Tampere University

ANISHA VISWANATHAN

Investigation of Molecular Mechanism, and Pre-clinical Evaluation of Multiple Classes of Novel Compounds for Treating Glioblastoma

Tampere University Dissertations 392

Tampere University Dissertations 392

ANISHA VISWANATHAN

Investigation of Molecular Mechanism, and Pre-clinical Evaluation of Multiple Classes of Novel Compounds for Treating Glioblastoma

ACADEMIC DISSERTATION
To be presented, with the permission of
the Faculty of Medicine and Health Technology
of Tampere University,
for public discussion at Tampere University
on 12th April 2021 at 11 o’clock am.

ACADEMIC DISSERTATION
Tampere University, Faculty of Medicine and Health Technology
Finland

Responsible supervisor	Adjunct professor Meenakshisundaram Kandhavelu Tampere University Finland	
Supervisor	Professor Olli Yli-Harja Tampere University Finland	
Pre-examiners	Professor Michela Buccioni University of Camerino Italy	Associate professor Vaiyapuri Subbarayan Periasamy King Saud University Kingdom of Saudi Arabia
Opponent	Associate professor Clement Penny University of Witwatersrand South Africa	
Custos	Professor Olli Yli-Harja Tampere University Finland	

The originality of this thesis has been checked using the Turnitin OriginalityCheck service.

Copyright ©2021 author

Cover design: Roihu Inc.

ISBN 978-952-03-1900-7 (print)
ISBN 978-952-03-1901-4 (pdf)
ISSN 2489-9860 (print)
ISSN 2490-0028 (pdf)
http://urn.fi/URN:ISBN:978-952-03-1901-4

PunaMusta Oy – Yliopistopaino
Joensuu 2021

Dear Mom and Dad,

You believed in me, before I believed in myself. Thank you for your boundless love and constant encouragement throughout my life. This achievement is dedicated to you !

ACKNOWLEDGEMENTS

I am deeply thankful to Adjunct Professor, Dr. Meenakshisundaram Kandhavelu and Prof.Olli Yli-Harja, my supervisors for doctoral research. Dr. Meenakshisundaram Kandhavelu is an amazing mentor and his continuous guidance and support throughout my project has helped me complete my work in time. He has guided me end-to-end during my lab experiments and I learned a lot from him as a person and supervisor. I also thank Prof. Olli for his valuable suggestions, encouragement and inspiration during my research.

I extend my sincere thanks to my pre examiners- Michela Buccioni, and V S Periasamy, for their proper review of the thesis draft, comments and recommendations. I take this opportunity to thank my colleagues, Phuong Doan, Anastasia Zurina, Dinesh Kute and Aliyu Musa for their generous help and wonderful teamwork for achieving completion of the work in a meticulous time. I remember with thanks Giulia Sebastianelli and Hien Le for your friendship and care during the course of my research.

I thank my amazing son Abhineeth, for being extremely cooperative, and for sacrificing many of his precious days for the sake of my studies. I express my deep gratitude to my husband Rupesh Chandran for letting me pursue my goal. I take this opportunity to mention that I am fully indebted to my parents and my sister for their great support and guidance, for standing by me during every ups and downs, and for endless things they have done for me since my childhood. I express my gratitude for my friends and well-wishers who has helped me to take every little step towards the success in my life.

Last, but not the least, I thank the department of MET, Tampere university for providing the financial support and infrastructure in order to complete my research work.

ABSTRACT

Glioblastoma multiforme (GBM) is the most complex, treatment-resistant, and non-curative brain cancer, accounting for 45% of all brain cancers. Despite the progressive discernment of the biological landscape of the disease, and numerous therapeutic agents in use or in trials, a lack of progress persists in GBM therapy. GBM possesses multiple sub-networks and extensive cross-talk between oncogenic pathways, promoting gliomagenesis, phenotypic variations, as well as adaptive mechanisms waning current treatment modes. A prospective outlook in GBM cure is to target the cross-talks between numerous sub-networks in GBM which promote tumorigenesis, therapeutic blockade, and phenotypic heterogeneity. The presence of adaptive mechanisms that help to bypass therapeutic blockade by mono-targeting agents, necessitates synergistic targeting of multiple oncoproteins or pathways. A multi-targeted, single drug molecule that horizontally inhibits various channels of tumorigenicity, such as angiogenesis or infiltration, represents a logical and alternative approach to drug cocktails to combat GBM, and can provide a guaranteed improvement in the clinical benefits. This thesis is a quest for identifying a potent multi-channel agent against GBM, which can bypass the current challenges of drug resistance and tumor recurrence.

This manuscript comprises of four publications, each detailing the extensive evaluation of novel compounds from four different chemical classes- diols, hydrazones, borons and thioesters, for their anti-GBM activity, *in vitro*. Each of the molecular classes has been evaluated for their cytotoxicity, apoptotic activity, cellular oxidative potential and caspase activity accounting for cell death. The possible targets were identified using docking studies and the detailed mechanism of action of the top compounds were analyzed using transcriptome studies.

The initial class of compounds described in this thesis is the decane-1,2-diol derivatives. The novel derivatives demonstrated fair cytotoxicity to GBM cell in the initial screening. Among a panel of twelve novel diol derivatives, the drug **DBT (decane-1,2-diyl bis-(p-toluenesulfonate))** was found to be the most cytotoxic to human cancer cell lines U-87 and LN229. **DBT** has shown cytotoxic activity with IC_{50} of 52 µM in U-87 cell line and 270 µM in LN229 cell line. Additionally, **DBT**

increased sensitivity to apoptotic pathways via caspase independent pathways, induced oxidative stress, prevented migratory activity effectively up to 6hrs post treatment at IC_{50} concentration and arrested cell cycle transition at G1/S phase. Molecular docking study identifies a strong interaction between NMDA receptor and **DBT** suggesting its possible mode of action.

The next class of compounds analyzed was arylhydrazones of active methylene compounds (AHAMCs). Among 23 novel derivatives, **R234 (2-(2-(2,4-dioxopentan-3-ylidene)hydrazineyl)benzonitrile)** was identified to possess the best anti-cancer features. **R234** displayed an IC_{50} of 107 µM in U-87 cells and 87 µM in LN229 cells. **R234** was found to reduce cell viability and proliferation, interrupt cell cycle at G1/S phase, drive apoptotic cell death, increase chemosensitivity and affect RTK pathways. Molecular profiling also supported the drug's characteristic as a strong cell cycle inhibitor. Docking studies cues that **R234** acts via NGFR receptor pathways.

The third class of compounds under study, detailed in this thesis, is boroxazolidones. The experimental results detected compound **JRB115 (2,2-bis(2,4-difluorophenyl)-4-isopropyl-1,3,2λ^4-oxazaborolidin-5-one** as the best candidate among an array of 6 novel L-valine derived boroxazolidones. **JRB115** exhibited dose-dependent cytotoxic effects in LN229 and SNB19 GBM cell lines with IC_{50} value of 53 µM and 49 µM, respectively. The compound **JRB115** was induced apoptosis via caspase 3/7 activation, caused toxicity via oxidative stress and instigated cell cycle arrest at G2/M phase.

The last class of compounds reported in this project is thioester derivatives. On analysis of 12 novel compounds containing α-thioether ketones and orthothioester moieties, our results highlights **5a (1,2-bis(4-hydroxy-3-methoxyphenyl)-2-((3((2-(4-hyroxy-3-methoxyphenyl)-1,3-dithian-2-yl)thio)propyl)thio)ethan-1-one**, as the most efficacious chemotherapeutic agent against GBM. **5a** was proven to possess an IC_{50} value of 27 µM in U-87 cell line and 23 µM in LN229 cell line. The top compound inhibited GBM proliferation, promoted caspase3/7 activation, inhibited cell cycle, and restricted MAPK signaling cascade. RNA-seq analysis of **5a** treated cells evidenced disfavoring of various tumorigenic pathways, notably proliferative and angiogenic signaling, and suggested inhibition of RTK signaling via EGFR. Docking studies indicated a solid interaction between **5a** and EGFR endorsing the mode of action via EGFR.

In general, our findings suggest that all the chemical classes investigated possess strong bioactivity against Glioblastoma, and had derivatives more potent than the current standard drug Cisplatin. Of the four different drugs considered for comprehensive evaluation, the study indicates that, the novel thioester derivative **5a** possesses multiple characteristics confronting various aspects of GBM oncogenesis. Specifically, **5a** is potent cytotoxic, genotoxic and a multi-kinase inhibitor leading to anti-angiogenic, anti-invasive effects, posing it as a best anti-GBM chemotherapy agent. Designing a precision medicine based on characteristics of this deadly tumor such as tumor subtype, mutagenic variations, specific molecular signatures, cross-talk of pathways involving in proliferation, angiogenesis, and drug resistance can be promising in anti-GBM therapy.

CONTENTS

ABSTRACT

PREFACE

LIST OF FIGURES

LIST OF TABLES

ABBREVIATIONS USED

LIST OF PUBLICATIONS

AUTHORS CONTRIBUTIONS

1 INTRODUCTION 1

  1.1. Introductory Overview 1

  1.2. Scope of the thesis……………………………………………………………. 2

  1.3. General sceheme of the study and limitations………. 3

  1.4. Thesis outline 3

2. REVIEW OF RELATED STUDIES………….. 5

  2.1. Glioblastoma multiforme-molecular subtypes, clinical challenges and therapeutic targeting….. 5

    Classification Based on Gene expression 5

    Classification based on Isocitrate dehydrogenase (IDH) mutation 6

  2.2. Molecular markers of Glioblastoma multiforme and their clinical correlation 6

  2.3. Glioblastoma multiforme: treatment challenges 8

    Glioblastoma stem cells (GSC) and therapeutic resistance 9

    Intra-tumoral heterogeneity 10
    Post-therapy resistance 10
2.4. Biology of Glioblastoma oncogenesis 10
2.5. Targeted therapies for Glioblastoma 12
    EGFR targeted inhibitors 13
    VEGF targeted inhibitors 13
    MET inhibitors 14
    MAPK/PI3K signaling pathway targeted therapy 14
    Multiple kinase inhibitors 14
    Immune checkpoint inhibitors 15
    DNA repair and cell cycle checkpoint inhibitors 15
2.6. Combination therapies 16
2.7. Drug design, discovery and development process 17
3. RATIONALE OF CHOICE OF DRUG CLASSES 20
3.1. Diols as anticancer agents 20
3.2. Hydrazones as anti-cancer agents 21
3.3. Thioesters as anti-cancer agents 22
3.4. Borons as anti-cancer agents 25
4. METHODOLOGY.. 27
4.1. Cell Culture 27
4.2. Trypan blue exclusion assay 28
4.3. Detection of apoptotic activity by Fluorescein dual staining with Annexin V FITC/Propidium iodide (PI) 29
4.4. Caspase Activation test 31
4.5. Intracellular Redox potential test using 2',7'-dichlorodihydrofluorescein diacetate (H2DCFDA) 32

4.6. Cell imaging using fluorescence microscopy 33
4.7. Transcriptome characterization using RNA-Seq data analysis 33
4.8. Molecular docking 38
4.9. Statistical Analysis 39
5. SUMMARY OF THE RESULTS. 41
6. INFERENCE AND DISCUSSION 51
7. CONCLUSION. 59
8. BIBLIOGRAPHY 60

List of Figures

Figure 1 .... Challenges associated with GBM treatment
Figure 2 .... Key pathways involved in Glioblastoma pathogenesis
Figure 3 .... General pipeline involved in drug discovery and development process
Figure 4 .... Structure of ethylene glycol- a simple diol
Figure 5 .... Basic structure of the hydrazone functional group
Figure 6 .... Basic structure of a thioester
Figure 7 .... Appearance of cells stained by Trypan blue dye, under an automated cell counter
Figure 8 .... Microscopic images of Apoptotic activity
Figure 9 .... Schematic representation of Apoptotic signaling via Caspase activation
Figure 10 .... Novel diol drug DBT exhibits strong anti- GBM activity
Figure 11 .... A sample molecular docking simulation of a ligand-receptor binding
Figure 12 .... Hydrazone drug R234 effectively downregulates various receptor tyrosine kinase pathways

Figure 13............ Thioester derivative 5a shows promising anti-GBM impact, demonstrating multidimensional toxic effects on key tumorigenic features

Figure 14 ... ……An overview of the enrichment of DEGs identified in each of the compound class

Figure 15...... Overall anti-tumor activities of DBT, R234 and 5a, identified by transcriptome profiling

Figure 16 .... MYC and EGFR are the hub nodes identified in 5a treatment

Figure 17……..….Key effector pathways of 5a and their interaction network

List of Tables

Table 1. ....Panel of diol derivatives considered for the study

Table 2. ....Chemical structure of hydrazone compounds, considered for the study

Table 3. .... Structure of Boron derivatives used for the study

Table 4. ....Structure of Thioester derivatives, used for the study

Table 5. ....List of DEGs disfavoring tumor growth, under 5a treated condition

ABBREVIATIONS USED

GBM	Glioblastoma Multiforme
WHO	World Health Organization
VEGF	Vascular Endothelial Growth Factor
ADME	Absorption, Distribution, Metabolism, and Excretion
CDKN2A	Cyclin-dependent kinase Inhibitor 2A
PTEN	Phosphatase and tensin homolog
NES	Nestin
EGFR	Epidermal growth factor receptor
TNF	Tumor Necrosis Factor
NF1	Neurofibromin1
TP53	Tumor Protein 53
TGCA	The Cancer Genome Atlas
TNF	Tumor Necrosis Factor
IDH1	Isocitrate dehydrogenase 1
NADPH	Nicotinamide adenine dinucleotide phosphate
MGMT	O-6-methylguanine-DNAmethyltransferase
EGFR	Epidermal Growth Factor Receptor
ATRX	α-thalassemia/mental retardation syndrome X-linked
TERT	Telomerase reverse transcriptase
GSC	Glioma Stem Cell
HIF	Hypoxia-inducible factors

RISC	Recurrence-initiating stem-like cancer cells
RTK	Receptor tyrosine kinase
RTKi	Receptor tyrosine kinase inhibitor
ATM	Ataxia telangiectasia mutated
PI3K	Phosphatidylinositol 3-kinase
pRB	Retinoblastoma protein
FGF	Fibroblast growth factor
PDGF	Platelet-derived growth factor
HGF	Hepatocyte growth factor
RT	Radiotherapy
PARP	Poly- (ADP ribose)- polymerase
CADD	Computer-Aided Drug Design
AMAP	2-[(arylmethyl)amino]-1,3-propanediol
α-CBD	α-2,7,11-cyprotermine-4,6-diol
CNS	Central Nervous System
NMDARs	N-methyl-D-aspartate receptors
CAMKs	Calmodulin-dependent kinase
NGFR	Nerve growth factor receptor
HDAC	Histone deacetylases
PI	Propidium iodide
NGS	Next-Generation Sequencing
ROS	Reactive Oxygen Species
H2DCFDA	2',7’-dichlorodihydrofluorescein diacetate
AHAMCs	Arylhydrazones of Active Methylene Compounds

ORIGINAL PUBLICATIONS

Publication I	Anisha Viswanathan, Anastasia Zhurina, Benedicta Assoah, Aleksi Paakkunainen, Aliyu Musa, Dinesh Kute, Konda Mani Saravanan, Olli Yli-Harja, Nuno R. Candeias, Meenakshisundaram Kandhavelu, ‘**Decane-1,2-diol derivatives as potential antitumor agents for the treatment of Glioblastoma**’, *European Journal of Pharmacology*, Volume 837, 15 October 2018, Pages 105-116. doi: 10.1016/j.ejphar.2018.08.041
Publication II	Anisha Viswanathan, Dinesh Kute; Aliyu Musa; Saravanan Konda Mani; Vili Sipilä; Frank Emmert-Streib; Fedor Zubkov; Atash V. Gurbanov; Olli Yli-Harja, Meenakshisundaram Kandhavelu, **‘2-(2-(2,4-dioxopentan-3-ylidene)hydrazineyl)benzonitrile as novel inhibitor of receptor tyrosine kinase and PI3K/AKT/mTOR signaling pathway in glioblastoma’**, *European Journal of Medicinal Chemistry*, Volume 166, 15 March 2019, Pages 291-303. doi.: 10.1016/j.ejmech.2019.01.021
Publication III	Anisha Viswanathan, Giulia Sebastianelli, Kenna Brown, Janne Raunio, Vili Sipilä, Rafael Candeias Nuno, Olli Yli-Harja, Meenakshisundaram Kandhavelu ‘***In vitro*** **anti-glioblastoma activity of L-valine derived boroxazolidones**’, European *Journal of Pharmacology*, Volume 854, 5 July 2019, Pages 194-200 doi: 10.1016/j.ejphar.2019.04.020
Publication IV	Anisha Viswanathan, Aliyu Musa, Akshaya Murugesan, João R. Vale, Saravanan Konda Mani, Carlos A. M. Afonso, Rafael Candeias Nuno, Olli Yli-Harja, Meenakshisundaram Kandhavelu ‘**Battling Glioblastoma: A Novel Tyrosine Kinase Inhibitor with Multi-dimensional Anti-tumor Effect’**, Cells, 12 Dec 2019, 8(12), 1624. doi: 10.3390/cells8121624

AUTHOR’S CONTRIBUTIONS

Publication I	Viswanathan A and Zhurina A performed the experimental work. Viswanathan A carried out the experimental data analysis, interpreted the results and is the primary author of the article. Konda M S did the docking study. Musa A performed RNA seq analysis. Kute D contributed to the cell cycle study. Musa A and Kute D did partial contribution to the manuscript. Assoah B, Paakkunainen A and Candeias N R synthesized the compounds. All authors partially contributed to the manuscript content. Kandhavelu M, Yli-Harja O, Candeias N R and conceived and managed the studies
Publication II	Viswanathan A and Kute D performed the *in vitro* experiments, and Musa A analyzed the RNA seq data. Zubkov F and Gurbanov V A synthesized and characterized the compounds. Viswanathan A is the primary author of the manuscript and all others partially contributed to the manuscript content. Kandhavelu M, Yli-Harja O, Streib E F and conceived and managed the studies
Publication III	Viswanathan A and Sebastianelli G executed the experiments and data analysis. Seppala V executed the cell cycle image analysis. Brown K performed the experiment on the normal brain cell line. Raunio J synthesized and characterized the compounds. All the authors contributed equally to the manuscript. Kandhavelu M, Yli-Harja O, Candeias N R and conceived and managed all the studies
Publication IV	Viswanathan A executed the experiments, performed data analysis, and primarily wrote the manuscript. Konda M executed docking studies. Murugesan A executed protein studies. Musa A analyzed RNA-seq data. All the authors contributed to the manuscript content. Kandhavelu M, Yli-Harja O, Candeias N R and conceived and managed the studies.

Kandhavelu M and Yli-Harja O supervised all the studies

1 INTRODUCTION

1.1. Introductory overview

Glioblastoma multiforme (GBM) is a WHO grade IV astrocytoma hallmarked by a heterogeneous cell population with variable genetics, high intrusion, rampant angiogenesis, and refractive to chemotherapy. GBM is one of the most complex and hardest to cure among all tumors. Despite continuous efforts, tumor recurrence and subsequent death are inevitable. Glioblastomas account for nearly 15% of all brain tumors and the mean survival time is 12-18 months. Only 25% of glioblastoma patients survive over a year, and only 5% of patients survive more than five years[1]. Traditional approaches for treating GBM, aimed at arresting cancer cell proliferation, have not led to any radical improvement in gliomas and have been replaced recently by more specific target-oriented therapies. Due to the acute complexity of the disease, single-target approaches have been futile. The global GBM market was estimated to be USD 464.8 million in 2016 and is predicted to grow nearly 1.15 billion by 2024 period mainly due to the rise in aging population[2].

Treatment of GBM is challenged by various factors. GBM is abundantly vascularized, consists of highly infiltrating cells hindering complete surgical removal. Also, GBM is histologically characterized by the altered expression of various genes that stimulate endothelial cell proliferation, migration, and survival. GBM exhibits cellular heterogeneity, with a small sub-population of tumor cells possessing stemness. Additionally, GBM present molecular heterogeneity depending on its tumor microenvironment as well as in various stress environments. Furthermore, symptomatic presentation of tumor occurs very late and even with the latest technological advancements, only dismal prognosis is possible.

Molecular profiling of GBM tumors demonstrates frequent alterations in GBM genes, enlisting amplification of various growth factor receptors, transcriptional regulators, checkpoint inhibitors and chromatin remodeling genes, being few among them. GBM must be confronted at various levels by synergistic modulation of several targets to incapacitate its tumorigenic properties. Trending in GBM chemotherapy research are multi-kinase inhibitors as evidenced by lately approved drugs, and many of those in preclinical or clinical development stages.

Recent reviews on current combinatorial therapies using standard drugs, remarks failure of complete cure and speedy recurrence. Presence of ingenious cell death evading mechanisms, stress-activated oncogenic genes and detoured tumor pathways warrant smarter therapeutic agents confronting multiple tumorigenic pathways. Resistance to chemotherapeutic activity of GBM primarily arises from the VEGF-A (Vascular Endothelial Growth Factor-A)-dependent angiogenesis and through activation of alternative angiogenic receptors. Therefore, the GBM research is keener on drugs that can resolve challenges of limited efficacy, safety, and resistance of single-targeted agents. The current study thus focuses on the discovery of an powerful chemotherapy agent, using unexplored novel derivatives, of four classes of compounds- diols, hydrazones, borons and thioesters that enables the discovery of effective and safe multi-target anticancer agents.

1.2. Scope of the Thesis

The whole study is based on the hypothesis that, concurrent targeting of tumorigenic pathways by a single drug molecule represents a sensible and safe substitute to drug cocktails, to combat GBM. Considering the evolving heterogeneity which is associated with the therapeutic resistance and recurrence exhibited by GBM cells, there is an urgent need to investigate the novel chemotherapeutics that can parallelly act on multiple features of tumor invasiveness. The recent studies demonstrate a varying response to medications, by different GBM subtypes. Thus, choosing a drug by its specific mode of action, or targeted biomarker, may assist not only in durable response and effective cure, but also may challenge tumor recurrence. Therefore, this study intends to identify a novel chemotherapeutic agent which is biomarker driven, as well as have a synchronous anti-oncogenic effect on various features of GBM.

Specific aims of the study are as follows:

i) To evaluate the anti-cancer activity of the novel compounds, belonging to four different classes.

ii) To screen and identify the top compound in each class, and to perform detailed molecular profiling to detect their mode of action.

iii) To identify possible target of each of the potential chemotherapeutic agent.

iv) To determine the most powerful drug candidate, which possess multiple onco-inhibitory features.

1.3. General scheme of the study and limitations

In general, we report the synthesis, bioactivity characterization and *in vitro* anti-tumor analysis of 53 novel drugs that belongs to four different classes of compounds such as Diols, Hydrazones, Borons and Thioesters, for their anti-GBM effect in multiple cell lines. The study proposes to accomplish detailed biological characterization at the molecular level using various biological assays and transcriptome analysis to elucidate the mechanism of the action of top compounds in each class.

This is a preliminary experimental report and therefore, the pharmacological refinement or the *in vivo* analysis of the drugs, has not been included in this study. Better understanding of various roles of these compounds in tumor microenvironment and *in vivo* conditions may aid optimizing the lead agents to provide better efficiency and drug activity. While current data highlights the possibility of these least explored drug classes as monotherapy agents for GBM, prospective studies are needed to evaluate their ADME (absorption, distribution, metabolism, and excretion) analysis, extensive pharmacokinetics and toxicological impact. Also, their combinatorial effect with other therapeutic agents should also be worth evaluating to progress the candidate drugs mentioned in this thesis, into the clinic.

1.4. Thesis Outline

This manuscript is organized into six different chapters. Chapter **I** outlines the major context, scope, and limitations of the current study and organization of the manuscript. This includes the basic overview of the whole content of the research, significance of the topic of consideration, and the overall sketch of the study design. Chapter **II** discusses the key topics from the extensive review of the literature associated with the study, which is essential to understand this thesis. This chapter sketch out the basic information on the complexity of the disease chosen for the study, challenges associated with it and attempt to summarize the biology of glioblastoma oncogenesis. Chapter **III** outlines the pharmacological significance of the drug families considered in this study, and the related research outcomes to date. Chapter **IV** presents the methods and approaches we have used for the characterization and identification of the most potent pharmacological scaffolds in each class. Chapter **V** features a summary of the results from each publication comprised in this thesis. Chapter **VI** presents the major inferences drawn from the observed results, discussion in context of the study and future directions of the current work. Finally the last chapter- **VII** summarizes the whole project and its significance.

2 REVIEW OF RELATED STUDIES

2.1 Glioblastoma multiforme-molecular subtypes, clinical challenges and therapeutic targeting

Global gene expression profiling of GBM has identified pathogenically diverse set of tumors demarcated by shared genomic, epigenomic, or transcriptional features called as ‘molecular subclasses. Therapeutic response and disease prognosis of Glioblastoma is thoroughly affected by the molecular subclass of GBM. Understanding these subtypes aids developing more effective, molecularly guided approaches for curing GBM.

Classification Based on Gene expression

The Cancer Genome Atlas (TCGA) cluster GBM into four clinically relevant subtypes based on its gene expression profile, namely- Classical, Mesenchymal, Proneural and Neural subtypes.

Classical GBM: Classical GBM is a molecular subtype of glioblastoma characterized by chromosome 7 amplification, Epidermal growth factor receptor (*EGFR*) amplification, *EGFRvIII* mutation and lack of *p53* mutations[3]. It is also characterized by the loss of chromosome 10 and Focal deletion of 9p21.3 that targets cyclin-dependent kinase Inhibitor 2A (*CDKN2A*)[4,5]. Also, the mutation in phosphatase and tensin (*PTEN*), neural precursor and stem cell marker Nestin (*NES*) overexpression, Notch (*NOTCH3, JAG1, LFNG*) and Sonic hedgehog (*SMO*, *GAS1, GLI2)* pathway activation, are detected in this subtype[5]. Classical GBM is more sensitive to chemotherapeutics targeting kinase inhibition.

Mesenchymal GBM: Associated with markers *CHI3L1* and *MET*, the mesenchymal subtype is characterized by focal heterozygous deletion of 17q11.2 containing neurofibromin 1 (*NF1*) and found co-mutated with *PTEN*. Mutations in tumor protein *p53* (TP53), and stimulation of Tumor Necrosis Factor(*TNF*) superfamily and NF-kB pathway are also observed in this subclass[5]. Mesenchymal GBM is more aggressive and resistant to treatment and leads to a shorter survival period.

Proneural GBM: This subclass is linked with point mutations in isocitrate dehydrogenase 1 (IDH1 and platelet-derived growth factor receptor alpha (PDGFRA)[5]. IDH mutant patients with proneural GBM were reported to have longer median survival time[6] and worse prognosis[7]. Proneural GBM exhibits normal *EGFR, NOTCH* and *PTEN* levels[6], whereas genes such as *NF1*, *SERPINE1, TIMP1,SOX, DCX, DLL3, ASCL1,* and *TCF4* are overexpressed[5,6].

Neural GBM: Neural GBM is sensitive to treatments and has a short prognosis[5]. This subtype is defined by the expression of various neuronal markers such as *NEFL, GABRA1, SYT1, SLC12A5*, and *EGFR* amplification along with MGMT methylation of 29%[5]. This neural subgroup has a robust relationship with oligodendrocytic, astrocytic and neuronal differentiation as reported by Verhaak et al[5].

Classification based on Isocitrate dehydrogenase (*IDH*) mutation

WHO has classified GBM in 2017 into three major subgroups, based on *IDH* mutation: Wild type, Mutated and non-determined. *IDH* encodes an enzyme that carries out oxidative decarboxylation of isocitrate to α-ketoglutarate (α-KG), releasing a nicotinamide adenine dinucleotide phosphate (NADPH). Mutation of *IDH* gene causes a reduction in α-KG[8] instead produce 2-hydroxyglutarate (2HG)[9]. d-2HG inhibits the activity of dioxygenases[10] resulting in aberrant gene expression and epigenetic changes, promoting glioma pathogenesis[8]. *IDH*-mutant tumors that arise from a lower grade glioma are termed “secondary glioblastoma”. GBMs that are IDH– wild-type are classically termed as “primary glioblastoma”. IDH-NOS or non-determined is designated for those tumors for which full IDH evaluation cannot be performed.

2.2 Molecular markers of Glioblastoma multiforme and their clinical correlation

A clear understanding of the type of genetic and epigenetic modifications are quite significant for a substantial prognosis and patient response to therapy, in case of GBM. Most recent studies identify molecular markers in GBM prognosis as follows.

O-6-methylguanine-DNA methyltransferase (MGMT)

The cell defense and DNA repair enzyme MGMT, hydrolyze alkyl groups from O6 position of guanine in DNA, leading to chemotherapeutic resistance to alkylating agents such as temozolomide[11]. Methylation of MGMT promoter silences MGMT gene in glioma cells, causing a reduction in DNA repair function, increased genome variability, and chemosensitivity[11]. The MGMT methylation of GBM significantly correlates with survival for patients undergoing treatment with alkylating agents[11].

Epidermal Growth Factor Receptor (EGFR)

EGFR is a transmembrane tyrosine kinase, well correlated with tumor characteristics such as cell proliferation, migration, and survival. *EGFR* mutation is stated in 40–60% of GBM tumors[12]. *EGFR* amplification and *EGFRvIII* mutation is frequently observed in adult GBMs[12–14]. EGFR mutations have been implied in glioblastoma pathogenesis and resistance to treatment[15].

IDH 1/2 mutation

Isocitrate dehydrogenase (*IDH*) is an enzyme participating in the Krebs cycle that converts isocitrate to α-ketoglutarate. Mutant IDH reductively converts α-ketoglutarate to D(R)-2-hydroxyglutarate (D-2-HG) increasing oxidative stress and tumorigenesis[16]. The presence of IDH mutation has a severe impact on methylation status, phospholipid, energy, and oxidative stress pathways as well as telomerase reverse transcriptase (TERT)[17,18].

1p/19q co-deletion

WHO revised the classification of gliomas, based on the presence of an *IDH* mutation, and whole-arm co-deletion of chromosomal arms 1p and 19q (1p/19q co-deletion). Oligodendrogliomas are signified by the loss of the entire chromosomal arms 1p and 19q[19,20] along with *IDH* mutation, whereas astrocytomas are further classified according to their IDH status and smaller losses of genetic material from 1p and 19q[21]. This diagnostic detection of allelic losses, and IDH mutation status favors an improved distinction in the prognosis of gliomas.

TP53 mutation

The p53 protein, encoded by the *TP53* tumor suppressor gene, orchestrates a variety of cellular responses such as cell cycle, DNA-damaging repair, apoptosis, genome stability, and cell differentiation. Alterations in *TP53* gene expression are very prominent in GBM and associated with its pathogenicity [22,23]. The p53-ARF-MDM2 pathway is dysregulated in 84% of glioblastoma (GBM) patients and 94% of GBM cell lines[24–26]. GBM cell lines possessing mutant p53 are found to be more resistant to DNA-damaging therapeutic drugs, such as Cisplatin[27].

ATRX mutation

The *ATRX* (α-thalassemia/mental retardation syndrome X-linked) gene is involved in chromatin remodeling, DNA methylation and genomic stability [28]. *ATRX* has a broad spectrum of roles involved in the epigenetic changes associated with GBM[29]. *ATRX* mutation is frequently associated with IDH mutations, but rarely with 1p19q co-deletions[28]. Cai and colleagues have observed lower *ATRX* expression can act as a malignancy marker as it is more obvious in primary GBM and anaplastic gliomas than grade II gliomas [30].

TERT mutation

Telomeres act as the caps at the ends of chromosomes and shortens with each round of cell division, limiting the proliferation of human cells to a finite number. Telomerase reverse transcriptase (*TERT*) is a catalytic subunit of telomerase enzyme that executes nucleotide addition to telomeres, preventing its shortening[31,32]. Gain-of-function mutations in the *TERT* promoter are recurrently mentioned in grade IV astrocytomas (up to 85% of GBM) and grade 2/3 oligodendrogliomas (approximately 80%)[31,33]. *TERT* mutations are testified to be strongly correlated with 1p19q co-deletion, [34,35] and a combination of *TERT* mutation and wild-type IDH is typical of GBM.

2.3 Glioblastoma multiforme: treatment challenges

Recent developments in understanding the molecular biology and pharmacology of GBM prompted the growth of targeted-drugs to tackle this fatal disease, however, the progress is dismal. Multiple factors contribute to this disease complexity. The presence of a striking degree of intratumoral heterogeneity, the exhibition of transcriptional and epigenetically regulated subclasses, intertumoral heterogeneity characterized by distinct molecular profiles, multiple-feedback cross-talk pathways that drive drug resistance, altered cellular metabolism favoring tumor growth, and the incidence of cancer stem cells, are some of the most notable of them (**Fig.1**).

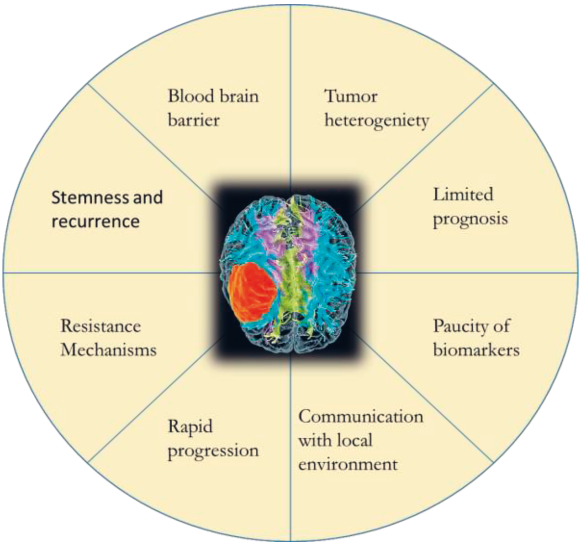
Blood brain barrier
Tumor heterogeniety
Stemness and recurrence
Limited prognosis
Resistance Mechanisms
Paucity of biomarkers
Rapid progression
Communication with local environment

Figure 1. Challenges associated with GBM treatment

Glioblastoma stem cells (GSC) and therapeutic resistance

Glioma stem cells (GSCs) comprises a fraction of slow-dividing cells within the tumor mass of GBM, responsible for post-treatment malignancy relapse. GSCs can recapitulate a whole tumor, and differentiate into other specific GBM sub-populations[36]. GSCs undergo genetic mutations as well as have a synergistic relationship within the tumor environment leading to various phenotypic transformations. The hypoxic niche supports GSC survival and proliferation via hypoxia-inducible factors (HIFs)[37]. CD133, a transmembrane glycoprotein, is the most widely recognized marker of neural stem cells, is common to GSCs as well[36]. Differential expression of proteins such as MGMT, BCRP1 and anti-apoptosis proteins in CD133+ GSCs were shown to contribute to the resistance to TMZ [38]. GSC plasticity through the generation of GSCs from non-GSCs, and upregulation of membrane transporters that are involved in expelling of drugs may also lead to therapeutic resistance.

Intra-tumoral heterogeneity

In order to effectively design therapeutics to GBM invasion, we must understand the molecular landscape underlying heterogeneity in tumor behaviors. Amplification oncogenic receptor tyrosine kinases, specifically, EGFR has been suggested to influence migratory behavior, clinical prognosis, and therapeutic efficacy[39]. IDH mutations also render variable susceptibility to treatments and therefore need to be targeted to prevent glioblastoma recurrence [40]. Metabolic heterogeneity in GBM is another aspect to be considered for effective cure of the tumor. Future molecularly targeted therapies for GBM should be designed based on the different properties such as divergent genetic alterations, selection pressure based on the tumor niche, capacity for dissemination.

Post-therapy resistance

Genetic modifications and rewiring cellular signaling pathways trigger the adaptive resistance of GBM cells, to current treatment modes leading to tumor recurrence. Numerous molecular mechanisms are associated with the post-therapy resistance in GBM: intra-tumoral heterogeneity at the cellular level, such as diverse transcription signatures for genes that regulate immune response, cell replication, hypoxia, stemness[41],and sub-clonal evolution[42] are a few to be specified. Recurrent tumors display variable degrees of genetic relatedness to the original tumor and involve complex evolutionary courses driving branched evolution resulting in divergent cell populations[43].

Recurrence-initiating stem-like cancer (RISC) cells are indebted to a number of molecular pathways linked to therapeutic resistance. This includes a number of extracellular signaling pathways mainly Wnt/β-catenin, Notch, receptor tyrosine kinase (RTK)/PI3K, NF-κB, SHH/GLI, and JAK/STAT signaling pathways as reviewed by latest reports[43,44]. Additionally, the apoptotic cancer cells send their signals via exosomes induced and released during apoptosis. Altered expression of the genes encoding Ataxia telangiectasia mutated (ATM), the cell cycle checkpoint protein RAD17, checkpoint kinases CHK1, CHK2, and the DNA repair enzyme *O*-6-Methylguanine-DNA methyltransferase (MGMT), also significantly correlate with resistance to chemotherapies[45,46]. Under hypoxic conditions, hypoxia-inducible transcription factors (HIF-1 and HIF-2) are also involved in tumor maintenance and angiogenesis[47].

2.4 Biology of Glioblastoma oncogenesis

Recent developments in the understanding of the oncogenic mechanism of GBM have summarized three core pathways- receptor tyrosine kinase [RTK]/RAS/phosphatidylinositol 3-kinase [PI3K], p53-ARF-MDM2/4 pathway, and retinoblastoma [RB] pathway- as major drivers of GBM characteristics[48]. The RTK/RAS/PI3K signaling pathway was found to be altered in approximately 86–89.6%, p53 pathway was altered approximately 85.3–87% and the pRB signaling pathway was found to be affected in approximately 77–78.9% of the GBM cases studied.

Downstream pathways triggered by RTKs involve RAS/MAPK/ERK and RAS/PI3K/AKT[49], which are implicated in controlling cell proliferation, survival, differentiation, and angiogenesis. PI3 kinases are activated by upstream signals from receptor tyrosine kinases (RTKs). PI3K catalyzes the production of the PIP_3, which actives both Akt and PKC favoring their kinase activity on multiple downstream substrates including mTOR. The protein phosphatase PTEN acts on PIP_3 to antagonize PI3K signaling and PTEN is frequently inactivated, deleted, or silenced in GBM. Mutations in GBM such as amplification of *EGFR*, gain-of-function in PIK3CA, or loss of PTEN, leads to tumor growth and invasion. RAS genes (Rat Sarcoma) are transforming oncogenes and belong to the G-protein family. RAS acts on MAPK through RAF kinase thus regulate downstream target gene transcription and cell activities. Deregulated RAS/MAPK pathway can trigger unchecked cell growth and proliferation, increasing aggressiveness. Various studies report over-expression of RAS in gliomas[50].

The p53 tumor suppressor integrates stress signals and negatively regulates cell division, induces senescence and apoptosis under normal growth conditions[51]. Aberrant p53 pathway components have been implicated in GBM cell invasion, migration, proliferation, evasion of apoptosis, and cancer cell stemness[26]. Amplification of oncogenes MDM2 and MDM4 can inactivate p53[52], leading to the loss of its function. CDKN2A/ ARF can promote MDM2 degradation, thereby preventing the degradation of p53 tumor suppressor activity. Also, ARF can induce tissue inhibitor of metalloproteinase-3 (TIMP3) thus reduce GBM cell migration. ARF is the most commonly deregulated component and found to undergo homozygous deletion in GBM.

The tumor suppressor retinoblastoma (pRB) protein controls cell cycle, and acts as a checkpoint to S-phase during division. RB protein is frequently altered in GBM[53]. The pRB is normally inactivated by Cyclin D/CDK4/CDK6-induced phosphorylation. Inactivation of CDKN2B which is a CDK inhibitor, and the amplification of CDK4 and CDK6 is commonly found in GBM[54] leading to tumorigenesis and glioma progression. Apart from the aforementioned pathways, other pathways such as JAK-STAT, Wnt, Sonic Hedgehog and Notch, can contribute to GBM progression.

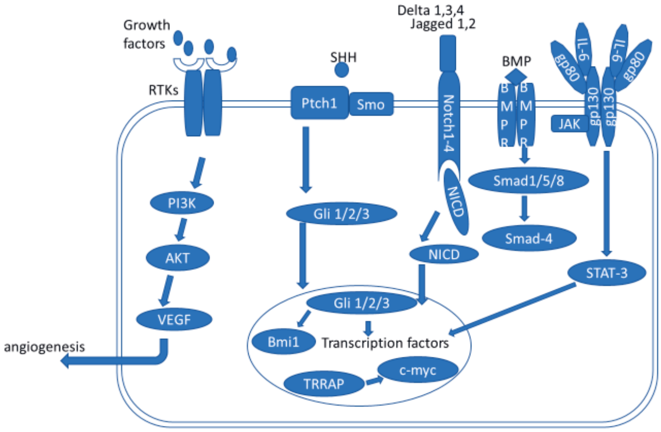
Growth factors
RTKs
SHH
Ptch1
Smo
Delta 1,3,4
Jagged 1,2
Notch1-4
NICD
BMP
BMPR
BMPR
IL-6
IL-6
gp80
gp80
gp130
gp130
JAK
PI3K
AKT
VEGF
angiogenesis
Gli 1/2/3
Smad1/5/8
Smad-4
NICD
STAT-3
Gli 1/2/3
Bmi1
Transcription factors
TRRAP
c-myc

Figure 2. Key pathways involved in Glioblastoma pathogenesis

2.5 Targeted therapies for Glioblastoma

Glioblastoma is highly resistant to conventional chemotherapy and radiotherapy. Most of the abnormalities in glioblastoma are associated with aberrant regulation of signal transduction pathways providing scope for potential new therapeutic targets. This necessitates the identification of the optimal therapeutic targets or those which have an amplifying effect down the signaling cascade, as a concomitant or adjuvant therapy. Several signal transduction inhibitors are under evaluation in preclinical and clinical malignant trials. This primarily includes anti-angiogenic agents (e.g.: bevacizumab, enzastaurin), and epidermal growth factor receptor tyrosine kinase inhibitors (e.g.: gefitinib and erlotinib), mTOR inhibitors (e.g.: temsirolimus, everolimus) and transmembrane protein inhibitors (e.g.: cilengitide). However, the results of the use of targeted agents are not so impressive in case of GBM, due to its heterogenic nature and resistance pathways.

The combination of different single-targeted drugs or the combination of targeted drugs with conventional chemotherapy and radiotherapy has also found no significant success. Therefore, most recent emphasis in GBM is on the combination of multi-targeted drugs along with surgery and radiotherapy, in order to overcome the resistance of tumors as opposed to single-agent targeted therapies.

EGFR targeted inhibitors

EGFR is amplified and mutated in a large number of GBMs. Considering the importance of EGFR and its variant EGFRvIII in GBM pathogenesis, clinical trials in progress include agents targeting EGFR. Unfortunately, targeting EGFR has not been effective so far. The first generation of EGFR inhibitors, gefitinib and erlotinib failed in GBM clinical trials[55,56]. Preliminary reports from the phase III randomized study of rindopepimut, another EGFR inhibitor, in newly diagnosed EGFRvIII-positive glioblastoma indicated no significance improvements, leading to closure of the trial[57]. An assortment of first and second generation EGFR/HER2 TKIs have been evaluated as monotherapy or as combination therapies, with limited success[58–61]. Further studies that evaluate novel anti-EGFR agents or combinations are required for an EGFR inhibition in specific molecular subtypes of GBM.

VEGF targeted inhibitors

Angiogenic factors, including vascular endothelial growth factor (VEGF), fibroblast growth factor (FGF), and platelet-derived growth factor (PDGF), are important drivers of angiogenesis promoting oxygen supply to the tumor. VEGF is an active mediator of tumor neovascularization and VEGF expression is linked with GBM tumorigenicity[62]. Furthermore, VEGF causes pericytes (perivascular cells that wrap around blood capillaries) disintegration leading to the formation of abnormal vascular permeability. This phenomenon is a hallmark of GBM[63] and has severe consequences on the blood brain barrier.

VEGF targeted therapies include blockade of VEGF (Bevacizumab) and VEGF trap (Aflibercept) and VEGFR TKIs (Pazopanib, Vandetanib, CT-322, Ramucirumab and Icrucumab). The most widely used targeted treatment against angiogenesis is the vascular endothelial growth factor (VEGF) monoclonal antibody bevacizumab. Vatalanib an anti-VEGF agent is well tolerated by patients, but it does not appear to result in effective tumor regression[64]. Cediranib, a VEGFR-2 tyrosine kinase inhibitor, failed to improve progression-free survival as a monotherapy and in conjunction with Lomustine[65]. The lack of a durable response and survival benefit demands the need to understand the mechanism underlying resistance to anti-angiogenic therapies and to develop multi-targeted therapeutics.

MET inhibitors

MET is a receptor tyrosine kinase that is involved in embryonic development and tissue repair[66] . MET and downstream signaling pathways, including RAS/MAPK, PI3K/AKT, and STAT are activated by Hepatocyte growth factor (HGF) [67]. The c-MET signaling pathway activation in glioblastoma, thus have pleotropic effects, promoting tumor growth, invasiveness, and drug resistance. Although many propitious MET inhibitors have been developed, resistance to single modality anti-MET drugs has been frequently reported, rendering these agents with limited success[68–70]. Ineffectiveness of Crizotinib, a c-MET/ALK inhibitor have been documented in GBM patients[71]. An in-depth analysis of the molecular basis of adaptive resistance to MET inhibitors can promote beneficial results as anti-GBM targeted therapy.

MAPK/PI3K signaling pathway targeted therapy

The RTK/PI3K/MAPK pathways are involved in glioblastoma cell migration and proliferation and are mutated in 90% of GBM[72,73]. Single-agent kinase inhibitors have had disappointing clinical results in gliomas due to limited brain penetrance and GBM adaptive mechanisms. Dual targeting PI3K and MAPK pathways, McNeill and colleagues observed synergistic effects accelerating GBM cell death, an advantageous effect over single-agent kinase therapies[74,75]. PX-866 (Sonolisib) a PI3K inhibiting drug, has been shown to inhibit angiogenesis, induce cell cycle arrest and restrict invasion of GBM cells *in vitro*[76]. The RAF multi-kinase inhibitor, Sorafenib, has been evaluated in several small phase I/II studies as monotherapy or as combination therapy[77–79] and exhibited limited efficacy in GBM.

Multiple kinase inhibitors

Drugs such as AEE788 and Vandetanib target both EGFR and VEGFR tyrosine kinases. In a phase II trial of a multi-modal therapy, including Vandetanib to the standard therapy regimen (surgery+ chemotherapy+ radiotherapy), yielded little effect on overall survival of the patients[80]. Regorafenib is an approved drug that was proven to inhibit VEGFRs and PDGFRs, in colon cancer as well was gastrointestinal stromal tumors[81]. TG02, a CDK inhibitor was reported to be effective in pediatric brain tumors with MYC overexpression[82]. Another multiple kinase inhibitor Lapatinib that targets both EGFR and HER2 tyrosine kinases also found limited success in phase I/II trial for recurrent GBM. Sunitinib is a multiple kinase inhibitor of VEGF, PDGFR, FLT1, FLT1/KDR, FLT3 and the RET kinases[83]. A phase II study for recurrent glioblastoma multiforme incorporating Sunitinib was found to be unsuccessful as a monotherapy with all patients' disease progressing despite treatment[84]. Imatinib, inhibitor of the PDGFR, KIT, and ABL kinases, also was less effective to outsmart GBM maintenance. Limited success of such multi-kinase inhibitors, warrants a relook into the molecular subtypes, resistance pathways and compensatory mechanisms in GBM.

Immune checkpoint inhibitors

Immunotherapy for glioblastoma has gained considerable interest over the past few years[85]. Few of the immune checkpoint blockers (ICBs) under clinical trials include nivolumab[85–87], Pembrolizumab[85,88], Atezolizumab [89,90] and Avelumab [91,92]. In GBM, the overexpression of TIM-3, a molecule expressed by CD4+ and CD8+ T cells involved in immune suppression, is associated with higher malignancy and is thus considered a strong prognostic indicator of the disease [93,94]. IDO is another immune checkpoint molecule and its overexpression is linked to poorer outcome in GBM patients[95,96]. Chemotherapeutics such as Epacadostat or Indoximod have shown positive results in *in vivo* models [97].

DNA repair and cell cycle checkpoint inhibitors

The cell cycle is a series of events involving cell growth and cell division that produces two new cells. The cell cycle consists of four-stages in which the cell increases in size (gap 1, or G1 stage), duplicates its DNA (synthesis, or S, stage), prepares to divide (gap 2, or G2 stage), and divides (mitosis, or M, stage)[98]. Cells use special proteins and checkpoint signaling systems to ensure faithful progression of the cell cycle. A complex system of regulatory molecules control cell-cycle process, with stringent control at two key control points - the G1 checkpoint (DNA quality), and at the end of the G2 checkpoint (chromosomal quality) ensuring high accuracy.

One of the major players in G1-S transition, is the Retinoblastoma (Rb) protein, which is in turn regulated by a series of proteins, including p16, cyclin-dependent kinases, cyclins, and E2F. In order for the DNA to replicate, cyclin D binds to CDK4/6 forming an active complex that phosphorylate Rb. The phosphorylated Rb then activate S phase specific transcription factors, permitting G1 to S phase transition. The p16 protein is one of the most important regulators of the CDK4-cyclin D complex. The binding of p16 to CDK4 blocks its complex formation with cyclin D, hindering Rb phosphorylation, thus arresting the cell in the G1 phase. Inactivation of p16 or Rb, increased cyclin D1, or CDK4/6 activity results in progression to the S phase and are common events in human glioma cells[99,100] . The p53 protein is upstream of Rb in controlling the G1 checkpoint. The mitotic checkpoint at the end of G2 phase ensures the chromosomal quality. Inhibitory phosphorylation of CDC2 lead to cell cycle arrest at G2. CDK1/CDC2 when in complex with cyclin B1 forms an active complex is required for progression from G2 to M phase. Key proteins involved here are CDC25C, ATR and p53. Following DNA damage, ATR phosphorylates CHK1 which in turn phosphorylates CDC25C. CDC25C is then not able to activate CDK1/CDC2 through its phosphatase activity, halting progression to Mitotic phase. Additional regulators of CDK1/CDC2 are WEE1 and MYT kinases. The p53 protein regulates G2 checkpoint via CyclinB1. Inactivation of Rb and p16 proteins and amplification of cyclin D1 and CDK4, are among the most frequent abnormalities that occur in Glioblastoma[101,102]. Numerous cell cycle checkpoint inhibitors have shown efficacy as anti-GBM agents in preclinical phase I and phase II studies[103–105].

2.6 Combination therapies

For resistant cancers like GBM, targeting two or more nodes in tumorigenic pathway, are found to be more effective than individual targeted therapies. Combination therapy works synergistically, or in an additive manner, and for a successful treatment, any single therapy agent used in the combination therapy shouldn't have cross resistance with the others.

The current standard drug used in GBM chemotherapy, temozolomide has been evaluated with many other agents such as morphine[106], nutlin3a[107], sulforaphane[108], XL765[109] and nimotuzumab[110] and has shown improved therapeutic response in comparison to single chemoagents. Use of drug cocktails such as the RIST (Rapamycin, Irinotecan, Sunitinib, Temozolomide) and the variant aRIST with GDC-0941 inhibit GBM cell growth in primary patient culture via up-regulation of apoptotic pathways[111]. Additionally, chemoagents in conjunction with Radiotherapy (RT) have also shown better results against GBM. Poly (ADP ribose) polymerase (PARP) inhibition is a new therapeutic approach in GBM[112,113]. RT and (PARP) inhibitors has been reported to radiosensitize glioma cells by inhibiting DNA repair[114]. Palbociclib is a selective inhibitor of CDK4/6 kinase, when co-administered with RT, showed a survival advantage in mice.

2.7 Drug design, discovery and development process

The hunt for new drugs is an integral part of medical research. Identification of novel therapeutic agents and right delivery vehicles for precision targeting is crucial for any type of pharmaceutical industry. Taking in a wider sense, drug design refers to random evaluation of natural or synthetic substances for medicinal properties, or inventing new drugs based on some bioactive compounds as templates, or synthesizing compounds by molecular modifications. This being a complicated, time consuming process, last few decades have started seeking the use of computational models to enhance the drug discovery procedure. The processes, termed as Computer-Aided Drug Design (CADD), is an alternative to another method that rely on a known structure of the biological target molecule, called Structure Based Drug Design. The in-silico drug design consists of various advanced techniques such as QSAR/QSPR, structure-based design, combinatorial library design, cheminformatics, bioinformatics and the increasing number of biological and chemical databases are used in the field. Drug discovery is multistage process, each stage consisting of several parallel and sequential sub-process (**Fig: 3**). In short, the stages of drug development have the following steps:

Selecting a disease: Choice of the disease is usually based on interest, significance or need. Once the disease is identified an attempt to explore the biochemical mechanisms underlying the disease will be performed to obtain better understanding of the targetable molecules or pathways.

Drug discovery: Following the selection of disease, many drug candidates will be evaluated for identifying a hit molecule. These drug molecules may by synthetic, natural or biologically-derived molecules. Methods of drug discovery includes, random screening, bioactivity analysis, target ligand interaction studies, refining/optimization of lead compounds to enhance the activity and preclinical studies. Next generation sequencing such as RNA-seq have revolutionized the drug discovery process by providing insight into pathways and regulations in biological processes. More importantly, it could be used to identify drug- induced gene expression changes aiding target identification of a particular drug.

Product Characterization: A promising drug molecule will be characterized for chemical and physical characteristics such as molecular features, stability, etc. Also, bioactivity analysis, including mode of action of the drug in body will be performed. Additionally, detailed analysis of optimal conditions and other factors affecting the performance of the drug will be carried out.

Formulation, Delivery, Packaging Development: All critical parameters that affect the bioavailability of the drug in the target tissues or cells are continuously refined and optimized during this stage. The drug formulation must remain effective, non-contaminated, safe and nontoxic to use. Appropriate mode of administration as capsules, tablets, aerosol or injectable, is evaluated.

Pharmacokinetics and Drug Disposition: The fate of the particular formulation inside the body depends on the course of its absorption, bioavailability, distribution, metabolism, and excretion, which is termed as pharmacokinetics. This would, to a good extend, depend on individual physiology, as well as, on chemical properties of the formulated drug. ADME analysis- Absorption, Distribution, Metabolism and Excretion, is performed at this stage. Following the administration, absorption of the therapeutic agent into plasma will happen, depending on the molecular weight, and solubility of the drug. Passage of the drug from blood plasma to the interstitial and intracellular fluids is termed as distribution. Permeability of the drug to the body cells would be affected by the blood-brain barrier, blood-testes barrier and blood-placenta barrier. Metabolism of the drug is performed by organs such as liver, kidney or other sites. This may be adversely of beneficially affected by interaction with other drugs. The final process involves removal of metabolites from the body through urine, bile and/or feces, called excretion.

Preclinical Toxicology Testing: The next step in this process involves safety, and efficacy testing and preparing drafts for clinical trials. Reproductive toxicity, Genetic toxicity, carcinogenicity studies, etc. are performed at this stage. Before entering clinical trials, bioanalytical Testing may also be carried out to improve quality and yield and to optimize the entire development process.

Clinical Trials: Clinical trials involve four phases.

Phase I trial is usually conducted healthy volunteers, in order to determine safety and dosing of the investigative drug.

Phase II trials performed in small numbers of patients to ensure safety and efficacy.

Phase III trials tested to determine safety and efficacy in sufficiently large numbers of patients with the targeted disease.

Phase IV trials are post-market trials that are carried out to identify long term effects of the drug.

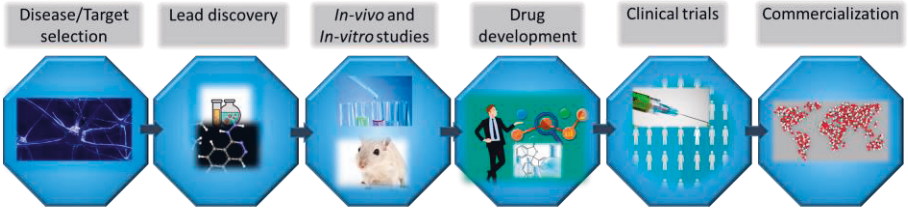

Figure 3. General pipeline involved in drug discovery and development process.

The success rate of a new drug is very low, only 0.001% of the candidate drugs qualify to test on humans. Capital costs for the whole drug development process is quite high and the computational drug discovery has drastically reduced the duration, costs and risks associated with drug discovery process.

3 RATIONALE OF CHOICE OF DRUG CLASSES

GBM is characterized by many aberrant pathways that provide the tumor cells with selective defense features and compensatory mechanisms, which in turn promote survival and proliferation in a hostile environment, as well as therapeutic resistance. For a successful multi-targeted agent, horizontal inhibition of various tumorigenic mechanism with a focus on the key nodes, which is selective to cancer cells, is required. In an attempt to identify a monotherapy for patients with recurrent glioblastoma, that targets multiple pathways involved in GBM ontogenesis, we aimed to elucidate the anti-tumor efficacy and drug mechanism of four novel classes of drugs- derivatives of diols, hydrazones, thioesters and borons. The significance of these drugs with anticipated activity as anti-tumor agents are mentioned below.

3.1 Diols as anticancer agents

A diol is a chemical compound containing two hydroxyl groups (–OH groups)[115] as represented in **Fig: 4**. An aliphatic diol is also called a glycol[116]. The most common industrial diol is ethylene glycol. Several natural and synthetic diol derivatives have been previously studied as small molecules capable of interacting with glioma cells[117–121].

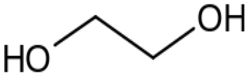

Figure 4. Structure of ethylene glycol- a simple diol

Earlier research has reported on the synthesis and biological screening of several natural or synthetic, aliphatic, aryl and long chain diols and their antitumor activities. A study reports on, 2-[(arylmethyl)amino]-1,3-propanediol derivatives (AMAPs) have shown its potential antitumor agents[122]. Diol derivatives of indenoisoquinoline have been identified as topoisomerase I inhibitors against cancer[123]. The neuro-steroid, 3-β androstene17-α diol (17-α-AED) is proven to possesses significant anti-glioma activity when used at pharmacologically relevant concentrations *in vitro*[124]. Similarly, a reduction of cell clones and inhibition of hepatocellular carcinoma cells were visible upon α-2,7,11-cyprotermine-4,6-diol (α-CBD) treatment in cancer cells [125]. Another pioneer study claims long chain 3-amino-1,2-diols have strong cytotoxicity against various cancer cell lines[126].

Straight chain diols have been previously studied as small molecules capable of interacting with glioma cells. N-alkanols, were reported to inhibit N-methyl-D-aspartate (NMDA) receptors [127–129]. Longer C9–C14 1,Ω-diols also identified as inhibitors of NMDA-activated signaling[129]. NMDA receptor signaling is triggered through Glutamate. Glutamate amino acid is an excitatory neurotransmitter of the central nervous system (CNS) and a principal mediator of neuronal precursor-cell proliferation, synaptic transmission, invasion, survival as well as cell death[130,131]. Extracellular glutamate binds to and activates multiple glutamate receptors namely- N-methyl-D-aspartate receptors (NMDARs), α-amino-3-hydroxy-5-methyl-4-isoazolepropionic acid (AMPA), and Kainate receptors. Glutamate promotes proliferation of neuronal progenitors by NMDA receptor-mediated mechanism[132]. Downstream effect of NMDAR is mainly through the activation of calcium-dependent signal transduction[133]. Upon binding of its cognate ligands, NMDAR permits Ca^{2+} influx that can elicit calmodulin (CaM) and calmodulin-dependent kinase (CaMKs) activation and subsequent protein kinase A (PKA) activity. Dysfunction in the glutamatergic signaling pathway has been well established as a frequent player in glioma pathogenesis and thus acts as a therapeutic target[134–136]. Recent studies have promoted NMDA receptors as potential targets for chemotherapy[137], considering that the blocking of the NMDA receptors can abrogate glioma proliferation[138].

In the light of previous reports on anti-cancer properties of diols and their interaction with NMDAR, we envisioned that, the non-polar derivatives of primary and secondary hydroxyl groups of decane-1,2-diols could be explored for their anti-cancer activity. The Publication I describes the detailed report on the design, synthesis, and the outcomes of bioactivity studies of the novel decane-1,2-diol derivatives.

3.2 Hydrazones as anti-cancer agents

Hydrazones are a class of organic compounds with the structure $R_1R_2C=NNH_2$[115] as shown in **Fig: 5**. They are related to ketones and aldehydes but possess NH_2

functional group instead of oxygen. They are formed usually by the action of hydrazine on ketones or aldehydes[139].

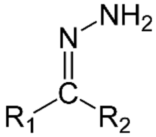

Figure 5. Basic structure of the hydrazone functional group

Hydrazones are attractive scaffolds in pharmacology due to its wide range of biological activities. A number of studies have demonstrated antimicrobial, anticonvulsant, analgesic, anti-inflammatory, anti-platelet, anti-tubercular and anti-tumor activities of hydrazones[140–142]. Natural and synthetic hydrazones are reported to interfere in a wide range of tumorigenic processes[143–145]. Acetylpyridine and benzoylpyridine derived hydrazones has been reported as agents against brain tumor[146].

A growing body of literature has examined the efficacy of hydrazone derivatives as anti-cancer drugs. *N*-phenylpyrazolyl-*N*-glycinyl-hydrazone derivatives were validated as TNF-α and p38 MAPK inhibitors by Lacerda et al[147]. 2-Acetylpyridine hydrazone derivatives of benzothiazole, benzoxazole, and benzimidazole were found to exhibit potent cytotoxic activity against the growth of murine and human leukemia and lymphoma cells[148]. N,N'-Bis[1-aryl-3-pyrrolidine-1-yl)propylidene]hydrazine dihydrochlorides has been indicated as cytotoxic by Kucukoglu et.al and suggests inhibition of mitochondrial respiration as a possible mechanism of action of the drug [149]. In another report, hydrazone compounds derived from salicylaldehyde were proven to be anti-proliferative agent against A549 cells. Potency of these compounds were related with the lipophilicity of the compound , as well as the capacity of compound chelating metal ions[150]. Additionally, there are many under preclinical and clinical trials as anti-cancer agents. N-acylhydrazones has been proven to hold multiple characteristics ensuring a strong motif in drug design and medicinal chemistry. N-acylhydrazone small-molecule pro-caspase activator, PAC-1, is currently in phase-1 clinical trials for Glioblastoma Multiforme (GBM) / Anaplastic Astrocytoma (AA) treatment[151]. PAC1 showed broad synergy with conventional chemotherapeutic agents in procaspase-3 over-expressing cell lines. Aldoxorubicin, a (maleinimidoalkanoyl)hydrazone derivative of doxorubicin is currently in phase III for the treatment of soft tissue sarcoma[152]. INNO-206 (DOXO-EMCH), an Albumin-

Binding Prodrug of Doxorubicin has potent antitumor activities in various cancer cell lines and in murine tumor models. The drug targeting Topoisomerase II is currently under development for Phase II Studies.

Nerve growth factor receptor (NGFR) is a transmembrane receptor of tyrosine kinase family. Neurotrophins mediate cell survival, proliferation, differentiation and cell death of neurons in the central nervous system. NGFRs include TrkA, TrkB, and TrkC and are found to be positively correlated with astrocytic gliomas. Role of NGFs in GBM growth is well established. Hampering NGF/Trk signaling via Trk inhibitors or anti-NGF antibodies are reported to reduce cell proliferation and tumorigenesis suggesting NGFR as a potential target in tumor treatment and prevention[153]. More recently, our group also studied effect of the panel of many hydrazone derivatives and their anti-proliferation effect on multiple human brain astrocytoma cells[154]. Taking into account numerous studies on hydrazone derivatives, as a potential anticancer compound, and tyrosine kinase inhibitors[155,156], we presume that this class of chemicals is of leading interest as active anti-GBM therapeutics. Publication II, appended in this manuscript reports the findings from our evaluation of a novel panel of hydrazone derivatives as anti-cancer agents and their possible mechanism of action.

3.3 Thioesters as anti-cancer agents

Thioesters are compounds with the functional group R–CO–SR'(**Fig: 6**). They are the product of esterification between a carboxylic acid and a thiol.

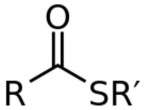

Figure 6. Basic structure of a thioester

Molecular targeted agents against tumors need not directly interfere to produce significant toxicity, instead indirectly disrupt intracellular processes through various critical pathways. They may be represented by receptor tyrosine kinase inhibitors, matrix metalloproteinase inhibitors, farnesyl transferase inhibitors, and angiogenesis inhibitors. Drugs that can act as multi-targeted agents can confront chemoresistance and recurrence exhibited by GBM as opposed to single targeted drugs. Developing multi-targeting drugs that target synergistic inhibition of multiple oncogenic pathways is an attractive strategy to combat GBM pathogenicity. Sorafenib is the first drug discovered and approved as a multikinase inhibitor[157]. Later, several multi-kinase inhibitors have evolved and approved, such as Nintedanib, Regorafenib, Vandetanib etc. Nintedanib is a tyrosine kinases inhibitor indicated for the treatment of idiopathic pulmonary fibrosis (IPF)[158]. Nintedanib inhibits PDGFR α and β, FGFR1-3, VEGFR1-3, and Fms-like tyrosine kinase-3 (FLT3). Regorafenib is indicated for the treatment of patients with metastatic colorectal cancer and inhibits the activity of Rearranged during Transfection (RET), VEGFR1-3, KIT, PDGFR α and β, FGFR1, 2, TIE2, DDR2, TrkA, Eph2A, RAF-1, BRAF, SAPK2, PTK5, and Abl. Vandetanib is a potent and selective inhibitor of VEGFR, EGFR and RET tyrosine kinases[159]. All the above-mentioned drugs are currently under clinical trials for GBM.

Numerous scientific studies indicate the relevance of thioester based derivatives as new antitumor compounds[160–163]. Thioester derivatives of the natural product psammaplin are reported as potent histone deacetylase inhibitors[164]. Histone deacetylases (HDACs) are a group of enzymes that remove acetyl groups from histones as well as non-histone proteins and regulate expression of tumor suppressor genes. Inhibitors of HDACs were found to be effective in cancers characterized by overexpression of HDACs and can revert the malignant phenotype. Hoque et al(2014) described mono and bicyclic tetrapeptides thioester as a potent inhibitor of histone deacetylase thereby acting as a strong anticancer agent[162]. A thioester derivative of leinamycin has been demonstrated a broad antitumor spectrum against human carcinoma xenografts[161]. Another study reports that thioester derivatives containing Arg-Gly-Asp (RGD) motif are proven to inhibit integrins and therefore they are potentially useful anti-angiogenic agents[165]. Gambogenic acid thioesters are evidenced to have anti-proliferative and anti-angiogenic agents [166]. El-Azab et al testified that derivatives of non-steroidal anti-inflammatory drugs S-cyclohexyl-2–(2-fluoro-[1,1′-biphenyl]-4-yl)propanethioate and S-cyclohexyl-2–(1-(4-chlorobenzoyl)-5-methoxy-2-methyl-1H-indol-3-yl)ethanethioate have broad-spectrum antitumor activity against HepG2 and MCF-7 cell lines, while S-phenyl-2–(2-((2,6-dichlorophenyl)amino)phenyl)ethanethioate exhibited broad-spectrum antitumor activity against the MCF-7 and Caco-2 cell lines[160]. Thus, owing to their biological and pharmacological properties, thioesters offer a rare opportunity to explore as a strong chemotherapeutic scaffold against GBM.

Angiogenesis is a significant feature of GBM, attributed to the overexpression of vascular endothelial growth factor (VEGF). Few of the most significant proangiogenic regulators that indirectly regulates VEGF mRNA expression, include growth factors (EGF, transforming growth factor [TGF]-α and β [TGF-β], tumor necrosis factor α [TNF-α], keratinocyte growth factor, insulin-like growth factor I (IGF-I), fibroblast growth factor (FGF), platelet-derived growth factor /(PDGF), and cytokines (interleukin (IL)-1α and IL-6)) and amplifications of *RAS/RAF* genes[167]. VEGF targeted therapies includes VEGF blockade, VEGF Trap, and suppression of VEGFR signaling via receptor tyrosine kinase inhibitors (TKIs)[168,169]. Some tumors become non-responsive during treatment with anti-VEGF agents, under hypoxic conditions when tumor cells upregulate rescue angiogenic molecules such as placental growth factor, FGFs, interleukin-8 etc. Cross-talk between VEGF and TGF-β1 signaling is known to convert p38 MAPK into a pro-apoptotic signal, representing a new target for anti-angiogenesis treatment[170]. Thus, considering the importance of the VEGF in angiogenesis and its close collaboration with other pathways involved in GBM oncogenesis and maintenance, we hypothesize that targeting VEGF, and the pathways involved in modulating it, would render it one of the most promising strategies in GBM therapy.

To be clinically relevant, molecularly targeted agents must be investigated for their effects on the intended targets and pathways. In this aspect, we evaluated a novel panel of thioester derivative as an agent for GBM monotherapy, as well as its specific action on various GBM pathways. Design, details and results of our evaluation are present in Publication III in this manuscript.

3.4 Borons as anti-cancer agents

The wealth of information accumulated during the past few decades on bioorganic and organometallic boron compounds that laid the foundation for the study and application of boron compounds as lipophilic pharmacophores and biologically active molecules. Due to their unique electronic, physicochemical, and biological properties, there is an increasing focus on boron-containing compounds as novel therapeutics. Boron is an electron-deficient non-metallic element, permitting them to form coordinate covalent bonds with nucleophiles. They are present in nature as orthoboric acid, as borates in the minerals, borax and colemanite and chemical properties of borons are more similar to that of carbon.

Boron containing therapeutics continues to increase that show multitude ways of inhibition against various biological targets. Due to its unique bioactivity, various boron based structures have been synthesized for the development of novel therapeutic agents[171–173]. Being electron deficient in nature, Boron-based inhibitors effectively interacts with nucleophilic side-chains such as serine, threonine, lysine and histidine. Considering the availability of residues at the binding site of a protein, design of drugs targeting synergistic binding would be more efficient.

Borons have been demonstrated to possess anti-microbial, anti-inflammatory and anti-tumor properties[174]. The biological activity of boron-containing molecules is mainly due to reversible covalent interactions with nucleophiles such as amino acid side chains in proteins or from sugar residues in nucleic acids. Many boron containing compounds like peptidyl boronic acids, benzoxaboroles, benzoxaborines, benzodiazaborines, amine carboxyboranes, and amine cyanoboranes have interesting and useful biological properties[175]. Alkyl or aryl boron-containing compounds have been demonstrated as serine protease inhibitors [176]. Hypoxia-inducible factor HIF-1α is a major physiological stimulus for expression of angiogenesis factors. A carboranyl boronic acid containing phenoxy acetanilide derivative was verified to be a potent inhibitor of hypoxia-induced HIF-1α by Shimizu et al[177].

Taking into account that the dipeptide boronic acid proteasome inhibitor bortezomib was approved by FDA for treatment of multiple myeloma[178] and mantle cell lymphoma[179], Lei et al. developed a series of dipeptidyl boronic acid inhibitors of 20S proteasome, displaying strong *in vivo* anti-cancer efficacy in human ARH77 xenograft mouse model[180]. Also, the compound was mentioned to inhibit chymotrypsin-like (CT-L) activities and cell cycle progression. Another study reports boronic acid chalcone analogue of combretastatin A-4, as a potent anti-proliferation agent against various human cancer cell lines[181].

Boron-containing anilinoquinazoline derivatives were detected to have strong bioactivity against Glioma cells and possesses the capability to interact intracellularly with EGFR[182]. Also, it was stated in the study that the cell growth was inhibited by these compounds through the arrest of G1 cell cycle, which induced apoptosis. In this context, it is appropriate to evaluate novel boron derivatives as anti-glioblastoma agents and their possible mechanism of action on GBM cells.

4 METHODOLOGY

The purpose of this chapter is to explain the methodologies employed in a detailed biological characterization of the pharmaceutical classes considered in this study. This also includes the details of characterizing the level of transcriptome and the effect of the new compounds on them.

4.1 Cell Culture

Human GBM cell lines, LN229 (Publication I, II, III and IV), U-87 (Publication I, II and IV) and SNB19 (Publication III) cells were used for *in vitro* studies to investigate the anti-tumor properties of novel compounds. Mouse embryonic fibroblast (MEF) cells were used as a control in Publication III.

J. Ponten and associates derived the U-87 MG cell line from glioma of a male patient in 1966. Since then it is one of the most regularly used cell line in neuro-oncology studies[183]. U-87 MG cell line is heterogenic in nature and possess many mutations such as deletion of p14ARF and p16. U-87 MG cells synthesize mutant form of tumor suppressor PTEN protein which in turn activates PI3K/Akt, that plays a key role in proliferation, angiogenesis and resistance to the apoptosis [184]. Also U-87 cell line expresses a wild-type p53, tumor suppressor protein[185]. The LN229 cell line was established in 1979 from right frontal parieto-occipital glioblastoma of a 60 years old female. The LN229 cells exhibits mutation at *p53* (TP53) and possible homozygous deletions in the *p16* and *p14ARF* tumor suppressor genes with the wild-type PTEN gene[24]. This cell line is an excellent choice for studies on apoptosis. The SNB19 cell line was established from the surgical resection of a left parieto-occipital glioblastoma from a 47-year-old man in 1980. This cell line exhibits biological characteristics that reflects the intrinsic properties associated with a GBM such as rapid proliferation capability to produce a potent angiogenic growth factor (basic fibroblast growth factor, bFGF), with high level of protease activity[186].The non-cancerous cells, MEFs, have an E10.5 genotype with Vin+/+

(Vinculin), was originally obtained from Wolfgang H. Ziegler (Hannover Medical School, Hannover, Germany).

U-87 cells were grown in Minimum Essential Medium (MEM, Product# 51416C, Sigma-Aldrich, St. Louis, MO) with 10% FBS 2mM sodium pyruvate (Product# S8636, Sigma-Aldrich, St. Louis, MO), 1% Penicillin-Streptomycin and 0.025mg/ml Amphotericin B. The human glioblastoma cell lines SNB19 and LN229 (ATCC® CRL-2611™/CRL-2611™) and mouse embryonal fibroblast (MEF, normal brain cells) were cultured in Dulbecco's Modified Eagle Medium - high glucose (DMEM, Catalog# L0102, Biowest) containing 5% FBS (Product # F1051, Sigma-Aldrich, St. Louis, MO), 1% Penicillin-Streptomycin (Product # P4333, Sigma-Aldrich, St. Louis, MO) and 0.025mg/ml Amphotericin B (Sigma-Aldrich, St. Louis, MO). Cells were maintained at 37°C in a humidified incubator supplemented with 5% CO_2. Biological and technical repeats were used for each condition throughout the experimentation.

4.2 Trypan blue exclusion assay

Trypan blue (Chemical formula-$C_{34}H_{24}N_6Na_4O_{14}S_4$) is a tetrasodium salt routinely used for *in vitro* toxicology studies as a method for cell viability measurement. Trypan blue is a cell death indicator stain as it can only stains cells with a compromised cell membrane. Live cell with intact cell is non permeable to the dye. Under light microscopy, the viable cells are visualized as a small, rounded, and refractive cell whereas dead cells are seen as swollen, large, and dark blue in color(**Fig. 7**).

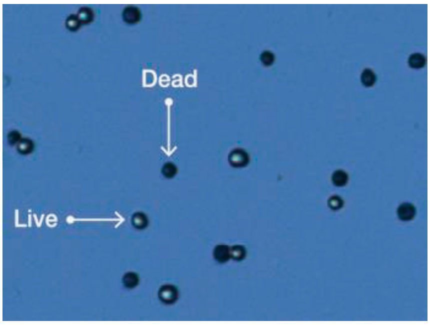

Figure 7. Appearance of cells stained by Trypan blue stain, under an automated cell counter. Live cells appear as to have bright centers and dark edges whereas dead cells are uniformly dark blue in appearance. (*Image modified from http://www.montreal-biotech.com/Brochures/EVE_User_manual_V08.pdf*)

A two-stage cytotoxicity assay was performed to determine the cell growth inhibitory effect of the compounds following the treatment for 48hrs on the GBM cell lines. Initially a high concentration (100 µM), of the compounds were analyzed, from which the top compound was selected and then IC_{50} was identified on treating with different concentrations (100 µM, 75 µM, 50 µM, 25 µM, and 10 µM) of the compounds. Treated cells were harvested by centrifugation at 1200 rpm for 10 min. Cell viability was determined using trypan blue dye (Catalog# 15250061, Thermo Fisher Scientific, USA) staining, by incubating 50 µl cell suspension with 10 µl trypan blue solution, for 1 min, at room temperature. After incubation, viable and dead cells were quantified using a Countess II Automated Cell Counter (Catalog # AMQAX1000, Thermo Fisher Scientific, USA).

Percentage of inhibition of cell proliferation was calculated using the following formula:

$$Proliferation\ inhibition\ (\%) = \frac{Mean\ No.of\ untreated\ cells\ (DMSO\ control) - Mean\ No.\ of\ treated\ cells\ \times 100}{Mean\ No.\ of\ untreated\ cells\ (DMSO\ control)} \qquad (1)$$

The proliferation inhibition percentage of each sample was determined using the above formula to determine the dose-response curve. From the dose-response curve, IC_{50} value of each compound was calculated.

4.3 Detection of apoptotic activity by Fluorescein dual staining with Annexin V FITC/Propidium iodide (PI)

Apoptosis is a physiological process involving highly specific and orderly set of biochemical changes and characteristic morphological changes leading to cell death and disposal. This includes morphological changes such as condensation of the cell cytoplasm and nucleus, DNA fragmentation, dissociation of cell organelles, and disruption of the cell plasma membrane. One of the biochemical changes in apoptosis is the translocation of phosphatidylserine to the outer side of the cell plasma membrane. Apoptosis can be prompted by stimuli from the extracellular medium (extrinsic pathway) or within the cell (intrinsic pathways). Apoptosis, in most cases involves the activation of cysteinyl aspartate-specific proteases (caspases). Apoptotic extrinsic pathway is activated by the tumor necrosis factor (TNF), which stimulates the death-inducing signaling complex. The intrinsic pathway is activated during cell stress, which cause the release of cytochrome c and other proteins from the mitochondria, eventually causing cytotoxic death. In order to evaluate the extend of cell death by apoptosis, fluorescein co-staining with dyes such as propidium iodide (a late stage cell apoptosis marker) and annexin V (an early commitment to apoptosis cell marker) was performed.

Annexin-V is a protein dye that has a strong affinity for phosphatidyl serine (PS) molecules, in the presence of Ca^{2+}. The dye serves as a marker of apoptosis by attaching to PS molecules, that have been redistributed to the outer layer of the cell membrane during the onset of apoptosis[187]. In healthy cells, PS molecules will be embedded in the inner layer of the cell membrane. Once attached to PS in the outer layer of the cell membrane, dying cells stain positive with Annexin-V and appear green and can be detected using a fluorescence microscope. The dye can be excited at 590 nm and it has a broad fluorescence emission with a peak at 617 nm that can be collected with a 650 nm or long-pass filter.

Propidium iodide (PI) (Chemical formula-$C_{27}H_{34}I_2N_4$) is a fluorescent dye with the ability to penetrate the cells with damaged cell membrane and bind to nuclear DNA by interlacing between the bases of the DNA. Apoptosis or programmed cell death starts with nuclear fragmentation, membrane damage and subsequent cytoskeletal collapse [188]. At this late stage, the cells become permeable to Propidium iodide (PI), which binds with the degenerated DNA in the nucleus and fluoresces red when detected by fluorescence microscope[189] (**Fig: 8**). The fluorescence excitation maximum of PI is 535 nm and has a wide-range fluorescence emission with a peak at 620 nm that can be collected with a 650 nm or long-pass filter.

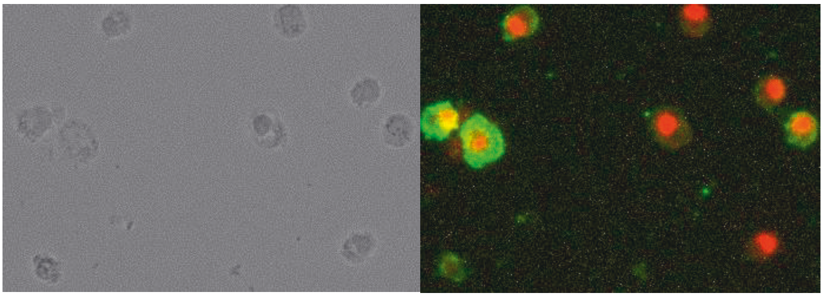

Figure 8. Microscopic images of Apoptotic activity. Apoptotic cells exhibit morphological changes such as disruption of cell membrane under a phase contrast image. Under a fluorescent microscope, annexin V-FITC bound cells will display green staining. The cells that have lost membrane integrity, will show a red (PI) stained nucleus, and a halo of green (FITC) stained plasma membrane.

In the experiments described in this report, apoptosis detection was carried out using the fluorescein dual staining with Annexin V/Propidium iodide. The cell lines were grown as described previously, followed by cells treatment with IC_{50} concentration of the selected drugs- **DBT/R234/JRB115/5a,** and incubated for 48 hrs. Untreated cells were considered as negative control and the standard drug (Cisplatin/Temozolomide) was considered as positive control for the study. Apoptosis/necrosis detection was carried out using Annexin V FITC and PI (Catalog# V13242, Thermo Fisher Scientific, USA). The apoptosis determination was performed following the standard protocol suggested by the manufacturer.

4.4 Caspase Activation test

Dysfunction of apoptotic machinery contributes to numerous diseases, including cancers. For their unchecked growth, tumor cells hijack normal cellular growth pathways and circumvent apoptosis machinery. Activation of caspases is a critical component of apoptosis. Alternative modes of cell death, e.g., necrosis may also mediate the cell death. The intrinsic pathway of apoptosis activated by various stimuli, can lead to the down-regulation of anti-apoptotic BCL-2 family members, permitting pro-apoptotic factors to perturb the mitochondria stability. The release of cytochrome c from mitochondria into the cytosol triggers caspase-9 activation, through the formation of the cytochrome c/Apaf-1/caspase-9-containing apoptosome complex, cleaving downstream targets, such as executioner caspase-3 and -7(**Fig:9**). The essential purpose of this test is, to understand whether the apoptotic activity resulting from the drug treatment, is promoted by caspase-3 and caspase-7 activity.

The *in vitro* caspase-3 and caspase-7 activity was determined using Caspase-Glo® 3/7 Assay Systems (Catalog# G8091, Promega Corporation, USA). The reagent was prepared as mentioned in the manufacturer’s protocol. Detailed report on the procedure is mentioned in individual publications. The study used quantitative analysis of the luminescence signal using Chameleon V Multi-label Detection Platform (Hidex oy, Finland) to reveal the effect of treatment. Magnitude of fold change in luminescence between treated and untreated cells were determined using the following formula:

$$Fold\ increase = \frac{F_{test} - F_{blank}}{F_{control} - F_{blank}} \qquad (2)$$

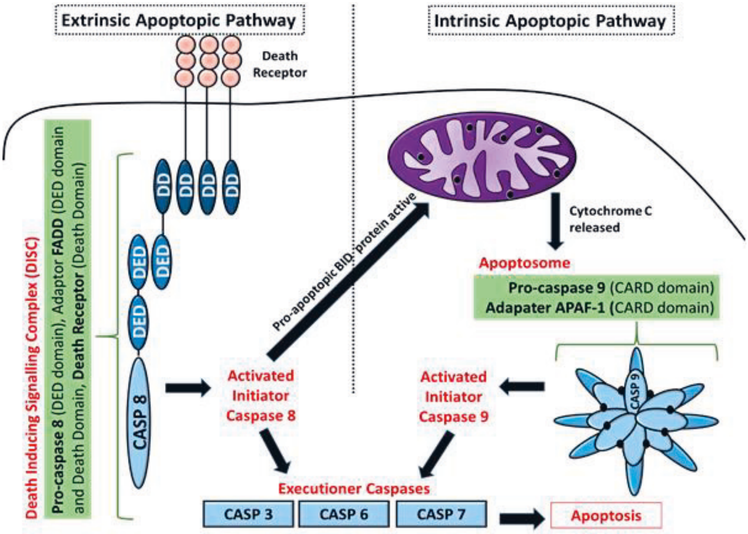
Extrinsic Apoptopic Pathway
Intrinsic Apoptopic Pathway
Death Receptor
Death Inducing Signalling Complex (DISC)
Pro-caspase 8 (DED domain), Adaptor FADD (DED domain and Death Domain, Death Receptor (Death Domain)
DD
DD
DD
DD
DED
DED
DED
CASP 8
Pro-apoptopic BID protein active
Cytochrome C released
Apoptosome
Pro-caspase 9 (CARD domain)
Adapater APAF-1 (CARD domain)
CASP 9
Activated Initiator Caspase 8
Activated Initiator Caspase 9
Executioner Caspases
CASP 3
CASP 6
CASP 7
Apoptosis

Figure 9. Schematic representation of Apoptotic signaling via Caspase activation. (Image Credits Gupta/ CC by 4.0)

4.5 Intracellular Redox potential test using 2',7’-dichlorodihydrofluorescein diacetate (H2DCFDA)

Reactive oxygen species (ROS) play a critical role in cellular physiopathology and are implicated in a variety of cellular processes such as cell proliferation, signal transduction, and oxidative stress triggered defense mechanisms. For the current study, oxidative flux imposed by the chosen drug was analyzed using Fluorescent H2DCFDA assay (Catalog # D399, Invitrogen, USA) using H_2O_2 as a positive control. The 2',7’-dichlorodihydrofluorescein diacetate (H2DCFDA) is a fluorogenic dye that is an indicator of reactive oxygen species (ROS) activity such as of hydroxyl and peroxyl residues within a cell. Cellular esterase enzymes can deacetylase DCFDA / H2DCFDA to a non-fluorescent compound once it is inside the cell, which is later oxidized by ROS into 2’,7’–dichlorofluorescein (DCF). DCF is a compound with strong fluorescence property, which can be detected using a fluorescence spectroscope on excitation / emission at 495 nm/ 529 nm. An increased fluorescence level is an indication of an increased amount of ROS[190]. We used Chameleon Multi-label Detection Platform (Hidex oy, Finland) to reveal the effect of treatment. Further details of the protocols are described in corresponding publications.

4.6 Cell imaging using fluorescence microscopy

General microscopy or phase-contrast microscopy has the limitations to identify and observe individual proteins. Fluorescent microscopes have features that uses a higher intensity light source which excites a fluorescent species in a sample of interest. In order to obtain a better understanding of the 3D nature of the samples and to identify individual molecular species, imaging in this thesis used fluorescence microscopy after treating the cells with fluorophores. All cell imaging for apoptotic and cell cycle studies, were performed using EVOS automated fluorescence microscope.

4.7 Transcriptome characterization using RNA-Seq data analysis

The use of *in vitro* assays to assess chemical safety, as alternatives to animal testing, has become an important undertaking in cytotoxicity research. Whole transcriptome analysis is an attractive option to obtain a deeper insight of identify candidate genes accounting for complex changes associated with a drug treatment. Transcriptome provides a real-time information about the full RNA content transcribed from the genome in a specific tissue or cell type, at a particular developmental stage, and under a certain physiological or pathological condition, or under a particular treatment condition. This section is focused in the use of transcriptional profiling in *in vitro* systems to determine the potential cytotoxic and genotoxic activity of chemicals of interest, as part of the assessment of toxic properties of the drugs mentioned in this study.

Target-based drug discovery relies heavily on modifying gene expression or enzymatic activity in response to small-molecule treatment. RNA sequencing is a next-generation sequencing (NGS) technique that is rapidly replacing traditional gene expression microarrays in many studies. RNA-seq technology has many advantages over other HTS methods. RNA-seq[191] allows to quantify, discover and profile RNAs- both coding and non-coding RNA, at splicing and allele-specific expression. Also, RNA-seq is useful in predicting with single base level precision, the SNP variations, RNA editing, splice sites, splice junctions, allele-specific expression, novel transcribing regions and differential gene expression analysis[192]. It has higher sensitivity for even low-level transcribing genes and has a wider range of expression level. Less variation, no bias, and more consistency are also other advantages. Furthermore, RNA-seq can be applied to species with previously unknown genome data.

The fluctuation in transcript levels in response to an environmental or experimental trigger, often indicates change in a function or protein activity. Transcript concentration is often assumed to reflect the expression levels of protein. However, exceptions can exist, due to various factors that affect the translation process, such as translational efficiency, temporal delay in translation, half-life of the synthesized protein, protein transport etc[193]. Transcriptome profiling using High-throughput Sequencing (HTS) technologies such as RNA-seq is widely being applied in molecular and clinical research to understand the effects of new drug treatments.

General workflow of RNA-seq experiment:

The preliminary step in RNA-seq analysis involves reverse transcription of RNA molecules to cDNA, followed by the construction of a sequencing library and deep sequencing using latest platforms like 'Illumina'. Deep sequencing produces raw data, which has to be further processed to produce a meaningful interpretation such as differential expression of genes. The reads produced from a sequencing experiment is then aligned to a genome or transcriptome. If a reference genome is absent for the organism*, de novo* assembly is used. Reads once aligned, are quantified to generate a read count in order to analyze the gene expression level.

An overview of RNA-seq experiment and data analysis is as follows:

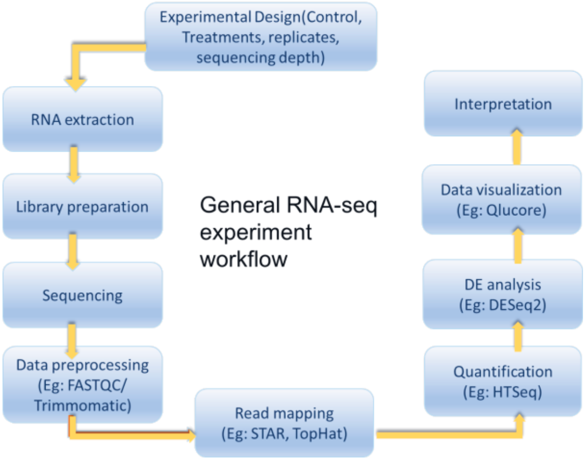
Experimental Design(Control, Treatments, replicates, sequencing depth)
RNA extraction
Library preparation
Sequencing
Data preprocessing (Eg: FASTQC/ Trimmomatic)
Read mapping (Eg: STAR, TopHat)
Quantification (Eg: HTSeq)
DE analysis (Eg: DESeq2)
Data visualization (Eg: Qlucore)
Interpretation
General RNA-seq experiment workflow

Quality Control (Pre-processing):

Data preprocessing starts with trimming of any adapter sequences, primer sequences if any, removal of low-quality reads, external reads and uncalled bases. Most common tools used for quality control are FastQC, Trimmomatic etc.

Read Alignment:

Read alignment or read mapping could be done either with the help of a reference genome or *de novo.* In the former method, the reads are mapped onto a reference genome, to infer the transcripts produced by each gene. In the later scheme, reads are assembled based on overlapping ends to create a long contig, onto which the reads are mapped back for quantification. The most popular mapper is ‘TopHat’ which uses the ‘Bowtie’ algorithm for unmapped reads and then unmapped reads are aligned to detect exon junctions. Read alignment produces BAM files which can be used for generating count matrices. Spliced Transcripts Alignment to a Reference (STAR) is an RNA-Seq read mapper which has high sensitivity and precision. Efficiency of STAR is due to a dual step process- an initial ‘seed’ searching and, a subsequent step that does clustering, stitching and scoring. STAR can detect splice reads and fusion transcripts[194].

Quantification:

Quantification step involves counting the number of reads aligned to each gene location. Transcript annotation for read mapping can be done with the help of the human gene annotation file (GTF) from Ensembl. Tools such as HTSeq-count generates raw read counts, which are to be normalized to reduce bias due to transcript length, sequencing depth and RNA composition. Any technical bias, reflected in the difference in aligned read count, can be reduced by normalization. The basic strategy is to identify a baseline and represent the read count relative to the baseline. Normalization methods such as RPKM (reads per kilobase of exon model per million reads) and its derivative FPKM (fragments per kilobase of exon model per million reads mapped), TPM (transcripts per kilobase million), and median of ratios etc., are effective in reducing biases. DESeq2 is preferred over others, for differential expression analysis, so that it can take into account depth and RNA composition. DESeq2 uses the median of ratios method which assumes that not ALL genes are differentially expressed. A normalized count is then generated by dividing each raw count value in a given sample by that sample's normalization factor.

Differential Expression Analysis (DE analysis):

DE analysis verifies, whether an observed difference in read counts is significant, or by chance. Various tools are used for DE analysis, such as Cuffdiff, edgeR, limma-voom, DESeq, and baySeq. The edgeR and DESeq are based on negative binomial (NB) distributions, whereas baySeq uses Bayesian approaches based on a negative binomial model[195]. DE analysis tools usually give a log2FoldChange value which gives a measure of magnitude of altered gene expression due to a particular treatment, when compared to control. The value is reported in a logarithmic scale to the base 2.

The studies mentioned in this thesis uses DESeq2 for DE analysis. In differential expression analysis, the hypothesis testing often achieved using 'p-value'. P-value can be defined as the lowest chosen 'α' of the test at which null hypothesis is rejected.

Null hypothesis or H_0 assumes that:

the gene g is not differentially expressed between the conditions.

Smaller the ‘p-value’, more likely that the null hypothesis is rejected. An ‘α’ of 0.05 denotes that the likelihood of observation if the null hypothesis is true, 5%.

DEseq2 generates an ‘adjusted p-value’ which is derived from False Discovery Rate (FDR) among the genes under a particular p-value cutoff. FDR identifies the proportion of false positives among all the genes identified as differentially expressed. DESeq2 determines the adjusted p-value using an algorithm called ‘Benjamini-Hochberg adjustment for multiple testing’.

There are several methods for visualizing and interpreting gene expression data such as a heatmap or clustering. Hierarchical method, K-means clustering, Model-based methods such as Self-organizing maps (SOMs) are few clustering methods widely used to infer hidden patterns in gene expression data.

Plotting the DE analysis data:

Once the DE analysis is performed the resulting data can be plotted to represent an overview of the experimental results using tools such as MA plot. MA plot denotes each gene as a dot in the graph where *x-axis* is the mean expression over all samples and *y-axis* is the log2 fold change of normalized counts between a treatment and a control. Other options for viewing the data are volcano plots, dispersion plots and histogram of the p-value.

Sample MA plot:

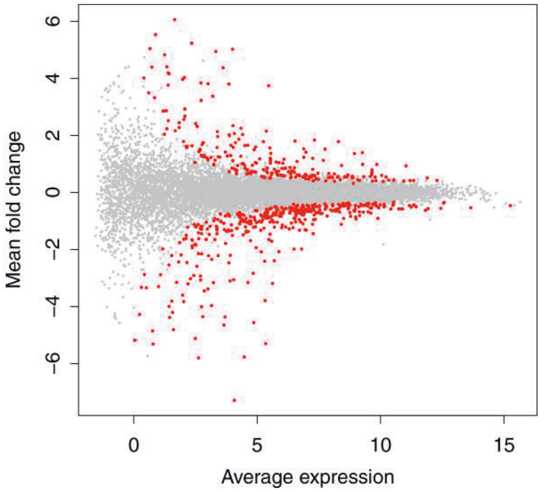

For a specific gene, a $\log_2$(fold change) of −1, for condition treated vs control, represents that the treatment resulted in a change in the observed expression level of $2^{-1} = 0.5$ when compared to the control condition. Likewise, a $\log_2$(fold change) of 1 represents the treatment altered for an observed expression level of $2^1 = 2$, compared to the control condition.

Experimental design for isolation of RNA for transcriptome analysis is mentioned in the original publications appended with the thesis. All trials were conducted in triplicates and RNA from all samples in profiling was isolated using GeneJET RNA purification kit (Catalog no. #K0731, Thermo Fisher Scientific, USA), according to the manufacturer's instructions. The yield was then measured spectrophotometrically using NanoDrop-1000 (Thermo Fisher Scientific, USA). RNA of >9.25ng/µL was considered for quality assessment by TapeStation and expression assay by Illumina Next Seq High Output profiling followed by analysis and validation studies. Sequence analysis was performed by starting with the conversion of sequence reads from ‘bcl’ format to ‘FASTQ’. For read mapping STAR [194] (version 2.6) was used. For assembly, SAM tools [196] (version 1.2) and the “union” mode of HTSeq [197] (version 0.9.1) was chosen, as the gene-level read counts could provide more flexibility in the differential expression analysis. Both STAR and HTSeq analyses were conducted using the high-performance research computing resources provided by TUT TCSC Merope computing cluster (http://merope.cc.tut.fi/) in the Linux operating system (version 2.6.32). Differential expression (DE) and statistical analysis was performed using DESeq2 [198] (release 3.3) in R (version 3.2.4). P-values were adjusted for multiple testing using the Benjamini-Hochberg procedure [199]. A false discovery rate adjusted p-value (i.e., q-value) < 0.05 was set for the selection of DE genes. Gene ontology [200] and ClusterProfiler package [201] was used for pathway analyses.

4.8 Molecular docking

Molecular docking permits the simulation of binding and interaction between two molecules. This permits the evaluation of the druggability and specificity of novel ligands with their target proteins. In addition, docking studies help understanding mechanism of action of various enzymes, accelerate virtual screening to identify lead compounds, identify target proteins. Docking programs, in general, attempt to converge to a minimal energy conformation of the ligand receptor complex, with the help of various search algorithms. This is achieved by taking into consideration the geometric fit, and various interaction energies such as van der Waals, electrostatic, coulombic, and hydrogen bonding between the interacting molecules. A sample image of a ligand-protein docking is given in **Fig:10**. Docking tools may use flexible or rigid docking depending on their algorithms. Rigid docking allows less degrees of freedom as it does not tolerate changes in internal geometry. On the other hand, flexible docking permits changes in the geometry of interacting partners to produce a better fit and interaction. There are a number of docking tools developed in the past few decades, of which few most widely used ones Autodock, GOLD, PatchDock, and GLIDE.

Search Algorithms:

As a primary step in molecular docking, search algorithms predict all possible conformations or orientations of complex formation between two molecules. The search space expands exponentially with the flexibilities of ligand and receptor and the size of the molecule. Search algorithms usually used are Simulated Annealing, Bayesian Geometric Hashing, Pose-Clustering matching and Incremental construction algorithms.

Scoring functions:

Scoring functions are computational methods that predict the accuracy or strength of a Docking simulation. Scoring functions assess the rank of a bound conformation of a protein-ligand structure, based on its binding affinity estimation. The basic types of scoring functions used are force-field, empirical, knowledge-based and descriptor based. Scoring function takes into consideration the sum of intermolecular and intramolecular contributions and tries to minimize the value using an optimization algorithm. The free energy of binding is them assessed from the intermolecular part of the lowest-scoring conformation.

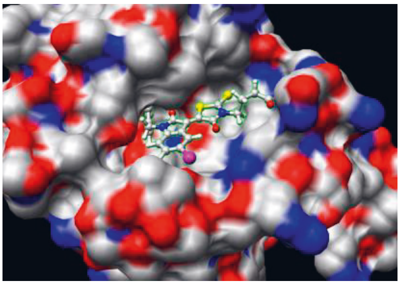

Figure 10. A sample molecular docking simulation of a ligand-receptor binding.

PatchDock program performs structural interaction predictions, depending on the shape complementarity of the molecules of interest. Patchdock first identifies various local patches from its surface representation, generates their corresponding transformations, and creates a scoring function. Calculation of this geometric score is based on the available contact surface area and atomic desolvation energy of the molecules involved in interaction. The tool considers all possible orientations and complementarity and ranks each complex to evaluate the best score. It matches local features of the docked molecules to account for complementary characteristics. PatchDock doesn't permit sidechain flexibility in the docking poses. The program take input as '.pdb' file format.

GLIDE offers a high precision prediction of protein - ligand interactions and flexible docking across a variety of receptor types. Glide uses an E-model scoring function to select between protein-ligand complexes of a given ligand and then rank-order the bound conformations using a GlideScore function. The former is mainly defined by the protein-ligand coulomb-van der Waals energy, whereas GlideScore calculates an empirical scoring function comprised of various interaction properties such as lipophilicity, hydrogen bonding, a rotatable bond penalty, and also coulomb-vdW energies.

4.9 Statistical Analysis

A proper experimental design requires to take in account the possible variations and uncertainities in the experiments. This requires that the experiments need to be replicated and readings should be repeated to produce a reliable and valid account of the variations in the study.

All samples are collected with proper randomization to reduce any bias. To avoid biological variations, all experiments described in the present study were performed with three biological repeats, so that the observations and inferences could be generalized. Every measurement has been taken in two technical repeats to reduce technical variabilities and handling error. The data were presented as the mean ± standard error of the mean. Statistical analysis between the two groups was performed by Student's t-test. Differences among multiple groups were tested by one-way analysis of variance followed by Dunnett's multiple comparison test (GraphPad Prism 7.04). $P<0.05$ was considered to indicate a statistically significant difference.

5 SUMMARY OF THE RESULTS

Aggressive metastasis and recurrence of Glioblastoma challenges all latest modes of therapy against this deadly cancer, calling for a shift in the design of anti-GBM therapeutic approaches. Use of selective single-targeted drugs is often defied by the development of resistance by cancer cells, hence the use of multi-targeted drugs is important to explore. A horizontal inhibition approach, using a multi-target ligand that interacts with different nodes of tumor cross-talk, will definitely improve the clinical benefits of GBM therapy by limiting the ability of cancer cells to develop escape mechanisms and resistance. Such a chemotherapy agent will possess several advantages, including a reduced risk of drug-drug interaction, an enhanced bioavailability, less vulnerable to resistance mechanisms and a better pharmacokinetic profile. Our hunt for a novel multi-targeted agent, evaluating four scantily explored chemical families, has funneled optimistic indications of a strong chemotherapeutic scaffold against GBM. This chapter summarizes the major observations from individual studies that led to each of the publications.

The first set of analysis examined the impact of diol derivatives on GBM tumor. An in-depth investigation report, on the bioactivity and molecular mechanism of action of an assortment of novel decane-1,2-diol derivatives in multiple glioma cell lines, is represented in **Publication I**. A panel of 12 decane-1,2-diol derivatives were synthesized (Table: 1) and evaluated in detail for their bioactivity. We observed that modification of the secondary hydroxyl group of the basic frame of decane-1,2-diol thoroughly affects its cytotoxicity. The top drug was recognized as decane-1,2-diyl bis-(p-toluenesulfonate) (**6, DBT**).

The diol drug **DBT** was identified to have IC_{50} value of 52 µM in U-87 cell line and 270 µM in LN229 cell line. As efficacy of the drug was higher than the standard drug in U-87 cell line but significantly less effective in LN229, hence further evaluations were carried out in U-87 cell line. **DBT** has shown high cytotoxic activity, increased sensitivity to apoptotic pathways, and induced high oxidation in GBM and has prevented migratory activity effectively up to 6hrs post treatment at IC_{50} concentration.

Table 1. Panel of diol derivatives considered for the study

CODE	Structure/Molar mass/Formula	CODE	Structure/Molar mass/Formula
APa13b	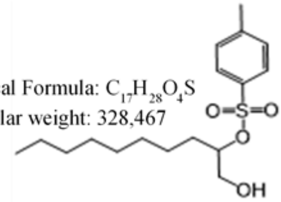 Chemical Formula: $C_{17}H_{28}O_4S$ Molecular weight: 328,467	BAB136A	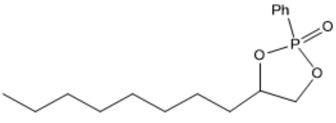 Chemical Formula: $C_{16}H_{25}O_3P$ Molecular Weight: 296,35
APa21b **(DBT)**	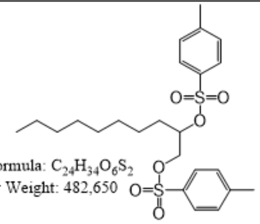 Chemical Formula: $C_{24}H_{34}O_6S_2$ Molecular Weight: 482,650	BAB136B	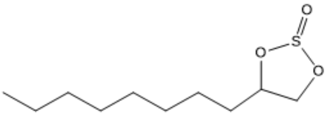 Chemical Formula: $C_{10}H_{20}O_3S$ Molecular Weight: 220,33
APa26	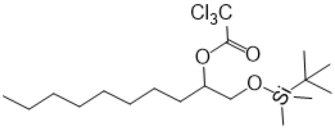 Chemical Formula: $C_{18}H_{35}Cl_3O_3Si$ Molecular Weight: 433,910	BAB136C	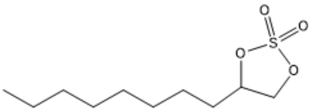 Chemical Formula: $C_{10}H_{20}O_4S$ Molecular Weight: 236,33
APa39a	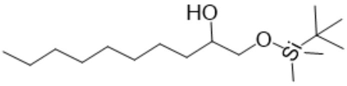 Chemical Formula: $C_{16}H_{36}O_2Si$ Molecular Weight: 288,547	BAB136D	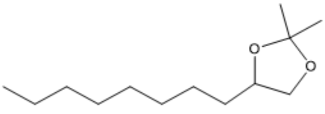 Chemical Formula: $C_{13}H_{26}O_2$ Molecular Weight: 214,35
APa21a	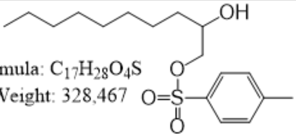 Chemical Formula: $C_{17}H_{28}O_4S$ Molecular Weight: 328,467	BAB136E	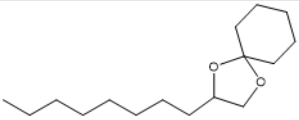 Chemical Formula: $C_{16}H_{30}O_2$ Molecular Weight: 254,41
pTsOH	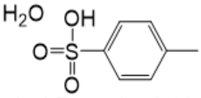 Chemical Formula: $C_7H_{10}O_4S$ Exact Mass: 190,030	BAB136F	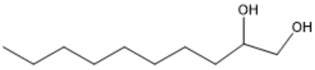 Chemical Formula: $C_{10}H_{22}O_2$ Molecular Weight: 174,28

Cancer cells, in general, demonstrate an elevated ROS sensitivity, therefore, the induction of oxidative stress appears to be a promising approach for the preferential killing of cancer cells. **DBT** induced oxidative stress in the GBM cells by

7.8-fold compared to untreated cells. Transcriptome profiling identified strong suppression of genes involved in migration and proliferation. It was also detected that the apoptotic activity of **DBT** was independent of caspase activation. Both *CASP3* and *CASP7* was found to be downregulated, concurring with the experimental results. Additionally, **DBT** has demonstrated its genotoxic activity by interfering with cell cycle genes. Expression of genes involved in the replication process, as well as angiogenic factors such as CREBBP, PTGS2, JAK, STAT and FOS were diminished upon the drug treatment.

Numerous studies have evidenced secretion of high levels of glutamate by gliomas[202,203], and that, NMDARs mediate glutamatergic signaling via the ERK1/2 and CREB pathways. Our docking studies indicated that DBT has a solid interaction with NMDA receptors, thereby diminishing proliferation and progression of cancer. As expected, the gene expression analysis identified 16 DEGS associated with neurotransmitter signaling. These results support the idea that, diol derivatives can be a targeted inhibitor of Glutamate signaling in GBM. A cumulative response of GBM cells to DBT is illustrated in the **Fig:11**. A progression of this work could be examining the effect of **DBT** on downstream effectors of NMDARs, and how their activity modulates GBM physiology and its cellular mechanics, in order to derive clinical benefits of long chain diols. Taking into account the collective effects of DBT, the study thus highlights the opportunity to consider the novel Diol drug to be advanced as a strong anti-cancer agent, against GBM.

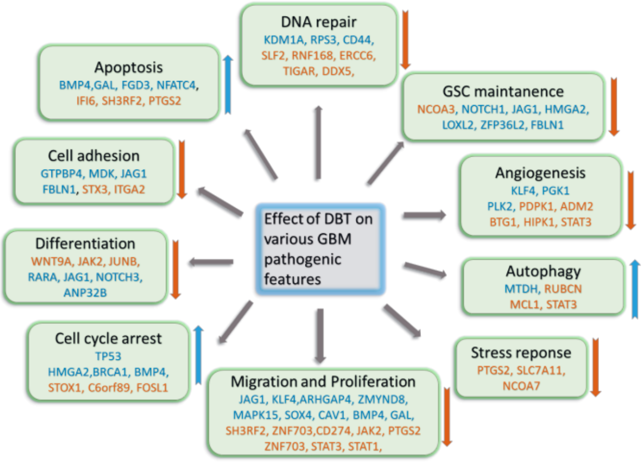
DNA repair
KDM1A, RPS3, CD44,
SLF2, RNF168, ERCC6,
TIGAR, DDX5,
Apoptosis
BMP4,GAL, FGD3, NFATC4,
IFI6, SH3RF2, PTGS2
GSC maintanence
NCOA3, NOTCH1, JAG1, HMGA2,
LOXL2, ZFP36L2, FBLN1
Cell adhesion
GTPBP4, MDK, JAG1
FBLN1, STX3, ITGA2
Angiogenesis
KLF4, PGK1
PLK2, PDPK1, ADM2
BTG1, HIPK1, STAT3
Effect of DBT on various GBM pathogenic features
Differentiation
WNT9A, JAK2, JUNB,
RARA, JAG1, NOTCH3,
ANP32B
Autophagy
MTDH, RUBCN
MCL1, STAT3
Cell cycle arrest
TP53
HMGA2,BRCA1, BMP4,
STOX1, C6orf89, FOSL1
Stress reponse
PTGS2, SLC7A11,
NCOA7
Migration and Proliferation
JAG1, KLF4,ARHGAP4, ZMYND8,
MAPK15, SOX4, CAV1, BMP4, GAL,
SH3RF2, ZNF703,CD274, JAK2, PTGS2
ZNF703, STAT3, STAT1,

.

Figure 11. Novel diol drug **DBT** exhibits strong anti- GBM activity. Top DEGs associated with each process is also mentioned. Blue font color indicates upregulated genes and red color indicates downregulation

The next class under evaluation was the hydrazone derivatives. The hydrazone moiety has been a key pharmacophore for various bioactive molecules. Our study has broadened the knowledge on this previously overlooked class of compounds as an anti-GBM agents. **Publication II** reports the details on the synthesis of 23 novel arylhydrazones of active methylene compounds (AHAMCs) compounds and their anti-proliferative activity against GBM cell lines, LN229 and U-87. It was identified that maximum cell lethality was induced by a hydrazone derivative **R234** (**Table 2**). The dose response analysis identified that **R234** effectively reduces cell viability and proliferation of GBM cells, with IC_{50} values of 107 µM in U-87 and 87 µM in LN229 cells. Dual staining test identified that **R234** hindered cell cycle by inducing G1/S arrest in both cell lines.

The experiment then proceeded to the detailed molecular profiling of drug activity in U-87 cells, using RNA-seq studies. It is critical to note that the maximum number of DEGS were associated with G1-S phase transition, with down regulation of multiple ORCs and MCMs, indicating blockade of DNA elongation. Importantly, **R234** was effective in activating P53, and subsequent downregulation of cyclins, cyclin-dependent kinases and other key molecules involved in cell cycle such as CCNE, E2F, CCND and CDK6. These results thus offer a compelling evidence for **R234** as genotoxic agent, causing cell cycle arrest at the G1/S phase leading to apoptosis, which prophesies its therapeutic aspect in cancer chemotherapy.

Moreover, **R234** enhanced pro-apoptotic genes such as *NOXA, PUMA, BIM*, and lowered Inhibitors of apoptosis proteins (IAPs), and heat shock proteins HSPs, which prohibits cell survival, suggesting the positive role **R234** in cancer cell apoptosis and chemosensitizing. Our experiments identified that **R234** provoke strong oxidative stress in U-87 cells and moderately oxidative in LN229. Induction of apoptosis was independent of caspase activation in both U-87 and LN229 cells. Altogether, **R234** disrupt various functions and pathways of GBM (**Fig: 12**). Genes identified as downregulated due to **R234** were enriched in KEGG pathways including Endocytosis, Cell cycle, Focal adhesion, p53 signaling pathway, Neurotrophin signaling pathway and cell cycle, whereas upregulated genes were associated with the pathways of Apoptosis, MAPK signaling pathway, Lysosome, Sphingolipid signaling pathway and Proteoglycans in cancer.

Table 2. Chemical structure of hydrazone compounds, considered for the study

Code	Compound structure	Code	Compound structure	Code	Compound structure
R2	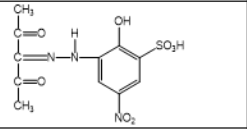	R8	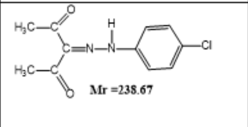	R10	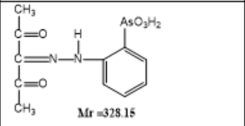
FeR2	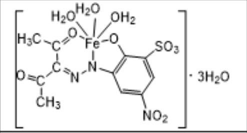	R9	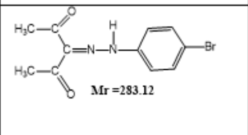	R235	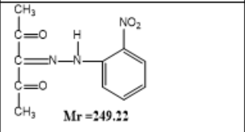
R212	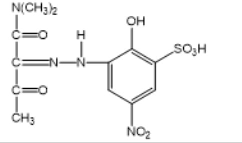	R283	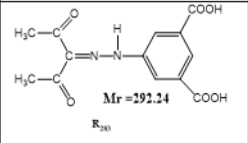	**R234**	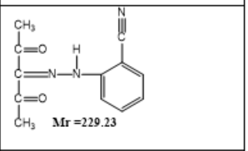
R31	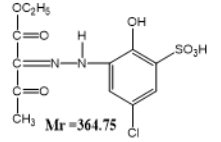	R243	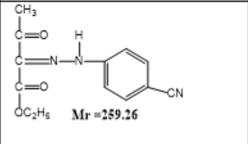	R246	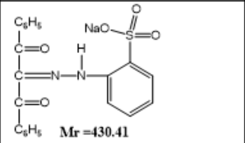
R142	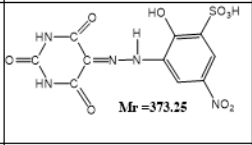	R244	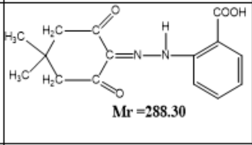	R237	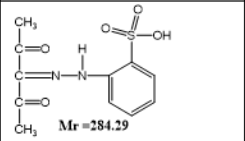
R46	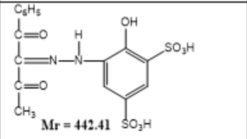	R221	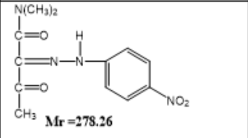	R40	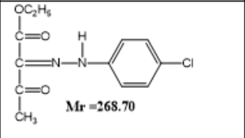
R237	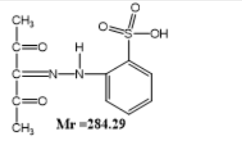	R48	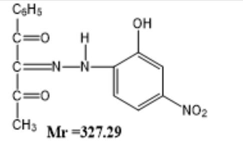	R236	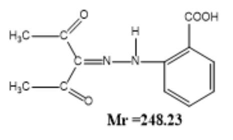
R241	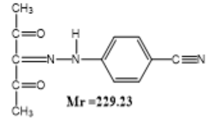	R246	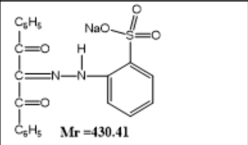		
R156	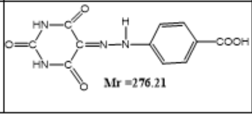	R313	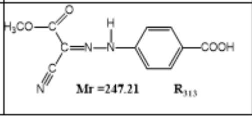		

Transcriptome profile also emphasize that, R234 exerts anti-proliferation effects on GBM cells via RTK pathways, and many significant genes of RTKs pathways such as mTOR, HIF1A, EIF4E, NRF2, MAP3K, GRB2, MAPK1, FOS and GSK3, where downregulated while it triggered p53, RBL2, Bim, Noxa, Puma, HDAC.

It could be inferred that the major implication of RTK mediated anti-GBM effects are through AKT signaling, affecting mTOR cascade, P53 pathways and JNK pathway. Coinciding with our initial observation of strong interaction with TrkA receptor, downregulation of NGFR downstream signaling pathway genes such as PI3K, JNK, NF-kb pathways indicates the potential of R234 to act as an antagonist of RTK pathways. R234 was found to effectively interact with high-affinity nerve growth factor receptor- TrkA and would possibly be an interesting compound in field of molecularly targeted therapies for GBM patients with TRK mutations. This finding is interesting in the context that the successful targeting on somatic genetic alterations rather than the histological subtype. Our results hint that the strong cytotoxicity, anti-angiogenic and apoptotic activity of R234 is chiefly via RTK signaling pathways. It would be interesting to further explore the prospective of hydrazones as a future therapeutic agent against GBM.

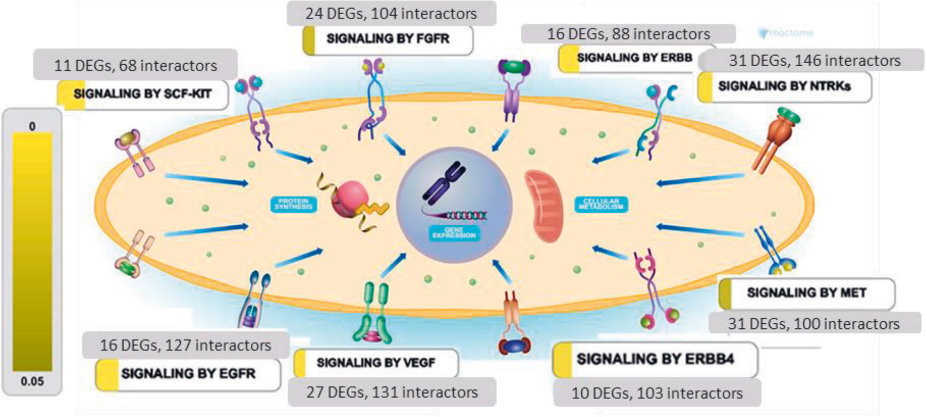
24 DEGs, 104 interactors
SIGNALING BY FGFR
16 DEGs, 88 interactors
SIGNALING BY ERBB
reactome
31 DEGs, 146 interactors
SIGNALING BY NTRKs
11 DEGs, 68 interactors
SIGNALING BY SCF-KIT
0
0.05
PROTEIN SYNTHESIS
GENE EXPRESSION
CELLULAR METABOLISM
SIGNALING BY MET
31 DEGs, 100 interactors
16 DEGs, 127 interactors
SIGNALING BY EGFR
SIGNALING BY VEGF
27 DEGs, 131 interactors
SIGNALING BY ERBB4
10 DEGs, 103 interactors

Figure 12. Hydrazone drug **R234** effectively downregulates various receptor tyrosine kinases pathways. Yellow colored portion denotes the fraction of molecules represented in the pathways, by DEGs due to **R234** treatment. Color scale represents p-value of outcome.

The third class of chemical under investigation was boron derivatives. Though the antitumor properties of boroxazolidones against brain astrocytoma and murine lymphoma cells, have been reported by other researches, its effect on GBM has remained unexplored. In the **Publication III**, we evaluated a series of novel boroxazolidones (**Table 3**) for its anti-neoplastic effects in GBM cell lines LN229 and SNB19. From six L-valine derived boroxazolidones (mentioned as **1–6 in the publication)**, it was identified a tetrafluorinated boron derivative ‘**6’/ ‘(JRB115)’** as the top cytotoxic compound.

The IC_{50} of compound **JRB115** was inferred to be 49 µM for LN229 and 53 µM for SNB19 and was higher than the standard drug TMZ. Annexin V/PI double staining identified that **JRB115** effectively induce apoptosis in both cell lines and was significantly higher than the TMZ in case of SNB19, and was comparable to TMZ in LN229. Caspase 3/7 test unveiled that the observed apoptosis by **JRB115** could possibly due to caspase activation in both cell lines. Interestingly, ROS level detection by H2DCFDA demonstrated a strong oxidative stress due to the drug in LN229, but SNB19 effectively countered the oxidative effect of the drug. This varying effect was also evident in the genotoxicity of the drug, as LN229 was arrested at G2/M phase whereas SNB19 was arrested at G1/S. Concisely, **JRB115** was proven to be an active cytotoxic agent that triggers apoptosis and has the potential to activate caspase 3/7 pathways, induce reactive oxygen species, and cell cycle arrest of GBM cells. Collectively, this data has given an opportunity to explore this previously underexplored compound class, to be modified or refined as an anti-GBM agent. The detailed report of the study is included in **Publication III.**

Table 3. Structure of Boron derivatives used for the study

CODE	Structure	CODE	Structure
RB63	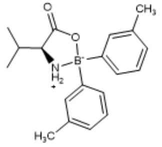	JRB85	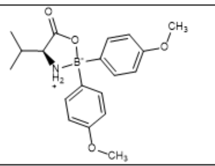
JRB115	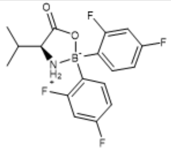	JRB61	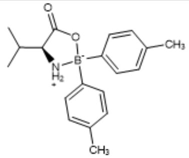
NK630	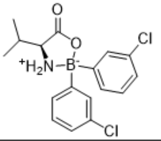	JRB119	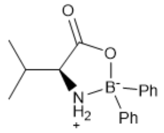

The last publication in this compilation thesis, **Publication IV**, presents the unpublished report on our investigation of thioesters derivatives, as a GBM chemotherapeutic agent. A panel of 12 new compounds containing α-thioether ketone and orthothioester functionalities were synthesized (**Table 4**). Our studies identified that five out of twelve novel thioester compounds analyzed, exhibited better cytotoxic profile when compared to standard drug Cisplatin. The top compound, mentioned as **5a** in the publication, was more cytotoxic and effective apoptotic driver than Cisplatin.

Table 4. Structure of Thioester derivatives, used for the study

CODE	Structure	CODE	Structure
RV195	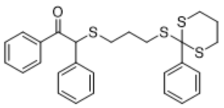	RV182	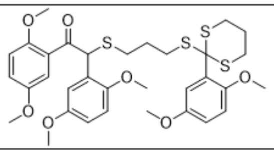
RV74	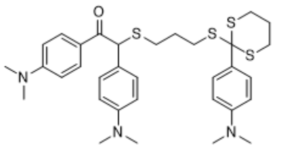	RV180	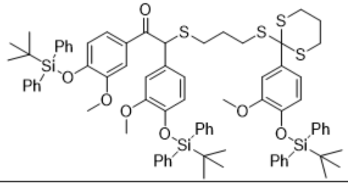
RV144	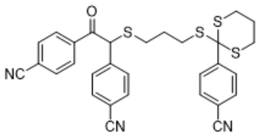	RV192	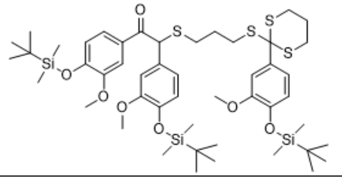
RV169	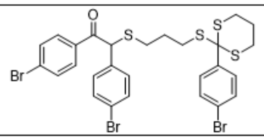	RV186	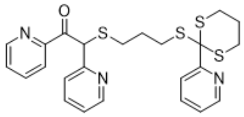
RV188	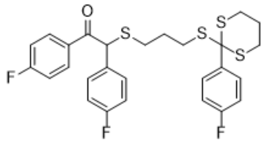	**RV114 (5a)**	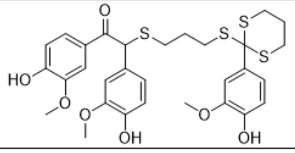
RV187	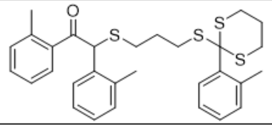	RV115	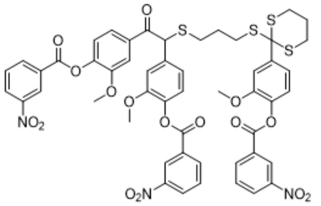
RV151	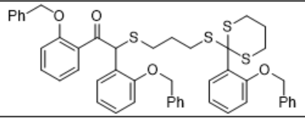		

Transcriptome analysis revealed that **5a** leads to inhibition of angiogenesis targeting VEGF pathway, via multiple pro-angiogenic regulators, and was found to preferentially interact with EGFR. Sole targeting of the EGFR signal pathway faces the issue of triggering alternative signaling pathways and quick acclimatization, however, an inhibitor such as **5a**, which can confront the multiple kinase pathways as well as other compensatory mechanisms of tumor resistance, that opens a new paradigm of GBM research. A cumulative list of signal transduction pathways hampered by **5a** is listed in **Table 5**.

Table 5. List of DEGs disfavoring tumor growth, under **5a** treated condition

Pathway name	**Entities found**
Signaling by VEGF	*NRP1; AHCYL1; CAV1; PXN; ITPR1; ITPR3; VEGFD; PGF; ACTG1; VEGFA; AXL; CTNNB1; FYN; CALM1; PRKACB; CRK; PDK1*
Signaling by Insulin receptor	*IRS1; ATP6V1B2; GRB10; FGFR4; ATP6V0D1; FGF2; PDK1*
Signaling by PDGF	*GRB7; STAT1; PDGFC; PDGFB; PDGFA; CRK; THBS1*
Signaling by SCF-KIT	*GRB7; KITLG; STAT1; GRB10; FYN*
Signaling by Type 1 Insulin-like Growth Factor 1 Receptor (IGF1R)	*IRS1; FGFR4; FGF2; PDK1*
Signaling by EGFR	*ADAM17; SH3KBP1; UBC; PXN; TGFA; SPRY1; AREG; EGFR; HBEGF*
Signaling by ERBB2	*GRB7; UBC; FYN; EGFR; HBEGF*
Signaling by MET	*SH3KBP1; UBC; CRK; MET; PTPN2*
Signaling by NTRKs	*TIAM1; RPS6KA5; IRS1; FYN; RALGDS; CRK; DUSP6*
Signaling by FGFR	*ESRP1; UBC; FGFR4; HNRNPA1; FGF2*
Signaling by ERBB4	*ADAM17; DLG4; STMN1; UBC; EGFR; HBEGF*

To underscore its anti-neoplastic effect, it should be mentioned here, that compound **5a** was found to have a negative impact on multiple pathways involved in tumor communication, such as MAPK pathway, Notch signaling and angiogenic signaling via TNF mediated expression of angiogenic factors. **5a** upregulated cell cycle inhibitory genes, as well as caused reduction of DNA repair proteins, suggesting its genotoxic effect as well. Additionally, **5a** is an effective IL-1R1 antagonist and downregulated IL-1a levels. IL-1 is involved in the regulation of diverse cells in the tumor microenvironment and acts jointly with VEGF to intensify and maintain tumor-mediated angiogenesis[204]. Another report points out that, IL-1a induces significant proliferation and migration of endothelial cells, by promoting the formation of tube-like structures -the hallmark of angiogenesis, *in vitro*, and such responses could be blocked by an IL-1 receptor antagonist (IL-1RA)[205]. Thioesters also possess the advantage that they are stable in the acidic conditions of the stomach and their hydrolysis occurs after their absorption into the bloodstream and therefore presents an excellent choice as a pharmacological scaffold. Decisively, **5a,** establishes its potential as a multidimensional anti-GBM agent having cytotoxic, genotoxic, anti-angiogenic, anti-invasive properties, posing it as a better anti-GBM monotherapy agent (**Fig: 13**).

One of the major pitfalls in blocking VEGF mediated angiogenesis in GBM, is the presence of VEGF- independent vascular growth. Another major consideration is that, blocking VEGF stimulates endothelial cell apoptosis, resulting in the damage of blood vessels, causing disruption of tissue homeostasis. If healthy blood vessels are affected along with tumor cells, it may result in hemorrhagic or thrombotic events. Thioesters as agents targeting DNA repair machinery and cell cycle control, also offers an exciting zone for novel therapeutic advances. As a genotoxic agent, the drug also faces another challenge, the sternness of tumors by promoting error-prone mechanisms of repair, thereby increasing mutation incidence and genomic variability which needs to be considered in future studies.

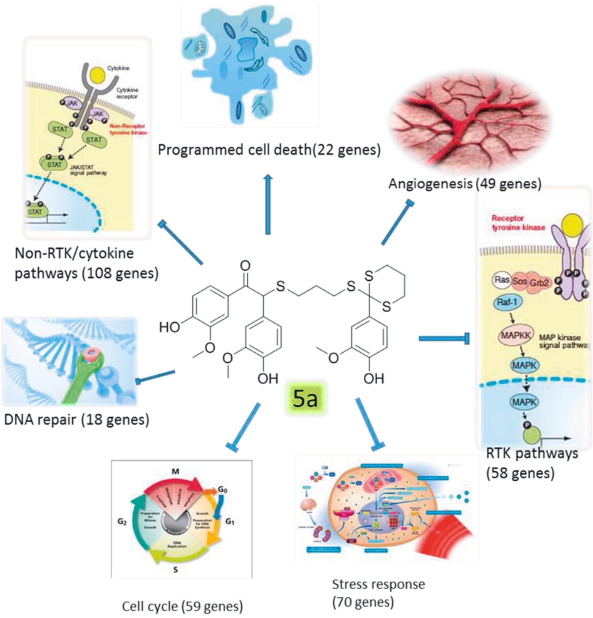
Cytokine
Cytokine receptor
JAK
JAK
STAT
STAT
Non-Receptor tyrosine kinase
STAT
JAK/STAT signal pathway
STAT
Programmed cell death(22 genes)
Angiogenesis (49 genes)
Non-RTK/cytokine pathways (108 genes)
O
S
S
S
S
HO
O
O
O
OH
OH
5a
Receptor tyrosine kinase
Ras
Sos
Grb2
Raf-1
MAPKK
MAP kinase signal pathway
MAPK
MAPK
RTK pathways (58 genes)
DNA repair (18 genes)
M
G₀
G₁
G₂
S
Cell cycle (59 genes)
Stress response (70 genes)

Figure 13. Thioester derivative **5a** shows promising anti-GBM impact, demonstrating multidimensional toxic effects on key tumorigenic features.

6 INFERENCE AND DISCUSSION

So far, we have discussed the comprehensive results from each compound class, in an attempt to identify a drug with multifaceted effects on GBM pathophysiology. Among the four classes of compounds analyzed- diols, hydrazones, borons and thioesters, all of them have shown various levels of anti-cancer characteristics, with thioester derivative displaying maximum cytotoxicity. Our experiments identified that, the top drug under each class was able to induce apoptosis higher than the standard drug used, except the diol derivative **DBT.** Apoptosis via caspase activation was observed in both the Boron derivative (**JRB115**) and the thioester derivative (**5a**). On the other hand, the diol derivative **DBT** and the hydrazone derivative **R234** inhibited Caspase expression suggesting activation of intrinsic pathways of cell death probably via caspase-independent pathways. All of the candidate drugs mentioned above induced oxidative stress in GBM cells.

The study considered the activity of **DBT**, **R234** and **5a** for detailed transcriptome profiling to explore molecular level anti-tumor activity, in GBM cells. Transcriptome study was performed in U-87 cell line for all the drug classes, except the boron class, as the compound JRB**115** was displaying unsatisfactory and inconsistent results in U-87. The reason for this rather contradictory result has still not been clear. Interestingly, the transcriptome profiling unveiled the three distinct modes of action for each of the drug analyzed. An overview of the various biological processes, molecular functions, and cellular components represented by DEGs of each class is portrayed in **Fig: 14**. The maximum number of DEGs was identified in **R234** treatment, but the most correlated activity by DEGs was displayed by **5a.**

Our findings suggest that **DBT** exerts its drug effect primarily via Glutamate receptor pathway, specifically NMDA receptor. On the other hand, **R234** was found to interact with the tyrosine kinase receptor NGFR. Varying from this, RNA-seq analysis indicates EGFR as a strong target to the thioester drug **5a**. Interestingly, gene expression analysis detects p53 activation by all the three compounds.

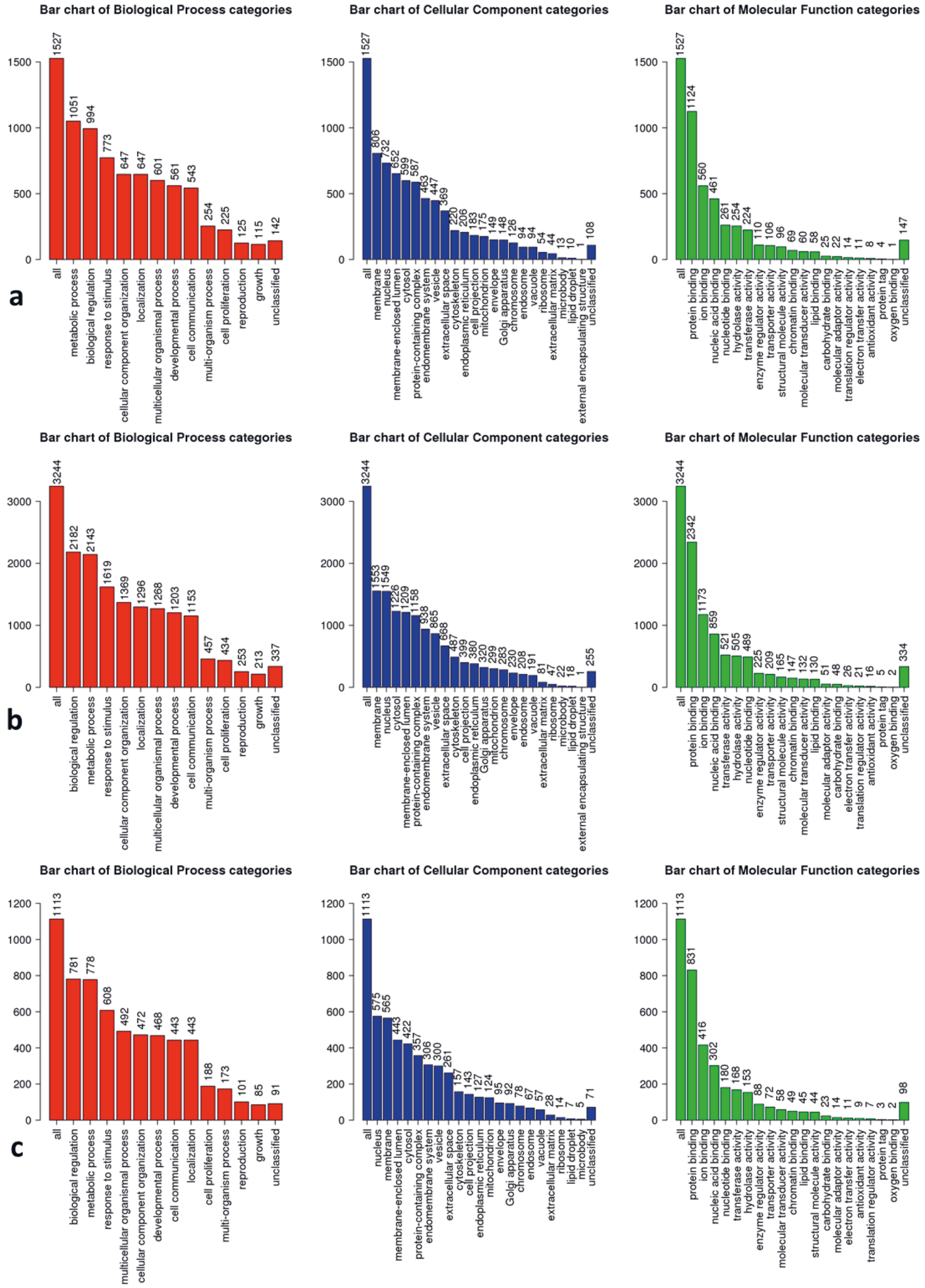

Figure 14. An overview of the enrichment of DEGs identified in each of the compound classes. a) categorization of DEGs under **DBT** treatment. b) categorization of DEGs under **R234** treatment .c) categorization of DEGs under **5a** treatment. 'x'-axis denotes the DEG count. P-value cut-off: 0.05

]

As reported above, the findings from our study has provided strong evidences to consider that the hydrazone derivative **R234,** and the thioester derivative **5a,** exhibited best advantages as anti-tumor agents for GBM, among the four classes evaluated. However, it was found that the hydrazone drug **R234** has IC_{50} value of 107 µM in U-87 and 87 µM in LN227 cells, whereas the thioester drug **5a** has IC_{50} value of 27 µM in U-87, and 23 µM in LN227 cells. Considering the aggregate effects, functionality as a TKI and the strong cytotoxicity over **R234**, we suggest **5a** as the top drug candidate against GBM. Overall statistics of the major features of all compounds under the higher-level analysis is given in the **Fig. 15** below.

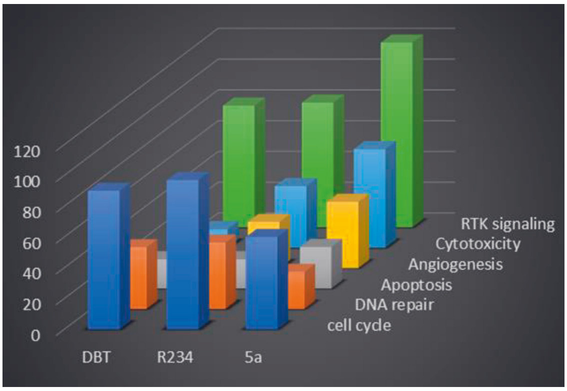

Figure 15. Overall anti-tumor activities of **DBT**, **R234** and **5a**, identified by transcriptome profiling.

Detailed analysis of drug effect on various pathways detects **5a** has the best cumulative effects as a multichannel antitumor drug. The x-axis denotes the treatment- top compound from derivatives of each class (diols- **DBT**, hydrazones- **R234** and thioesters-**5a),** and y-axis denotes the number of DEGs in each pathway. P-value cutoff for the DEGs is 0.05.

The most striking observation from the comprehensive evaluation of transcriptome profiling of **5a** treatment is that, the *MYC* and *EGFR* are the two hub nodes among 1147 DEGs (**Fig: 16 a**). It must also be noted that the functional annotation distinguished MAPK signaling among the top ten altered pathways. Activation of p53 signaling as well as attenuation of Notch signaling boosts the onco-suppressing nature of **5a**.

The Myc family of protooncogenes controls an array of cellular activities including cell growth, differentiation, stemness and tumor initiation. *Myc* driven oncogenesis in GBM is partially ascribed to glycolytic pathway dependency[206], and inhibition of *Myc* is also reported to restrict the hypoxic response in GBM[207]. The tumor suppressor *p53,* which is often de-railed in GBM, depends on *Myc* to control differentiation, self-renewal and tumor cell initiation in glioblastoma[208].

Indication of an apparent activation of p53 signaling pathway, in the **5a** treated condition, thus well correlates with the observation of huge amount of DEGs associated with *Myc*. Considering the past reports, this interplay of *Myc* and *p53* depends on various microRNAs and lncRNAs[209–211], notabily through the initiation of the tumor suppressor *miR-145*[210]. 16 genes associated with p53 pathway were found to be differently expressed upon the drug treatment (**Fig:17 a**). The *p53* expression activates *p21* that block formation of Cdk4/Cyclin D and Cdk2/Cyclin E complexes [212], and thus prevent the cell cycle progression. Restoration of *p53* function can activate genes that are implicated in cell cycle arrest and apoptosis[209]. Combined targeting of *p53* and *Myc* was reported to be effective in leukemia stem cells[213].

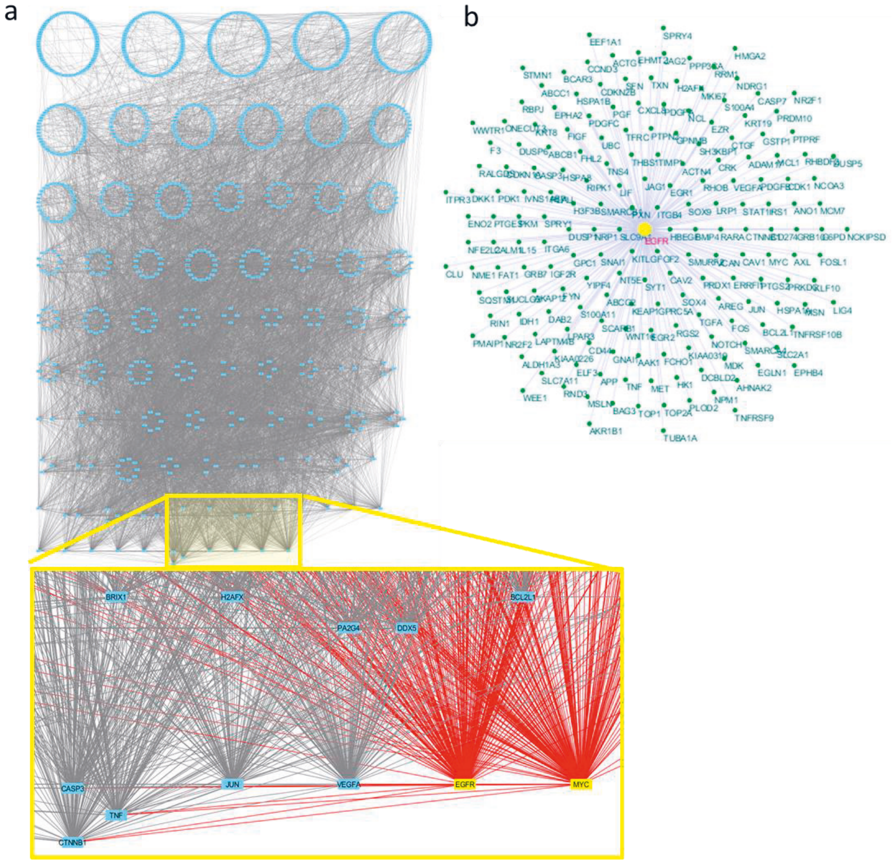

Figure 16. MYC and EGFR as the hub nodes in **5a** treatment. **a**. Grouped attribute layout based on degree of nodes, of entire DEGs identified in **5a** treatment. EGFR and MYC, the top two hub nodes are highlighted in yellow. **b**. EGFR, the hub node (highlighted in yellow) and its 189 first neighbors arranged in an organic layout. The networks are generated using Cytoscape[214]. All DEGs are identified with a q-value<0.05

Tumor hypoxic environment triggers activation of Hypoxia Inducible Factors(*HIFs*) and subsequent *EGFR* expression[215] in cancer cells. Identified as a hub node in the DEG network in **5a** treated cells (**Fig: 17 b**), in conjunction with the molecular docking predictions, reinforces EGFR as valid target for **5a**. Its worthy to note that the oncogenic potential of EGFR consists two distinct signaling modes, the surface receptor mode and the nuclear mode[216]. The surface receptor mode operates through *PLC-γ, RAS, PI3-K , JAK2* and *STAT*. Strikingly, a prominent way of action of EGFR in the nucleus is as a co-activator of other transcription regulators, including *Myc*[217]. A substantial amount of study reveals the consequence of targeting membrane bound EGFR, such as the use of erlotinib and lapatinib, however a study by Brand et al. also discusses the concern of nuclear EGFR as a target in Glioblastoma[218]. The *STAT1* gene expression is enhanced by nuclear EGFR via cooperation with *STAT3*[219]*,* therefore targeted binding of EGFR is expected to reduce STAT1 levels. As indicated, we observed an evident repression of *STAT1,* and of other JAK-STAT pathway components such as *CYP1B1, AKR1B1, CAV1 and HMGA2*. These evidences converge to the aspect that **5a** have a strong interaction with EGFR, thus affecting its partner molecules, diminishing various GBM tumor pathogenic characteristics.

Another effector molecule of EGFR is NF-kB - a dimeric transcription factor that is activated by the EGFR signaling pathway mainly via RIPK1[220]. TNF-α is another activator of NF-kB. NF-kB helps GBM cells to evade apoptotic machinery and its required for tumor growth, vascularization and invasion[221]. Our study evidenced a marked destabilization of NF-kB signaling cued by downregulation of genes such as *TNF, HMOX1, HSPA1, CLU, RIPK1* and *BCL10*. BCL10 is required for the activation of *NF-kB* via IKK-β-PHlPP2 interaction. Besides, the tumor niche dependent phenotypic shift from proneural-to-mesenchymal is dependent on TNF/NF-kB[222] and activation of NF-kB triggers TNFα production and eventually cell migration and invasion[223]. Also, the antiapoptotic activity of NF-kB is activated by TNFα through its death receptors TNFR1. Weakening of NF-kB observed in our experiment could be explained by a steep decline in the TNF expression level (Log_2FC: -6.62). Furthermore, pro-inflammatory mediator IL-1 plays an important role in tumor-mediated angiogenesis by elevating the expression of NF-kB and VEGF. A significant study by Lee et al. claims that the expression of FGF-2 by IL-1 could be blocked by inhibitors to NF-κB activation[224], which is coherent with our observation of distinct downregulation of FGF2 and NF-kB pathway.

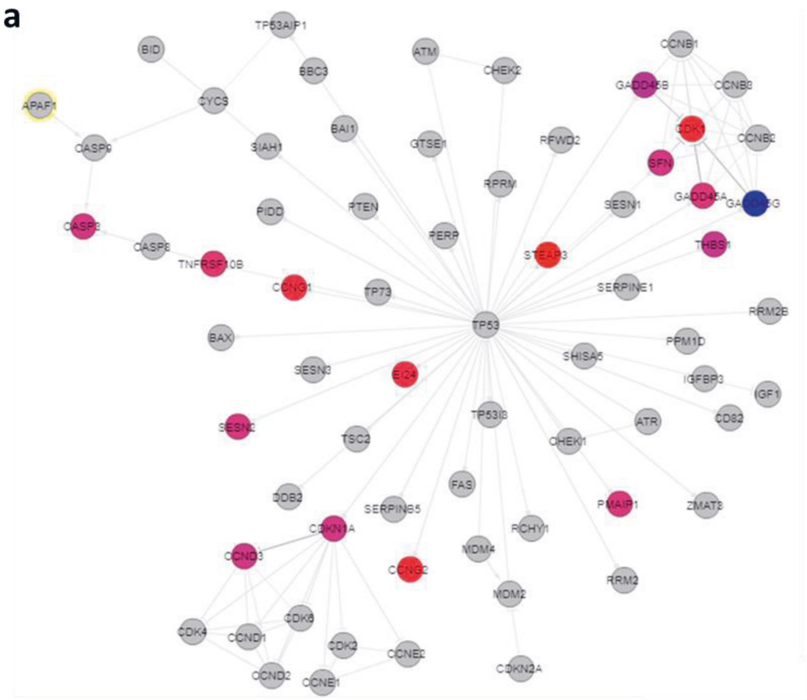
a
TP53AIP1
BID
ATM
CCNB1
BBC3
CHEK2
GADD45B
CCNB3
APAF1
CYCS
CDK1
BAI1
CCNB2
CASP9
SIAH1
GTSE1
RFWD2
SFN
RPRM
GADD45A
GADD45G
SESN1
PIDD
PTEN
CASP3
PERP
THBS1
CASP8
STEAP3
TNFRSF10B
SERPINE1
CCNG1
TP73
RRM2B
TP53
BAX
PPM1D
SHISA5
SESN3
EI24
IGFBP3
IGF1
TP53I3
ATR
CD82
SESN2
TSC2
CHEK1
FAS
DDB2
SERPINB5
PMAIP1
ZMAT3
CDKN1A
RCHY1
CCND3
MDM4
CCNG2
RRM2
MDM2
CDK6
CDK4
CCND1
CDK2
CCNE2
CCND2
CCNE1
CDKN2A

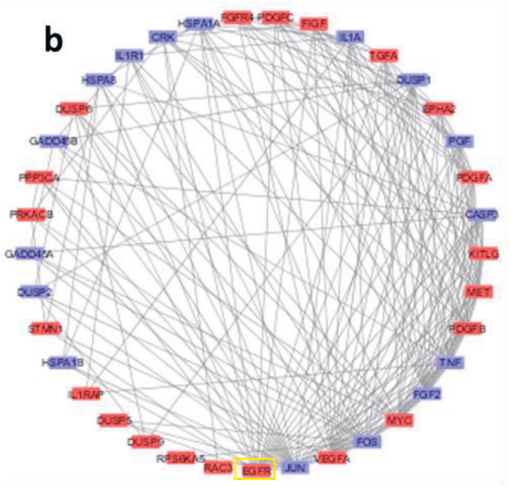
b
HSPA1A
FGFR4
PDGFC
FIGF
CRK
IL1A
IL1R1
TGFA
HSPA8
DUSP1
DUSP6
EPHA2
GADD45B
PGF
PPP3CA
PDGFA
PRKACB
CASP3
GADD45A
KITLG
DUSP2
MET
STMN1
PDGFB
HSPA1B
TNF
IL1RAP
FGF2
DUSP5
MYC
DUSP9
FOS
RPS6KA5
VEGFA
RAC3
EGFR
JUN

Genes represented in MAPK pathway

Gene Symbol	Log2(FC)	Gene Symbol	Log2(FC)
TNF	-6.62	DUSP6	0.45
VEGFD	-4.46	VEGFA	0.46
HSPA1B	-3.90	STMN1	0.55
HSPA1A	-3.68	FLNC	0.65
IL1A	-2.64	PPP3CA	0.69
FOS	-2.42	EPHA2	0.73
DUSP2	-2.34	DUSP5	0.73
GADD45B	-1.49	FGFR4	0.76
HSPA8	-1.40	EGFR	0.77
PGF	-1.22	PRKACB	0.80
FGF2	-1.22	TGFA	0.86
IL1R1	-1.04	RAC3	0.95
JUN	-1.01	PDGFC	0.97
DUSP1	-0.90	MET	1.03
CASP3	-0.86	DUSP9	1.07
LAMTOR3	-0.70	IL1RAP	1.15
PPM1B	-0.63	RPS6KA5	1.23
GADD45A	-0.63	PDGFA	1.27
CRK	-0.55	PDGFB	1.31
		MYC	1.36
		KITLG	1.81

Figure 17. Key effector pathways of **5a** and their interaction network **a**. The p53 gene and its interacting partners identified in **5a** treated cells. Color code is based on the expression levels downregulated genes in blue and upregulated genes in red. Gradient intensity is based on the magnitude of gene expression. **b.** Network of genes overrepresented in MAPK pathway represented in degree sorted circle layout. EGFR the hub node in highlighted in yellow box. Nodes are color coded as downregulated genes in blue and upregulated genes in red. All DEGs are selected with a q-value < 0.05

High affinity ligands of EGFR- TGFβ and EGF, are reported to induce *VEGF* expression, whereas EGFR inhibitors attenuate *VEGF* expression[225]. *VEGF* expression is also contributed by MAPK, ERK1/2, STAT and PI3K signaling cascade[226]. Considering the aspect that VEGFD binds to VEGFR2 as well as VEGFR3, downregulation of *VEGFD* would result in the attenuation of the consecutive pathways mentioned above. Our results reveal a clear-cut decline in the VEGFD level, which is in line with previous findings. One possible explanation of ineffectiveness of sole VEGF targeted chemotherapeutics, could be the compensatory activation of Notch signaling in GBM cells [227]. Notch signaling regulates stem cell maintenance, apoptosis and angiogenesis[227–231]. Notch signaling is an attractive therapeutic target as it functions in intimate association with VEGF pathway in tumor angiogenesis. Inhibition of Notch communication causes disruption of vascular niche eliminating the survival advantage of tumor cells, also conferring anti-angiogenic activity. *Notch* is also involved in the regulation of *cyclin D1, Myc, HER2, NRAR* and *NF-κB*. Molecular profiling also unveiled that **5a** commendably mitigated Notch signaling. Given that, it is reasonable to deduce that **5a** partially imparts its anti-tumor activity via Notch blockade, thus begetting anti-angiogenicity, reducing stemness, altering cell fate and imperiling tumor cell survival.

Targeted therapy using small molecules against RTKs were reported to be effective against a variety of cancers. Particularly, RTK inhibitors (RTKis) targeting EGFR, PDGFR, IGF-R, VEGFR and FGFR are of prime focus. Many of them are already tested as a single agent, or as a part of the combination regimen, in preclinical studies or approved for clinical trials. Despite that, resistance to RTKis have been reported due to the presence of compensatory pathways in GBM. A solution to this problem is concomitant inhibition of multiple RTK receptors. Alternatively, deterring of multiple molecular components of same cellular signaling must also give better results. All told, it is evident that a powerful anti-GBM drug should inhibit parallel and converging compensatory signaling that exists in GBM cells.

A multitarget RTKi Sitravatinib was mentioned to exhibit strong anti-tumor activity in preclinical models of sarcoma[232].Similarly, Ganetespib was cited to act on multiple levels of the RTK signaling cascade in breast cancer cells[233]. A dual target drug ZD6474, that blocks VEGFR and EGFR were found effective against multiple nervous system tumors[234]. Another significant notion of a multi-target drug has been made by Chung et al., which reports a novel drug that concurrently targets VEGF, FGF and PDFG-β signaling[235]. A recent review article on this topic proposes potential of multiple RTKIs that simultaneously block several proangiogenic factors and stabilize vascular normalization as an effective approach in GBM treatment[236]. Advocating the same strategy, our results promote **5a** as a powerful anti-tumor agent against GBM, acting on a wide array of tumorigenic aspects as RTK signaling, angiogenesis, vascularization, chemoresistance and evasion of immunosurvival and apoptosis.

Further development of this study would include evaluation of the candidate drug **5a** in 3D and animal models, tracking the response of the tumor microenvironment to the drug, ADME profiling, detailed pharmacokinetic profiling, possible refinements and precisely controlled and targeted release of the drug to the tumor cells. Additionally, it would be worth evaluating the combined effect of the candidate drug with other standard chemotherapy agents or with other treatment modes. One wider level, any personalized treatment regimen that takes into account multiple features of GBM- the dynamic behavior of cells in response to therapeutic interventions, the complex series of molecular processes involved in epigenetic evolution, the role of biomechanical modification in the tumor microenvironment and identification of unique drivers of brain metastasis development, would be prospective in GBM treatment.

7 CONCLUSION

GBM harbors complex signaling tactics to evade conventional therapies, including surgical resection, radiation, and chemotherapy using current standard drugs, resulting in a poor survival rate. Regardless of a number of anti-GBM agents in development, preclinical and clinical trials, it is hard to ignore the copious death statistics of Glioblastoma. While the development of numerous kinase inhibitors continues to be actively pursued, successful treatment requires precise targeting of multiple contributors of tumor pathway. Targeted therapies such as RTKis avoid negatively affecting the normal cells, thus enhance safety, and reduce undesirable effects. Yet, resistance to RTKis have been reported due to the intracellular signal interchanges, necessitating concurrent blocking of multiple receptors. Our project intended to identify a potent multi-channel chemotherapy agent for GBM, from 53 novel compounds, belonging to four different chemical classes. All the compound families evaluated constitutes active anti-GBM agents, and was more cytotoxic than current first-line chemotherapeutic agent Cisplatin. Among the four classes under consideration, our study proposes a thioester drug **5a** (as mentioned in **Publication IV**) as the most active pharmacological template possessing multi-faceted inhibitory action, leading to a significant reduction in tumor proliferation, angiogenesis, and resistance. Tested against multiple GBM cell lines, **5a** was found to be an active RTK. This research is only a preclinical experimental study and poses many questions in need of further investigation. Further validation of the recommended drug targets, the possibility of refining the drug structure to enhance the bioactivity, the combined effects with other drugs, identifying precise delivery agents etc. are just a few of them. However, an effective anti-GBM therapy should consider a careful blend of diagnosis, stratification, and patient-specific biology, to confront this deadly cancer.

BIBLIOGRAPHY

1. Glioblastoma Prognosis | Brain Tumour Survival Rates. https://www.thebraintumourcharity.org/brain-tumour-diagnosis-treatment/types-of-brain-tumour-adult/glioblastoma/glioblastoma-prognosis/. Accessed May 22, 2019.

2. Glioblastoma Multiforme Market, 2024 | GBM Industry Research Report. https://www.hexaresearch.com/research-report/glioblastoma-multiforme-gbm-market. Accessed June 5, 2019.

3. Index of /ftp1/NCI_Thesaurus. https://evs.nci.nih.gov/ftp1/NCI_Thesaurus/. Accessed April 15, 2019.

4. Olar A, Aldape KD. Using the molecular classification of glioblastoma to inform personalized treatment. *J Pathol*. 2014. doi:10.1002/path.4282.

5. Verhaak RGW, Hoadley KA, Purdom E, et al. Integrated Genomic Analysis Identifies Clinically Relevant Subtypes of Glioblastoma Characterized by Abnormalities in PDGFRA, IDH1, EGFR, and NF1. *Cancer Cell*. 2010. doi:10.1016/j.ccr.2009.12.020.

6. Phillips HS, Kharbanda S, Chen R, et al. Molecular subclasses of high-grade glioma predict prognosis, delineate a pattern of disease progression, and resemble stages in neurogenesis. *Cancer Cell*. 2006. doi:10.1016/j.ccr.2006.02.019.

7. Sturm D, Witt H, Hovestadt V, et al. Hotspot Mutations in H3F3A and IDH1 Define Distinct Epigenetic and Biological Subgroups of Glioblastoma. *Cancer Cell*. 2012. doi:10.1016/j.ccr.2012.08.024.

8. Ichimura K. Molecular pathogenesis of IDH mutations in gliomas. In: *Brain Tumor Pathology*. ; 2012. doi:10.1007/s10014-012-0090-4.

9. Dang L, White DW, Gross S, et al. Cancer-associated IDH1 mutations produce 2-hydroxyglutarate. *Nature*. 2009. doi:10.1038/nature08617.

10. Xu W, Yang H, Liu Y, et al. Oncometabolite 2-hydroxyglutarate is a competitive inhibitor of α-ketoglutarate-dependent dioxygenases. *Cancer Cell*. 2011. doi:10.1016/j.ccr.2010.12.014.

11. Hegi ME, Diserens A-C, Gorlia T, et al. MGMT Gene Silencing and Benefit from Temozolomide in Glioblastoma . *N Engl J Med*. 2005. doi:10.1056/nejmoa043331.

12. Thorne AH, Zanca C, Furnari F. Epidermal growth factor receptor targeting and challenges in glioblastoma. *Neuro Oncol*. 2016. doi:10.1093/neuonc/nov319.

13. Karsy M, Neil JA, Guan J, Mahan MA, Colman H, Jensen RL. A practical review of prognostic correlations of molecular biomarkers in glioblastoma. *Neurosurg Focus*. 2015. doi:10.3171/2015.1.focus14755.

14. Reardon DA, Wen PY, Mellinghoff IK. Targeted molecular therapies against epidermal growth factor receptor: Past experiences and challenges. *Neuro Oncol*. 2014. doi:10.1093/neuonc/nou232.

15. Huang PH, Xu AM, White FM. Oncogenic EGFR signaling networks in glioma. *Sci Signal*. 2009. doi:10.1126/scisignal.287re6.

16. Molenaar RJ, Radivoyevitch T, Maciejewski JP, van Noorden CJF, Bleeker FE. The driver and passenger effects of isocitrate dehydrogenase 1 and 2 mutations in oncogenesis and survival prolongation. *Biochim Biophys Acta - Rev Cancer*. 2014. doi:10.1016/j.bbcan.2014.05.004.

17. Fack F, Tardito S, Hochart G, et al. Altered metabolic landscape in IDH-mutant gliomas affects phospholipid, energy, and oxidative stress pathways. *EMBO Mol Med*. 2017. doi:10.15252/emmm.201707729.

18. Ohba S, Mukherjee J, Johannessen TC, et al. Mutant IDH1 expression drives TERT promoter reactivation as part of the cellular transformation process. *Cancer Res*. 2016. doi:10.1158/0008-5472.CAN-16-0696.

19. Jenkins RB, Blair H, Ballman K V., et al. A t(1;19)(q10;p10) mediates the combined deletions of 1p and 19q and predicts a better prognosis of patients with oligodendroglioma. *Cancer Res*. 2006. doi:10.1158/0008-5472.CAN-06-1796.

20. Reifenberger J, Reifenberger G, Liu L, James CD, Wechsler W, Collins VP. Molecular genetic analysis of oligodendroglial tumors shows preferential allelic deletions on 19q and 1p. *Am J Pathol*. 1994.

21. Vogazianou AP, Chan R, Bäcklund LM, et al. Distinct patterns of 1p and 19q alterations identify subtypes of human gliomas that have different prognoses. *Neuro Oncol*. 2010. doi:10.1093/neuonc/nop075.

22. Krex D, Mohr B, Appelt H, et al. Genetic Analysis of A Multifocal Glioblastoma Multiforme: A Suitable Tool to Gain New Aspects in Glioma Development. *Neurosurgery*. 2003. doi:10.1227/01.NEU.0000093426.29236.86.

23. Cho SY, Park C, Na D, et al. High prevalence of TP53 mutations is associated with poor survival and an EMT signature in gliosarcoma patients. *Exp Mol Med*. 2017. doi:10.1038/emm.2017.9.

24. Ishii N, Maier D, Merlo A, et al. Frequent Co-alterations of TP53, p16/CDKN2A, p14(ARF), PTEN tumor suppressor genes in human glioma cell lines. *Brain Pathol*. 1999. doi:10.1111/j.1750-3639.1999.tb00536.x.

25. Wang TJ, Huang MS, Hong CY, Tse V, Silverberg GD, Hsiao M. Comparisons of tumor suppressor p53, p21, and p16 gene therapy effects on glioblastoma tumorigenicity in Situ. *Biochem Biophys Res Commun*. 2001. doi:10.1006/bbrc.2001.5565.

26. Zhang Y, Dube C, Gibert M, et al. The p53 Pathway in Glioblastoma. *Cancers (Basel)*. 2018. doi:10.3390/cancers10090297.

27. Park CM, Park MJ, Kwak HJ, et al. Induction of p53-mediated apoptosis and recovery of chemosensitivity through p53 transduction in human glioblastoma cells by cisplatin. *Int J Oncol*. 2006.

28. Nandakumar P, Mansouri A, Das S. The Role of ATRX in Glioma Biology. *Front Oncol*. 2017. doi:10.3389/fonc.2017.00236.

29. Haase S, Garcia-Fabiani MB, Carney S, et al. Mutant ATRX: uncovering a new therapeutic target for glioma. *Expert Opin Ther Targets*. 2018. doi:10.1080/14728222.2018.1487953.

30. Cai J, Chen J, Zhang W, et al. Loss of ATRX, associated with DNA methylation pattern of chromosome end, impacted biological behaviors of astrocytic tumors. *Oncotarget*. 2015. doi:10.18632/oncotarget.3906.

31. Herndon JE, Gallia GL, Killela PJ, et al. TERT PROMOTER MUTATIONS OCCUR FREQUENTLY IN GLIOMAS AND A SUBSET OF TUMORS DERIVED FROM CELLS WITH LOW RATES OF SELF-RENEWAL. *Neuro Oncol*. 2014. doi:10.1093/neuonc/nou206.18.

32. Blackburn EH, Greider CW, Henderson E, Lee MS, Shampay J, Shippen-Lentz D. Recognition and elongation of telomeres by telomerase. *Genome*. 1989;31(2):553-560. doi:10.1139/g89-104.

33. Eckel-Passow JE, Lachance DH, Molinaro AM, et al. Glioma Groups Based on 1p/19q, IDH , and TERT Promoter Mutations in Tumors . *N Engl J Med*. 2015. doi:10.1056/nejmoa1407279.

34. Nguyen HS, Shabani S, Awad AJ, Kaushal M, Doan N. Molecular markers of therapy-resistant glioblastoma and potential strategy to combat resistance. *Int J Mol Sci*. 2018. doi:10.3390/ijms19061765.

35. Koelsche C, Sahm F, Capper D, et al. Distribution of TERT promoter mutations in pediatric and adult tumors of the nervous system. *Acta Neuropathol*. 2013. doi:10.1007/s00401-013-1195-5.

36. Singh SK, Hawkins C, Clarke ID, et al. Identification of human brain tumour initiating cells. *Nature*. 2004. doi:10.1038/nature03128.

37. Seidel S, Garvalov BK, Wirta V, et al. A hypoxic niche regulates glioblastoma stem cells through hypoxia inducible factor 2α. *Brain*. 2010. doi:10.1093/brain/awq042.

38. Liu G, Yuan X, Zeng Z, et al. Analysis of gene expression and chemoresistance of CD133+ cancer stem cells in glioblastoma. *Mol Cancer*. 2006. doi:10.1186/1476-4598-5-67.

39. Parker JJ, Canoll P, Niswander L, Kleinschmidt-DeMasters BK, Foshay K, Waziri A. Intratumoral heterogeneity of endogenous tumor cell invasive behavior in human glioblastoma. *Sci Rep*. 2018. doi:10.1038/s41598-018-36280-9.

40. Li F, He X, Ye D, et al. NADP+-IDH Mutations Promote Hypersuccinylation that Impairs Mitochondria Respiration and Induces Apoptosis Resistance. *Mol Cell*. 2015. doi:10.1016/j.molcel.2015.10.017.

41. Patel AP, Tirosh I, Trombetta JJ, et al. Single-cell RNA-seq highlights intratumoral heterogeneity in primary glioblastoma. *Science (80-)*. 2014;344(6190):1396-1401. doi:10.1126/science.1254257.

42. Wang J, Cazzato E, Ladewig E, et al. Clonal evolution of glioblastoma under therapy. *Nat Genet*. 2016. doi:10.1038/ng.3590.

43. Osuka S, Van Meir EG. Overcoming therapeutic resistance in glioblastoma: The way forward. *J Clin Invest*. 2017. doi:10.1172/JCI89587.

44. Schonberg DL, Lubelski D, Miller TE, Rich JN. Brain tumor stem cells: Molecular characteristics and their impact on therapy. *Mol Aspects Med*. 2013. doi:10.1016/j.mam.2013.06.004.

45. Bao S, Wu Q, McLendon RE, et al. Glioma stem cells promote radioresistance by preferential activation of the DNA damage response. *Nature*. 2006. doi:10.1038/nature05236.

46. Esteller M, Garcia-Foncillas J, Andion E, et al. Inactivation of the DNA-Repair Gene MGMT and the Clinical Response of Gliomas to Alkylating Agents . *N Engl J Med*. 2002. doi:10.1056/nejm200011093431901.

47. Calabrese C, Poppleton H, Kocak M, et al. A Perivascular Niche for Brain Tumor Stem Cells. *Cancer Cell*. 2007. doi:10.1016/j.ccr.2006.11.020.

48. McLendon R, Friedman A, Bigner D, et al. Comprehensive genomic characterization defines human glioblastoma genes and core pathways. *Nature*. 2008. doi:10.1038/nature07385.

49. Regad T. Targeting RTK signaling pathways in cancer. *Cancers (Basel)*. 2015. doi:10.3390/cancers7030860.

50. TSURUSHIMA H, TSUBOI K, YOSHII Y, OHNO T, MEGURO K, NOSE T. Expression of N-ras Gene in Gliomas. *Neurol Med Chir (Tokyo)*. 1996;36(10):704-708. doi:10.2176/nmc.36.704.

51. Kastenhuber ER, Lowe SW. Putting p53 in Context. *Cell*. 2017. doi:10.1016/j.cell.2017.08.028.

52. England B, Huang T, Karsy M. Current understanding of the role and targeting of tumor suppressor p53 in glioblastoma multiforme. *Tumor Biol*. 2013;34(4):2063-2074. doi:10.1007/s13277-013-0871-3.

53. Chow LML, Endersby R, Zhu X, et al. Cooperativity within and among Pten, p53, and Rb Pathways Induces High-Grade Astrocytoma in Adult Brain. *Cancer Cell*. 2011. doi:10.1016/j.ccr.2011.01.039.

54. Y. P. Lam, E. di Tomaso, H.-K. Ng, P. Expression of p19 INK4d, CDK4, CDK6 in glioblastoma multiforme. *Br J Neurosurg*. 2002. doi:10.1080/02688690042870.

55. Reardon DA, Desjardins A, Vredenburgh JJ, et al. Phase 2 trial of erlotinib plus sirolimus in adults with recurrent glioblastoma. *J Neurooncol*. 2010. doi:10.1007/s11060-009-9950-0.

56. Rich JN, Reardon DA, Peery T, et al. Phase II trial of gefitinib in recurrent glioblastoma. *J Clin Oncol*. 2004. doi:10.1200/JCO.2004.08.110.

57. Weller M, Butowski NA, Tran DD, et al. OS11.5 ACT IV: An international, double-blind, phase 3 trial of rindopepimut in newly diagnosed, EGFRvIII-expressing glioblastoma. *Neuro Oncol*. 2017. doi:10.1093/neuonc/nox036.076.

58. Neyns B, Sadones J, Joosens E, et al. Stratified phase II trial of cetuximab in patients with recurrent high-grade glioma. *Ann Oncol*. 2009. doi:10.1093/annonc/mdp032.

59. Lv S, Teugels E, Sadones J, et al. Correlation of EGFR, IDH1 and PTEN status with the outcome of patients with recurrent glioblastoma treated in a phase II clinical trial with the EGFR-blocking monoclonal antibody cetuximab. *Int J Oncol*. 2012. doi:10.3892/ijo.2012.1539.

60. Reardon DA, Nabors LB, Mason WP, et al. Phase I/randomized phase II study of afatinib, an irreversible ErbB family blocker, with or without protracted temozolomide in adults with recurrent glioblastoma. *Neuro Oncol*. 2015. doi:10.1093/neuonc/nou160.

61. Reardon DA, Groves MD, Wen PY, et al. A phase I/II trial of pazopanib in combination with lapatinib in adult patients with relapsed malignant glioma. *Clin Cancer Res*. 2013. doi:10.1158/1078-0432.CCR-12-1707.

62. Cheng SY, Huang HJ, Nagane M, et al. Suppression of glioblastoma angiogenicity and tumorigenicity by inhibition of endogenous expression of vascular endothelial growth factor. *Proc Natl Acad Sci*. 2002. doi:10.1073/pnas.93.16.8502.

63. Dvorak HF. Tumors: Wounds That Do Not Heal--Redux. *Cancer Immunol Res*. 2015. doi:10.1158/2326-6066.cir-14-0209.

64. Gerstner ER, Eichler AF, Plotkin SR, et al. Phase I trial with biomarker studies of vatalanib (PTK787) in patients with newly diagnosed glioblastoma treated with enzyme inducing anti-epileptic drugs and standard radiation and temozolomide. *J Neurooncol*. 2011. doi:10.1007/s11060-010-0390-7.

65. Batchelor TT, Mulholland P, Neyns B, et al. Phase III randomized trial comparing the efficacy of cediranib as monotherapy, and in combination with lomustine, versus lomustine alone in patients with recurrent glioblastoma. *J Clin Oncol*. 2013. doi:10.1200/JCO.2012.47.2464.

66. Awad AJ, Burns TC, Zhang Y, Abounader R. Targeting MET for glioma therapy. *Neurosurg Focus*. 2014. doi:10.3171/2014.9.focus14520.

67. Abounader R, Laterra J. Scatter factor/hepatocyte growth factor in brain tumor growth and angiogenesis. *Neuro Oncol*. 2005. doi:10.1215/s1152851705000050.

68. Nehoff H, Parayath NN, McConnell MJ, Taurin S, Greish K. A combination of tyrosine kinase inhibitors, crizotinib and dasatinib for the treatment of glioblastoma multiforme. *Oncotarget*. 2015. doi:10.18632/oncotarget.5698.

69. Morley R, Cardenas A, Hawkins P, et al. Safety of onartuzumab in patients with solid tumors: Experience to date from the onartuzumab clinical trial program. *PLoS One*. 2015. doi:10.1371/journal.pone.0139679.

70. Zhang Y, Guessous F, Kofman A, Schiff D, Abounader R. XL-184, a MET, VEGFR-2 and RET kinase inhibitor for the treatment of thyroid cancer, glioblastoma multiforme and NSCLC. *IDrugs*. 2010.

71. Le Rhun E, Chamberlain MC, Zairi F, et al. Patterns of response to crizotinib in recurrent glioblastoma according to ALK and MET molecular profile in two patients. *CNS Oncol*. 2015. doi:10.2217/cns.15.30.

72. Brennan CW, Verhaak RGW, McKenna A, et al. The somatic genomic landscape of glioblastoma & supp. *Cell*. 2013. doi:10.1016/j.cell.2013.09.034.

73. Zohrabian VM, Forzani B, Chau Z, Murali R, Jhanwar-Uniyal M. Rho/ROCK and MAPK signaling pathways are involved in glioblastoma cell migration and proliferation. *Anticancer Res*. 2009.

74. Schultz CR, Golembieski WA, King DA, Brown SL, Brodie C, Rempel SA. Inhibition of HSP27 alone or in combination with pAKT inhibition as therapeutic approaches to target SPARC-induced glioma cell survival. *Mol Cancer*. 2012. doi:10.1186/1476-4598-11-20.

75. McNeill RS, Canoutas DA, Stuhlmiller TJ, et al. Combination therapy with potent PI3K and MAPK inhibitors overcomes adaptive kinome resistance to single agents in preclinical models of glioblastoma. *Neuro Oncol*. 2017. doi:10.1093/neuonc/nox044.

76. Koul D, Shen R, Kim YW, et al. Cellular and in vivo activity of a novel PI3K inhibitor, PX-866, against human glioblastoma. *Neuro Oncol*. 2010. doi:10.1093/neuonc/nop058.

77. Hainsworth JD, Ervin T, Friedman E, et al. Concurrent radiotherapy and temozolomide followed by temozolomide and sorafenib in the first-line treatment of patients with glioblastoma multiforme. *Cancer*. 2010. doi:10.1002/cncr.25275.

78. Galanis E, Anderson SK, Lafky JM, et al. Phase II study of bevacizumab in combination with sorafenib in recurrent glioblastoma (N0776): A North Central Cancer Treatment Group Trial. *Clin Cancer Res*. 2013. doi:10.1158/1078-0432.CCR-13-0708.

79. Zustovich F, Landi L, Lombardi G, et al. Sorafenib plus daily low-dose temozolomide for relapsed glioblastoma: A phase ii study. *Anticancer Res*. 2013.

80. Lee EQ, Kaley TJ, Duda DG, et al. A multicenter, phase II, randomized, noncomparative clinical trial of radiation and temozolomide with or without vandetanib in newly diagnosed glioblastoma patients. *Clin Cancer Res*. 2015. doi:10.1158/1078-0432.CCR-14-3220.

81. Lombardi G, De Salvo GL, Eoli M, et al. REGOMA: A randomized, multicenter, controlled open-label phase II clinical trial evaluating regorafenib (REG) activity in relapsed glioblastoma (GBM) patients (PTS). *J Clin Oncol*. 2017. doi:10.1200/jco.2017.35.15_suppl.tps2085.

82. Wadhwa E, Meetze K, Nicolaides T. PDTM-41. TG02, A NOVEL MULTIKINASE INHIBITOR, IS EFFECTIVE IN PEDIATRIC BRAIN TUMORS, WITH SELECTIVE POTENCY IN THOSE WITH MYC EXPRESSION. *Neuro Oncol*. 2017. doi:10.1093/neuonc/nox168.804.

83. Balaña C, Gil MJ, Perez P, et al. Sunitinib administered prior to radiotherapy in patients with non-resectable glioblastoma: results of a Phase II study. *Target Oncol*. 2014. doi:10.1007/s11523-014-0305-1.

84. Neyns B, Sadones J, Chaskis C, et al. Phase II study of sunitinib malate in patients with recurrent high-grade glioma. *J Neurooncol*. 2011. doi:10.1007/s11060-010-0402-7.

85. Preusser M, Lim M, Hafler DA, Reardon DA, Sampson JH. Prospects of immune checkpoint modulators in the treatment of glioblastoma. *Nat Rev Neurol*. 2015. doi:10.1038/nrneurol.2015.139.

86. Reardon DA, Sampson JH, Sahebjam S, et al. Safety and activity of nivolumab (nivo) monotherapy and nivo in combination with ipilimumab (ipi) in recurrent glioblastoma (GBM): Updated results from checkmate-143. *J Clin Oncol*. 2018. doi:10.1200/jco.2016.34.15_suppl.2014.

87. J.H. S, G. V, S. S, et al. Preliminary safety and activity of nivolumab and its combination with ipilimumab in recurrent glioblastoma (GBM): CHECKMATE-143. *J Clin Oncol*. 2015.

88. D.A. R, J.F. DG, H. C, et al. Safety of pembrolizumab in combination with bevacizumab in recurrent glioblastoma (rGBM). *J Clin Oncol*. 2016.

89. Weathers S-P, Kamiya-Matsuoka C, Dervin S, et al. ATIM-37. SAFETY RUN-IN RESULTS OF A PHASE I/II STUDY TO EVALUATE THE SAFETY AND CLINICAL EFFICACY OF ATEZOLIZUMAB (ATEZO; aPDL1) IN COMBINATION WITH TEMOZOLOMIDE (TMZ) AND RADIATION IN PATIENTS WITH NEWLY DIAGNOSED GLIOBLASTOMA (GBM). *Neuro Oncol*. 2018. doi:10.1093/neuonc/noy148.032.

90. Lukas R V., Rodon J, Becker K, et al. Clinical activity and safety of atezolizumab in patients with recurrent glioblastoma. *J Neurooncol*. 2018. doi:10.1007/s11060-018-2955-9.

91. Ben Salama L, Duerinck J, Du Four S, et al. Safety of axitinib plus avelumab in patients with recurrent glioblastoma. *J Clin Oncol*. 2018. doi:10.1200/jco.2018.36.15_suppl.e14082.

92. Chi AS, Eisele S, Arrillaga-Romany I, et al. ATIM-01. A PHASE II, OPEN-LABEL, SINGLE ARM, MULTICENTER STUDY OF AVELUMAB WITH HYPOFRACTIONATED RE-IRRADIATION IN ADULT SUBJECTS WITH TRANSFORMED IDH MUTANT GLIOBLASTOMA. *Neuro Oncol*. 2017. doi:10.1093/neuonc/nox168.098.

93. Du W, Yang M, Turner A, et al. Tim-3 as a target for cancer immunotherapy and mechanisms of action. *Int J Mol Sci*. 2017. doi:10.3390/ijms18030645.

94. Han S, Feng S, Xu L, et al. Tim-3 on Peripheral CD4 + and CD8 + T Cells Is Involved in the Development of Glioma . *DNA Cell Biol*. 2014. doi:10.1089/dna.2013.2306.

95. Prendergast GC, Smith C, Thomas S, et al. Indoleamine 2,3-dioxygenase pathways of pathogenic inflammation and immune escape in cancer. *Cancer Immunol Immunother*. 2014. doi:10.1007/s00262-014-1549-4.

96. Adams S, Teo C, McDonald KL, et al. Involvement of the kynurenine pathway in human glioma pathophysiology. *PLoS One*. 2014. doi:10.1371/journal.pone.0112945.

97. Cheong JE, Ekkati A, Sun L. A patent review of IDO1 inhibitors for cancer. *Expert Opin Ther Pat*. 2018. doi:10.1080/13543776.2018.1441290.

98. The Editors of Encyclopaedia Britannica. Cell cycle. Encyclopaedia Britanica. https://www.britannica.com/science/cell-cycle. Published 2014. Accessed April 25, 2019.

99. Sherr CJ. The pezcoller lecture: Cancer cell cycles revisited. In: *Cancer Research*. ; 2000.

100. Maher EA, Furnari FB, Bachoo RM, et al. Malignant glioma: Genetics and biology of a grave matter. *Genes Dev*. 2001. doi:10.1101/gad.891601.

101. Ueki K, Ono Y, Henson JW, Efird JT, Von Deimling A, Louis DN. CDKN2/p16 or RB alterations occur in the majority of glioblastomas and are inversely correlated. *Cancer Res*. 1996.

102. Büschges R, Weber RG, Actor B, Lichter P, Collins VP, Reifenberger G. Amplification and Expression of Cyclin D Genes (CCND1 CCND2 and CCND3) in Human Malignant Gliomas . *Brain Pathol*. 2010. doi:10.1111/j.1750-3639.1999.tb00532.x.

103. Sarcar B, Kahali S, Prabhu AH, et al. Targeting Radiation-Induced G2 Checkpoint Activation with the Wee-1 Inhibitor MK-1775 in Glioblastoma Cell Lines. *Mol Cancer Ther*. 2011. doi:10.1158/1535-7163.mct-11-0469.

104. Begemann M, Kashimawo SA, Heitjan DF, Schiff PB, Bruce JN, Weinstein IB. Treatment of human glioblastoma cells with the staurosporine derivative CGP 41251 inhibits CDC2 and CDK2 kinase activity and increases radiation sensitivity. *Anticancer Res*. 1998.

105. Ajit Kumar Saxena GC. Targetting Cdks in Cancer: An Overview and New Insights. *J Cancer Sci Ther*. 2015. doi:10.4172/1948-5956.1000313.

106. Iorio AL, da Ros M, Genitori L, et al. Tumor response of temozolomide in combination with morphine in a xenograft model of human glioblastoma. *Oncotarget*. 2017. doi:10.18632/oncotarget.19875.

107. Wang H, Cai S, Bailey BJ, et al. Combination therapy in a xenograft model of glioblastoma: enhancement of the antitumor activity of temozolomide by an MDM2 antagonist. *J Neurosurg*. 2016. doi:10.3171/2016.1.jns152513.

108. Lan F, Yang Y, Han J, Wu Q, Yu H, Yue X. Sulforaphane reverses chemo-resistance to temozolomide in glioblastoma cells by NF-κB-dependent pathway downregulating MGMT expression. *Int J Oncol*. 2016. doi:10.3892/ijo.2015.3271.

109. Prasad G, Sottero T, Yang X, et al. Inhibition of PI3K/mTOR pathways in glioblastoma and implications for combination therapy with temozolomide. *Neuro Oncol*. 2011. doi:10.1093/neuonc/noq193.

110. Nitta Y, Shimizu S, Shishido-Hara Y, Suzuki K, Shiokawa Y, Nagane M. Nimotuzumab enhances temozolomide-induced growth suppression of glioma cells expressing mutant EGFR in vivo. *Cancer Med*. 2016. doi:10.1002/cam4.614.

111. Nonnenmacher L, Westhoff MA, Fulda S, et al. RIST: A potent new combination therapy for glioblastoma. *Int J Cancer*. 2015. doi:10.1002/ijc.29138.

112. Murai J, Zhang Y, Morris J, et al. Rationale for Poly(ADP-ribose) Polymerase (PARP) Inhibitors in Combination Therapy with Camptothecins or Temozolomide Based on PARP Trapping versus Catalytic Inhibition. *J Pharmacol Exp Ther*. 2014. doi:10.1124/jpet.113.210146.

113. Tentori L, Ricci-Vitiani L, Muzi A, et al. Pharmacological inhibition of poly(ADP-ribose) polymerase-1 modulates resistance of human glioblastoma stem cells to temozolomide. *BMC Cancer*. 2014. doi:10.1186/1471-2407-14-151.

114. Lesueur P, Chevalier F, El-Habr EA, et al. Radiosensitization Effect of Talazoparib, a Parp Inhibitor, on Glioblastoma Stem Cells Exposed to Low and High Linear Energy Transfer Radiation. *Sci Rep*. 2018. doi:10.1038/s41598-018-22022-4.

115. March J. *Advanced Organic Chemistry : Reactions, Mechanisms, and Structure*. 3rd ed. New York: Wiley; 1985.

116. Moss GP, Smith PAS, Tavernier D. Glossary of class names of organic compounds and reactivity intermediates based on structure (IUPAC Recommendations 1995). *Pure Appl Chem*. 1995;67(8-9):1307-1375. doi:10.1351/pac199567081307.

117. H W, H F, Y Z. Resveratrol inhibits hypoxia-induced glioma cell migration and invasion by the p-STAT3/miR-34a axis. *Neoplasma*. 2012. doi:10.4149/neo.

118. Kang S-H, Cho HT, Devi S, et al. Antitumor Effect of 2-Methoxyestradiol in a Rat Orthotopic Brain Tumor Model. *Cancer Res*. 2006;66(24):11991-11998. doi:10.1158/0008-5472.CAN-06-1320.

119. Jia W, Loria RM, Park MA, Yacoub A, Dent P, Graf MR. The neuro-steroid, 5-androstene 3β,17α diol; induces endoplasmic reticulum stress and autophagy through PERK/eIF2α signaling in malignant glioma cells and transformed fibroblasts. *Int J Biochem Cell Biol*. 2010;42(12):2019-2029. doi:10.1016/j.biocel.2010.09.003.

120. Graf MR, Jia W, Johnson RS, Dent P, Mitchell C, Loria RM. Autophagy and the functional roles of Atg5 and beclin-1 in the anti-tumor effects of 3β androstene 17α diol neuro-steroid on malignant glioma cells. *J Steroid Biochem Mol Biol*. 2009. doi:10.1016/j.jsbmb.2009.03.013.

121. Kumar S, Narasimhan B, Lim SM, Ramasamy K, Mani V, Shah SAA. Design, Synthesis and Biological Potential of 5-(2-Amino-6-(3/4-bromophenyl)pyrimidin-4-yl)benzene-1,3-diol Scaffolds as Promising Antimicrobial and Anticancer agents. *Mini-Reviews Med Chem*. 2018;18. doi:10.2174/1389557518666181009141924.

122. Bair KW, 1·1 ’, Tuttle RL, Knick VC, Cory M, Mckee1 DD. *(L-Pyrenylmethyl)Amino Alcohols, a New Class of Antitumor DNA Intercalators. Discovery and Initial Amine Side Chain Structure-Activity Studies*. Vol 33.; 1990. https://pubs.acs.org/sharingguidelines. Accessed May 13, 2019.

123. Peterson KE, Cinelli MA, Morrell AE, et al. Alcohol-, diol-, and carbohydrate-substituted indenoisoquinolines as topoisomerase I inhibitors: investigating the relationships involving stereochemistry, hydrogen bonding, and biological activity. *J Med Chem*. 2011;54(14):4937-4953. doi:10.1021/jm101338z.

124. Graf MR, Jia W, Lewbart ML, Loria RM. The anti-tumor effects of androstene steroids exhibit a strict structure-activity relationship dependent upon the orientation of the hydroxyl group on carbon-17. *Chem Biol Drug Des*. 2009;74(6):625-629. doi:10.1111/j.1747-0285.2009.00900.x.

125. Yuan X-L, Mao X-X, Du Y-M, Yan P-Z, Hou X-D, Zhang Z-F. Anti-Tumor Activity of Cembranoid-Type Diterpenes Isolated from Nicotiana tabacum L. *Biomolecules*. 2019;9(2). doi:10.3390/biom9020045.

126. Padrón J, Martin VS, Hadjipavlou-Litina D, et al. Synthesis, in vitro cytotoxicity and in vivo anti-inflammatory activity of long chain 3-amino-1,2-diols. *Bioorg Med Chem Lett*. 1999;9(6):821-826. doi:10.1016/S0960-894X(99)00084-0.

127. Brosnan RJ, Pham TL. Hydrocarbon molar water solubility predicts NMDA vs. GABAA receptor modulation. *BMC Pharmacol Toxicol*. 2014. doi:10.1186/2050-6511-15-62.

128. Dildy-Mayfield JE, Mihic SJ, Liu Y, Deitrich RA, Harris RA. Actions of long chain alcohols on GABAA and glutamate receptors: relation to in vivo effects. *Br J Pharmacol*. 1996. doi:10.1111/j.1476-5381.1996.tb15413.x.

129. Peoples RW, Ren H. Inhibition of N-methyl-D-aspartate receptors by straight-chain diols: implications for the mechanism of the alcohol cutoff effect. *Mol Pharmacol*. 2002;61(1):169-176. doi:10.1124/mol.61.1.169.

130. Luján R, Shigemoto R, López-Bendito G. Glutamate and GABA receptor signalling in the developing brain. *Neuroscience*. 2005. doi:10.1016/j.neuroscience.2004.09.042.

131. Schlett K. Glutamate as a Modulator of Embryonic and Adult Neurogenesis. *Curr Top Med Chem*. 2006. doi:10.2174/156802606777323665.

132. Luk KC, Kennedy TE, Sadikot AF. Glutamate promotes proliferation of striatal neuronal progenitors by an NMDA receptor-mediated mechanism. *J Neurosci*. 2003.

133. Traynelis SF, Wollmuth LP, McBain CJ, et al. Glutamate Receptor Ion Channels: Structure, Regulation, and Function. *Pharmacol Rev*. 2010. doi:10.1124/pr.109.002451.

134. Sontheimer H. A role for glutamate in growth and invasion of primary brain tumors. *J Neurochem*. 2008. doi:10.1111/j.1471-4159.2008.05301.x.

135. Takano T, Lin JHC, Arcuino G, Gao Q, Yang J, Nedergaard M. Glutamate release promotes growth of malignant gliomas. *Nat Med*. 2001;7(9):1010-1015. doi:10.1038/nm0901-1010.

136. Arcella A, Carpinelli G, Battaglia G, et al. Pharmacological blockade of group II metabotropic glutamate receptors reduces the growth of glioma cells in vivo. *Neuro Oncol*. 2005. doi:10.1215/S1152851704000961.

137. Deutsch SI, Tang AH, Burket JA, Benson AD. NMDA receptors on the surface of cancer cells: Target for chemotherapy? *Biomed Pharmacother*. 2014. doi:10.1016/j.biopha.2014.03.012.

138. Ramaswamy P, Aditi Devi N, Hurmath Fathima K, Dalavaikodihalli Nanjaiah N. Activation of NMDA receptor of glutamate influences MMP-2 activity and proliferation of glioma cells. *Neurol Sci*. 2014;35(6):823-829. doi:10.1007/s10072-013-1604-5.

139. Stork G, Benaim J. Monoalkylation of α,β-Unsaturated Ketones via Metalloenamines: 1-butyl-10-methyl-$\Delta^{1(9)}$-2-octalone. *Org Synth*. 1977;57:69. http://www.orgsyn.org/demo.aspx?prep=cv6p0242. Accessed April 30, 2019.

140. Rollas S, Küçükgüzel ŞG. Biological activities of hydrazone derivatives. *Molecules*. 2007;12(8):1910-1939. doi:10.3390/12081910.

141. Singh M, Raghav N. Biological activities of hydrazones: A review. *Int J Pharm Pharm Sci*. 2011;3(4):26-32. doi:10.1186/1752-153X-5-2; Rollas, S., Kiiciikguzel, S.G., Biological Activities of Hydrazone Derivatives (2007) Molecules, 12, pp. 1910-1939; Yadav, J., Pandeya, S.N., Nath, G., Singh, S.P., Synthesis and antibacterial evaluation of some hydrazones of flavanoid derivatives (2010) J Chem Pharm Res, 2 (4), pp. 558-563; Khan, S.U., Mullick, P., Pandit, S., Kaushik, D., Synthesis of hydrazones derivatives of Quinoxaline-prospective antimicrobial and anti-inflammatory agents (2009) Acta Polonica Pharmac.

142. Suvarapu LN, Seo YK, Baek SO, et al. A Review on Biological Importance of Hydrazones. *Eur J Med Chem*. 2013. doi:10.1016/j.ejmech.2015.05.010.

143. Wardakhan WW, El-Sayed NNE, Mohareb RM. Synthesis and anti-tumor evaluation of novel hydrazide and hydrazide-hydrazone derivatives. *Acta Pharm*. 2013. doi:10.2478/acph-2013-0004.

144. Mandewale MC, Patil UC, Shedge S V., Dappadwad UR, Yamgar RS. A review on quinoline hydrazone derivatives as a new class of potent antitubercular and

anticancer agents. *Beni-Suef Univ J Basic Appl Sci*. 2017. doi:10.1016/j.bjbas.2017.07.005.

145. Loncle C, Brunel JM, Vidal N, Dherbomez M, Letourneux Y. Synthesis and antifungal activity of cholesterol-hydrazone derivatives. *Eur J Med Chem*. 2004;39(12):1067-1071. doi:10.1016/j.ejmech.2004.07.005.

146. Despaigne AAR, Parrilha GL, Izidoro JB, et al. 2-Acetylpyridine- and 2-benzoylpyridine-derived hydrazones and their gallium(III) complexes are highly cytotoxic to glioma cells. *Eur J Med Chem*. 2012. doi:10.1016/j.ejmech.2012.01.051.

147. Lacerda RB, da Silva LL, de Lima CKF, et al. Discovery of Novel Orally Active Anti-Inflammatory N-Phenylpyrazolyl-N-Glycinyl-Hydrazone Derivatives That Inhibit TNF-α Production. *PLoS One*. 2012. doi:10.1371/journal.pone.0046925.

148. Hall IH, Peaty NJ, Henry JR, Easmon J, Heinisch G, Pürstinger G. Investigations on the mechanism of action of the novel antitumor agents 2-benzothiazolyl, 2-benzoxazolyl, and 2-benzimidazolyl hydrazones derived from 2-acetylpyridine. *Arch Pharm (Weinheim)*. 1999. doi:10.1002/(SICI)1521-4184(19994)332:4<115::AID-ARDP115>3.0.CO;2-G.

149. Kucukoglu K, Gul M, Gul HI, Cetin-Atalay R, Geny B. Cytotoxicities of novel hydrazone compounds with pyrrolidine moiety: inhibition of mitochondrial respiration may be a possible mechanism of action for the cytotoxicity of new hydrazones. *Med Chem Res*. 2018;27(9):2116-2124. doi:10.1007/s00044-018-2220-y.

150. Xia Y, Fan C-D, Zhao B-X, Zhao J, Shin D-S, Miao J-Y. Synthesis and structure–activity relationships of novel 1-arylmethyl-3-aryl-1H-pyrazole-5-carbohydrazide hydrazone derivatives as potential agents against A549 lung cancer cells. *Eur J Med Chem*. 2008;43(11):2347-2353. doi:10.1016/J.EJMECH.2008.01.021.

151. Danciu OC, Nicholas MK, Holdhoff M, et al. Phase I study of procaspase activating compound-1 (PAC-1) for treatment of advanced malignancies. *J Clin Oncol*. 2018;36(15_suppl):TPS2621-TPS2621. doi:10.1200/JCO.2018.36.15_suppl.TPS2621.

152. Sachdev E, Sachdev D, Mita M. Aldoxorubicin for the treatment of soft tissue sarcoma. *Expert Opin Investig Drugs*. 2017. doi:10.1080/13543784.2017.1371134.

153. Festuccia C, Muzi P, Gravina GL, et al. Tyrosine kinase inhibitor CEP-701 blocks the NTRK1/NGF receptor and limits the invasive capability of prostate cancer cells in vitro. *Int J Oncol*. 2007.

154. Palanivel S, Zhurina A, Doan P, et al. In vitro characterization of arylhydrazones of active methylene derivatives. *Saudi Pharm J SPJ Off Publ Saudi Pharm Soc*. 2018;26(3):430-436. doi:10.1016/j.jsps.2017.12.018.

155. Xu G, Abad MC, Connolly PJ, et al. 4-Amino-6-arylamino-pyrimidine-5-carbaldehyde hydrazones as potent ErbB-2/EGFR dual kinase inhibitors. *Bioorganic Med Chem Lett*. 2008. doi:10.1016/j.bmcl.2008.07.020.

156. Sawutz DG, Bode DC, Briggs GM, et al. In vitro characterization of a novel series of platelet-derived growth factor receptor tyrosine kinase inhibitors. *Biochem Pharmacol*. 1996. doi:10.1016/0006-2952(96)00112-8.

157. Wilhelm S, Carter C, Lynch M, et al. Discovery and development of sorafenib: A multikinase inhibitor for treating cancer. *Nat Rev Drug Discov*. 2006. doi:10.1038/nrd2130.

158. Richeldi L, Costabel U, Selman M, et al. Efficacy of a Tyrosine Kinase Inhibitor in Idiopathic Pulmonary Fibrosis. *N Engl J Med*. 2011. doi:10.1056/NEJMoa1103690.

159. Morabito A, Piccirillo MC, Falasconi F, et al. Vandetanib (ZD6474), a Dual Inhibitor of Vascular Endothelial Growth Factor Receptor (VEGFR) and Epidermal Growth Factor Receptor (EGFR) Tyrosine Kinases: Current Status and Future Directions. *Oncologist*. 2009. doi:10.1634/theoncologist.2008-0261.

160. El-Azab AS, Abdel-Aziz AAM, Abou-Zeid LA, et al. Synthesis, antitumour activities and molecular docking of thiocarboxylic acid ester-based NSAID scaffolds: COX-2 inhibition and mechanistic studies. *J Enzyme Inhib Med Chem*. 2018. doi:10.1080/14756366.2018.1474878.

161. Ashizawa T, Kawashima K, Kanda Y, et al. Antitumor activity of KF22678, a novel thioester derivative of leinamycin. *Anticancer Drugs*. 1999. doi:10.1097/00001813-199910000-00006.

162. Hoque MA, Islam N, Kato T, Nishino N, Ito A, Yoshida M. Design and synthesis of mono and bicyclic tetrapeptides thioester as potent inhibitor of histone deacetylases. doi:10.1007/s00726-014-1800-5.

163. Baud MGJ, Leiser T, Petrucci V, et al. Thioester derivatives of the natural product psammaplin A as potent histone deacetylase inhibitors. *Beilstein J Org Chem*. 2013;9(1):81-88. doi:10.3762/bjoc.9.11.

164. Baud MGJ, Leiser T, Petrucci V, et al. Thioester derivatives of the natural product psammaplin A as potent histone deacetylase inhibitors. *Beilstein J Org Chem*. 2013;9(1):81-88. doi:10.3762/bjoc.9.11.

165. Kohli RM, Takagi J, Walsh CT. The thioesterase domain from a nonribosomal peptide synthetase as a cyclization catalyst for integrin binding peptides. *Proc Natl Acad Sci*. 2002. doi:10.1073/pnas.251668398.

166. Chen T, Zhang RH, He SC, et al. Synthesis and anti-angiogenic activity of novel gambogic acid derivatives. *Molecules*. 2012. doi:10.3390/molecules17066269.

167. Ferrara N, Gerber HP, LeCouter J. The biology of VEGF and its receptors. *Nat Med*. 2003. doi:10.1038/nm0603-669.

168. Ferrara N, Hillan KJ, Gerber HP, Novotny W. Discovery and development of bevacizumab, an anti-VEGF antibody for treating cancer. *Nat Rev Drug Discov*. 2004. doi:10.1038/nrd1381.

169. Holash J, Davis S, Papadopoulos N, et al. VEGF-Trap: A VEGF blocker with potent antitumor effects. *Proc Natl Acad Sci*. 2002. doi:10.1073/pnas.172398299.

170. Ferrari G, Pintucci G, Seghezzi G, Hyman K, Galloway AC, Mignatti P. VEGF, a prosurvival factor, acts in concert with TGF-beta1 to induce endothelial cell apoptosis. *Proc Natl Acad Sci*. 2006. doi:10.1073/pnas.0605556103.

171. I. Scorei R, Popa R. Boron-Containing Compounds as Preventive and Chemotherapeutic Agents for Cancer. *ACAMC*. 2010;10(4):346-351. doi:10.2174/187152010791162289.

172. Jolanta D. Żołnierczyk, Agnieszka B. Olejniczak, Adam Mieczkowski, Jerzy Z. Błoński, Zofia M. Kiliańska, Tadeusz Robak, Zbigniew J. Leśnikowskie. In Vitro Antileukemic Activity of Novel Adenosine Derivatives Bearing Boron Cluster Modification. *Bioorg Med Chem*. 2016;24(21):5076-5087.

173. Soriano-Ursúa MA, Das BC, Trujillo-Ferrara JG. Boron-containing compounds: chemico-biological properties and expanding medicinal potential in prevention, diagnosis and therapy. *Expert Opin Ther Pat*. 2014. doi:10.1517/13543776.2014.881472.

174. Yang F, Zhu M, Zhang J, Zhou H. Synthesis of biologically active boron-containing compounds. *Medchemcomm*. 2018;9(2):201-211. doi:10.1039/c7md00552k.

175. Yang F, Zhu M, Zhang J, Zhou H. Synthesis of biologically active boron-containing compounds. *Medchemcomm*. 2018. doi:10.1039/c7md00552k.

176. Philipp M, Bender ML. Inhibition of serine proteases by arylboronic acids. *Proc Natl Acad Sci U S A*. 1971;68(2):478-480. doi:10.1073/pnas.68.2.478.

177. Shimizu K, Maruyama M, Yasui Y, Minegishi H, Ban HS, Nakamura H. Boron-containing phenoxyacetanilide derivatives as hypoxia-inducible factor (HIF)-1α

inhibitors. *Bioorg Med Chem Lett*. 2010;20(4):1453-1456. doi:10.1016/J.BMCL.2009.12.037.

178. Richardson PG, Sonneveld P, Schuster MW, et al. Bortezomib or High-Dose Dexamethasone for Relapsed Multiple Myeloma. *N Engl J Med*. 2005. doi:10.1056/NEJMoa043445.

179. Robak T. Bortezomib in the treatment of mantle cell lymphoma. *Futur Oncol*. 2015. doi:10.2217/fon.15.191.

180. Lei M, Feng H, Bai E, et al. Design, synthesis, in vitro and in vivo evaluation, and structure-activity relationship (SAR) discussion of novel dipeptidyl boronic acid proteasome inhibitors as orally available anti-cancer agents for the treatment of multiple myeloma and mechanism studies. *Bioorg Med Chem*. 2018;26(14):3975-3981. doi:10.1016/J.BMC.2018.06.020.

181. Kong Y, Wang K, Edler MC, et al. A boronic acid chalcone analog of combretastatin A-4 as a potent anti-proliferation agent. *Bioorganic Med Chem*. 2010. doi:10.1016/j.bmc.2009.11.003.

182. Ban HS, Usui T, Nabeyama W, Morita H, Fukuzawa K, Nakamura H. Discovery of boron-conjugated 4-anilinoquinazoline as a prolonged inhibitor of EGFR tyrosine kinase. *Org Biomol Chem*. 2009;7(21):4415. doi:10.1039/b909504g.

183. Urbańska K, Mandal CC. Advanced Views of Glioblastoma Multiforme U-87 Cells for Therapy of Brain Tumor. *Ijcbr*. 2014.

184. Jacobs VL, Valdes PA, Hickey WF, De Leo JA. Current Review of in Vivo GBM Rodent Models: Emphasis on the CNS-1 Tumour Model . *ASN Neuro*. 2011. doi:10.1042/an20110014.

185. Cerrato JA, Yung WKA, Liu T-J. Introduction of mutant <I>p53</I> into a wild-type <I>p53</I>-expressing glioma cell line confers sensitivity to Ad-p53-induced apoptosis. *Neuro Oncol*. 2004. doi:10.1215/s1522851700000430.

186. Welch WC, Morrison RS, Gross JL, et al. Morphologic, immunologic, biochemical, and cytogenetic characteristics of the human glioblastoma-derived cell line, SNB-19. *Vitr Cell Dev Biol - Anim J Soc Vitr Biol*. 1995. doi:10.1007/BF02634314.

187. Burgoyne RD, Geisow MJ. The annexin family of calcium-binding proteins. Review article. *Cell Calcium*. 1989. doi:10.1016/0143-4160(89)90038-9.

188. Trump BF, Berezesky IK, Chang SH, Phelps PC. The pathways of cell death: Oncosis, apoptosis, and necrosis. In: *Toxicologic Pathology*. ; 1997. doi:10.1177/019262339702500116.

189. Riccardi C, Nicoletti I. Analysis of apoptosis by propidium iodide staining and flow cytometry. *Nat Protoc*. 2006. doi:10.1038/nprot.2006.238.

190. Labuschagne CF, Brenkman AB. Current methods in quantifying ROS and oxidative damage in Caenorhabditis elegans and other model organism of aging. *Ageing Res Rev*. 2013. doi:10.1016/j.arr.2013.09.003.

191. Wang Z, Gerstein M, Snyder M. RNA-Seq: a revolutionary tool for transcriptomics. *Nat Rev Genet*. 2009. doi:10.1038/nrg2484.

192. Han Y, Gao S, Muegge K, Zhang W, Zhou B. Advanced applications of RNA sequencing and challenges. *Bioinform Biol Insights*. 2015. doi:10.4137/BBI.S28991.

193. Liu Y, Beyer A, Aebersold R. On the Dependency of Cellular Protein Levels on mRNA Abundance. *Cell*. 2016. doi:10.1016/j.cell.2016.03.014.

194. Dobin A, Davis CA, Schlesinger F, et al. STAR: Ultrafast universal RNA-seq aligner. *Bioinformatics*. 2013. doi:10.1093/bioinformatics/bts635.

195. Rapaport F, Khanin R, Liang Y, et al. Comprehensive evaluation of differential gene expression analysis methods for RNA-seq data. *Genome Biol*. 2013. doi:10.1186/gb-2013-14-9-r95.

196. Li H, Handsaker B, Wysoker A, et al. The Sequence Alignment/Map format and SAMtools. *Bioinformatics*. 2009. doi:10.1093/bioinformatics/btp352.

197. Anders S, Pyl PT, Huber W. HTSeq-A Python framework to work with high-throughput sequencing data. *Bioinformatics*. 2015. doi:10.1093/bioinformatics/btu638.

198. Love MI, Huber W, Anders S. Moderated estimation of fold change and dispersion for RNA-seq data with DESeq2. *Genome Biol*. 2014. doi:10.1186/s13059-014-0550-8.

199. Benjamini Y, Hochberg Y. Controlling the false discovery rate: a practical and powerful approach to multiple testing. *J R Stat Soc Ser B*. 1995. doi:10.2307/2346101.

200. Ashburner M, Ball CA, Blake JA, et al. Gene ontology: Tool for the unification of biology. *Nat Genet*. 2000. doi:10.1038/75556.

201. Yu G, Wang L-G, Han Y, He Q-Y. clusterProfiler: an R Package for Comparing Biological Themes Among Gene Clusters. *Omi A J Integr Biol*. 2012. doi:10.1089/omi.2011.0118.

202. Noch E, Khalili K. Molecular mechanisms of necrosis in glioblastoma: The role of glutamate excitotoxicity. *Cancer Biol Ther*. 2009. doi:10.4161/cbt.8.19.9762.

203. van Lith SAM, Navis AC, Verrijp K, et al. Glutamate as chemotactic fuel for diffuse glioma cells: Are they glutamate suckers? *Biochim Biophys Acta - Rev Cancer*. 2014. doi:10.1016/j.bbcan.2014.04.004.

204. Voronov E, Carmi Y, Apte RN. The role IL-1 in tumor-mediated angiogenesis. *Front Physiol*. 2014. doi:10.3389/fphys.2014.00114.

205. Salmeron K, Aihara T, Redondo-Castro E, Pinteaux E, Bix G. IL-1alpha induces angiogenesis in brain endothelial cells in vitro: Implications for brain angiogenesis after acute injury. *J Neurochem*. 2016. doi:10.1111/jnc.13422.

206. Tateishi K, Iafrate AJ, Ho Q, et al. Myc-Driven glycolysis is a therapeutic target in glioblastoma. *Clin Cancer Res*. 2016. doi:10.1158/1078-0432.CCR-15-2274.

207. Mongiardi MP, Savino M, Falchetti ML, et al. c-MYC inhibition impairs hypoxia response in glioblastoma multiforme. *Oncotarget*. 2016. doi:10.18632/oncotarget.8921.

208. Zheng H, Ying H, Yan H, et al. Pten and p53 converge on c-Myc to control differentiation, self-renewal, and transformation of normal and neoplastic stem cells in glioblastoma. In: *Cold Spring Harbor Symposia on Quantitative Biology*. ; 2008. doi:10.1101/sqb.2008.73.047.

209. Mei Y, Wu M. Noncoding RNAs regulating p53 and c-Myc signaling. In: *Advances in Experimental Medicine and Biology*. ; 2016. doi:10.1007/978-981-10-1498-7_13.

210. Sachdeva M, Zhu S, Wu F, et al. p53 represses c-Myc through induction of the tumor suppressor miR-145. *Proc Natl Acad Sci U S A*. 2009. doi:10.1073/pnas.0808042106.

211. Lin T, Hou PF, Meng S, et al. Emerging roles of p53 related lncRNAs in cancer progression: A systematic review. *Int J Biol Sci*. 2019. doi:10.7150/ijbs.33218.

212. He G, Siddik ZH, Huang Z, et al. Induction of p21 by p53 following DNA damage inhibits both Cdk4 and Cdk2 activities. *Oncogene*. 2005. doi:10.1038/sj.onc.1208474.

213. Abraham SA, Hopcroft LEM, Carrick E, et al. Dual targeting of p53 and c-MYC selectively eliminates leukaemic stem cells. *Nature*. 2016. doi:10.1038/nature18288.

214. Shannon P, Markiel A, Ozier O, et al. Cytoscape: A software Environment for integrated models of biomolecular interaction networks. *Genome Res*. 2003. doi:10.1101/gr.1239303.

215. Franovic A, Gunaratnam L, Smith K, Robert I, Patten D, Lee S. Translational up-regulation of the EGFR by tumor hypoxia provides a nonmutational explanation for its overexpression in human cancer. *Proc Natl Acad Sci U S A*. 2007. doi:10.1073/pnas.0702387104.

216. Lo HW, Hung MC. Nuclear EGFR signalling network in cancers: Linking EGFR pathway to cell cycle progression, nitric oxide pathway and patient survival. *Br J Cancer*. 2006. doi:10.1038/sj.bjc.6602941.

217. Jaganathan S, Yue P, Paladino DC, Bogdanovic J, Huo Q, Turkson J. A functional nuclear epidermal growth factor receptor, Src and Stat3 heteromeric complex in pancreatic cancer cells. *PLoS One*. 2011. doi:10.1371/journal.pone.0019605.

218. Brand TM, Iida M, Li C, Wheeler DL. The nuclear epidermal growth factor receptor signaling network and its role in cancer. *Discov Med*. 2011.

219. Han W, Carpenter RL, Cao X, Lo HW. STAT1 gene expression is enhanced by nuclear EGFR and HER2 via cooperation With STAT3. *Mol Carcinog*. 2013. doi:10.1002/mc.21936.

220. Puliyappadamba VT, Chakraborty S, Chauncey SS, et al. Opposing effect of EGFRWT on EGFRvIII-mediated NF-κB activation with RIP1 as a cell death switch. *Cell Rep*. 2013. doi:10.1016/j.celrep.2013.07.025.

221. Xia Y, Shen S, Verma IM. NF-κB, an active player in human cancers. *Cancer Immunol Res*. 2014. doi:10.1158/2326-6066.CIR-14-0112.

222. Bhat KPL, Balasubramaniyan V, Vaillant B, et al. Mesenchymal Differentiation Mediated by NF-κB Promotes Radiation Resistance in Glioblastoma. *Cancer Cell*. 2013. doi:10.1016/j.ccr.2013.08.001.

223. Tchoghandjian A, Jennewein C, Eckhardt I, Rajalingam K, Fulda S. Identification of non-canonical NF-kB signaling as a critical mediator of smac mimetic-stimulated migration and invasion of glioblastoma cells. *Cell Death Dis*. 2013. doi:10.1038/cddis.2013.70.

224. Lee JG, Kay EDP. NF-κB is the transcription factor for FGF-2 that causes endothelial mesenchymal transformation in cornea. *Investig Ophthalmol Vis Sci*. 2012. doi:10.1167/iovs.11-9102.

225. Larsen AK, Ouaret D, El Ouadrani K, Petitprez A. Targeting EGFR and VEGF(R) pathway cross-talk in tumor survival and angiogenesis. *Pharmacol Ther*. 2011. doi:10.1016/j.pharmthera.2011.03.012.

226. Demyanets S, Kaun C, Rychli K, et al. Oncostatin M-enhanced vascular endothelial growth factor expression in human vascular smooth muscle cells involves PI3K-, p38 MAPK-, Erk1/2- and STAT1/STAT3-dependent pathways and is attenuated by interferon-γ. *Basic Res Cardiol*. 2011. doi:10.1007/s00395-010-0141-0.

227. Li JL, Harris AL. Cross-talk of VEGF and Notch pathways in tumour angiogenesis: Therapeutic implications. *Front Biosci*. 2009. doi:10.2735/3438.

228. Yahyanejad S, King H, Iglesias VS, et al. Targeting notch pathway in glioblastoma. *Radiother Oncol*. 2016.

229. Ying M, Wang S, Sang Y, et al. Regulation of glioblastoma stem cells by retinoic acid: Role for Notch pathway inhibition. *Oncogene*. 2011;30(31):3454-3467. doi:10.1038/onc.2011.58.

230. Aguirre A, Rubio ME, Gallo V. Notch and EGFR pathway interaction regulates neural stem cell number and self-renewal. *Nature*. 2010. doi:10.1038/nature09347.

231. Bazzoni R, Bentivegna A. Role of Notch Signaling Pathway in Glioblastoma Pathogenesis. *Cancers (Basel)*. 2019. doi:10.3390/cancers11030292.

232. Patwardhan PP, Ivy KS, Musi E, Stanchina E de, Schwartz GK. Significant blockade of multiple receptor tyrosine kinases by MGCD516 (Sitravatinib), a novel small molecule inhibitor, shows potent anti-tumor activity in preclinical models of sarcoma. *Oncotarget*. 2016. doi:10.18632/oncotarget.6547.

233. Lee H, Saini N, Howard EW, et al. Ganetespib targets multiple levels of the receptor tyrosine kinase signaling cascade and preferentially inhibits ErbB2-overexpressing breast cancer cells. *Sci Rep*. 2018. doi:10.1038/s41598-018-25284-0.

234. Rich JN, Sathornsumetee S, Keir ST, et al. ZD6474, a novel tyrosine kinase inhibitor of vascular endothelial growth factor receptor and epidermal growth factor receptor, inhibits tumor growth of multiple nervous system tumors. *Clin Cancer Res*. 2005. doi:10.1158/1078-0432.CCR-05-0319.

235. Chung SW, Bae SM, Lee M, et al. LHT7, a chemically modified heparin, inhibits multiple stages of angiogenesis by blocking VEGF, FGF2 and PDGF-B signaling pathways. *Biomaterials*. 2015. doi:10.1016/j.biomaterials.2014.10.004.

236. Shan Y, Wang B, Zhang J. New strategies in achieving anti-angiogenic effect: Multiplex inhibitors suppressing compensatory activations of RTKs. *Med Res Rev*. 2018. doi:10.1002/med.21517.

PUBLICATIONS

PUBLICATION

I

Decane-1,2-diol derivatives as potential antitumor agents for the treatment of Glioblastoma

Anisha Viswanathan, Anastasia Zhurina, Benedicta Assoah, Aleksi Paakkunainen, Aliyu Musa, Dinesh Kute, Konda Mani Saravanan, Olli Yli-Harja, Nuno R. Candeias, Meenakshisundaram Kandhavelu

European Journal of Pharmacology, Volume 837, 15 October 2018, Pages 105-116
https://doi.org/10.1016/j.ejphar.2018.08.041

Publication reprinted with the permission of the copyright holders.

European Journal of Pharmacology 837 (2018) 105–116

Contents lists available at ScienceDirect

European Journal of Pharmacology

journal homepage: www.elsevier.com/locate/ejphar

Molecular and cellular pharmacology

Decane-1,2-diol derivatives as potential antitumor agents for the treatment of glioblastoma

Anisha Viswanathan[a], Anastasia Zhurina[a], Benedicta Assoah[b], Aleksi Paakkunainen[b], Aliyu Musa[c], Dinesh Kute[a], Konda Mani Saravanan[d], Olli Yli-Harja[a,e], Nuno R. Candeias[b,*], Meenakshisundaram Kandhavelu[a,*]

[a] Molecular Signaling Lab, Computational Systems Biology Research Group, BioMediTech and Faculty of Biomedical Sciences and Engineering, Tampere University of Technology, P.O. Box 553, 33101 Tampere, Finland
[b] Laboratory of Chemistry and Bioengineering, Tampere University of Technology, Korkeakoulunkatu 8, 33101 Tampere, Finland
[c] Predictive Medicine and Data Analytics Lab, Faculty of Biomedical Sciences and Engineering, Tampere University of Technology, P.O. Box 553, 33101 Tampere, Finland
[d] Centre of Advanced Study in Crystallography & Biophysics, University of Madras, Chennai 600025, India
[e] Institute for Systems Biology, 1441N 34th Street, Seattle, WA 98103-8904, USA

ARTICLE INFO

Keywords:
Alcohols
Anti-cancer drugs
Glioblastoma

ABSTRACT

Glioblastoma remains the most common and aggressive type of malignant brain tumor among adults thus, considerable attention has been given to discovery of novel anti-tumor drugs for its treatment. This study reports the synthesis of a series of twelve novel decane-1,2-diol derivatives and evaluation of its anti-tumor activity in mammalian glioblastoma cell lines, U87 and LN229. Starting from decane-1,2-diol, several derivatives were prepared using a diversity oriented synthesis approach through which a small library composed of esters, silyl ethers, sulfonates, sulfites, sulfates, ketals, and phosphonates was built. The decane-1,2-diol ditosylated derivative, DBT, found to have higher cytotoxicity than the standard drug cisplatin, has IC_{50} value of 52 μM in U87 and 270 μM in LN229. Migration analysis of U87 cell line treated with the DBT indicated its ability to effectively suppress proliferation during initial hours of treatment and decrease anti-proliferative property over time. Additionally, DBT was assessed for its role in apoptosis, oxidative stress and caspase 3/7 activation in U87. Interestingly, our experiments indicated that its cytotoxicity is independent of Reactive oxygen species induced caspase 3/7 activity. The compound also exhibited caspase independent apoptosis activity in U87. DBT treatment led to G1/S cell cycle arrest and apoptosis induction of glioma cell lines. In addition, we identified 1533 genes with significant changes at the transcriptional level, in response to DBT. A molecular docking study accounting for the interaction of DBT with NMDA receptor disclosed several hydrogen bonds and charged residue interactions with 17 amino acids, which might be the basis of the DBT cytotoxicity observed. We conclude that this molecule exerts its cytotoxicity *via* caspase 3/7 independent pathways in glioblastoma cells. Concisely, simple decane-1,2-diol derivatives might serve as scaffolds for the development of effective anti-glioblastoma agents.

1. Introduction

Increasing recurrence of brain tumors and challenges in the current oncology treatments points to an urgent need to develop alternative or synergistic anticancer drugs, for tumor progression reduction. Glioblastoma, also known as glioblastoma multiforme (GBM) is the most aggressive cancer that affects the glial tissues of the brain. It is a grade IV brain cancer with poor prognosis, short median survival (Wen and Kesari, 2008) and limited response to current treatment methods (Jue and McDonald, 2016). The current standard of care for GBM includes maximal safe surgical removal of tumor and irradiation with or without adjuvant chemotherapeutics (Chinot et al., 2014; Stupp et al., 2005). The exclusion of current drugs due to the blood–brain barrier (BBB) (Pardridge, 2005; Weidle et al., 2015) together with the scarce distribution of therapeutics within the tumor region (Agarwal et al., 2011) make adequate drug delivery a critical challenge in advancing glioblastoma treatment. High intra-tumoral heterogeneity (Davis, 2016; Patel et al., 2014), high proliferation rate and chemo-resistance (Garrido et al., 2014; Hombach-Klonisch et al., 2017) are among the factors that make the cure of glioblastoma quite complex.

---

* Corresponding authors.
E-mail addresses: nuno.rafaelcandeias@tut.fi (N.R. Candeias), meenakshisundaram.kandhavelu@tut.fi (M. Kandhavelu).

https://doi.org/10.1016/j.ejphar.2018.08.041
Received 18 May 2018; Received in revised form 29 August 2018; Accepted 30 August 2018
Available online 01 September 2018
0014-2999/ © 2018 Elsevier B.V. All rights reserved.

The inflammatory process occurring inside glioblastoma tumor cells is related with the hyper-activation of *N*-methyl-D-aspartate (NMDA) receptors eventually resulting in cell death (Takano et al., 2001). Blocking the activation of NMDA receptors abrogates glioma cells proliferation (Ramaswamy et al., 2014). Fingolimod (FTY720) has been reported to be a potential therapeutic agent for the treatment of GBM (Estrada-Bernal et al., 2012), and it can also inhibit NMDA-induced intracellular calcium ($[Ca^{2+}]i$) increase, suggesting a negative modulatory effect on NMDA receptor in neurons (Yan et al., 2015). Consequently, NMDA receptors have been pointed as potential targets for chemotherapy (Deutsch et al., 2014) and object of studies in the development of anti-tumor agents for glioblastoma treatment (Cacciatore et al., 2017; Markert et al., 2001; Stepulak et al., 2014).

Straight chain diols have been previously studied as small molecules capable of interacting with glioma cells. *N*-Alkanols, particularly 1-octanol and 1-nonanol, were reported to inhibit NMDA receptors (IC_{50} = 1.2 and 1.39 mM, respectively) whilst a cutoff effect was observed for longer alcohols (Brosnan and Pham, 2014; Dildy-Mayfield et al., 1996). Follow-up studies, focused on straight-chain diols and on the importance of the relative position of the hydroxyl groups demonstrated that the observed cutoff could not be explained by a size exclusion mechanism, since longer C_9–C_{14} 1,Ω-diols also inhibited NMDA-activated current (Peoples, 2002). Generally, diols were stronger NMDA receptor inhibitors than straight chain alcohols with similar carbon content. Comparison of C_6 and C_8 1,2-diols with the corresponding 1,Ω-diols, led to stronger inhibition by the vicinal diols which was suggested to arise from their increased hydrophobicity. Furthermore, more hydrophobic decane-1,2- and 1,10-diols were determined to have stronger inhibitory properties (IC_{50} = 1.44 and 1.61 mM, respectively), although in similar degree. While the NMDA receptor inhibition mechanism by the alcohols and diols remained elusive, the hydrophobic interactions were deemed important to achieve some degree of inhibition.

With such preliminary studies in mind, we envisioned that the different reactivity of the primary and secondary hydroxyl groups of decane-1,2-diol could be explored to prepare non-polar derivatives of this diol. While the new derivatives would have increased lipophilicity when compared with the synthetic precursor, namely by obviation of the hydrogen bond donor group, the introduction of other functional groups able to act as hydrogen bond acceptors could lead to the establishment of interactions with different regions of the receptor. Hence, novel non-polar decane-1,2-diol derivatives were designed, synthesized, and their potential inhibition of tumor growth and progression evaluated in GBM cell lines.

Cisplatin is a well-known chemotherapeutic drug for treating numerous human cancers including bladder, lung, ovarian, testicular and glial cancers. It interferes with DNA repair mechanisms, DNA damage, and inducing apoptosis in cancer cells. Thus in the present study, cisplatin is used as a positive control drug and the observed results are compared with the activity of the diol derivatives.

2. Materials and methods

2.1. Chemical synthesis of decane-1,2-diol derivatives

2.1.1. General remarks

All synthesis were carried out in oven-dried glassware under inert atmosphere. Triethylamine was purified and dried before use. Dichloromethane (DCM) was dried by distillation under argon with calcium hydride. All other chemicals were used as received from suppliers. Decane-1,2-diol was used in synthesis and biological assays as received from TCI. Reactions were monitored through thin-layer chromatography (TLC) with commercial silica gel plates (Merck silica gel, 60 F254). Visualization of the developed plates was performed under UV lights at 254 nm and by staining with cerium ammonium molybdate. Flash column chromatography was performed on silica gel 60 (40–63 μm) as stationary phase.

^{1}H NMR spectra were recorded at 300 MHz, ^{13}C NMR spectra were recorded at 75 MHz in a 300 MHz Varian Mercury spectrometer, using $CDCl_3$ as solvent. Chemical shifts (δ) are reported in ppm referenced to the $CDCl_3$ residual peak (δ 7.26) or TMS peak (δ 0.00) for

^{1}H NMR and to $CDCl_3$ (δ 77.16) for ^{13}C NMR. The following abbreviations were used to describe peak splitting patterns: s = singlet, d = doublet, t = triplet, m = multiplet. Coupling constants, J, were reported in Hertz (Hz). High-resolution mass spectra were recorded on a Waters ESI-TOF MS spectrometer. Structural elucidation of all compounds tested in biological assays was performed by

^{1}H and ^{13}C NMR, and HRMS. All compounds of interest were isolated by chromatography and their purity (> 97%) assessed by NMR (please see Supplementary material 1 for NMR spectra).

2.1.2. 1-((tert-butyldimethylsilyl)oxy)decan-2-ol (2)

A solution of *tert*-butyldimethylsilyl chloride (3.02 g, 20 mmol) in dichloromethane (40 mL) was added dropwise to a 0 °C solution of triethylamine (2.8 mL, 20 mmol) and decane-1,2-diol (4.18 g, 24 mmol) in dichloromethane (20 mL). After stirring at room temperature for 48 h, water (50 mL) was added and the aqueous layer extracted with dichloromethane (2 × 80 mL). The combined organic layers were washed with brine and dried over Na_2SO_4, after which the crude compound was concentrated under reduced pressure. The residue was purified by silica gel column chromatography using hexane/EtOAc (97:3) as eluent, to yield **2** (4.43 g, 77%) as a colorless oil, and similar spectral characterization as previously reported (Attygalle et al., 2008).

^{1}H NMR ($CDCl_3$, 300 MHz,): δ 3.64–3.59 (m, 2H), 3.41–3.34 (m, 1H), 2.42 (d, J = 3.2 Hz, 1H), 1.43–1.27 (m, 14H), 0.91–0.85 (m, 12H), 0.07 (s, 6H); ^{13}C NMR ($CDCl_3$, 75 MHz): δ 72.1, 67.5, 33.0, 32.1, 30.0, 29.8, 29.5, 26.1, 25.8, 22.9, 18.5, 14.3.

2.1.3. 1-((tert-butyldimethylsilyl)oxy)dec-2-yl 2,2,2-trichloroacetate (3)

To a stirred solution of **2** (392 mg, 1.36 mmol) in Et_2O (4.5 mL) at 0 °C under argon, triethylamine (0.25 mL, 1.77 mmol) was added, after which trichloroacetyl chloride (0.17 mL, 1.5 mmol) was added dropwise. The reaction was stirred for 1 h 40 min, after which the formed precipitate was dissolved into a small amount of water. The organic layer was washed with brine, dried over Na_2SO_4 and concentrated under reduced pressure to obtain **3** as a colorless oil (488 mg, 83%).

^{1}H NMR ($CDCl_3$, 300 MHz): δ 5.08–5.00 (m, 1H), 3.74–3.72 (d, J = 5.6 Hz, 2H), 2.32–2.28 (m, 1H), 1.65–1.72 (m, 2H), 1.25–1.39 (m, 12H), 0.91–0.82 (m, 12H), 0.06 (s, 3H), 0.05 (s, 3H); ^{13}C NMR ($CDCl_3$, 75 MHz): δ 162.0, 81.1, 64.0, 32.0, 30.3, 29.6, 29.4, 26.0, 25.1, 22.9, 18.4, 14.3; HRMS (ESI) *m/z* cald for $[C_{18}H_{35}Cl_3O_3Si + Na]^+$ 455.1313, found 455.1320.

2.1.4. 2-(p-toluenesulfonyl)decan-1-ol (4)

To a stirred solution of **2** (1.47 g, 5.1 mmol) in CH_2Cl_2 (20 mL) at room temperature under argon, triethylamine (2.84 mL, 20 mmol), 4-dimethylaminopyridine (810 mg, 6.6 mmol) and *p*-toluenesulfonyl chloride (1.27 g, 6.6 mmol) were added. The reaction was allowed to stir at room temperature for 48 h, after which saturated NH_4Cl (20 mL) was added and the aqueous layer extracted with CH_2Cl_2 (3 × 20 mL). The organic layers were combined, washed with brine (80 mL), dried over Na_2SO_4 and concentrated in vacuum. The residue was purified by silica gel column chromatography with hexane/EtOAc (95:5) to yield 1-((*tert*-butyldimethylsilyl)oxy)dec-2-yl *p*-toluenesulfonate (2.01 g, 89%) as a yellow solid.

^{1}H NMR ($CDCl_3$, 300 MHz): δ 7.80 (d, J = 8.5 Hz, 2H), 7.32 (d, J = 8.2 Hz, 2H), 4.50–4.45 (m, 1H), 3.71–3.60 (m, 2H), 2.45 (s, 3H), 1.66–1.57 (m, 3H), 1.30–1.17 (m, 12H), 0.88 (t, J = 7.0 Hz, 3H), 0.84 (s, 12H), 0.00 (s, 6H); ^{13}C NMR ($CDCl_3$, 75 MHz): δ 144.4, 134.5, 129.6, 127.8, 83.4, 64.0, 31.8, 31.0, 29.3, 29.2, 29.1, 25.8, 24.6, 22.6, 21.5, 18.2, 14.1.

The obtained 1-((*tert*-butyldimethylsilyl)oxy)dec-2-yl *p*-toluenesulfonate (734 mg, 1.7 mmol) was dissolved in methanol (20 mL) under argon, and NH_4F (1.2 g, 33 mmol) was added. The mixture was stirred at room temperature for 26 h, after which the solvent was removed under reduced pressure. The residue obtained was re-suspended in CH_2Cl_2 (10 mL) and saturated NH_4Cl (10 mL) and the aqueous layer extracted with CH_2Cl_2 (3 × 10 mL). The combined organic layers were dried over $MgSO_4$ and the solvent removed under reduced pressure. The residue was purified by silica gel column chromatography with hexane/EtOAc (75:25) to yield **4** (427 mg, 79%) as a yellow oil, with similar spectral characterization as previously described (Ogawa et al., 1987).

^{1}H NMR ($CDCl_3$, 300 MHz): δ 7.81 (d, J = 8.5 Hz, 2H), 7.34 (d, J = 7.9 Hz, 2H), 4.61–4.52 (m, 1H), 3.75–3.61 (m, 2H), 2.45 (s, 3H), 2.26 (d, J = 3.0 Hz, 1H), 1.63–1.49 (m, 2H), 1.32–1.06 (m, 12H), 0.87 (t, J = 6.9 Hz, 3H). ^{13}C NMR ($CDCl_3$, 75 MHz): δ 144.9, 133.8, 129.8, 127.9, 84.7, 64.4, 31.8, 30.9, 29.3, 29.1, 29.1, 24.8, 22.6, 21.6, 14.1.

2.1.5. 1-(p-toluenesulfonyl)decan-2-ol (5)

To a stirred solution of decane-1,2-diol (405 mg, 2.3 mmol) in CH_2Cl_2 (23 mL) at room temperature under argon, triethylamine (0.67 mL, 4.8 mmol), 4-dimethylaminopyridine (21.5 mg, 0.18 mmol) and *p*-toluenesulfonyl chloride (659 mg, 3.46 mmol) were added. The reaction was stirred at room temperature for 23 h, after which the mixture was diluted with Et_2O (50 mL) and water (75 mL) was added. The organic layer was washed with brine (75 mL), dried over Na_2SO_4, filtered and concentrated under reduced pressure. The residue was purified by silica gel column chromatography with toluene/AcOEt (95:5) to yield **5** (478 mg, 63%) as a colorless solid, with similar spectral characterization as previously reported (Ogawa et al., 1987).

^{1}H NMR ($CDCl_3$, 300 MHz): δ 7.79 (d, J = 8.2 Hz, 2H), 7.35 (d, J = 8.2 Hz, 2H), 4.05–4.01 (m, 1H), 3.90–3.80 (m, 2H), 2.44 (s, 3H), 2.15–2.10 (m, 1H), 1.42–1.35 (m, 3H), 1.35–1.20 (m, 11H), 0.86 (t, J = 6.9 Hz, 3H). ^{13}C NMR ($CDCl_3$, 75 MHz): δ 145.3, 132.9, 130.2, 128.2, 74.2, 69.7, 32.9, 32.1, 29.4, 25.4, 22.9, 21.9, 14.3.

2.1.6. decane-1,2-diyl bis-(p-toluenesulfonate) (6, DBT)

To a stirred solution of decane-1,2-diol (100 mg, 0.57 mmol) in CH_2Cl_2 (5 mL) at room temperature under argon, triethylamine (0.32 mL, 2.3 mmol), 4-dimethylaminopyridine (70 mg, 0.57 mmol) and *p*-toluenesulfonyl chloride (329 mg, 1.7 mmol) were added. The reaction was stirred at room temperature for 7 h, after which the mixture was diluted with Et_2O (13 mL), followed by addition of water (20 mL). The organic layer was washed with brine (20 mL), dried over $MgSO_4$, filtered and solvent removed under vacuum. The residue was purified by silica gel column chromatography with toluene/AcOEt (83:17) to yield **6** (248 mg, 89%) as a colorless oil.

^{1}H NMR ($CDCl_3$, 300 MHz): δ 7.75–7.68 (m, 4H), 7.35–7.28 (m, 4H), 4.63–4.52 (m, 1H), 4.03 (d, J = 5.0 Hz, 2H), 2.46 (s, 3H), 2.45 (s, 3H), 1.68–1.52 (m, 3H), 1.36–1.02 (m, 11H), 0.88 (t, J = 6.9 Hz, 3H); ^{13}C NMR ($CDCl_3$, 75 MHz): δ 145.1, 145.0, 133.5, 132.3, 129.9, 129.8, 128.0, 127.9, 78.9, 69.4, 31.8, 31.0, 29.2, 29.1, 29.0, 24.4, 22.6, 21.7, 14.1; HRMS (ESI) *m/z* calcd for $[C_{24}H_{34}O_6S_2 + Na]^+$ 505.1689, found 505.1712.

2.1.7. 2,2-dimethyl-4-octyl-1,3-dioxolane (7)

Decane-1,2-diol (8.7 g, 50 mmol) and $FeCl_3{\cdot}6H_2O$ (1.4 g, 5 mmol) were dissolved in acetone (50 mL) and left stirring at room temperature until the disappearance of the diol as monitored by TLC. The mixture was concentrated and the crude obtained purified on silica gel flash chromatography using hexane: EtOAc (97:3) to yield the desired product as a clear oil (7.46 g, 35 mmol, 70%).

^{1}H NMR ($CDCl_3$, 300 MHz): δ = 4.03 (d, J = 7.0 Hz, 2H), 3.49 (s, 1H), 1.58–1.70 (m, 1H), 1.44–1.54 (m, 1H), 1.40 (s, 3H), 1.35 (s, 3H),1.19–1.33 (m, 12H), 0.87 ppm (s, 3H); ^{13}C NMR ($CDCl_3$, 75 MHz): δ = 119.2, 108.5, 69.5, 33.6, 31.8, 29.7, 29.5, 29.2, 26.9, 25.8, 22.6, 14.1 ppm; HRMS (ESI) *m/z* calcd for $[C_{13}H_{26}O_2 + H]^+$: 215.2011, found 215.2019.

2.1.8. 2-octyl-1,4-dioxaspiro[4.5]decane (8)

A reaction flask charged with $FeCl_3{\cdot}6H_2O$ (1.4 g, 5 mmol), THF (50 mL), cyclohexanone (5.2 mL, 50 mmol) and decane-1,2-diol (8.7 g, 50 mmol) was stirred at room temperature overnight. The mixture was concentrated under reduced pressure and the crude obtained purified on silica gel flash chromatography using hexane. The desired product was obtained as a clear oil (7.57 g, 29.75 mmol, 60%).

^{1}H NMR ($CDCl_3$, 300 MHz): δ = 3.93–4.16 (m, 2H), 3.39–3.58 (m, 1H), 1.12–1.76 (m, 25H), 0.87 ppm (s, 3H); ^{13}C NMR ($CDCl_3$, 75 MHz): δ = 120.8, 109.0, 75.7, 69.2, 36.6, 35.3, 33.8, 31.8, 29.4, 25.8, 25.2, 23.9, 22.6, 14.1 ppm; HRMS (ESI) *m/z* calcd for $[C_{16}H_{30}O_2 + H]^+$: 255.2324, found 255.2324.

2.1.9. 4-octyl-2-phenyl-1,3,2-dioxaphospholane 2-oxide (9)

To a stirred solution of decane-1,2-diol (1 g, 5.74 mmol) and *N,N*-diisopropylethylamine (1.48 g, 11.48 mmol) in chloroform (15 mL) was added dropwise phenylphosphonic dichloride (1.12 g, 5.74 mmol) for 10 min at room temperature under argon. The resulting reaction mixture was stirred for an additional 10 min and left standing overnight without stirring. The mixture was then diluted with chloroform (20 mL), washed with water (30 mL), the organic layer separated, dried with anhydrous Mg_2SO_4 and solvent evaporated. The crude residue was purified by silica gel flash chromatography using Hexane: EtOAc (1:1) to afford the phenyl phosphinate ester **9** (0.96 g, 3.24 mmol, 56%) as a pale yellow oil containing an inseparable mixture of *cis/trans* (1:1) isomers.

^{1}H NMR ($CDCl_3$, 300 MHz): δ = 7.72–7.95 (m, 4H), 7.53–7.67 (m, 2H), 7.44–7.53 (m, 4H), 4.74–4.87 (m, 1H), 4.53–4.69 (m, 2H), 4.38–4.52 (m, 1H), 4.15–4.27 (m, 2H), 3.90–4.02 (m, 1H), 1.13–1.58 (m, 28H), 0.87 ppm (t, J = 6.4 Hz, 6H); ^{13}C NMR ($CDCl_3$, 75 MHz): δ = 133.0, 131.9, 128.6, 80.0, 78.3, 72.1, 70.8, 33.7, 31.8, 29.2, 24.2, 14.1 ppm; HRMS (ESI) *m/z* calcd for $[C_{16}H_{25}O_3P + H]^+$: 297.1614, found 297.1627.

2.1.10. 4-octyl-1,3,2-dioxathiolane 2-oxide (10)

Triethylamine (5.52 mL, 37.88 mmol) and thionyl chloride (1.4 mL, 17.92 mmol) were added to a solution of decane-1,2-diol (2 g, 11.48 mmol) in dichloromethane (40 mL) at 0 °C, and the reaction mixture was stirred at 0 °C for 10 min. The reaction mixture was partitioned between dichloromethane and water, and the organic layer was washed with brine, dried with anhydrous $MgSO_4$, filtered, and evaporated. The residue was purified by silica gel flash chromatography using Hexane: EtOAc (96:4) to give the cyclic sulfite **10** (2.5 g, 11.19 mmol, 97%) as a yellow oil in a 1:1 diastereoisomeric mixture, as previously described (Nandanan et al., 1999)

^{1}H NMR ($CDCl_3$, 300 MHz): δ = 4.88–5.06 (m, 1H), 4.66 (s, 1H), 4.38–4.57 (m, 1H), 4.21–4.38 (m, 1H), 3.78–4.01 (m, 1H), 1.47–2.06 (m, 4H), 1.09–1.49 (m, 24H), 0.88 ppm (s, 6H); ^{13}C NMR ($CDCl_3$, 75 MHz): δ = 84.2, 80.2, 71.7, 70.2, 33.4, 32.0, 29.2, 25.6, 22.6, 14.1 ppm; HRMS (ESI) *m/z* calcd for $[C_{10}H_{20}O_3S + Na]^+$: 243.1031, found 243.1024.

2.1.11. 4-octyl-1,3,2-dioxathiolane 2,2-dioxide (11)

To a cold solution of the cyclic sulfite **10** (1.33 g, 6.02 mmol) in dichloromethane (3.5 mL) at 0 °C was added a cold solution of H_2SO_4 (0.95 mL, 17.80 mmol) in water (14 mL). Granules of $KMnO_4$ (1.05 g, 6.64 mmol) were added in small portions to the reaction mixture to afford an intensely purple colored solution. It was left stirring overnight at room temperature until a brown color of the reaction mixture was observed on a filter paper. $NaHSO_3$ was added in portions until all the brown color disappeared. The organic layer was extracted with dichloromethane (3 × 10 mL), washed with $NaHCO_3$, dried over $MgSO_4$ and solvent evaporated. The crude residue was purified by silica gel flash chromatography using Hexane: EtOAc (9:1) to obtain the cyclic sulfate **11** (0.30 g, 1.27 mmol, 21%) as a clear oil, as previously described (Ramírez-Contreras and Morandi, 2016).

^{1}H NMR (CDCl$_3$, 300 MHz): δ = 4.97 (tt, J = 8.2, 5.6 Hz, 1H), 4.71 (dd, J = 8.5, 6.2 Hz, 1H), 4.23–4.48 (m, 1H), 1.86–2.05 (m, 1H), 1.65–1.85 (m, 1H), 1.18–1.49 (m, 12H), 0.88 ppm (t, J = 7.0 Hz, 3H); ^{13}C NMR (CDCl$_3$, 75 MHz): δ = 82.9, 72.8, 32.2, 31.7, 29.2, 29.1, 29.0, 24.6, 22.6, 14.1 ppm; HRMS (ESI) *m/z* calcd for $[C_{10}H_{20}O_4S + Na]^+$: 259.0980, found 259.0981.

2.2. Cell culture

U87 cells were grown in Minimum Essential Medium (MEM, Product# 51416C, Sigma-Aldrich, St. Louis, MO) with 10% FBS 2 mM sodium pyruvate(Product# S8636, Sigma-Aldrich, St. Louis, MO), 1% Penicillin-Streptomycin and 0.025 mg/mL Amphotericin B. LN229 cells were cultured in Dulbecco's Modified Eagle Medium - high glucose (DMEM, Catalog# L0102, Biowest) containing 5% FBS(Product # F1051, Sigma-Aldrich, St. Louis, MO), 1% Penicillin-Streptomycin (Product # P4333, Sigma-Aldrich, St. Louis, MO) and 0.025 mg/mL Amphotericin B (Sigma-Aldrich, St. Louis, MO). Cells were maintained at 37 °C in a humidified incubator supplemented with 5% CO$_2$. Three biological repeats and two technical and were performed for each condition.

2.3. In vitro cytotoxicity assay and IC$_{50}$ calculation

Cytotoxicity assay was performed to determine the cell growth inhibitory effect of the compounds following treatment for 48 h on the GBM cell lines, U87 and LN229. This assay was performed in two stages. To begin with, a high concentration, 100 µM, was used for all the compounds as well as for the positive control cisplatin (Sigma-Aldrich, USA). In the second stage, the compounds which exhibited better activity in the previous step, were selected and different concentrations were used to determine the IC$_{50}$ of each compound. For U87 cell line, 150 µM, 100 µM, 75 µM, 50 µM and 25 µM were used for both PC and DBT. For LN229, same concentration were used for PC, while higher concentrations 400 µM, 300 µM, 200 µM, 100 µM were used for DBT due to minimal cytotoxicity effect. Treated cells were harvested by centrifugation at 1200 rpm for 10 min. Cell viability was determined using trypan blue staining, using a Countess II Automated Cell Counter (Thermo Fisher Scientific, USA) to count the number of live and dead cells. The inhibition percentage of each sample was determined using the following formula to determine the dose-response curve. From the dose-response curve, IC$_{50}$ value of each compound was calculated.

Proliferation Inhibition (%) was calculated using the following formula:

$$\text{Proliferation inhibition (\%)} = \frac{(\textit{Mean No. of untreated cells (DMSO control)} - \textit{Mean No. of treated cells}) \times 100}{\textit{Mean No. of untreated cells (DMSO control)}}$$

2.4. Migration assay

To assess the effect of **DBT** on migration profile of the U87 cells, a scratch migration assay was performed (Liang et al., 2007). A cell density of 1 * 105 cells/well was used to culture the cells in 12-well plates and grown overnight at 37 °C with 5% CO$_2$ to obtain the monolayer, which was scratched using a thin tip. The debris was removed and the edge of the scratch was smoothened by washing the cells with 1 mL of complete culture medium. After washing, 1 mL of 2% FBS containing culture medium supplemented with the IC$_{50}$ of the compounds was added. Cells cultured with medium containing 2% FBS alone was used as a control. The scratch area were imaged using an EVOS FL Cell Imaging System (Thermo Fisher Scientific, USA), immediately after the scratch and monitored every 2 h for a period of 10 h.

2.5. Double staining assay

In order to quantify the extent of apoptosis in glioblastoma cell culture due to the treatment with **DBT**, a double staining assay using Annexin V/Propidium iodide was performed (Schutte et al., 1998). U87 cell line was grown as described previously for 24 h, followed by treatment with **DBT** at IC$_{50}$ value and incubated for 24 h. Negative and positive controls were also used. Cells were then harvested, washed and resuspended in PBS. Apoptotic cells were identified by ´Alexa Fluor® 488 Annexin V/Dead Cell Apoptosis Kit (Thermo Fisher Scientific, USA) according to the manufacturer's instructions. Stained cells were observed using EVOS FL Cell Imaging System to distinguish apoptotic cells. Approximately 300 cells were used for each analysis. Three biological repeats and two technical were used for each condition.

2.6. Caspase activity assay

In vitro caspase-3 and caspase-7 activity leading to apoptosis was determined using Caspase-Glo® 3/7 Assay Systems (Promega Corporation). The reagent was prepared as mentioned by the manufacturer. The U87 cells were grown overnight in a 96-well-plate and were treated with **DBT** at IC$_{50}$. Negative control, positive control and blank (medium + DMSO + dye) were maintained. Cells were incubated at 37 °C in a humidified incubator supplemented with 5% CO$_2$ for 5 h and then equilibrated at room temperature for 30 min. 100 µL of Caspase-Glo 3/7 reagent was added to 100 µL of cells/well and was incubated in a dark-chamber. The luminescence signal was quantified (Chameleon Multi-label Detection Platform) one hour after treatment. Basal Activity due to blank was deducted. Magnitude of fold change in luminescence, proportional to caspase activity, between treated and untreated cells were determined using the following formula:

$$\text{Fold change (\%)} = \frac{(\textit{Untreated cells} - \textit{Treated cells}) \times 100}{\textit{Untreated cells}}$$

2.7. Intracellular redox potential test

To evaluate the redox potential of **DBT**, a comparative test, using H$_2$O$_2$ and standard drug against untreated cells, was performed using H2DCFDA (Catalog no. # D399, Life Technologies, USA). The U87 cells were grown overnight in a 96-well-plate and were treated with **DBT** at IC$_{50}$ for 5 h at 37 °C in a humidified incubator supplemented with 5% CO$_2$. Negative control, positive control and blank were maintained. Baseline effect due to solvent was determined as well. After 5 h of treatment, cells were harvested by centrifugation at 3000 rpm for 10 min and incubated with 200 µL of 2 µM H2DCFDA for 30 min at 37 °C in the CO$_2$ incubator. Cells were then washed with pre-warmed PBS and resuspended in 200 µL of pre-warmed medium.100 µL of suspension was then transferred to each well, in a 96-well-plate and incubated at room temperature for 20 min. Finally, fluorescence signal was measured using Chameleon Multi-label Detection Platform (Excitation 485 nm, Emission 535 nm). Magnitude of fold change in fluorescence due to Reactive oxygen species levels, between treated and untreated cells, were determined using the following formula:

$$\text{Fold change (\%)} = \frac{(\textit{Untreated cells} - \textit{Treated cells}) \times 100}{\textit{Untreated cells}}$$

2.8. Cell cycle assay

Propidium iodide analysis of DNA content was performed to identify the drug intervention at various cell cycle stages. Briefly, U87 cells were plated in a six-well-plate (3 * 10^5/well) as described previously for 24 h, followed by treatment with DBT and PC at IC$_{50}$ concentration. Negative and Positive controls (Cisplatin) were maintained. The cells were harvested after 24 h treatment, washed and resuspended in 100 µL of cold PBS. Subsequently, cells were fixed with 900 µL of 70% ethanol. Following that, cells were incubated on ice for 30 min, pelleted by centrifugation and resuspended in 50 µL of PI-Triton-RNase (1 µL Triton X-100, 20 µL RNaseA, and 2 µL Propidium iodide/mL PBS). Samples were then incubated at 37 °C, 5% CO_2 for 15 min. Images were captured using EVOS FL Cell Imaging System and analyzed by MATLAB R2013b to distinguish various cell cycle stages.

2.9. Transcriptome profiling and pathway analysis

Total RNA of the U87 cells were isolated using GeneJET RNA Purification Kit (ThermoFisher Scientific) prior to sequencing using Illumina NextSeq. 500 by Biomedicum Functional Genomics Unit (FuGU, University of Helsinki, Finland). The quality of the sequencing reads was assessed with FASTQC (version 0.11.2)(Andrews, 2010). RNA sequencing reads were trimmed and filtered on length ($\geq$ 25 bp) using Trimmomatic (Bolger et al., 2014). Sequences were aligned to the Human genome (Homo sapiens human release 92; ftp://ftp.ensembl.org/pub/release-92/gtf/homo_sapiens) using STAR (version 2.6) (Dobin et al., 2013), with default parameters. For assembly, we chose SAMtools (Li et al., 2009) (version 1.2) and the "union" mode of HTSeq (Anders et al., 2015) (version 0.9.1), as the gene-level read counts to provide accuracy. The RNAseq pipeline (within SAMtools) was employed with uniquely mapped reads to generate a set of probes covering every mRNA in the genome, which were quantified based on the number of reads falling within the exons of those mRNAs (ignoring any reads found in introns). The log-transformed counts produced were corrected for the total number of sequences in each sample. Differential expression analysis between the replicate sets was performed on raw counts with annotated mRNAs *via* the DESeq. 2 Filter in R (Love et al., 2014). This output was combined with the Intensity Difference Filter, a statistical based fold change filter that works by constructing a local distribution of differences for mRNAs with similar average intensity to the mRNA being examined. Genes were considered significantly differentially expressed when the adjusted p-value was < 0.05 and 2 fold change. In other words, the P-value represents the likelihood that a given gene is significantly differentially expressed by chance, taking into consideration the absolute expression level and how variable other genes are that are expressed at a similar level. In general, highly expressed genes have low variability and lowly expressed genes have high variability. Differentially expressed genes were used to enriched GO categorization using PANTHER database with default settings (Mi et al., 2009). PANTHER Over-representation Test (released on Feb 03, 2018) in PANTHER version 13.1 (http://www.pantherdb.org/, released on October 24, 2016) was used. The list of top 20 pathways is represented in Table 1 with P-value < 0.05 were set as cutoff value.

2.10. DBT interaction with NMDA receptor

The molecular interactions between NMDA receptors and twelve compounds were investigated using PatchDock protein-ligand automated molecular docking tool (Schneidman-Duhovny et al., 2005). The protein databank identifier 3OEM, a high-resolution NMDA receptor structure of rat was used in the present study (Berman et al., 2000). The compound structures were drawn by using Pubchem sketcher tool to generate three dimensional molecular format files. PatchDock program is made up of three efficient algorithms like molecular shape representation, surface patch matching and filtering, and scoring. The PatchDock program outputs ten top docked models and we considered the top score for our further analysis.

3. Results

3.1. Chemistry

Compounds **2–11** were prepared according to Scheme 1. Modification of the secondary hydroxyl group was achieved by prior regioselective silylation of the less hindered hydroxy group (Chaudhary and Hernandez, 1979; Patschinski et al., 2014) yielding **2**, which was further transformed into trichloroacetate derivative **3** and tosylate **4** after desilylation. The tosylated decane-1,2-diol derivatives **5** and **6** were obtained through tosylation of the vicinal diol with different stoichiometric amounts of tosyl chloride. The regioselective tosylation of the primary hydroxy group was achieved in 63% upon use of 1.5 equivalents of tosyl chloride, in accordance with previously reported procedures. The ditosylated compound **6** was obtained in reasonable yield upon increase of tosyl chloride to 2.9 equivalents and increase of DMAP from catalytic to stoichiometric amounts. Ketal derivatives **7** and **8** were obtained in reasonable yields upon reaction of **1** with corresponding ketones in presence of catalytic amounts of iron(III) trichloride (Karamé et al., 2011). The cyclic ester of phenylphosphonic acid **9** was prepared from phenylphosphonic dichloride and the vicinal diol in the presence of *N*,*N*-diisopropylethylamine (Holý, 1998). The cyclic sulfite **10** was obtained as a 1:1 mixture of diastereomers through reaction of **1** with thionyl chloride and further oxidized with $KMnO_4$ in a biphasic solvent system to yield cyclic sulfate **11** (Berridge et al., 1990; Lee et al., 2011; Lohray, 1992).

3.2. Biological studies

3.2.1. Effect of diol-derivatives on GBM cell viability

Diol derivatives **2–11** were screened in-vitro for their antitumor properties in U87 cell line. Fig. 1(A) shows that the cytotoxic effect of novel diol derivatives on U87 demonstrated minimal cytotoxic activity.

Table 1

Gene ontology analysis of the over-represented biological processes/pathways based on sets of statistically significant upregulated/downregulated genes (q-value < 0.01).

Pathway	ID	Overrepresented categories	q-value
Cell cycle	GO:0044843	Cell cycle G1/S phase transition	0.003265412
	GO:0000082	G1/S transition of mitotic cell cycle	0.004841737
	GO:0090068	Positive regulation of cell cycle process	0.004896813
Apoptosis	GO:2001233	Regulation of apoptotic signalling pathway	3.30580e − 05
	GO:2001235	Positive regulation of apoptotic signalling pathway	
	GO:0008630	Intrinsic apoptotic signalling pathway in response to DNA damage	1.17202e − 03
	GO:0097193	Intrinsic apoptotic signalling pathway	1.52529e − 03
	GO:0097191	Extrinsic apoptotic signalling pathway	1.92567e − 03
	GO:0051402	Neuron apoptotic process	4.21502e − 03
DNA damage	GO:2001022	Positive regulation of response to DNA damage stimulus	0.002205668
	GO:0042770	Signal transduction in response to DNA damage	0.002609157
	GO:0030330	DNA damage response, signal transduction by p53 class mediator	0.003417336

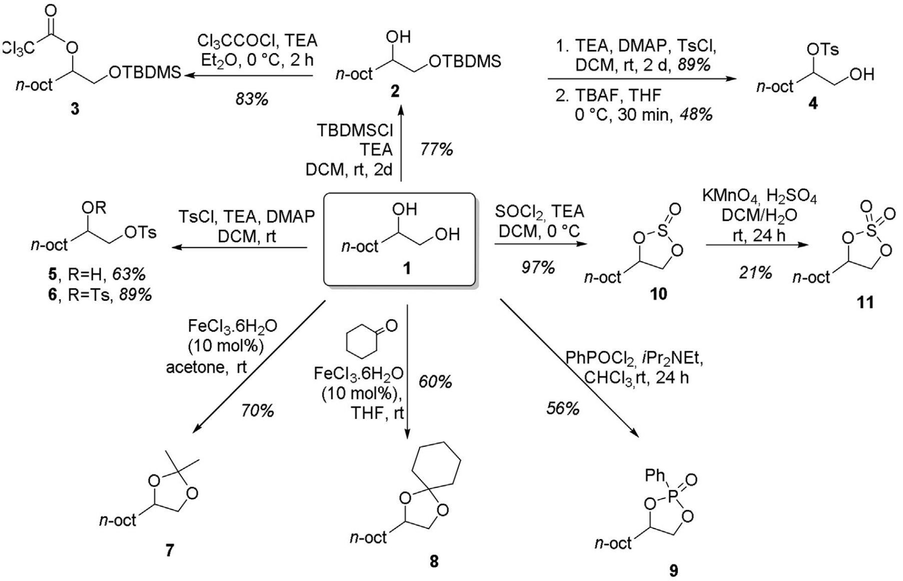

Scheme 1. Synthesis of decane-1,2-diol derivatives.

The compound **DBT** exhibited maximum mortality effect followed by **2**, **5**, and **3**, respectively. **DBT** exhibited 0.9% higher cytotoxicity than the positive control cisplatin, and hence chosen for further studies. The high cytotoxicity of **DBT** prompted us to consider the formation of its synthetic precursor in the medium; therefore, we performed the independent evaluation of *p*-TsOH and **1** on U87. As evident from Fig. 1(B), although **1** exhibited 52.3% activity and *p*-TsOH residual cytotoxicity (2.3%), **DBT** was superior hence ruling out such consideration.

3.2.2. *Dose dependent effect of DBT*

To determine the IC_{50} of **DBT** in U87 and LN229 cell lines, a dose-response study was performed. As expected, there was a gradient increase in mortality with increased dosage in both cell lines, and the IC_{50} values of **DBT** were calculated as 52 µM in U87 and 270 µM in LN229. The IC_{50} values of cisplatin were found to be 66 µM for U87 and 108.7 for LN229 (Fig. 2A, B). The experiment allowed to conclude that **DBT** is more effective in U87 cell line showing 21.2% higher potential than the standard drug cisplatin. Cell line LN229 was less sensitive to both drugs under consideration. Therefore, **DBT** was selected for further studies in U87 cell line to investigate its cellular mechanisms of action.

3.2.3. *Migration inhibition test: scratch assay*

Scratch assay was performed to evaluate the effect of **DBT** on the cell migration properties of malignant tumor cells (Albini et al., 1987). Evaluation of migratory property of the U87 cells when treated with **DBT** and the standard drug revealed a similar trend of increasing migration over time (Fig. 3A, B). Both drugs prevented migration effectively at the 2nd h of treatment, where **DBT** inhibited migration in 59.1% and cisplatin in 61.7%, as compared to migration activity of untreated cells. A similar, although less pronounced effect was observed at the 4th (29.5% for DBT and 42.6% for cisplatin) and 6th (19.5% for DBT and 18.0% for cisplatin) hours of post-treatment. However, at the 8th h, this effect was only 0.6% and 18% respectively for **DBT** and cisplatin. Interestingly, as the percentage of inhibition remained steady at 6th and 8th h for cisplatin, **DBT** had almost lost its anti-migratory activity by 8 h post treatment. Our results indicate that, **DBT** is effective in preventing/reducing migration during initial hours of treatment and decreases its anti-invasive property over time.

3.2.4. *Estimation of apoptosis effect: double staining assay*

To confirm the role of apoptotic pathways in cell death, a double staining method was carried out as above described. The Annexin V/PI

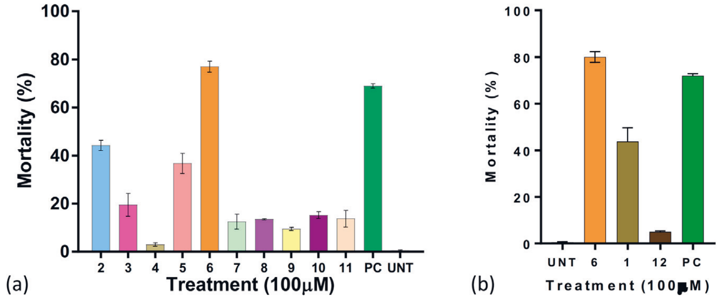

Fig. 1. Cytotoxicity assay of **1–11** (a) Evaluation of the new panel of **2–11**, positive control (cisplatin) and untreated conditions in U87 cell line. (b) Additional assessment of **DBT** and its synthetic precursors for their cytotoxicity.

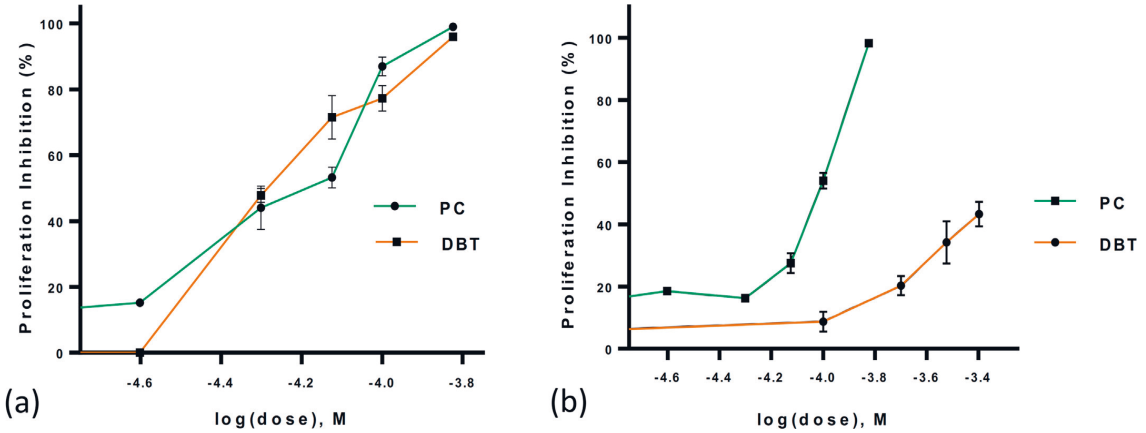

Fig. 2. (a) Dose-response effect of **DBT** and cisplatin in U87 and (b) LN229 after 48 h of incubation time. Baseline effect of vehicle (DMSO) has been deducted. PC – cisplatin. Each data point represents mean ± S.E.M of biological and technical replicates. The results are statistically significant as per Dunnett's multiple comparisons test, alpha cut off. 0.05.

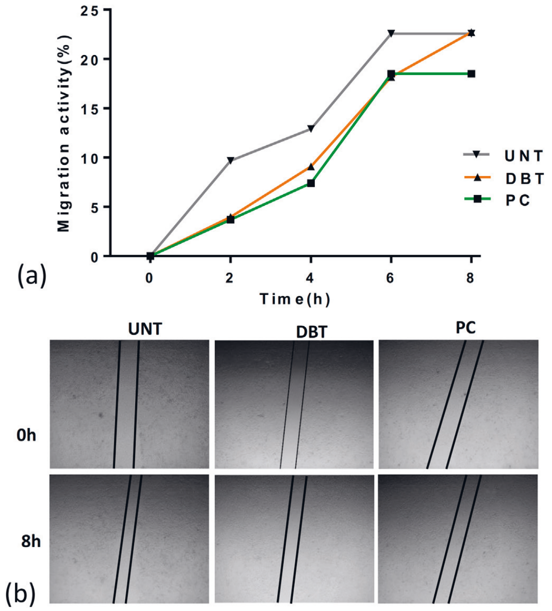

Fig. 3. (a) Migration of scratch area by U87 cells over the time. PC – Cisplatin, UNT – Untreated. (b) Migration activity of U87 cells treated with **DBT,** as indicated by scratch assay at 0 h. (c) Migration activity of U87 cells treated with **DBT,** as indicated by scratch assay at 8 h. Each data point represents an average of biological and technical replicates.

assay effectively detects both early and late stage apoptosis in cells (Schutte et al., 1998). In general, PI do not stain live or early apoptotic cells due to the plasma membrane barrier, therefore stained cells indicate apoptotic or late apoptotic cells. Annexin V is a highly fluorescent stain, which can effectively bind to phosphatidyl serine molecules translocated to the outer plasma membrane during intermediate apoptotic stage, and are exposed to the extra cellular environment. After 24 h of treatment, images were captured using EVOS FL Cell Imaging System, in both phase contrast and fluorescence mode (Fig. 4A, B). Apoptotic cells were detected by its high fluorescence due to the reporter dyes. These results indicate that cell treatment with **DBT** at IC_{50} caused apoptosis of 29.6% of the total number of the cells analyzed whereas that of the standard drug caused apoptosis of 58.9% cells (Fig. 4C). This marked a 12.8% and 39.6% increase in apoptotic fraction when compared to untreated cells. The difference between treated and untreated conditions was confirmed to be statistically significant per ANOVA test ($P\text{-value} < 0.05$).

3.2.5. Evaluation of oxidative stress and caspase activation

Reactive oxygen species mediated caspase activation and subsequent cell death has been repeatedly reported by various studies (Izeradjene et al., 2005; Moungjaroen et al., 2006). Both intracellular Reactive oxygen species and caspase in U87 cells were quantified. The oxidative potential of **DBT** was determined by Reactive oxygen species assay using H2DCFDA indicator. After exposure of cells to **DBT** at IC_{50} for 5 h, we detected an oxidative increase of 7.8% fold change in the treated cells when compared to untreated cells. The standard drug cisplatin and positive control H_2O_2 on the other hand, marked 3.7% and 1.6% respectively (Fig. 5A). The difference between treated and untreated conditions was confirmed to be statistically significant per ANOVA test ($P\text{-value} < 0.05$).

Considering the role of Reactive oxygen species in caspase-mediated apoptosis, we determined the caspase activity of U87 cells using caspase 3/7 assay after a treatment period of 5 h with **DBT** at IC_{50}. Interestingly, U87 **DBT**-treated cells displayed a reduction of caspase 3/7, displaying a 19.1% fold decrease in comparison to untreated cancer cells, whereas positive control displayed 7.2% fold reduction in caspase activity (Fig. 5B), a clear indication of the caspase independent apoptotic process. The difference between treated and untreated conditions was confirmed to be statistically significant per ANOVA test ($P\text{-value} < 0.05$).

3.2.6. RNA-seq analysis detects the pathways

We analyzed the total gene expression profile using RNA sequencing data to understand the effect of **DBT** on human glioblastoma cell functions. In the treated cells, 1531 genes were significantly over/under-expressed at the 95% confidence level ($P \leq 0.05$) (Supplementary file 2). Comprehensive analysis revealed that critical signalling pathways involved in cell cycle, apoptosis and DNA damage has been affected. Functional analysis of DEGs using Reactomes showed the involvement of 76 DEGs in cell cycle, 42 DEGS in DNA damage and

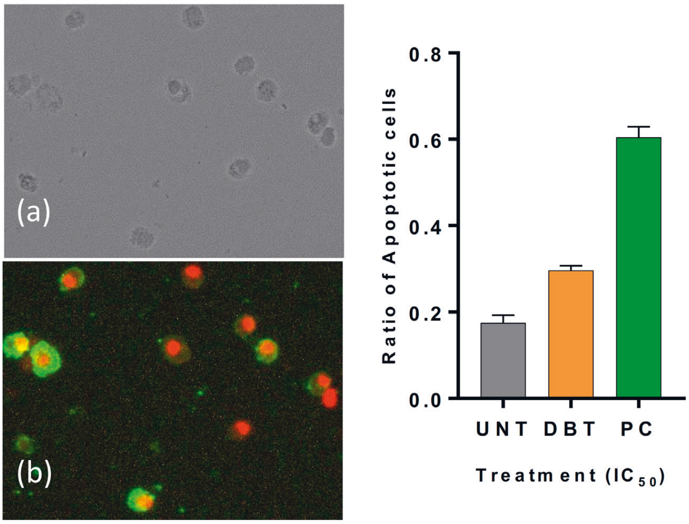

Fig. 4. (a) Phase contrast image of cells after 24 h of treatment. (b) Cellular tagging of reporter dyes Annexin V/ Propidium iodide. Enhanced fluorescence by early and intermediate apoptotic cells stained by Annexin V. (c) Apoptotic activity of **DBT** and standard drug from double staining assay. PC – Cisplatin, UNT – Untreated. Each bar represents mean ± S.E.M. Baseline effect due to DMSO has been deducted (ANOVA test, P value of < 0.05).

repair, 23 genes in Apoptosis and 28 DEGs related to P53 mediated pathway. Among 76 DEGs engaged in the cell cycle, 24 genes were associated with G1/S transition, and 26 genes in G2/M transition. A prolonged G1/S phase and low fraction of cells in G2/M phase in DBT treated condition was also observed per the experimental analysis (Fig. 6). One possibility of this scenario is due to the over expression of *WEE1* preventing the S phase cells to enter into mitosis. RNA-seq analysis also identifies downregulation of caspase genes (*CASP3* and *CASP7* with $\log_2$(fold change) values -0.82 and -0.57, respectively) in **DBT** treated conditions, which confirms the experimental findings.

Gene ontology analysis of the over-represented biological processes based on sets of differentially expressed genes (DEGs) are enlisted in Table 1 and the top 20 DEGs, which are involved in the cell cycle, apoptosis and DNA damage, are listed out in Table 2.

3.2.7. NMDA interaction with the DBT

The neuronal calcium flux elicited by the stimulation of NMDA calcium-permeable ion channels favours cell survival through multiple mechanisms (Portt et al., 2011). Considering the action of straight chain diols on NMDA receptors, we have investigated the gene expression profile of the major pathways involved in glutamate-associated processes. Twenty-eight DEGs were associated with NMDA receptor mediated pathways (Fig. 7A), where notable downregulation of genes encoding for *GCLC, GCLM, CALM1, CAPN2, CREBBP* and *MCL1*, hinting the interaction of DBT with NMDA receptors could be observed. NMDA receptor blockade reduces calcium influx and thereby reduces migration rates and inhibits cell invasiveness, as well as affects various downstream processes mediated *via* Ca^{2+}/calmodulin-dependent signalling. Here, we also observed the downregulation of *GCL* genes which is involved in GSH synthesis, proliferation and cell cycle progression (Traverso et al., 2013). The results indicate that inhibition of *GCL* genes, glutamate-cysteine ligase modifier subunit (*GCLM*) and glutamate-cysteine ligase catalytic subunit (*GCLC*), caused GSH depletion and thus sensitizes the cells to chemotherapy by affecting the redox

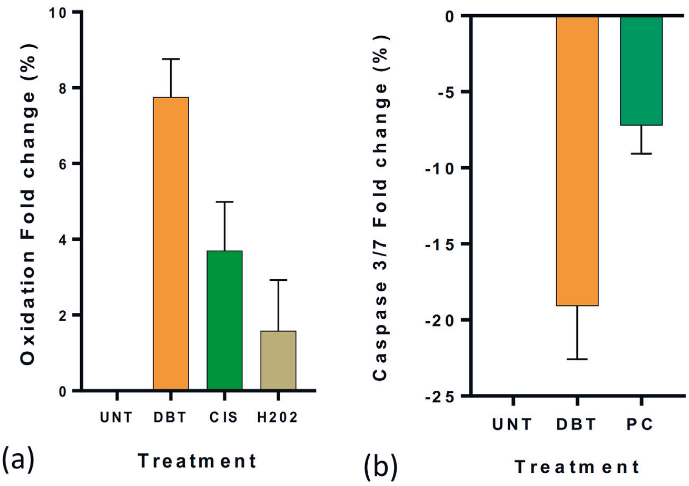

Fig. 5. (a) Oxidative effect of compounds after a treatment period of 5 h with **DBT** at IC_{50}, standard drug and positive control, respectively, as estimated by fluorescence activity due to Reactive oxygen species (ROS) indicator H2DCFDA. Each bar represents a mean ± S.E.M. Each treatment was performed with biological and technical replicates b) Quantification of caspase activity after a treatment period of 5 h with **DBT** and positive control, respectively, as estimated by luminescence activity. PC – Cisplatin, UNT – Untreated. Each bar represents a mean ± S.E.M. Each treatment was performed with biological and technical replicates. The results are statistically significant as per Dunnett's multiple comparisons test, alpha cut off: 0.05.

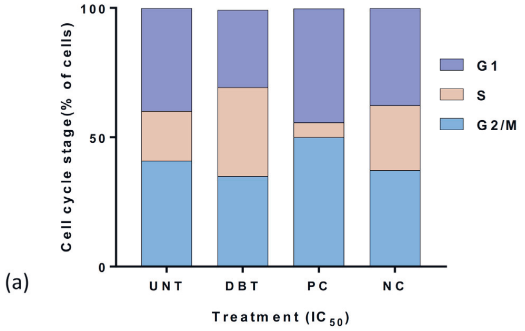

(b)

	UNT	DBT	PC	NC
G1	39.75	29.83	44.04	37.51
S	19.2	34.37	5.63	25.09
G2/M	40.92	34.96	50.05	37.29

Fig. 6. (a) Analysis of percentage of cell population in G1, S, and G2/M phases. (b) Percentage of cell population in each cell stage as determined from histogram of Propidium iodide intensity, in Tabular form. UNT – Untreated, PC – Cisplatin, NC – DMSO.

mechanism upon stress. In addition, downregulation of *CREBBP* and *MCL1* suggest an increase in sensitivity to sub-lethal apoptosis inducing by DBT.

Finally, the interaction of **1–12** with NMDA receptor was computationally validated using molecular docking procedures. The 12 compounds along with their codes and PatchDock score is given in Supplementary file 2. Among the series, **DBT** has highest PatchDock score (6086) and compound 12 the lowest (4014). The 2D protein-ligand interaction diagram for top scoring protein-ligand complex is shown in Fig. 7B. The docking of **DBT** with the receptor is characterized by interactions with 17 amino acid residues, specifically very strong interactions with charged residues like GLU13, LYS87, ARG196 and GLU 198 and 21 hydrogen bonds between the complex. These findings in conjugation with the pathway analysis suggest NMDA receptor as one possible target for **DBT**.

3.2.8. *Statistical analysis*

Results are expressed as the Mean ± Standard Error of Mean (S.E.M) of biological and technical replicates. The statistical significance between the control and the treatment groups was calculated using one-way ANOVA test. GraphPad Prism 7 was used to analyze the data. $P < 0.05$ was considered to indicate a statistically significant difference.

4. Discussion

Diols are widely used in pharmaceutical formulations and antimicrobial agents, solvent and absorption enhancers. Although the antimycotic and anti-bacterial properties of diol derivatives are well studied, the antitumor activity of decane-1,2-diol derivatives has never been reported. Treatment of human glioblastoma cell lines (U87 and LN229) with the newly synthesized decane-1,2-diol derivatives unveiled mild to moderate cytotoxicity, induction of apoptosis and reduction of migration during early hours of treatment. Even though the mechanism of action of the diol derivatives presented in this study has not yet fully been established, it is now evident that the manipulation of the vicinal diol moiety can infer considerable higher biological activity against human glioblastoma cells. The considerable activity of decane-1,2-diol (**1**) against U87 cell lines was increased by two-fold by converting its hydroxyl groups to bistosylate **DBT**. Although one could reason that such activity could be to some extent due to hydrolysis of the tosylate groups, this seems now unlikely since monotosylates **4** and **5** showed completely different activity profiles. Interestingly, the transformation of a single hydroxyl group to tosylate led to a cytotoxicity decrease as observed for **4,** while tosylation of the primary hydroxyl group had no effect as observed for **5**. Similarly, the transformation of the hydroxyl groups to other functional groups such as silyl ethers or esters resulted in unchanged or a decrease in cytotoxicity as observed for **2** and **3**. Nevertheless, while conversion of the primary hydroxyl to silyl ethers or tosylate has little or no effect on the activity, the manipulation of the secondary hydroxyl group has a considerable impact on the cytotoxicity of the decane-1,2-diol derivatives. This aspect could be also confirmed by the constrained cyclic structures **7–11**, which resulted in the loss of the cytotoxicity against U87 cell line previously observed for **1**. The excellent leaving group ability of the tosylate groups, and the structural similarity of compound **6** with well-

Table 2
The top 20 DEGs which are involved in the Cell cycle, Apoptosis and DNA damage. The DEGs were labelled, with the corresponding fold changes and p-values (cut-off: p-value < 0.01) of the up- and down-regulated genes.

	Gene Symbol	*Fold change*	*P-value*		*Gene Symbol*	*Fold change*	*P-value*		*Gene Symbol*	*Fold change*	*P-value*
Cell cycle	**MYC**	1.4202936	1.558971e-74	Apoptosis	**GPI**	1.8525727	3.081624e-15	DNA damage	**MYC**	1.4202936	1.558971e-74
	ANXA1	1.2807115	4.009410e-65		**KITLG**	2.2159959	1.774290e-11		**SOX4**	1.2669231	3.304103e-47
	SOX4	1.2669231	3.304103e-47		**CAV1**	1.4027915	1.050548e-82		**CD44**	1.1313734	8.988581e-42
	NPM1	1.0159993	1.160413e-34		**BMP4**	1.6989839	2.680824e-67		**NPM1**	1.0159993	1.160413e-34
	APEX1	1.0854840	2.149509e-32		**ENO1**	1.1010958	1.632984e-50		**APEX1**	1.0854840	2.149509e-32
	MCM7	1.1327413	3.538445e-23		**BNIP3**	1.3423552	9.210894e-46		**MCL1**	-0.9516929	3.097983e-31
	SUSD2	2.4826163	1.488256e-19		**CD44**	1.1313734	8.988581e-42		**CLU**	-1.0849446	7.819125e-28
	PLK2	1.1014042	4.558871e-17		**MCL1**	-0.9516929	3.097983e-31		**NDRG1**	0.9336335	8.554999e-25
	MYBBP1A	1.0585463	1.850603e-16		**CLU**	-1.0849446	7.819125e-28		**PLK2**	1.1014042	4.558871e-17
	TP53	0.6330290	6.488401e-13		**FAM162A**	1.0236904	1.303485e-25		**AEN**	0.9023050	1.901990e-15
	UBE2C	0.9094918	1.197034e-12		**AARS**	0.6845547	2.207134e-19		**DDX5**	-0.6404172	4.708530e-14
	CDT1	1.1727941	2.226547e-12		**TCF7L2**	1.0967135	2.442031e-19		**BCL2L1**	0.6465268	4.623821e-13
	PRMT1	0.9050000	3.481567e-12		**HSPA5**	0.6084979	1.347699e-18		**TP53**	0.6330290	6.488401e-13
	HMGA2	0.8812668	1.766184e-10		**NLE1**	1.4827916	3.068248e-17		**PRMT1**	0.9050000	3.481567e-12
	ORC1	1.4921658	1.976674e-10		**MYBBP1A**	1.0585463	1.850603e-16		**HMGA2**	0.8812668	1.766184e-10
	SFPQ	-0.5534240	3.700804e-10		**NQO2**	-1.0123799	2.398154e-16		**SESN2**	-0.6680803	2.834512e-10
	TGFA	0.7277016	6.299998e-10		**HSPD1**	0.6906440	5.870919e-16		**NFATC4**	2.2287951	3.052642e-09
	MCM2	0.9725794	7.496943e-10		**HSP90AB1**	0.6260079	9.367473e-16		**PRKDC**	0.7396542	7.873338e-09
	PPP3CA	0.6883943	9.131796e-10		**GCLM**	-1.0354542	1.699349e-15		**TIMELESS**	0.8018258	1.962788e-08
	DACT1	1.4403240	4.810058e-09		**PEA15**	-0.8294305	1.820591e-15		**FAM175A**	1.1576120	9.792904e-08

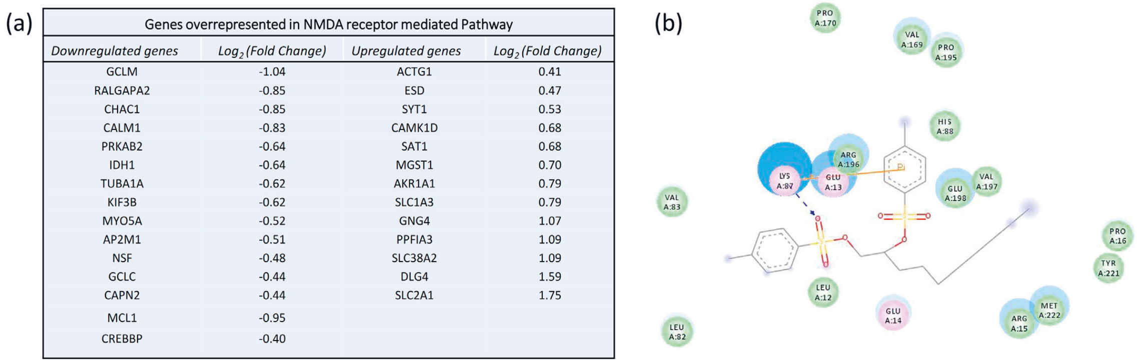

(a)

Genes overrepresented in NMDA receptor mediated Pathway			
Downregulated genes	*Log$_2$(Fold Change)*	*Upregulated genes*	*Log$_2$(Fold Change)*
GCLM	-1.04	ACTG1	0.41
RALGAPA2	-0.85	ESD	0.47
CHAC1	-0.85	SYT1	0.53
CALM1	-0.83	CAMK1D	0.68
PRKAB2	-0.64	SAT1	0.68
IDH1	-0.64	MGST1	0.70
TUBA1A	-0.62	AKR1A1	0.79
KIF3B	-0.62	SLC1A3	0.79
MYO5A	-0.52	GNG4	1.07
AP2M1	-0.51	PPFIA3	1.09
NSF	-0.48	SLC38A2	1.09
GCLC	-0.44	DLG4	1.59
CAPN2	-0.44	SLC2A1	1.75
MCL1	-0.95		
CREBBP	-0.40		

Fig. 7. (a) Genes differentially expressed by DBT treated cells, in NMDA receptor mediated pathway (P value < 0.05). (b) Two-dimensional protein-ligand interaction diagram of NMDA receptor-C2 complex.

established chemotherapeutic busulfan analogues known to crosslink DNA (Galaup and Paci, 2013; Kokotos et al., 2001), might suggest an alkylation process on the basis of the observed cytotoxicity.

Considering the hallmarks of cancer cells such as uncontrolled growth and proliferation, increased invasiveness, altered redox potential, evading apoptotic pathways, and use of alternative pathways, it is essential to evaluate novel antitumor molecules in these contexts. In line with this reasoning, an extensive study of **DBT** was carried out in significant characteristics such as apoptosis, Reactive oxygen species level, caspase activation and scratch migration. Bypass of apoptosis is widely believed to be a signature of cancer cells (Evan and Vousden, 2001; Kerr et al., 1994). Apoptosis is mediated *via* a cascade of distinct signalling pathways, which are often deregulated in cancer. The ability to exploit these pathways will offer effective therapies for GBMs (Krakstad and Chekenya, 2010). Synergistic treatments targeting apoptosis will certainly shift target from cytostatic effect to cytotoxic therapeutic responses owing to greater therapeutic benefits. Our results show higher level of apoptosis in treated conditions, showing that treatment with **DBT** renders the U87 cells sensitive to apoptotic pathways. Enhancing redox perturbation is proven to be an effective strategy to kill glioma cells (Rinaldi et al., 2016; Sharma et al., 2007). Increasing the intracellular Reactive oxygen species to a high level can cause cellular damage and eventually cell death (Schumacker, 2006; Pelicano et al., 2004). As **DBT** demonstrates almost double efficacy as an oxidative agent comparing to the standard drug, it can be seen as a scaffold in the development on anti-cancer agents.

Human glioblastoma cells are reported to exhibit a constitutive activation of caspases *in vivo* and *in vitro* (Gdynia et al., 2007). Also, the inhibition of caspases by peptide inhibitors are reported to decrease the migration of cells in scrape mobility assays and the invasiveness of cells in spheroid assays (Gdynia et al., 2007). It has been suggested that the administration of low doses of caspase inhibitors that block the mobility of glioma cells without affecting the execution of apoptotic cell death, may be exploited as a novel strategy for the treatment of glioblastomas (Gdynia et al., 2007). This correlates well with our observation of reduction of caspase activity due to **DBT** and consequent suppression of scratch migration. Although the mechanism of action of **DBT** or the role of the *p*-toluene sulfonyl moiety remains elusive, it should be mentioned that other sulfonates have been previously reported to effect the fate of glioblastoma cells. For instance, resveratrol monosulfate was reported to be one of the primary metabolites of anticancer *trans*-resveratrol due to sulfotransferases activity (Shu et al., 2011; Sun et al., 2012), and 2,5-dihydroxyphenylsulfonate has also been reported to stimulate the apoptosis of tumor cells, inhibit glioblastoma invasion and suppress angiogenesis (Cuevas et al., 2011). On the other hand, busulfan induces apoptotic death with caspase activation, cleavage of Bcl-2 and PARP proteins in myeloid P39 cell line model (Hassan et al., 2001). In order to decipher the physiological role of caspase independent apoptosis by diols, and understand the extension of NMDA receptors involvement in the process, there will be a need for future research in these important avenues.

5. Conclusion

In conclusion, this study demonstrated the anti-glioma activity of a new panel of diverse decane-1,2-diol derivatives in multiple glioma cell lines. Evaluation in U87 and LN229 demonstrated mild to moderate anti-glioma activity and the synthetic derivative **DBT** was found to be the best cytotoxic compound among the library tested. Additionally, the magnitude of anti-glioma efficacy was found comparable to the currently available platinum drug cisplatin. From the library of compounds tested, it is concluded that modification of the secondary hydroxyl group of the very simple skeleton of decane-1,2-diol has a strong effect on its cytotoxicity. The study also revealed that the cytotoxic effect, at least in part, is due to the apoptotic pathways. Future work will shed more light on its structure-activity relationships as well as detailed mechanism of action. These results indicate that decane-1,2-diol derivatives may have the potential to be used as a chemotherapy for treating glioma.

Acknowledgements

We also thank Dr. Rahul Mangayil and Prof. Ville Santala for providing the access to Fluorescence Plate reader instrumental facility at TUT.

Author contributions

BA, AP and NRC synthesized and characterized the compounds, AV and AZ executed the experiments and data analysis. AM performed RNAseq analysis. KMS executed the docking studies. DK executed the cell cycle studies. MK, OY and NRC conceived and managed all studies. All the authors contributed to writing the manuscript.

Funding sources

MK, AV and OYH acknowledge the Academy of Finland for the project grant support (decision no. 297200) and Tampere University of Technology for Instrumental facility grant support. NRC acknowledges the Academy of Finland (decision no. 287954) for the financial support. MK supervised the full study.

Disclosure of potential conflicts of interest

The authors declare no potential conflicts of interest.

Supplementary data

Supplementary Data are available online: NMR data of all the compounds tested.

Appendix A. Supplementary material

Supplementary data associated with this article can be found in the online version at doi:10.1016/j.ejphar.2018.08.041.

References

Agarwal, S., Sane, R., Oberoi, R., Ohlfest, J.R., Elmquist, W.F., 2011. Delivery of molecularly targeted therapy to malignant glioma, a disease of the whole brain. Expert Rev. Mol. Med. https://doi.org/10.1017/S1462399411001888.

Albini, A., Iwamoto, Y., Kleinman, H.K., Martin, G.R., Aaronson, S.A., Kozlowski, J.M., McEwan, R.N., 1987. A rapid in vitro assay for quantitating the invasive potential of tumor cells. Cancer Res. 47, 3239–3245. https://doi.org/10.1158/0008-5472.can-04-0754.

Anders, S., Pyl, P.T., Huber, W., 2015. HTSeq-A Python framework to work with high-throughput sequencing data. Bioinformatics. https://doi.org/10.1093/bioinformatics/btu638.

Andrews, S., 2010. FastQC: a quality control tool for high throughput sequence data. [WWW Document]. 〈Http://Www.Bioinformatics.Babraham.Ac.Uk/Projects/Fastqc/〉. 〈https://doi.org/citeulike-article-id:11583827〉.

Attygalle, A.B., Bialecki, J.B., Nishshanka, U., Weisbecker, C.S., Ruzicka, J., 2008. Loss of benzene to generate an enolate anion by a site-specific double-hydrogen transfer during CID fragmentation of o-alkyl ethers of ortho-hydroxybenzoic acids. J. Mass Spectrom. 43, 1224–1234. https://doi.org/10.1002/jms.1399.

Berman, H.M., Westbrook, J., Feng, Z., Gilliland, G., Bhat, T.N., Weissig, H., Shindyalov, I.N., Bourne, P.E., 2000. The protein data bank. Nucleic Acids Res. https://doi.org/10.1093/nar/28.1.235.

Berridge, M.S., Franceschini, M.P., Rosenfeld, E., Tewson, T.J., 1990. Cyclic sulfates: useful substrates for selective nucleophilic substitution. J. Org. Chem. 55, 1211–1217. https://doi.org/10.1021/jo00291a020.

Bolger, A.M., Lohse, M., Usadel, B., 2014. Trimmomatic: a flexible trimmer for Illumina sequence data. Bioinformatics. https://doi.org/10.1093/bioinformatics/btu170.

Brosnan, R.J., Pham, T.L., 2014. Hydrocarbon molar water solubility predicts NMDA vs. GABAA receptor modulation. BMC Pharmacol. Toxicol. https://doi.org/10.1186/2050-6511-15-62.

Cacciatore, I., Fornasari, E., Marinelli, L., Eusepi, P., Ciulla, M., Ozdemir, O., Tatar, A., Turkez, H., Di Stefano, A., 2017. Memantine-derived drugs as potential antitumor agents for the treatment of glioblastoma. Eur. J. Pharm. Sci. 109, 402–411. https://doi.org/10.1016/j.ejps.2017.08.030.

Chaudhary, S.K., Hernandez, O., 1979. 4-Dimethylaminopyridine: an efficient and selective catalyst for the silylation of alcohols. Tetrahedron Lett. 20, 99–102. https://doi.org/10.1016/S0040-4039(01)85893-7.

Chinot, O.L., Wick, W., Mason, W., Henriksson, R., Saran, F., Nishikawa, R., Carpentier, A.F., Hoang-Xuan, K., Kavan, P., Cernea, D., Brandes, A.A., Hilton, M., Abrey, L., Cloughesy, T., 2014. Bevacizumab plus radiotherapy–temozolomide for newly diagnosed glioblastoma. N. Engl. J. Med. 370, 709–722. https://doi.org/10.1056/NEJMoa1308345.

Cuevas, P., Carceller, F., Angulo, J., González-Corrochano, R., Cuevas-Bourdier, A., Giménez-Gallego, G., 2011. Antiglioma effects of a new, low molecular mass, inhibitor of fibroblast growth factor. Neurosci. Lett. 491, 1–7. https://doi.org/10.1016/j.neulet.2010.12.047.

Davis, M.E., 2016. Glioblastoma: overview of disease and treatment. Clin. J. Oncol. Nurs. 20, 1–8. https://doi.org/10.1188/16.CJON.S1.2-8.

Deutsch, S.I., Tang, A.H., Burket, J.A., Benson, A.D., 2014. NMDA receptors on the surface of cancer cells: target for chemotherapy? Biomed. Pharmacother. https://doi.org/10.1016/j.biopha.2014.03.012.

Dildy-Mayfield, J.E., Mihic, S.J., Liu, Y., Deitrich, R.A., Harris, R.A., 1996. Actions of long chain alcohols on GABAA and glutamate receptors: relation to in vivo effects. Br. J. Pharmacol. https://doi.org/10.1111/j.1476-5381.1996.tb15413.x.

Dobin, A., Davis, C.A., Schlesinger, F., Drenkow, J., Zaleski, C., Jha, S., Batut, P., Chaisson, M., Gingeras, T.R., 2013. STAR: Ultrafast universal RNA-seq aligner. Bioinformatics. https://doi.org/10.1093/bioinformatics/bts635.

Estrada-Bernal, A., Palanichamy, K., Chaudhury, A.R., Van Brocklyn, J.R., 2012. Induction of brain tumor stem cell apoptosis by FTY720: a potential therapeutic agent for glioblastoma. Neuro Oncol. https://doi.org/10.1093/neuonc/nos005.

Evan, G.I., Vousden, K.H., 2001. Proliferation, cell cycle and apoptosis in cancer. Nature 411, 342–348. https://doi.org/10.1038/35077213.

Galaup, A., Paci, A., 2013. Pharmacology of dimethanesulfonate alkylating agents: busulfan and treosulfan. Expert Opin. Drug Metab. Toxicol. https://doi.org/10.1517/17425255.2013.737319.

Garrido, W., Rocha, J.D., Jaramillo, C., Fernandez, K., Oyarzun, C., San Martin, R., Quezada, C., 2014. Chemoresistance in high-grade gliomas: relevance of adenosine signalling in stem-like cells of glioblastoma multiforme. Curr. Drug Targets 15, 931–942(〈https://doi.org/CDT-EPUB-61957[pii]〉).

Gdynia, G., Grund, K., Eckert, A., Böck, B.C., Funke, B., Macher-Goeppinger, S., Sieber, S., Herold-Mende, C., Wiestler, B., Wiestler, O.D., Roth, W., 2007. Basal caspase activity promotes migration and invasiveness in glioblastoma cells. Mol. Cancer Res. 5, 1232–1240. https://doi.org/10.1158/1541-7786.MCR-07-0343.

Hassan, Z., Hassan, M., Hellström-Lindberg, E., 2001. The pharmacodynamic effect of busulfan in the P39 myeloid cell line in vitro. Leukemia. https://doi.org/10.1038/sj.leu.2402193.

Holý, A., 1998. Simple method for cleavage of phosphonic acid diesters to monoesters. Synthesis 1998 (4), 381–385. https://doi.org/10.1055/s-1998-2047.

Hombach-Klonisch, S., Mehrpour, M., Shojaei, S., Harlos, C., Pitz, M., Hamai, A., Siemianowicz, K., Likus, W., Wiechec, E., Toyota, B.D., Hoshyar, R., Seyfoori, A., Sepehri, Z., Ande, S.R., Khadem, F., Akbari, M., Gorman, A.M., Samali, A., Klonisch, T., Ghavami, S., 2017. Glioblastoma and chemoresistance to alkylating agents: involvement of apoptosis, autophagy, and unfolded protein response. Pharmacol. Ther. https://doi.org/10.1016/j.pharmthera.2017.10.017.

Izeradjene, K., Douglas, L., Tillman, D.M., Delaney, A.B., Houghton, J.A., 2005. Reactive oxygen species regulate caspase activation in tumor necrosis factor-related apoptosis-inducing ligand-resistant human colon carcinoma cell lines. Cancer Res. 65, 7436–7445. https://doi.org/10.1158/0008-5472.CAN-04-2628.

Jue, T.R., McDonald, K.L., 2016. The challenges associated with molecular targeted therapies for glioblastoma. J. Neurooncol. https://doi.org/10.1007/s11060-016-2080-6.

Karamé, I., Alamé, M., Kanj, A., Baydoun, G.N., Hazimeh, H., El Masri, M., Christ, L., 2011. Mild and efficient protection of diol and carbonyls as cyclic acetals catalysed by iron (III) chloride. Comptes Rendus Chim. 14, 525–529. https://doi.org/10.1016/j.crci.2010.12.001.

Kerr, J.F.R., Winterford, C.M., Harmon, B.V., 1994. Apoptosis. Its significance in cancer and cancer Therapy. Cancer 73, 2013–2026. https://doi.org/10.1002/1097-0142(19940415)73:8<2013::AID-CNCR2820730802>3.0.CO;2-J.

Kokotos, G., Constantinou-Kokotou, V., Padrón, J.M., Peters, G.J., 2001. Synthesis and in vitro cytotoxicity of novel long chain busulphan analogues. Bioorg. Med. Chem. Lett. https://doi.org/10.1016/S0960-894X(01)00084-1.

Krakstad, C., Chekenya, M., 2010. Survival signalling and apoptosis resistance in glioblastomas: opportunities for targeted therapeutics. Mol. Cancer. https://doi.org/10.1186/1476-4598-9-135.

Lee, H.W., Nam, S.K., Choi, W.J., Kim, H.O., Jeong, L.S., 2011. Stereoselective synthesis of MLN4924, an inhibitor of NEDD8-activating enzyme. J. Org. Chem. 76, 3557–3561. https://doi.org/10.1021/jo2001897.

Li, H., Handsaker, B., Wysoker, A., Fennell, T., Ruan, J., Homer, N., Marth, G., Abecasis, G., Durbin, R., 2009. The sequence alignment/Map format and SAMtools. Bioinformatics. https://doi.org/10.1093/bioinformatics/btp352.

Liang, C.-C., Park, A.Y., Guan, J.-L., 2007. In vitro scratch assay: a convenient and inexpensive method for analysis of cell migration in vitro. Nat. Protoc. 2, 329–333. https://doi.org/10.1038/nprot.2007.30.

Lohray, B.B., 1992. Cyclic sulfites and cyclic sulfates: epoxide like synthons. Synthesis 1992, 1035–1052. https://doi.org/10.1055/s-1992-26295.

Love, M.I., Huber, W., Anders, S., 2014. Moderated estimation of fold change and dispersion for RNA-seq data with DESeq. 2. Genome Biol. https://doi.org/10.1186/s13059-014-0550-8.

Markert, J.M., Fuller, C.M., Gillespie, G.Y., Bubien, J.K., McLean, L.A., Hong, R.L., Lee, K., Gullans, S.R., Mapstone, T.B., Benos, D.J., 2001. Differential gene expression profiling in human brain tumors. Physiol. Genom(〈https://doi.org/5/1/21[pii]〉).

Mi, H., Dong, Q., Muruganujan, A., Gaudet, P., Lewis, S., Thomas, P.D., 2009. PANTHER version 7: improved phylogenetic trees, orthologs and collaboration with the Gene Ontology Consortium. Nucleic Acids Res. https://doi.org/10.1093/nar/gkp1019.

Moungjaroen, J., Nimmannit, U., Callery, P.S., Wang, L., Azad, N., Lipipun, V., Chanvorachote, P., Rojanasakul, Y., 2006. Reactive oxygen species mediate caspase activation and apoptosis induced by lipoic acid in human lung epithelial cancer cells through Bcl-2 down-regulation. J. Pharmacol. Exp. Ther. 319, 1062–1069. https://doi.org/10.1124/jpet.106.110965.glutathione.

Nandanan, E., Phukan, P., Sudalai, A., 1999. An efficient method to chiral β-hydroxy acids: synthesis of lipid-A side chain. Indian J. Chem. – Sect. B Org. Med. Chem. 38, 893–896.

Ogawa, K., Ohta, S., Okamoto, M., 1987. Reaction of terminal oxiranes with arenesulfonic acid. Synthesis 281–284. https://doi.org/10.1055/s-1987-27918.

Pardridge, W.M., 2005. The blood-brain barrier: bottleneck in brain drug development. NeuroRx. https://doi.org/10.1602/neurorx.2.1.3.

Patel, A.P., Tirosh, I., Trombetta, J.J., Shalek, A.K., Gillespie, S.M., Wakimoto, H., Cahill, D.P., Nahed, B.V., Curry, W.T., Martuza, R.L., Louis, D.N., Rozenblatt-Rosen, O., Suvà, M.L., Regev, A., Bernstein, B.E., 2014. Single-cell RNA-seq highlights intratumoral heterogeneity in primary glioblastoma. Science (80-) 344, 1396–1401. https://doi.org/10.1126/science.1254257.

Patschinski, P., Zhang, C., Zipse, H., 2014. The lewis base-catalyzed silylation of alcohols-a mechanistic analysis. J. Org. Chem. 79, 8348–8357. https://doi.org/10.1021/jo5016568.

Pelicano, H., Carney, D., Huang, P., 2004. ROS stress in cancer cells and therapeutic implications. Drug Resist. Updat. https://doi.org/10.1016/j.drup.2004.01.004.

Peoples, R.W., 2002. Inhibition of N-methyl-D-aspartate receptors by straight-chain diols: implications for the mechanism of the alcohol cutoff effect. Mol. Pharmacol. https://doi.org/10.1124/mol.61.1.169.

Portt, L., Norman, G., Clapp, C., Greenwood, M., Greenwood, M.T., 2011. Anti-apoptosis and cell survival: a review. Biochim. Biophys. Acta – Mol. Cell Res. https://doi.org/10.1016/j.bbamcr.2010.10.010.

Ramaswamy, P., Aditi Devi, N., Hurmath Fathima, K., Dalavaikodihalli Nanjaiah, N.,

2014. Activation of NMDA receptor of glutamate influences MMP-2 activity and proliferation of glioma cells. Neurol. Sci. 35, 823–829. https://doi.org/10.1007/s10072-013-1604-5.

Ramírez-Contreras, R., Morandi, B., 2016. Chemo- and regioselective functionalization of polyols through catalytic C(sp3)-C(sp3) Kumada-type coupling of cyclic sulfate esters. Org. Lett. 18, 3718–3721. https://doi.org/10.1021/acs.orglett.6b01745.

Rinaldi, M., Caffo, M., Minutoli, L., Marini, H., Abbritti, R.V., Squadrito, F., Trichilo, V., Valenti, A., Barresi, V., Altavilla, D., Passalacqua, M., Caruso, G., 2016. ROS and brain gliomas: an overview of potential and innovative therapeutic strategies. Int. J. Mol. Sci. https://doi.org/10.3390/ijms17060984.

Schneidman-Duhovny, D., Inbar, Y., Nussinov, R., Wolfson, H.J., 2005. PatchDock and SymmDock: servers for rigid and symmetric docking. Nucleic Acids Res. https://doi.org/10.1093/nar/gki481.

Schumacker, P.T., 2006. Reactive oxygen species in cancer cells: live by the sword, die by the sword. Cancer Cell. https://doi.org/10.1016/j.ccr.2006.08.015.

Schutte, B., Nuydens, R., Geerts, H., Ramaekers, F., 1998. Annexin V binding assay as a tool to measure apoptosis in differentiated neuronal cells. J. Neurosci. Methods 86, 63–69. https://doi.org/10.1016/S0165-0270(98)00147-2.

Sharma, V., Joseph, C., Ghosh, S., Agarwal, A., Mishra, M.K., Sen, E., 2007. Kaempferol induces apoptosis in glioblastoma cells through oxidative stress. Mol. Cancer Ther. 6, 2544–2553. https://doi.org/10.1158/1535-7163.MCT-06-0788.

Shu, X.H., Li, H., Sun, X.X., Wang, Q., Sun, Z., Wu, M.L., Chen, X.Y., Li, C., Kong, Q.Y., Liu, J., 2011. Metabolic patterns and biotransformation activities of resveratrol in human glioblastoma cells: relevance with therapeutic efficacies. PLoS One 6. https://doi.org/10.1371/journal.pone.0027484.

Stepulak, A., Rola, R., Polberg, K., Ikonomidou, C., 2014. Glutamate and its receptors in cancer. J. Neural Transm. 121, 933–944. https://doi.org/10.1007/s00702-014-1182-6.

Stupp, R., Mason, W., van den Bent, M.J., Weller, M., Fisher, B.M., Taphoorn, M.J.B., Belanger, K., Brandes, A.A., Marosi, C., Bogdahn, U., Curschmann, J., Janzer, R.C., Ludwin, S.K., Gorlia, T., Allgeier, A., Lacombe, D., Cairncross, G., Eisenhauer, E., Mirimanoff, R.O., 2005. Radiotherapy plus concomitant and adjuvant temozolomide for glioblastoma. N. Engl. J. Med. 987–996. https://doi.org/10.1056/NEJMoa043330.

Sun, Z., Li, H., Shu, X.H., Shi, H., Chen, X.Y., Kong, Q.Y., Wu, M.L., Liu, J., 2012. Distinct sulfonation activities in resveratrol-sensitive and resveratrol-insensitive human glioblastoma cells. FEBS J. 279, 2381–2392. https://doi.org/10.1111/j.1742-4658.2012.08617.x.

Takano, T., Lin, J.H.C., Arcuino, G., Gao, Q., Yang, J., Nedergaard, M., 2001. Glutamate release promotes growth of malignant gliomas. Nat. Med. 7, 1010–1015. https://doi.org/10.1038/nm0901-1010.

Traverso, N., Ricciarelli, R., Nitti, M., Marengo, B., Furfaro, A.L., Pronzato, M.A., Marinari, U.M., Domenicotti, C., 2013. Role of glutathione in cancer progression and chemoresistance. Oxid. Med. Cell. Longev. https://doi.org/10.1155/2013/972913.

Weidle, U.H., Niewohner, J., Tiefenthaler, G., 2015. The blood-brain barrier challenge for the treatment of brain cancer, secondary brain metastases, and neurological diseases. Cancer Genom. Proteom. 12, 167–178.

Wen, P.Y., Kesari, S., 2008. Malignant gliomas in. N. Engl. J. Med. 359, 492–507. https://doi.org/10.1056/NEJMra0708126.

Yan, M., Liu, A.L., Zhou, S.J., Tang, L.P., Ou, Y.Q., Yin, W., Chen, X.Y., Su, X.W., Qiu, P.X., Huang, Y.J., Zhang, J.X., Yan, G.M., Leng, T.D., 2015. Characterization of a synthetic steroid 24-keto-cholest-5-en-3β, 19-diol as a neuroprotectant. CNS Neurosci. Ther. https://doi.org/10.1111/cns.12378.

PUBLICATION
II

2-(2-(2,4-dioxopentan-3-ylidene)hydrazineyl)benzonitrile as novel inhibitor of receptor tyrosine kinase and PI3K/AKT/mTOR signaling pathway in glioblastoma

Anisha Viswanathan, Dinesh Kute; Aliyu Musa; Saravanan Konda Mani; Vili Sipilä; Frank Emmert-Streib; Fedor Zubkov; Atash V. Gurbanov; Olli Yli-Harja, Meenakshisundaram Kandhavelu

European Journal of Medicinal Chemistry., Volume 166, 15 March 2019, Pages 291-303
http://dx.doi.org/10.1016/j.ejmech.2019.01.021

Publication reprinted with the permission of the copyright holders.

European Journal of Medicinal Chemistry 166 (2019) 291–303

Contents lists available at ScienceDirect

European Journal of Medicinal Chemistry

journal homepage: http://www.elsevier.com/locate/ejmech

Research paper

2-(2-(2,4-dioxopentan-3-ylidene)hydrazineyl)benzonitrile as novel inhibitor of receptor tyrosine kinase and PI3K/AKT/mTOR signaling pathway in glioblastoma

Anisha Viswanathan [a], Dinesh Kute [a], Aliyu Musa [b], Saravanan Konda Mani [c], Vili Sipilä [a], Frank Emmert-Streib [b], Fedor I. Zubkov [d], Atash V. Gurbanov [e, f], Olli Yli-Harja [g, h], Meenakshisundaram Kandhavelu [a, *]

[a] *Molecular Signaling Lab, Faculty of Medicine and Health Technology, Tampere University and BioMediTech, P.O. Box 553, 33101, Tampere, Finland*
[b] *Predictive Medicine and Data Analytics Lab, Faculty of Medicine and Health Technology, Tampere University and BioMediTech, P.O. Box 553, 33101 Tampere, Finland*
[c] *Centre of Advanced Study in Crystallography & Biophysics, University of Madras, Chennai, 600 025, India*
[d] *Organic Chemistry Department, Faculty of Science, Peoples' Friendship University of Russia (RUDN University), 6 Miklukho-Maklaya St., Moscow, 117198, Russian Federation*
[e] *Centro de Química Estrutural, Instituto Superior Técnico, Universidade de Lisboa, Av. Rovisco Pais, 1049–001 Lisbon, Portugal*
[f] *Department of Chemistry, Baku State University, Z. Xalilov Str. 23, Az 1148 Baku, Azerbaijan*
[g] *Computaional Systems Biology Group, Faculty of Medicine and Health Technology, Tampere University and BioMediTech, P.O. Box 553, 33101 Tampere, Finland*
[h] *Institute for Systems Biology, 1441N 34th Street, Seattle, WA, 98103-8904, USA*

ARTICLE INFO

Article history:
Received 16 November 2018
Received in revised form
9 January 2019
Accepted 9 January 2019
Available online 22 January 2019

ABSTRACT

Nerve growth factor receptor (NGFR), a member of kinase protein, is emerging as an important target for Glioblastoma (GBM) treatment. Overexpression of NGFR is observed in many metastatic cancers including GBM, promoting tumor migration and invasion. Hydrazones have been reported to effectively interact with receptor tyrosine kinases (RTKs). We report herein the synthesis of 23 arylhydrazones of active methylene compounds (AHAMCs) compounds and their anti-proliferative activity against GBM cell lines, LN229 and U87. Compound **R234**, 2-(2-(2,4-dioxopentan-3-ylidene)hydrazineyl)benzonitrile, was identified as the most active anti-neoplastic compound, with the IC_{50} value ranging 87 μM - 107 μM. Molecular docking simulations of the synthesized compounds into the active site of tyrosine receptor kinase A (TrkA), demonstrated a strong binding affinity with **R234** and concurs well with the obtained biological results. **R234** was found to be a negative regulator of PI3K/Akt/mTOR pathway and an enhancer of p53 expression. In addition, **R234** treated GBM cells exhibited the downregulation of cyclins, cyclin-dependent kinases and other key molecules involved in cell cycle such as CCNE, E2F, CCND, CDK6, indicating that **R234** induces cell cycle arrest at G1/S. **R234** also exerted its apoptotic effects independent of caspase3/7 activity, in both cell lines. In U87 cells, **R234** induced oxidative effects whereas LN229 cells annulled oxidative stress. The study thus concludes that **R234**, being a negative modulator of RTKs and cell cycle inhibitor, may represent a novel class of anti-GBM drugs.

© 2019 Elsevier Masson SAS. All rights reserved.

1. Introduction

Glioblastoma Multiforme (GBM) is WHO grade IV astrocytoma, representing a highly heterogeneous group of neoplasms that are among the most aggressive and challenging cancers to treat. Though highly heterogeneous, GBM shares common essential characteristics with other tumors, such as, uncontrolled proliferation, evading of apoptosis, invasiveness, avoidance of immune surveillance, resistance to chemotherapy and Reactive Oxygen Species (ROS) generation and angiogenesis [1].

Receptor tyrosine kinases (RTKs) are important regulators of intracellular signal-transduction pathways mediating cellular

---

* Corresponding author.
E-mail address: meenakshisundaram.kandhavelu@tuni.fi (M. Kandhavelu).

https://doi.org/10.1016/j.ejmech.2019.01.021
0223-5234/© 2019 Elsevier Masson SAS. All rights reserved.

processes, including metabolism, cell-cycle control, survival, proliferation, motility and differentiation, and are often deregulated in cancer [2,3]. RTKs consist of families of growth factor receptors such as the platelet-derived growth factor receptor (PDGFR), fibroblast growth factor receptor (FGFR), vascular endothelial growth factor receptor (VEGFR), and epidermal growth factor receptor (EGFR), nerve growth factor receptor (NGFR) and 15 other subfamilies. Most of the members of RTK family are strongly associated with oncological diseases through gain-of-function mutations or through receptor/ligand overexpression [4]. GBM being high in intratumoral heterogeneity exhibits amplification of RTK expression on tumor cells [5], affecting the sensitivity to various chemo treatments [6]. The main signaling pathways activated by RTKs are PI3K/Akt, Ras/Raf/ERK1/2 and signal transduction and activator of transcription (STAT) pathways [7].

Among several RTKs linked with cancer, the NGFR is found to be positively correlated with astrocytic gliomas and several reports suggests the role of NGFs in GBM growth [8–10]. NGFRs includes two distinct family of receptor Trks and p75NTR and are found to be differentially expressed in glioblastoma and are identified as effective drugable targets for GBM [8,11–15]. NGFR is a transmembrane receptor for the neurotrophin family. Neurotrophins regulate the proliferation and differentiation of neurons in the central nervous system via NGFRs by activating specific tyrosine kinase receptors which include TrkA, TrkB, and TrkC [12]. Recent reports suggest that inhibition of NGFR could be a therapeutic target considering its role in cell proliferation and survival [16], differentiation, cell cycle progression [17], apoptosis [11,18], neurite outgrowth and retraction [19] myelination [20] cell migration and invasion. The NGF-NGFR cascade is reported to activate nuclear factor-κB (NF-κB), leading to inhibition of apoptosis [21]. NGFR is also involved in feedback regulation of P53 and it has been reported that down regulation of NGFR, induced p53-dependent apoptosis and cell growth arrest, as well as suppressed tumor growth [22]. Neurotrophin binding to NGFR activates the c-Jun N-terminal kinase (JNK) signaling cascade, resulting in the activation of p53 and expression of pro-apoptotic genes such as Bcl-2 [23]. Alternatively, combined activation of NGFR and tumor necrosis factor receptor member TRAF6 has been shown to promote downstream activation of NF-κB signaling, which primarily promotes cell survival [24]. Blockade of NGF/Trk signaling via anti-NGF antibodies or Trk inhibitors reduced cell proliferation and tumorigenesis in a muscarinic acetylcholine receptor-3 dependent manner, suggesting NGF as an potential target in tumor treatment and prevention [25,26].

Currently the most targeted molecules in GBM pathway are Protein kinase inhibitors such as Lonarfanib [27], Sorafenib [28], Topoisomerase targeting Irinotecan [29], PKC inhibitors such as Enzastaurin [30] and Integrin inhibitors such as Cilengitide [31] and RTK inhibitors. The use of small-molecule inhibitors targeted against EGFR (Cetuximab and Panitututmab) is a common antitumor therapeutic strategy [32–35]. Anti- PDGFR agent Imatinib has been shown to inhibit GBM cell proliferation and induces cell cycle arrest in the G1 phase of the cell cycle [36]. Similarly, inhibitors of IGFR can modify sensitivity to several chemotherapeutic agents [37–40]. There is still considerable need of more effective chemotherapeutics targeting RTK signaling pathways in GBM disease.

Hydrazones are a potential class of compounds for new drug development, considering its established properties as anticonvulsant [41–43], anti-depressant [44,45], analgesic [46,47], anti-inflammatory [46,48,49], anti-microbial [45], anti-mycobacterial [50], anti-tumoral [51,52] activities. Among several potential arylhydrazones, Di- and tri-organotin(IV) complexes of arylhydrazones of methylene active compounds have shown better anti-proliferative effect against the growth of HCT116 and HEPG2 cancer cells [53]. In addition, hydrazone derivatives were also identified as potential anti-prostate cancer compounds [54]. These compounds induces the apoptosis by caspase 9 and 3 activation [55,56]. Lanthanide chelation with hydrazone derivatives have also expressed higher cytotoxic effect on colon cancer [57]. More recently, we also studied effect of the panel of many hydrazone derivatives on multiple human brain astrocytoma cells and the results showed a better anti-proliferation effect at micro molar level [58]. Considering the prior studies on hydrazone derivatives as a potential anticancer compound and tyrosine kinase inhibitors [59,60] the current study intend to correlate the pharmacodynamic behavior of the top hydrazone derivative under evaluation, with the genomic data, to identify the key pathways affected in the anti-neoplastic behavior, specifically via tyrosine kinase inhibition.

2. Methodology

2.1. Chemistry

A series of new 3-(2-(1-(dimethylamino)-1,3-dioxobutan-2-ylidene)hydrazineyl)-2-hydroxy-5-nitrobenzenesulfonic acid (**3, R212**), N,N-dimethyl-2-(2-(4-nitrophenyl)hydrazineylidene)-3-oxobutanamide (**16, R221**), 4-(2-(2,4,6-trioxotetrahydropyrimidin-5(2H)-ylidene)hydrazineyl)benzoic acid (**19, R156**), sodium 2-(2-(1,3-dioxo-1,3-diphenylpropan-2-ylidene)hydrazineyl)benzenesulfonate (**20, R246**), ethyl 2-(2-(4-chlorophenyl)hydrazineylidene)-3-oxobutanoate (**21, R40**), 4-(2-(1-cyano-2-methoxy-2-oxoethylidene) hydrazineyl)benzoic acid (**22, R313**), 5-(2-(2,4-dioxopentan-3-ylidene)hydrazineyl)isophthalic acid (**23, R283**) and known, 3-(2-(2,4-dioxopentan-3-ylidene)hydrazineyl)-2-hydroxy-5-nitrobenzenesulfonic acid (**1, R2**), triaqua[2-(hydroxy-κ*O*)-5-nitro-3-{2-[2-oxo-4-(oxo-κ*O*)pentan-3-ylidene]hydrazinyl-κN^1} benzenesulfonato(2-)]iron trihydrate (**2, FeR2**), (2-(2-(2,4-dioxopentan-3-ylidene)hydrazineyl) phenyl)arsonic acid (**4, R10**), 5-chloro-3-(2-(1-ethoxy-1,3-dioxobutan-2-ylidene)hydrazineyl)-2-hydroxybenzenesulfonic acid (**5, R31**), 2-hydroxy-5-nitro-3-(2-(2,4,6-trioxotetrahydropyrimidin-5(2H)-ylidene)hydrazineyl)benzenesulfonic acid (**6, R142**), 5-(2-(1,3-dioxo-1-phenylbutan-2-ylidene)hydrazineyl)-4-hydroxybenzene-1,3-disulfonic acid (**7, R46**), 2-(2-(2,4-dioxopentan-3-ylidene)hydrazineyl) benzenesulfonic acid (**8, R237**), 4-(2-(2,4-dioxopentan-3-ylidene)hydrazineyl)benzonitrile (**9, R241**), 2-(2-(2,4-dioxopentan-3-ylidene) hydrazineyl)benzonitrile (**10, R234**), 2-(2-(2,4-dioxopentan-3-ylidene)hydrazineyl) benzoic acid (**11, R236**), 3-(2-(2-nitrophenyl) hydrazineylidene)pentane-2,4-dione (**12, R235**), 3-(2-(4-chlorophenyl)hydrazineylidene)pentane-2,4-dione (**13, R8**), 3-(2-(4-bromophenyl)hydrazineylidene) pentane-2,4-dione (**14, R9**), ethyl 2-(2-(4-cyanophenyl) hydrazineylidene)-3-oxobutanoate (**15, R243**), 2-(2-(4,4-dimethyl-2,6-dioxocyclohexylidene) hydrazineyl) benzoic acid (**17, R244**), 2-(2-(2-hydroxy-4-nitrophenyl) hydrazineylidene)-1-phenylbutane-1,3-dione (**18, R48**) arylhydrazones of active methylene compounds (AHAMCs) have been prepared. Synthesis scheme of know compound is give in the supplemental file 1 while novel compounds synthesis scheme is given below.

2.2. Synthesis of novel arylhydrazone derivatives

The aryl hydrazones R212, R221, R156, R246, R40, R313 and R283 were synthesized via Japp–Klingemann reaction [61–74] between the substituted aryldiazonium chloride and active methylene compounds in water solution containing sodium hydroxide (Table 1).

2.2.1. Diazotization

0.025 mol of substituted aniline was dissolved in 50 mL of water

Table 1
Arylhydrazones of active methylene compounds (AHAMCs).

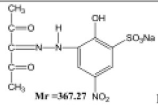 Mr =367.27 R_{2} 1	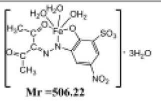 Mr =506.22 FeR2 2	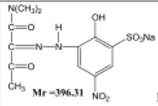 Mr =396.31 R_{212} 3
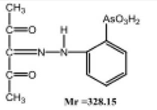 Mr =328.15 R_{10} 4	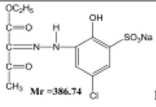 Mr =386.74 R_{31} 5	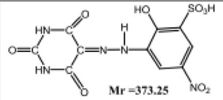 Mr =373.25 R_{142} 6
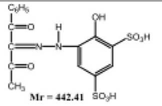 Mr = 442.41 R_{46} 7	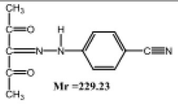 Mr =229.23 R_{241} 9	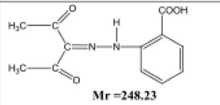 Mr =248.23 R_{236} 11
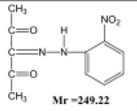 Mr =249.22 R_{235} 12	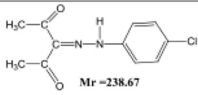 Mr =238.67 R_{8} 13	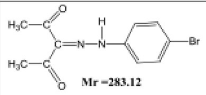 Mr =283.12 R_{9} 14
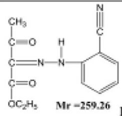 Mr =259.26 R_{243} 15	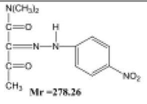 Mr =278.26 R_{221} 16	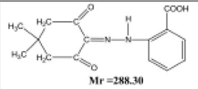 Mr =288.30 R_{244} 17
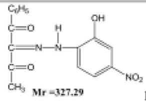 Mr =327.29 R_{48} 18	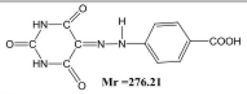 Mr =276.21 R_{156} 19	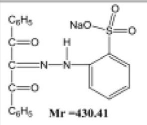 Mr =430.41 R_{246} 20
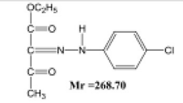 Mr =268.70 R_{40} 21	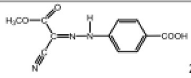 22 R313	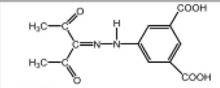 23 R283

and then 0.025 mol of crystalline NaOH was added. The solution was cooled in an ice bath to 273 K and then 0.025 mol of $NaNO_2$ was added; after that 5.00 mL (33%) HCl was added in portions for 1 h. The temperature of the mixture should not exceed 278 K. The resulting diazonium solution was used directly in the following coupling procedure.

2.2.2. Coupling

0.025 mol of NaOH was added to a mixture of 0.025 mol of active methylene compound with 50 mL of water. The solution was cooled in an ice bath to *ca.* 273 K, and a suspension of aryldiazonium chloride (see above) was added in three portions under vigorous stirring for 1 h.

3, R212: yield, 77% (based on N,N-dimethyl-3-oxobutanamide), yellow powder, soluble in water, methanol, ethanol, and insoluble in chloroform. Anal. Calcd for $C_{12}H_{14}N_4O_8S$ ($M = 374.3$): C, 38.50; H, 3.77; N, 14.97. Found: C, 38.42; H, 3.64; N, 14.84%. IR, cm^{-1}: 3459 ν(OH), 2944 ν(NH), 1681 ν(C=O), 1628 ν(C=O···H), 1535 ν(C=N), 742 δ(C–H, Ar). ^1H NMR of a mixture of enol-azo and hydrazo tautomers, (300.13 MHz, D_2O). Enol-azo, δ: 2.55 CH_3, 2.97 and 3.08 $N(CH_3)_2$, 7.98–8.11 (2H, C_6H_2). Hydrazo, δ: 2.32 CH_3, 3.13 and 3.18 $N(CH_3)_2$, 7.98–8.11 (2H, C_6H_2). ^1H NMR of a mixture of enol-azo and hydrazo tautomers, (300.13 MHz, DMSO-d_6). Enol-azo, δ: 2.47 CH_3, 2.77 and 2.96 $N(CH_3)_2$, 7.98–8.18 (2H, C_6H_2), 9.94 (s, 1H, HO–Ar), 11.96 (s, 1H, HO-enol). Hydrazo, δ: 2.28 CH_3, 3.02 and 3.10 $N(CH_3)_2$, 7.98–8.18 (2H, C_6H_2), 9.94 (s, 1H, HO–Ar), 13.60 (s, 1H, NH). $^{13}C\{^1H\}$ NMR (100.61 MHz, DMSO-d_6). Enol-azo, δ: 24.7, 34.0 and 34.8 (CH_3), 109.1 (Ar–N=N), 116.2 (C–N), 125.6 and 131.6 (2Ar–H), 136.4 (Ar–SO_3H), 139.7 (Ar–NO_2), 146.8 (Ar–OH), 162.0 (CH_3C–O), 194.5 ($N(CH_3)_2C$=O). Hydrazo, δ: 28.8, 37.3 and 38.1 (CH_3), 116.9 and 123.5 (2Ar–H), 123.5 (Ar–NH–N), 130.7 (Ar–SO_3H), 132.2 (C=N), 139.6 (Ar–NO_2), 145.4 (Ar–OH), 194.5

($N(CH_3)_2C{=}O$), 196.0 ($CH_3C{=}O$). ^1H NMR of a mixture of enol-azo and hydrazo tautomers, (300.13 MHz, CD_3OD). Enol-azo, 2.54 CH_3, 2.92 $N(CH_3)_2$, δ: 8.23–8.36 (2H, C_6H_2). Hydrazo, δ: 2.34 CH_3, 3.18 and 3.18 $N(CH_3)_2$, 8.23–8.36 (2H, C_6H_2). $^{13}C\{^1H\}$ NMR (100.61 MHz, CD_3OD). Enol-azo, δ: 24.8, 29.8 and 34.7 (CH_3), 107.5 (Ar–N=N), 109.2 (C–N), 117.9 and 121.0 (2Ar–H), 133.4 (Ar–SO_3H), 140.5 (Ar–NO_2), 148.0 (Ar–OH), 164.5 (CH_3C–O), 196.7 ($N(CH_3)_2C{=}O$). Hydrazo, δ: 28.8, 38.2 and 38.8 (CH_3), 110.7 and 111.1 (2Ar–H), 112.3 (Ar–NH–N), 118.4 (Ar–SO_3H), 133.2 (C=N), 134.8 (Ar–NO_2), 141.8 (Ar–OH), 196.7 ($N(CH_3)_2C{=}O$), 200.4 ($CH_3C{=}O$).

16, R221: yield 72% (based on N,N-dimethyl-3-oxobutanamide), orange powder soluble in DMSO, methanol, ethanol and acetone, and insoluble in water. Elemental analysis: $C_{12}H_{14}N_4O_4$ (M = 278.27); C 51.75 (calc. 51.80); H 5.02 (5.07); N 20.08 (20.13) %. IR (KBr): 2930 ν(NH), 1663 ν(C=O), 1634 ν(C=O···H), 1595 ν(C=N) cm^{-1}.^1H NMR in DMSO-d_6, δ (ppm): 2.42 (3H, CH_3), 2.78 (3H, CH_3), 2.99 (6H, CH_3), 7.38–7.49 (4H, Ar–H), 12.68 (1H, N–H). ^{13}C-$\{^1H\}$ NMR in DMSO-d_6, δ (ppm): 24.4 (CH_3), 33.7 (CH_3), 36.4 (CH_3), 116.1 (2Ar–H), 126.0 (2Ar–H), 129.1 (C=N), 138.4 (Ar–NO_2), 142.4 (Ar–NH–N), 163.3 and 194.3 (C=O).

19, R156: yield, 67% (based on barbituric acid), yellow powder, soluble in water, methanol, ethanol, and insoluble in chloroform. Anal. Calcd for $C_{11}H_8N_4O_5$ (M = 276.20): C, 47.83; H, 2.92; N, 20.28. Found: C, 47.65; H, 2.90; N, 20.11%. IR, cm^{-1}: 3365 ν(OH), 3214, 3019, 2855 ν(NH), 1715 ν(C=O), 1657 ν(C=O), 1592 ν(C=O···H), 1563 ν(C=N). ^1H NMR (300.13 MHz, DMSO-d_6) δ: 7.94–8.21 (4H, C_6H_4), 11.35 (s, 1H, NH), 11.54 (s, 1H, NH) and 14.31 (s, 1H, NH). $^{13}C\{^1H\}$ NMR (100.61 MHz, DMSO-d_6) δ: 111.3 and 117.9 (4Ar–H), 125.4 (Ar–COOH), 136.2 (C=N), 146.8 (Ar–NH–N =), 151.8, 157.6, 159.1 and 163.9 (C=O).

20, R246: yield 64% (based on 1,3-diphenylpropane-1,3-dione), grey powder is soluble in DMSO, methanol, ethanol and acetone, and insoluble in hexane. Elemental analysis: $C_{21}H_{15}N_2NaO_5S$ (M = 43041; C 58.45 (calc. 58.60); H 3.43 (3.51); N 6.34 (6.51) %. IR (KBr): 3450 ν(OH), 3045 ν(NH), 1681 ν(C=O), 1607 ν(C=O···H), 1587 ν(C=N) cm^{-1}.^1H NMR in DMSO, internal TMS, δ (ppm): 7.12–7.98 (14H, Ar–H), 13.42 (s, 1H, N–H). ^{13}C NMR in DMSO, internal TMS, δ (ppm): 125.42 (Ar–H), 127.13 (Ar–H), 128.25 (Ar–H), 128.36 (Ar–H), 128.43 (Ar–H), 128.56 (Ar–H), 128.90 (Ar–H), 129.49 (Ar–H), 130.38 (Ar–H), 132.43 (Ar–H), 132.85 (Ar–H), 133.08 (Ar–H), 133.729 (Ar–H), 134.05 (Ar–H), 134.67 (C=N), 138.19 (Ar–CO), 137.21 (Ar–CO), 138.16 (Ar–NH–N), 146.45 (Ar–SO_3Na), 191.44 (C=O), 192.52 (C=O).

21, R40: yield 96% (based on ethyl 3-oxobutanoate), yellow powder soluble in DMSO, methanol, ethanol, chloroform and acetone, and insoluble in water. Elemental analysis: $C_{12}H_{13}ClN_2O_3$ (M = 268.70); C 53.55 (calc. 53.64); H 4.74 (4.88); N 10.37 (10.43)%. IR (KBr): 3453 (NH), 1676 (C=O), 1643 (C=O···H), 1610 (C=N) cm^{-1}.^1H NMR in DMSO-d_6, δ (ppm): 1.31 (s, 3H, CH_3), 2.40 (s, 3H, CH_3), 4.04 (2H, CH_2), 7.23–7.76 (4H, Ar–H), 13.23 (s, 1H, N–H). ^{13}C–$\{^1H\}$ NMR in DMSO-d_6, d (ppm): 13.29 (CH_3), 32.33 (CH_3), 60.48 (CH_2), 116.48 (2Ar–H), 119.24 (Ar–Cl), 134.20 (2Ar–H), 135.44 (C=N), 144.28 (Ar–NH–N), 196.12 (C=O), 197.66 (C=O).

22, R313: yield 87% (based on methyl 2-cyanoacetate), yellow powder soluble in DMSO, methanol, ethanol, chloroform and acetone, and insoluble in water. Elemental analysis: $C_{11}H_9N_3O_4$ (M = 247.21); C 53.38 (calc. 53.44); H 3.54 (3.67); N 16.95 (17.00)%. IR (KBr): 3470 (OH), 3349 (NH), 1670 (C=O), 1646 (C=O···H), 1614 (C=N) cm^{-1}.^1H NMR in DMSO-d_6, δ (ppm): 3.56 (s, 3H, OCH_3), 7.28–7.86 (4H, Ar–H), 11.70 (s, 1H, O–H). 13.08 (s, 1H, N–H). ^{13}C–$\{^1H\}$ NMR in DMSO-d_6, d (ppm): 58.20 (OCH_3), 116.40 (2Ar–H), 124.58 (Ar–COOH), 133.72 (2Ar–H), 135.13 (C=N), 145.04 (Ar–NH–N), 162.06 (C=O), 196.29 (C=O), 197.80 (C=O).

23, R283: yield 94% (based on pentane-2,4-dione), yellow powder soluble in DMSO, methanol, ethanol, chloroform and acetone, and insoluble in water. Elemental analysis: $C_{13}H_{12}N_2O_6$ (M = 292.25); C 53.37 (calc. 53.43); H 4.08 (4.14); N 9.46 (9.59)%. IR (KBr): 3378 (OH), 3290 (NH), 1668 (C=O), 1626 (C=O···H), 1607 (C=N) cm^{-1}.^1H NMR in DMSO-d_6, δ (ppm): 2.43 (s, 3H, CH_3), 2.46 (s, 3H, CH_3), 8.13–8.31 (3H, Ar–H), 13.99 (s, 1H, N–H). ^{13}C–$\{^1H\}$ NMR in DMSO-d_6, δ (ppm): 26.27 (CH_3), 31.29 (CH_3), 119.34 (2Ar–H), 126.76 (Ar–H), 134.02 (Ar–COOH), 135.45 (Ar–COOH), 136.18 (C=N), 141.80 (Ar–NH–N), 167.71 (C=O), 167.94 (C=O), 196.32 (C=O), 197.01 (C=O).

2.3. Computational assessment of ligand-receptor interaction

The structures of 23 ligands were drawn in SDF format using the tool Marvin Sketch [Marvin Draw 5.1.5, 2008, Chemaxon Ltd., Budapest]. The ligands were prepared for docking simulations using the LigPrep module of the Schrödinger suite of tools. Most probable tautomers and all possible stereo isomers were generated to study the activity of individual stereotypes of each ligand. In the final stage of LigPrep, compounds were minimized with OPLS-2001 Force field [75]. The Human nerve growth receptor structure with PDBID 1HE7 (Resolution- 2 Å) is downloaded from Protein Data Bank [76]. The protein structure was prepared using the 'Protein Preparation Wizard' of the Schrödinger suite (Schrödinger, LLC, New York, NY, 2009). The docking grid on the receptor has been generated based on the co-crystallized ligand. Docking was performed on prepared receptor and 23 ligands by using the Glide docking program [Glide, version 5.5, Schrödinger, LLC, New York, NY, 2009].

2.4. Cell culture

Human GBM cell lines, U87 cells were grown in Minimum Essential Medium (MEM, Product# 51416C, Sigma-Aldrich, St. Louis, MO) with 10% FBS 2 mM sodium pyruvate (Product# S8636, Sigma-Aldrich, St. Louis, MO), 1% Penicillin-Streptomycin and 0.025 mg/ml Amphotericin B. LN229 cells were cultured in Dulbecco's Modified Eagle Medium - high glucose (DMEM, Catalog# L0102, Biowest) containing 5% FBS (Product #F1051, Sigma-Aldrich, St. Louis, MO), 1% Penicillin-Streptomycin (Product #P4333, Sigma-Aldrich, St. Louis, MO) and 0.025 mg/ml Amphotericin B (Sigma-Aldrich, St. Louis, MO). Cells were maintained at 37 °C in a humidified incubator supplemented with 5% CO_2. Biological and technical repeats were used for each condition.

2.5. In vitro cytotoxicity assay

Cytotoxicity assay was performed to determine the cell growth inhibitory effect of the compounds following treatment for 48hrs on the GBM cell lines, U87 and LN229. This assay was performed in two stages. First, a high concentration, 100 μM, was used for all the compounds as well as for the positive control Cisplatin (Sigma-Aldrich, USA). Following which, in the second stage, the compounds, which exhibited better activity in the previous step, were selected, and different concentrations (100 μM, 75 μM, 50 μM, 25 μM, and 10 μM) were used to determine the IC_{50} of each compound. Treated cells were harvested by centrifugation at 1200 rpm for 10min. Cell viability was determined using trypan blue staining, using a Countess II Automated Cell Counter (Thermo Fisher Scientific) to count the number of live and dead cells. The inhibition percentage of each sample was determined using the following formula to determine the dose-response curve. From the dose-response curve, IC_{50} value of each compound was calculated.

Mortality % was calculated using the following formula:

$$\text{Mortality } (\%) = \frac{Mean\ No.\ of\ untreated\ cells\ (DMSO\ control) - Mean\ No.\ of\ treated\ cells \times 100}{Mean\ No.\ of\ untreated\ cells\ (DMSO\ control)}$$

2.5.1. Double staining assay

U87 and LN229 cell lines were grown as described previously, for 24hrs, followed by treatment with IC_{50} value of **R234** and incubated for 48hrs. Negative (untreated) and positive (Cisplatin) controls were maintained. Apoptosis/necrosis detection was carried out using Annexin V FITC and PI (Thermo Fisher Scientific). The apoptosis determination was performed following the standard protocol from the manufacture. Briefly, the cells were cultured in 6 well-plate with the initial cell density of 7×10^5 cells/well. The cells were incubated for 48hrs with **R234**, positive control and untreated cells conditions and then harvested and washed in cold PBS. The cell pellets were then resuspended in 1X Annexin-binding buffer provided in the kit. Consequently, 5 μL of FITC conjugated Annexin V and 1 μL of the 100 μg/ml PI working solutions were added to the 100 μL of cell suspension. The cells were incubated in dark for 15 min, at room temperature, after which the stained cells were observed for fluorescence to distinguish apoptotic cells. The image acquisition was done by using EVOS imaging system (ThermoFisher Scientific) with 20X objective magnification. Approximately 300 cells were used for each analysis.

2.6. Caspase activity assay

In vitro caspase-3 and caspase-7 activity leading to apoptosis was determined using Caspase-Glo® 3/7 Assay Systems (Promega Corporation). The reagent was prepared as mentioned by the manufacturer. The U87and LN229 cells were grown overnight in a 96-well-plate and were treated with IC_{50} of R234. Negative control, positive control and blank (medium + DMSO + dye) were maintained. Cells were incubated at 37 °C in a humidified incubator supplemented with 5% CO_2 for 5hrs and then equilibrated at room temperature for 30 min. 100 μL of Caspase-Glo 3/7 reagent was added to 100 μL of cells/well and was incubated in a dark-chamber. The luminescence signal was quantified (Chameleon Multi-label Detection Platform) at 1 h after treatment. Magnitude of fold change in luminescence between treated and untreated cells were determined using the following formula:

$$Fold\ increase = \frac{F_{test} - F_{blank}}{F_{control} - F_{blank}}$$

2.7. Intracellular redox potential test

To evaluate the redox potential of **R234**, a comparative test, using H_2O_2 and standard drug against untreated cells, was performed using H2DCFDA (Catalog no.#D399 Life Technologies, USA). The U87 and LN229 cells were grown overnight in a 96-well-plate and were treated with IC_{50} of **R234** for 5 h at 37 °C in a humidified incubator supplemented with 5% CO_2. Negative control, positive control and blank were maintained. Baseline effect due to solvent was determined as well. After 5hrs of treatment, cells were harvested by centrifugation at 3000 rpm for 10min and incubated with 200 μL of 2 μM H2DCFDA for 30 min at 37 °C in the CO_2 incubator. Cells were then washed with pre-warmed PBS and resuspended in 200 μL of pre-warmed medium.100 μL of suspension was then transferred to each well, in a 96-well plate and incubated at room temperature for 20min. Finally, fluorescence signal was measured using Chameleon Multi-label Detection Platform (Excitation 485 nm, Emission 535 nm).

2.8. Cell cycle intervention test

To elucidate the effect of the newly synthesized compound on the cell cycle progression, **R234** was examined against U87 and LN229 cells. A cell density of 1×10^6 cells were grown overnight at 37 °C in a humidified incubator supplemented with 5% CO_2, cells were exposed to **R234** at its IC_{50} concentration for 48hrs. The cells then were collected by trypsinization, washed with cold phosphate buffered saline (PBS) and pellet was resuspended in 100 μL of cold PBS. Subsequently, the cell suspension was added with 900 μL of 70% ethanol and stored at 4 °C for 30min. Following that, the cells were harvested by centrifugation at 3000 rpm, rinsed again by centrifugation with 1 mL cold PBS. The cells were then stained with 20 μL of DNA fluorochrome PI in a solution containing Triton X-100 and RNase and incubated at 37 °C in a humidified incubator supplemented with 5% CO_2, for 15 min. Finally, the fluorescence was detected by imaging using an EVOS FL Cell Imaging System.

2.9. RNA isolation and gene expression evaluation

Cell were incubated with IC_{50} of test compound and standard drug Cisplatin for 48 h at 37 °C in a humidified incubator supplemented with 5% $CO_{2.}$ A negative control was maintained as well. All conditions were conducted in triplicated RNA from all samples in profiling was isolated using same protocol. Total RNA of >9.25ng/uL was isolated using GeneJET RNA purification kit (Catalog no.#K0731), according to the manufacturer's instructions. The yield was then measured spectrophotometrically using NanoDrop-1000 (Thermoscientific, USA). After quantification, the cells were considered for quality assessment by TapeStation and expression assay by Illumina Next Seq High Output profiling followed by analysis and validation studies.

2.10. Statistical analysis

All experiments described in the present study were performed as with three biological and technical repeats. The data were presented as the mean ± standard error of mean. Statistical analyses between two groups were performed by Student's t-test. Differences among multiple groups were tested by one-way analysis of variance following by a Dunnett's multiple comparison test (GraphPad Prism 7.04). $P < 0.05$ was considered to indicate a statistically significant difference.

3. Results

3.1. AHAMCs interaction with receptor tyrosine kinase, TrkA

AHAMCs **1**–**23** were prepared according to Scheme of (Fig. 1a). Purity of all compounds (≥95%) was verified by melting point, NMR, elemental analysis and mass spectrometry measurements (see Supporting Information). Structures of these compounds are presented in Table 1. To obtain a deeper insight into the mode of

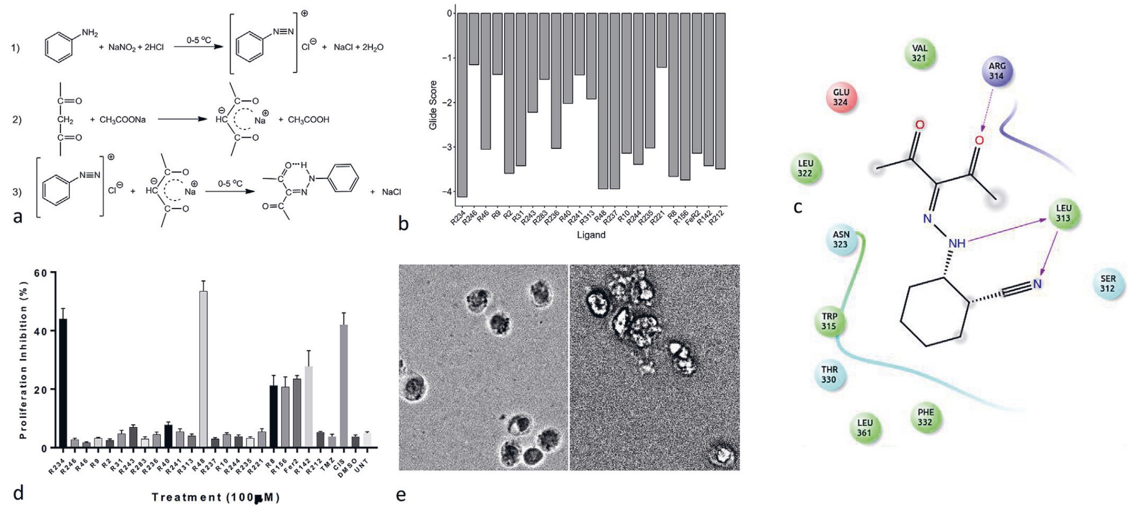

Fig. 1. a. Scheme: Japp-Klingemann synthesis of hydrazones [61–74]. b. Docking scores of a panel of 23 novel aryl hydrazones of active methylene compounds (AHMACs) with tyrosine kinase TrkA. c. Structure activity relationship of R234 with TrkA receptor. d. Cytotoxicity assay of 23 AHAMCs in U87 cell line. e. Phase contrast image of U87 cells under apoptosis (non-apoptotic-left, apoptotic-right).

action of all the novel derivatives (**1**–**23**) docking study was carried out against human NGFR protein, receptor tyrosine kinase, TrkA**.** The Glide docking results of the TrkA of interest with 23 ligands were presented in Fig. 1. b. The ligand **R234** shows better binding with the receptor compared with other 22 ligands with a highest Glide score (−4.12). **R234** forms interactions with 11 amino acid residues, which is shown as two-dimensional interaction diagram (Fig. 1c). There are six hydrophobic amino acid residues, three polar residues and two charged amino acid residues form interaction with the receptor. The amino acid residues 313LEU and 314ARG form hydrogen-bonding interactions with the R234. The hydrogen bonding interaction between the TrkA and R234 is shown with arrow marks in the two-dimensional ligand interaction diagram.

3.2. R234 effectively reduces cell viability and proliferation of GBM cells

To evaluate the efficiency of the AHMACs molecules as anti-GBM agents, effect on cell proliferation and viability was assessed for all synthesized compounds. Test compounds were initially screened against U87 cell line at 100uM concentration (Fig. 1d). Temolozamide and Cisplatin were used as positive control drugs and effects were evaluated against untreated cells. Baseline effect due to solvent was deducted. We have found the compound **R46** to have least cytotoxic activity. R234 and R48 induced higher anti-proliferative effect. However, docking of **R234** and R48 along with other compounds showed that **R234** has higher affinity than R48 with the TrkA receptor (Fig. 1b). Hence, the **R234** was further investigated to confirm the does- and time - dependent cytotoxic effect and found to be cytotoxic in GBM cell lines (Fig. 1e) To generalize the potency of **R234** activity we used multiple GBM cell lines, LN229 and U87. The dose-response study was performed as described in the methods section and IC_{50} was determined for both cell lines. As expected, there was a gradient increase in mortality with increasing dosage in both cell lines, and IC_{50} value of **R234** was calculated as 107 μM in U87 and 87 μM in LN229, whereas IC_{50} value of Cisplatin was found to be 53 μM and 101 μM in U87 and LN229, respectively (Fig. 2a and b). Surprisingly, there was steady increase in cytotoxicity over first 48hrs whereas a loss in cytotoxic activity was observed after 48 h, in both U87 and LN229 cell lines) (Fig. 2 c and d). In addition, R234 was also tested against the growth of normal brain cells (Mouse Embryonic Fibroblasts, MEF). At 100 μM treatment the cells expressed less than 20% death suggesting that R234 cytotoxic effect is specific to GBM cells (data not show).

3.3. R234 interrupts of cell cycle by inducing G1/S arrest

In order to investigate whether **R234** induces cell cycle disturbances in GBM cells, cell cycle analysis was performed using Propidium iodide staining method as described in method section, following **R234** treatment at IC_{50} for 24 h. Cells exhibit fluorescence bright red, proportionate to their DNA content in each cell phase (Fig. 3a and b). Significant G1/S transition arrest was observed in U87 cells treated with R234, with a concomitant reduction in the fraction of cells in S phase. Fraction of cells in G1 phase was 47.7% in **R234** treatment, 44.0% in positive control Cisplatin and 39.7% in untreated cells. In S phase, the percentage of the population was 2.8% in **R234** treatment, 5.6% in positive control and 19.2% in untreated cells (Fig. 3c). Baseline effect due to DMSO was negligible. However, in LN229, a similar trend of minimal cell fraction in S phase cells were observed, in treated condition in comparison to untreated condition. Particularly, higher fraction of cells at G1 phase in was observed in **R234** treatment. Low fraction of cells in G2/M in **R234** treated cells clearly indicates that the drug induces cell cycle arrest at G1/S (Fig. 3d).

Cell cycle gene expression analysis of U87 cell line revealed differential expression of 77 genes associated with G1-S phase, 82 in S phase and 74 in G2/M phase. Down regulation of ORCs (ORC1, ORC6) and MCMs (MCM3-7) were observed clearly indicating the blocking of DNA elongation. Gene expression analysis highlighted the P53 activation and subsequent downregulation of cyclins, cyclin-dependent kinases and other key molecules involved in cell cycle such as CCNE, E2F, CCND, CDK6 etc. (Fig. 3e). The high fraction of cell population in G1 phase in **R234** treated cells could be

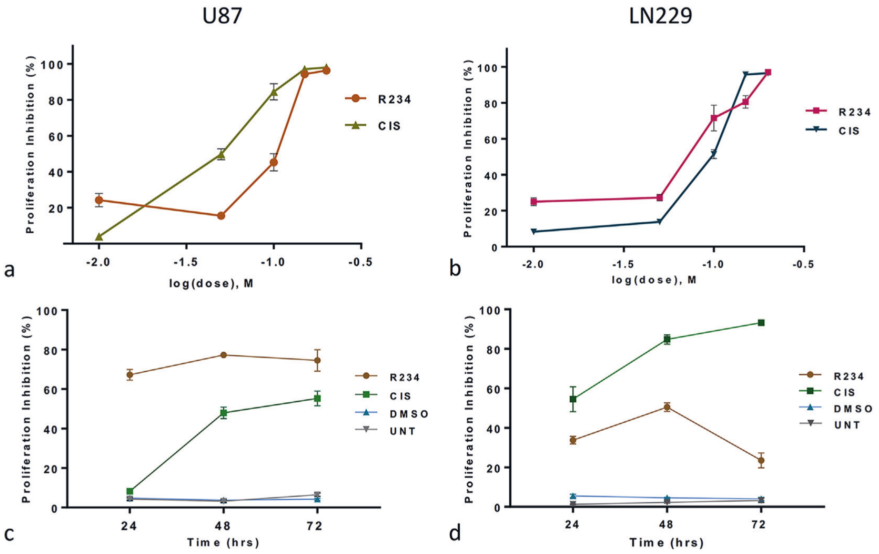

Fig. 2. R234 inhibits GBM cell proliferation in a time and dose dependent manner. a. U87 cells were treated for 5hrs with 0–200 μM quantity of R234, after 24hrs of cell growth. Cellular viability was measured by the Trypan Blue exclusion method. Datapoints and error bars represent mean ± S.E.M ($n = 4$ per group). *$P < 0.05$ per one-way ANOVA. b. U87 cells were treated for 5hrs, with 0–200 μM quantity of R234, after 24 h of cell growth. Datapoints and error bars represent mean ± S.E.M ($n = 4$ per group). *$P < 0.05$ per one-way ANOVA. c. U87 cells were harvested after 24 h of cell growth and subsequently treated with IC_{50} value of R234 upto 72hrs. Proliferation Inhibition was monitored every 24hrs. Data points and error bars represent mean ± S.E.M ($n = 4$ per group). *$P < 0.05$ per one-way ANOVA. d. LN229 cells were harvested after 24hrs of cell growth and subsequently treated with IC_{50} value of R234 upto 72hrs. Proliferation Inhibition was monitored every 24hrs. Datapoints and error bars represent mean ± S.E.M ($n = 4$ per group). *$P < 0.05$ per one-way ANOVA. (For interpretation of the references to color in this figure legend, the reader is referred to the Web version of this article.)

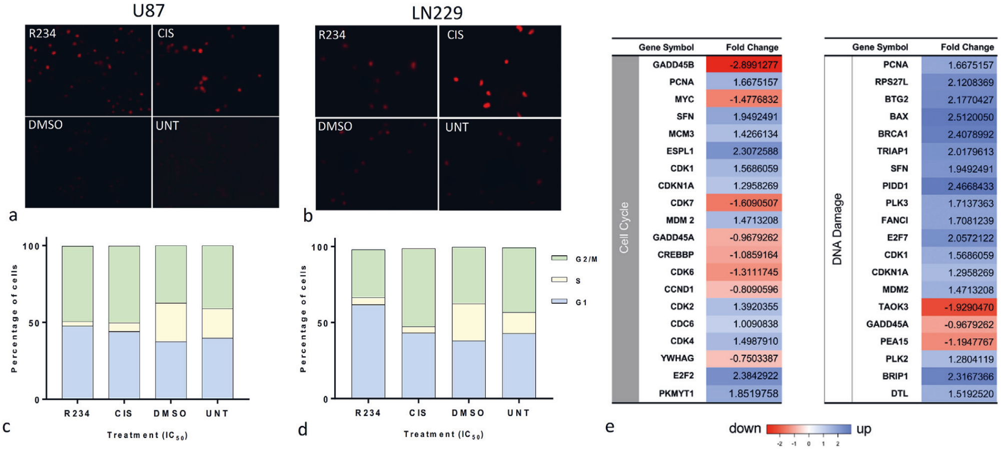

	Gene Symbol	Fold Change
Cell Cycle	GADD45B	-2.8991277
	PCNA	1.6675157
	MYC	-1.4776832
	SFN	1.9492491
	MCM3	1.4266134
	ESPL1	2.3072588
	CDK1	1.5686059
	CDKN1A	1.2958269
	CDK7	-1.6090507
	MDM 2	1.4713208
	GADD45A	-0.9679262
	CREBBP	-1.0859164
	CDK6	-1.3111745
	CCND1	-0.8090596
	CDK2	1.3920355
	CDC6	1.0090838
	CDK4	1.4987910
	YWHAG	-0.7503387
	E2F2	2.3842922
	PKMYT1	1.8519758

	Gene Symbol	Fold Change
DNA Damage	PCNA	1.6675157
	RPS27L	2.1208369
	BTG2	2.1770427
	BAX	2.5120050
	BRCA1	2.4078992
	TRIAP1	2.0179613
	SFN	1.9492491
	PIDD1	2.4668433
	PLK3	1.7137363
	FANCI	1.7081239
	E2F7	2.0572122
	CDK1	1.5686059
	CDKN1A	1.2958269
	MDM2	1.4713208
	TAOK3	-1.9290470
	GADD45A	-0.9679262
	PEA15	-1.1947767
	PLK2	1.2804119
	BRIP1	2.3167366
	DTL	1.5192520

Fig. 3. R234 induces cell cycle arrest in GBM cells. Cells were treated with DMSO (negative control), Cisplastin (positive control) and R234 for 48hrs. Microscopic image analysis was performed for cell-cycle distribution. The DNA content was evaluated with Propidium iodide (PI) staining and fluorescence measured and analyzed. **a.** Representative fluorescence microscopy images for each treated or untreated groups in U87, in S phase. **b.** Representative fluorescence microscopy images for each treated or untreated groups in LN229 cells. c. Percentage of U87 cells in various phases is fraction of whole population. d. Percentage of LN229 cells in various phases is fraction of whole population. Data represented as mean ± S.E.M of triplicates, *$p < 0.05$ as compared with the control group. **e.** Fold change for the list of representative genes in the cell cycle and DNA damage pathways. The blue and red colors represent those genes that were upregulated and downregulated, respectively. (For interpretation of the references to color in this figure legend, the reader is referred to the Web version of this article.)

explained by the Rb mediated downregulation of Cyclin E (CCNE), which is required for the transition from G1 to S phase of the cell cycle.

3.4. R234 induces apoptosis by negatively regulating stress protective mechanisms and DNA damage repair

Apoptosis assay was performed using Annexin V/PI test to

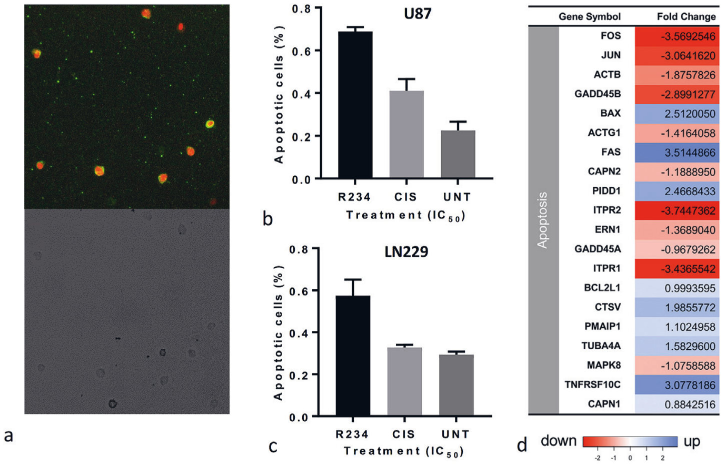

Fig. 4. Annexin V/PI double-staining assay of GBM cells treated with R234 for 48 h indicates that the drug effectively induced apoptosis as compared to control cells. **a**. Fluorocytogram of U87 cells exhibited upon Annexin V/PI double-staining (top). Phase contrast image of the treated cells(bottom). **b.** The histogram represents the percentage of PI_positive cells, in the U87 population. **c.** The percentage of PI positive cells, in the U87 population. **d.** Key genes involved in Apoptotic process and their Log2(Fold Change), that are differentially expressed upon R234 treatment, compared to untreated. *p < 0.05 as produced by ANOVA test.

determine the fraction of apoptotic cells. Apoptotic cells appeared bright red, necrotic cells as bright green and apo-nectrotic cells as bright orange (Fig. 4a). In U87 cell line, 68.7% of population under R234 treatment were found to be apoptotic, followed by 41.0% in Cisplatin treatment, and 22.4% in untreated cells (Fig. 4b). In LN229 cell line, this was 57.3% of the population under R234 treatment, followed by 32.6% in Cisplatin treatment, and 29.3% in untreated cells (Fig. 4c). Relevantly, the key differentially expressed genes involved in apoptotic process were identified as FOS, JUN, ITPR, ACTB and ACTG1(Fig. 4d) Transcriptome analysis identified upregulation of pro-apoptotic genes such as NOXA, PUMA, BIM, and downregulation of IAPs, HSPs (Supplementary file 2), that favours cell survival, suggesting the positive role **R234** in cancer cell apoptosis and chemosensitizing. Also, DNA repair genes such as GADD45s and SESNs were found to be notably downregulated. Genes such as TUBB3, ACTB, TESK1, PARVA, and ACTN1 were also found to be downregulated suggesting negatively affecting cellular integrity and survival. Stress response genes such as NQO1, GSTs and TrxR1 were also downregulated, which is sensitizes the cell to chemotherapy.

Reactive oxygen species (ROS) mediated caspase activation and subsequent cell death has been repeatedly reported by various studies [77–79]. Both intracellular ROS and caspase in U87 cells were quantified to assess redox flux as subsequent caspase activation due to the treatment with candidate molecule. The oxidative potential of **R234** was determined by ROS assay using H2DCFDA indicator as described in methods section. The results shows that oxidative stress increase of 9.5% in the **R234** treated U87 cells when compared to untreated cells, whereas the standard drug cisplatin and positive control H_2O_2 marked 3.7% and 1.6% respectively. However, in LN229 cell line there was no statistically significant difference found between treated and untreated cell (Fig. 5a). These results suggest that ROS may not played a major role in R234 induced GBM cell death.

Considering the role of ROS in caspase-mediated apoptosis, we determined the caspase activity of both cell lines using caspase 3/7 assay after a treatment period of 5hrs with IC_{50} of **R234**. Interestingly, U87 cells treated with **R234** displayed a reduction of caspase 3/7, displaying a decrease of 60.2% in comparison to untreated cancer cells, whereas positive control displayed 1.03% increase in caspase activity. In LN229, both candidate drug as well as positive control exhibited a reduction in caspase activity with 36.1% and 56.4% respectively (Fig. 5b). The difference between **R234** treated and untreated conditions, was confirmed to be statistically significant, per ANOVA test (P-value < 0.05). Over all, these observations suggest that ROS-independent and caspase-depended apoptosis is induced by R234.

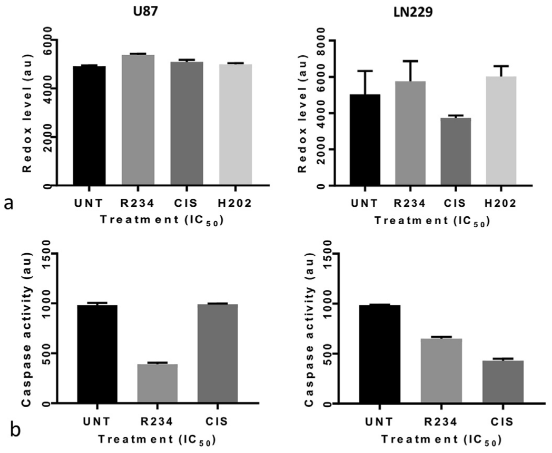

Fig. 5. a. Effect of R234 on intracellular ROS production by GBM cells(U87 cells-left, LN229 cells-right). R234 treatment marginally increased cellular oxidation in both cell lines. **b**. Caspase activity displayed by GBM cells analyzed using caspase3/7 luminescence assay kit. Decrease in caspase activity of cells was observed after treatment with IC_{50} of R234 for 5hrs compared to control. The values are expressed as means ± SEM of triplicate measurements of at least two independent experiments. Significant differences compared between control and treated cells (*p < 0.05).

3.5. Differentially expressed genes between GBM cells treated with R234 and control samples

In the DEGs analysis, 22,260 genes were mapped by at least one read in each sample profile. In total, 5619 DEGs with a q-value $<$ 0.05 and fold change $>$1.5 were detected over the 2 comparisons of R234 with Untreated and R234 with Cisplatin in DESeq2 (Supplementary file 2). The numbers of differentially expressed genes with more than 2-fold change were higher in negative control. Therefore, there were higher number of differentially expressed genes in R234 cell line when analyzed with untreated cell line. We applied the MA plot function in DESeq2 to visualize the top genes with the smallest q-values (Fig. 6a). We investigated the similarity in differential gene expression profiles regulated untreated samples and Cisplatin treated samples. The fold-changes in overlapped genes filtered by the q-value $<$ 0.05 were plotted for U87 cell line. Venn diagrams indicated overlap in genes whose expression was regulated in the same direction (Fig. 6b). The total number and up- or down-regulated number of DEGs ($>=$2-fold change, p-value 0.05) for untreated, Cisplatin and Both (Fig. 6c). We identified 3256 DEGs between R234 and Untreated (negative control) samples (q-value $<$ 0.05). We also compared the R234 and Cisplatin samples as a positive control group, both individually and combined as a single “affected” group. In these comparisons, 2442 number of DEGs were identified, with the largest number of DEGs identified in comparison with the untreated samples, and 1321 out of 5619 DEGs are common in both comparison (Supplementary file 2 and Fig. 6b). The complete lists of DEGs from the cell line analysis and all pairs of comparisons are presented in Supplementary file 2.

3.6. R234 disrupt the functions and pathways of GBM

Pathway effects were elucidated by Gene Ontology analysis to analyze up and down regulated genes concerning DNA damage, cell cycle and apoptosis for R234 and untreated sample comparison. GO analysis identified the list of genes that were enriched in DNA replication, protein folding and regulation of transcription in response to stress. These biological processes are involved in the DNA replication pathway for Cisplatin (Fig. 6d left). Enrichment analysis for GO molecular function and pathways clearly demonstrated related phenotypes associated with GBM (Fig. 6d right). GO terms cadherin binding, damaged DNA binding for molecular function appeared to be significantly overrepresented, and none significantly underrepresented. Cadherin binding, a type I membrane protein involved in cell adhesion and damaged DNA binding, interacting selectively and non-covalently with damaged DNA have coordinated effect on regulation and function in DNA damage (will discuss the list of pathways to add).

There were 3256 DEGs, including 1595 upregulated and 1661 downregulated DEGs, between **R234**-treated and untreated expression profiles. Interestingly, 1866 DEGs were found to have overrepresented in both in Cisplatin as well as **R234** treatment. Genes downregulated due to **R234** were enriched in KEGG pathways including Endocytosis, Cell cycle, Focal adhesion, p53 signaling pathway, Neurotrophin signaling pathway and cell cycle, whereas upregulated genes were associated with the pathways of Apoptosis, MAPK signaling pathway, Lysosome, Spingolipid signaling pathway and Proteoglycans in cancer(Supplementary file 2). Top20 overrepresented genes associated with significant processes such as cell cycle, DNA Damage and Apoptosis are given in Fig. 5c. It is interesting to note that following **R234** treatment, a

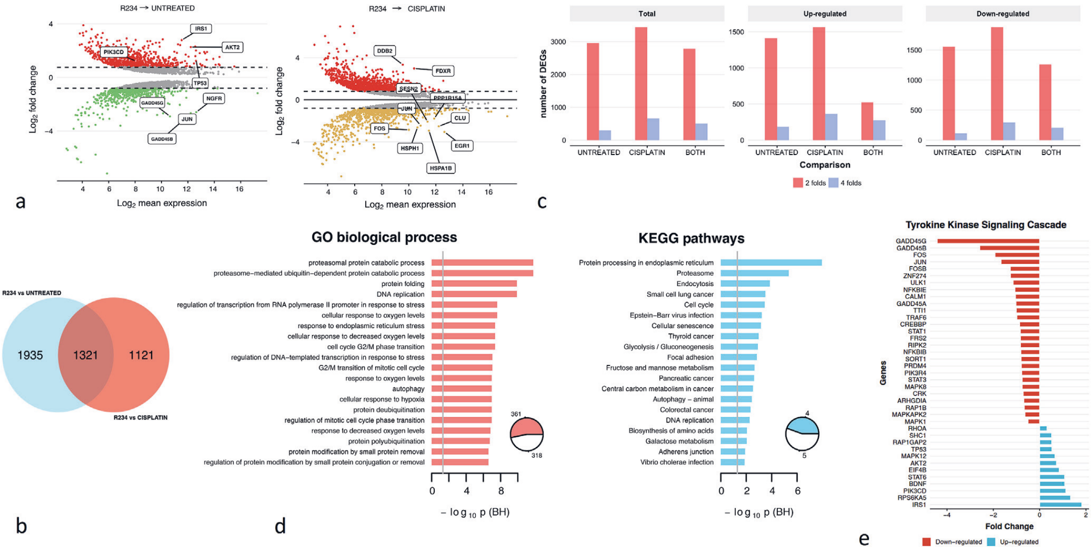

Fig. 6. a. The MA-plot from means and log fold changes. It shows differential gene expression from the two inter-group comparisons (R224 vs. Untreated; R224 vs. Cisplatin). **b.** Overlapping DEGs in Untreated vs R234 and Cisplatin vs R234 compared. For the comparison, only genes with a q-value $<$ 0.05 were considered as DEGs. The number of DEGs found at each comparison are indicated. **c.** The total number and up- or down-regulated number of DEGs ($>=$ twofold change, p-value 0.05) for Untreated, Cisplatin and Both. **d.** Biological processes represented by the DEGs ($<=$ twofold cutoff, p-value $<$ 0.05) for R224 in comparison with untreated samples, using GO enrichment analysis. The percentage showed that the number of DEGs hit against total number of genes belonging to each GO terms in the categories(left). KEGG enrichment analysis identifying the most affected signaling pathways ($>=$ twofold cutoff, p-value $<$ 0.05) (right). **e.** RNA-Seq analysis of the expression representative of 40 genes by comparing the R224 and Untreated samples from the gene expression in U87 cell line. It shows the up- and down-regulated genes associated with Tyrokine Kinase Signaling cascade, and the log fold changes.

significant reduction in HSPs, IAPs, Proto-oncogenes, pro-survival genes as well as increase in pro-apoptotic genes were observed, suggesting increased chemo-sensitivity and low survival [80]. Also many of the genes providing cell stability was found to be downregulated such as TUBB3, ACTB, MCL1, PARP, SPTAN1, MITF etc (Supplementary file 2).

3.7. R234 exerts antiproliferation effects on GBM cells via RTK pathways

The molecular mechanisms of **R234**-mediated growth inhibition of GBM cells further investigated by gene expression analysis as described in method section. The effects of R234 on oncogenic RTK signaling were investigated using RNA seq analysis. R234 decreased the activation of significant genes in RTK pathway such as JUN, FOS, MAPK8 etc (Fig. 6e). Additionally many other significant genes involved in the pathway was found to be suppressed by R234, such as, mTOR, HIF1A, EIF4E, NRF2, MAP3K, GRB2, MAPK1, FOS and GSK3, while increasing TP53, RBL2, Bim, Noxa, Puma, HDAC etc. (Supplementary file 2). The major implication of RTK mediated anti-GBM effects are through AKT signaling, affecting mTOR cascade, P53 pathways, JNK pathway, FOXOs, IAPs and other significant molecules affecting cell cycle, growth, proliferation, cell survival and cellular metabolism (Supplementary file 2). One interesting observation was the downregulation of NGFR downstream signaling pathway genes such as PI3K, JNK, NF-kβ pathways demonstrating the potential of R234 to act as an antagonist of RTK pathways.

In detail, the gene expression analysis also revealed that **R234** significantly downregulates NGFR mediated signaling indicated by downregulation of MAP3K, GRB2, MKK3, and JNK1 (Supplementary file 2). This subsequently affects key genes such as mTOR and P53 via Akt signaling leading to cell cycle arrest, proliferation inhibition, anti-angiogenesis and chemo-sensitization, via multiple pathways. The PI3K/Akt/mTOR signaling pathway promotes cellular growth, migration, protein synthesis, survival and metabolism in tumor cells [81–83]. The expression of PI3K/Akt/mTOR pathway was significantly reduced in **R234** treated cells, compared to control as evident from the gene expression profile.

4. Discussion

Despite huge efforts being taken to develop potent drugs to fight glioblastoma, only a minority of patients benefit with currently approved chemotherapies. In the present study, we have demonstrated that a novel hydrazone derivative **R234** exerts cytotoxic, antiangiogenic and pro-apoptotic activity via RTK signaling pathways. **R234** demonstrated the effective anti-proliferative activity in a dose- and time-dependent manner. This observation is supported by earlier studies published on hydrazone derivatives as potent anti-tumor [84–88] agents.

Interestingly, **R234** exposure at an IC_{50} concentration for 24 h caused cell cycle arrest at the G1/S phase and subsequent apoptosis, which may be a therapeutic aspect for its use in cancer chemotherapy. **R234** effectively reduces CCNE, CDK6 and E2Fs whereas upregulates RBL1 (RB family protein), which may explain the G1/S transition arrest. Cells advancement from G1 to S-phase irreversibly relies on cyclin E/cdk2 phosphorylation of pRB to release activator E2Fs that transcribe cyclin E [89]. Down regulation of CCNE thus negatively regulates G1 to S phase transition. The downregulation of MCMs and ORCs gene expression affecting the pre-replicative (pre-RC) complex demarks the origin to be licensed, to be triggered and initiate DNA synthesis. Also it has been shown that, pRB can physically localize to replication origins in S-phase to arrest DNA synthesis, through unknown molecular mechanisms by which it blocks synthesis [90]. This justifies our observation of a longer G1 phase and a short S phase in case of **R234** treated cells.

Gene expression profile analysis also revealed the increased levels of FOXO4, which negatively regulates the cell cycle, whereas low NRF2 increase chemo-sensitivity as well as stress-induced death susceptibility. **R234** also negatively regulates cell growth and differentiation via CREB, as indicated by low levels of CREBBP. **R234** effectively promotes cell apoptosis and cell cycle arrest via elevating p53 level, which is often downregulated in most cancers. The p53 gene exerts its effect via p21 by downregulating cell cycle proteins such as CCND, CCNE, CDK6 and E2F, as well as upregulating RBL2, HDAC as evident from our transcriptome analysis. Increase in p53 also affects other tumorigenic features such as promoting apoptosis via upregulation of pro-apoptotic genes like Noxa, Puma, Bim, FAS, BAX, PIDD and reducing proliferation and damage repair via downregulation of GADD45s, SESNs and BAX as supported by our results.

Further gene expression analysis also revealed the anti-cancer effects of **R234** via other pathways such as JAK-STAT pathway, as marked by downregulation of genes such as JAK1, STAT3, STAT1, GRB2, PIM1, CCND, also affecting the MAPK pathway and JNK pathway indicated by downregulation of significant genes such as JUN and FOS, decreasing angiogenesis and proliferation. In addition, the drug increase chemo-sensitivity by suppressing MITF, and affecting cytoskeletal proteins such as TUBB3, MCL1, ACTB and SPTAN1. Over all, inhibitory activity of PI3K/Akt/mTOR signaling pathway and cell cycle pathways were found and correlated with the cell death activation, which suggest that this class of compound might function by inhibiting multiple key proteins involved in the RTK signaling pathways. In addition, the top compound **R234 was identified to have** interactions with 11 amino acid residues of TrkA. The amino acid residues 313LEU and 314ARG formed hydrogen-bonding interactions with this compound. Compared all the tested compounds R234 had higher hydrogen bonding interaction between the TrkA. Thus, newly synthesized compound R234 could be considered as promising RTK inhibitors for the development of potential anti-GBM drug.

Author contributions

FZ and AG synthesized and characterized the compounds; AV and DK performed the *in vitro* experiments, and AM analyzed the RNA-seq data; FES supervised the gene expression and pathway analysis. MK and OY conceived and supervised the work, wrote and revised the manuscript. All authors approved the submitted version.

Conflicts of interest

The authors declare there are no conflict of interest.

Appendix A. Supplementary data

Supplementary data to this article can be found online at https://doi.org/10.1016/j.ejmech.2019.01.021.

Funding

MK, AV and OYH acknowledge the Academy of Finland for the project grant support (decision no. 297200) and Tampere University of Technology for Instrumental facility grant support. The publication was prepared with the support of the “RUDN University Program 5–100”.

References

[1] J. Chen, R.M. McKay, L.F. Parada, Malignant glioma: lessons from genomics, mouse models, and stem cells, Cell (2012), https://doi.org/10.1016/j.cell.2012.03.009.

[2] C.W. Brennan, R.G.W. Verhaak, A. McKenna, B. Campos, H. Noushmehr, S.R. Salama, S. Zheng, D. Chakravarty, J.Z. Sanborn, S.H. Berman, R. Beroukhim, B. Bernard, C.J. Wu, G. Genovese, I. Shmulevich, J. Barnholtz-Sloan, L. Zou, R. Vegesna, S.A. Shukla, G. Ciriello, W.K. Yung, W. Zhang, C. Sougnez, T. Mikkelsen, K. Aldape, D.D. Bigner, E.G. Van Meir, M. Prados, A. Sloan, K.L. Black, J. Eschbacher, G. Finocchiaro, W. Friedman, D.W. Andrews, A. Guha, M. Iacocca, B.P. O'Neill, G. Foltz, J. Myers, D.J. Weisenberger, R. Penny, R. Kucherlapati, C.M. Perou, D.N. Hayes, R. Gibbs, M. Marra, G.B. Mills, E. Lander, P. Spellman, R. Wilson, C. Sander, J. Weinstein, M. Meyerson, S. Gabriel, P.W. Laird, D. Haussler, G. Getz, L. Chin, C. Benz, W. Barrett, Q. Ostrom, Y. Wolinsky, B. Bose, P.T. Boulos, M. Boulos, J. Brown, C. Czerinski, M. Eppley, T. Kempista, T. Kitko, Y. Koyfman, B. Rabeno, P. Rastogi, M. Sugarman, P. Swanson, K. Yalamanchii, I.P. Otey, Y.S. Liu, Y. Xiao, J.T. Auman, P.C. Chen, A. Hadjipanayis, E. Lee, S. Lee, P.J. Park, J. Seidman, L. Yang, S. Kalkanis, L.M. Poisson, A. Raghunathan, L. Scarpace, R. Bressler, A. Eakin, L. Iype, R.B. Kreisberg, K. Leinonen, S. Reynolds, H. Rovira, V. Thorsson, M.J. Annala, J. Paulauskis, M. Curley, D. Hatfield, S. Mallery, T. Morris, C. Shelton, M. Shelton, P. Sherman, L. Yena, F. Cuppini, M. DiMeco, E. Eoli, B. Maderna, M. Pollo, S. Saini, K.A. Balu, L. Hoadley, C.R. Li, Y. Miller, M.D. Shi, J. Topal, G. Wu, C. Dunn, B.A. Giannini, Y. Aksoy, L. Antipin, E. Borsu, J. Cerami, B. Gao, A. Gross, M. Jacobsen, A. Ladanyi, Y. Lash, B. Liang, N. Reva, R. Schultz, N.D. Shen, A. Socci, M.L. Viale, Q.R. Ferguson, J.A. Chen, L.A.L. Demchok, K.R. Dillon, M. Mills Shaw, R. Sheth, Z. Tarnuzzer, L. Wang, T. Yang, M.S. Davidsen, B.A. Guyer, H.J. Ozenberger, J. Sofia, J. Bergsten, J. Eckman, C. Harr, K. Smith, C. Tucker, L.A. Winemiller, J.Y. Zach, G. Ljubimova, B. Eley, M.A. Ayala, A. Jensen, T.D. Kahn, D.A. Pihl, Y. Pot, N. Wan, P. Hansen, B. Hothi, Lin, N. Shah, J.G. Yoon, C. Lau, M. Berens, K. Ardlie, S.L. Carter, A.D. Cherniack, M. Noble, J. Cho, K. Cibulskis, D. DiCara, S. Frazer, S.B. Gabriel, N. Gehlenborg, J. Gentry, D. Heiman, J. Kim, R. Jing, E.S. Lander, M. Lawrence, P. Lin, W. Mallard, R.C. Onofrio, G. Saksena, S. Schumacher, P. Stojanov, B. Tabak, D. Voet, H. Zhang, N.N. Dees, L. Ding, L.L. Fulton, R.S. Fulton, K.L. Kanchi, E.R. Mardis, R.K. Wilson, S.B. Baylin, L. Harshyne, M.L. Cohen, K. Devine, A.E. Sloan, S.R. Van Den Berg, M.S. Berger, D. Carlin, B. Craft, K. Ellrott, M. Goldman, T. Goldstein, M. Grifford, S. Ma, S. Ng, J. Stuart, T. Swatloski, P. Waltman, J. Zhu, R. Foss, B. Frentzen, R. McTiernan, A. Yachnis, Y. Mao, R. Akbani, O. Bogler, G.N. Fuller, W. Liu, Y. Liu, Y. Lu, A. Protopopov, X. Ren, Y. Sun, W.K.A. Yung, J. Zhang, K. Chen, J.N. Weinstein, M.S. Bootwalla, P.H. Lai, T.J. Triche, D.J. Van Den Berg, D.H. Gutmann, N.L. Lehman, D. Brat, J.J. Olson, G.M. Mastrogianakis, N.S. Devi, Z. Zhang, E. Lipp, R. McLendon, The somatic genomic landscape of glioblastoma, Cell 155 (2013), https://doi.org/10.1016/j.cell.2013.09.034.

[3] R. McLendon, A. Friedman, D. Bigner, E.G. Van Meir, D.J. Brat, G.M. Mastrogianakis, J.J. Olson, T. Mikkelsen, N. Lehman, K. Aldape, W.K.A. Yung, O. Bogler, J.N. Weinstein, S. VandenBerg, M. Berger, M. Prados, D. Muzny, M. Morgan, S. Scherer, A. Sabo, L. Nazareth, L. Lewis, O. Hall, Y. Zhu, Y. Ren, O. Alvi, J. Yao, A. Hawes, S. Jhangiani, G. Fowler, A. San Lucas, C. Kovar, A. Cree, H. Dinh, J. Santibanez, V. Joshi, M.L. Gonzalez-Garay, C.A. Miller, A. Milosavljevic, L. Donehower, D.A. Wheeler, R.A. Gibbs, K. Cibulskis, C. Sougnez, T. Fennell, S. Mahan, J. Wilkinson, L. Ziaugra, R. Onofrio, T. Bloom, R. Nicol, K. Ardlie, J. Baldwin, S. Gabriel, E.S. Lander, L. Ding, R.S. Fulton, M.D. McLellan, J. Wallis, D.E. Larson, X. Shi, R. Abbott, L. Fulton, K. Chen, D.C. Koboldt, M.C. Wendl, R. Meyer, Y. Tang, L. Lin, J.R. Osborne, B.H. Dunford-Shore, T.L. Miner, K. Delehaunty, C. Markovic, G. Swift, W. Courtney, C. Pohl, S. Abbott, A. Hawkins, S. Leong, C. Haipek, H. Schmidt, M. Wiechert, T. Vickery, S. Scott, D.J. Dooling, A. Chinwalla, G.M. Weinstock, E.R. Mardis, R.K. Wilson, G. Getz, W. Winckler, R.G.W. Verhaak, M.S. Lawrence, M. O'Kelly, J. Robinson, G. Alexe, R. Beroukhim, S. Carter, D. Chiang, J. Gould, S. Gupta, J. Korn, C. Mermel, J. Mesirov, S. Monti, H. Nguyen, M. Parkin, M. Reich, N. Stransky, B.A. Weir, L. Garraway, T. Golub, M. Meyerson, L. Chin, A. Protopopov, J. Zhang, I. Perna, S. Aronson, N. Sathiamoorthy, G. Ren, J. Yao, W.R. Wiedemeyer, H. Kim, W.K. Sek, Y. Xiao, I.S. Kohane, J. Seidman, P.J. Park, R. Kucherlapati, P.W. Laird, L. Cope, J.G. Herman, D.J. Weisenberger, F. Pan, D. Van Den Berg, L. Van Neste, M.Y. Joo, K.E. Schuebel, S.B. Baylin, D.M. Absher, J.Z. Li, A. Southwick, S. Brady, A. Aggarwal, T. Chung, G. Sherlock, J.D. Brooks, R.M. Myers, P.T. Spellman, E. Purdom, L.R. Jakkula, A.V. Lapuk, H. Marr, S. Dorton, G.C. Yoon, J. Han, A. Ray, V. Wang, S. Durinck, M. Robinson, N.J. Wang, K. Vranizan, V. Peng, E. Van Name, G.V. Fontenay, J. Ngai, J.G. Conboy, B. Parvin, H.S. Feiler, T.P. Speed, J.W. Gray, C. Brennan, N.D. Socci, A. Olshen, B.S. Taylor, A. Lash, N. Schultz, B. Reva, Y. Antipin, A. Stukalov, B. Gross, E. Cerami, Q.W. Wei, L.X. Qin, V.E. Seshan, L. Villafania, M. Cavatore, L. Borsu, A. Viale, W. Gerald, C. Sander, M. Ladanyi, C.M. Perou, D.N. Hayes, M.D. Topal, K.A. Hoadley, Y. Qi, S. Balu, Y. Shi, J. Wu, R. Penny, M. Bittner, T. Shelton, E. Lenkiewicz, S. Morris, D. Beasley, S. Sanders, A. Kahn, R. Sfeir, J. Chen, D. Nassau, L. Feng, E. Hickey, A. Barker, D.S. Gerhard, J. Vockley, C. Compton, J. Vaught, P. Fielding, M.L. Ferguson, C. Schaefer, J. Zhang, S. Madhavan, K.H. Buetow, F. Collins, P. Good, M. Guyer, B. Ozenberger, J. Peterson, E. Thomson, Comprehensive genomic characterization defines human glioblastoma genes and core pathways, Nature (2008), https://doi.org/10.1038/nature07385.

[4] P. Blume-Jensen, T. Hunter, Oncogenic kinase signalling, Nature (2001), https://doi.org/10.1038/35077225.

[5] N.J. Szerlip, A. Pedraza, D. Chakravarty, M. Azim, J. McGuire, Y. Fang, T. Ozawa, E.C. Holland, J.T. Huse, S. Jhanwar, M.A. Leversha, T. Mikkelsen, C.W. Brennan, Intratumoral heterogeneity of receptor tyrosine kinases EGFR and PDGFRA amplification in glioblastoma defines subpopulations with distinct growth factor response, Proc. Natl. Acad. Sci. (2012), https://doi.org/10.1073/pnas.1114033109.

[6] J.M. Stommel, A.C. Kimmelman, H. Ying, R. Nabioullin, A.H. Ponugoti, R. Wiedemeyer, A.H. Stegh, J.E. Bradner, K.L. Ligon, C. Brennan, L. Chin, R. a DePinho, Coactivation of receptor tyrosine kinases affects the response of tumor cells to targeted therapies, Science (2007), https://doi.org/10.1126/science.1142946.

[7] T. Regad, Targeting RTK Signaling Pathways in Cancer, Cancers (Basel), 2015, https://doi.org/10.3390/cancers7030860.

[8] S. Lawn, N. Krishna, A. Pisklakova, X. Qu, D.A. Fenstermacher, M. Fournier, F.D. Vrionis, N. Tran, J.A. Chan, R.S. Kenchappa, P.A. Forsyth, Neurotrophin signaling via TrkB and TrkC receptors promotes the growth of brain tumor-initiating cells, J. Biol. Chem. (2015), https://doi.org/10.1074/jbc.M114.599373.

[9] S. Wadhwa, T.C. Nag, A. Jindal, R. Kushwaha, A.K. Mahapatra, C. Sarkar, Expression of the neurotrophin receptors Trk A and Trk B in adult human astrocytoma and glioblastoma, J. Biosci. (2003), https://doi.org/10.1007/BF02706217.

[10] M. Bassili, E. Birman, N.F. Schor, H.U. Saragovi, Differential roles of Trk and p75 neurotrophin receptors in tumorigenesis and chemoresistance ex vivo and in vivo, Cancer Chemother. Pharmacol. (2010), https://doi.org/10.1007/s00280-009-1110-x.

[11] D.E. Bredesen, S. Rabizadeh, p75(NTR) and apoptosis: Trk-dependent and Trk-independent effects, Trends Neurosci. (1997), https://doi.org/10.1016/S0166-2236(96)01049-1.

[12] M. Barbacid, The Trk family of neurotrophin receptors, J. Neurobiol. (1994), https://doi.org/10.1002/neu.480251107.

[13] Y. Wang, C. Hagel, W. Hamel, S. Müller, L. Kluwe, M. Westphal, Trk A, B, and C are commonly expressed in human astrocytes and astrocytic gliomas but not by human oligodendrocytes and oligodendroglioma, Acta Neuropathol. (1998), https://doi.org/10.1007/s004010050906.

[14] A.M. Lange, H.W. Lo, Inhibiting TRK proteins in clinical cancer therapy, Cancers (Basel) (2018), https://doi.org/10.3390/cancers10040105.

[15] J. Meldolesi, Neurotrophin Trk receptors: new targets for cancer therapy, Rev. Physiol. Biochem. Pharmacol. (2017), https://doi.org/10.1007/112_2017_6.

[16] J.J. Gentry, P. Casaccia-Bonnefil, B.D. Carter, Nerve growth factor activation of nuclear factor ??B through its p75 receptor is an anti-apoptotic signal in RN22 schwannoma cells, J. Biol. Chem. (2000), https://doi.org/10.1074/jbc.275.11.7558.

[17] A. Chittka, J.C. Arevalo, M. Rodriguez-Guzman, P. Pérez, M.V. Chao, M. Sendtner, The p75NTR-interacting protein SC1 inhibits cell cycle progression by transcriptional repression of cyclin E, J. Cell Biol. (2004), https://doi.org/10.1083/jcb.200301106.

[18] A. Nykjaer, R. Lee, K.K. Teng, P. Jansen, P. Madsen, M.S. Nielsen, C. Jacobsen, M. Kliemannel, E. Schwarz, T.E. Willnow, B.L. Hempstead, C.M. Petersen, Sortilin is essential for proNGF-induced neuronal cell death, Nature (2004), https://doi.org/10.1038/nature02319.

[19] S. Rabizadeh, S. Rabizadeh, X. Ye, J.J.L. Wang, D.E. Bredesen, Neurotrophin dependence mediated by p75(NTR): contrast between rescue by BDNF and NGF, Cell Death Differ. (1999), https://doi.org/10.1038/sj.cdd.4400614.

[20] L. Notterpek, Neurotrophins in myelination: a new role for a puzzling receptor, Trends Neurosci. (2003), https://doi.org/10.1016/S0166-2236(03)00099-7.

[21] B.D. Carter, C. Kaltschmidt, B. Kaltschmidt, N. Offenhauser, R. Bohm-Matthaei, P.A. Baeuerle, Y.A. Barde, Selective activation of NF-kappa B by nerve growth factor through the neurotrophin receptor p75, Science 80 (1996), https://doi.org/10.1126/science.272.5261.542.

[22] X. Zhou, Q. Hao, P. Liao, S. Luo, M. Zhang, G. Hu, H. Liu, Y. Zhang, B. Cao, M. Baddoo, E.K. Flemington, S.X. Zeng, H. Lu, Nerve growth factor receptor negates the tumor suppressor p53 as a feedback regulator, Elife (2016), https://doi.org/10.7554/eLife.15099.

[23] S. Verbeke, E. Tomellini, F. Dhamani, S. Meignan, E. Adriaenssens, L.B. Xuefen, Extracellular cleavage of the p75 neurotrophin receptor is implicated in its pro-survival effect in breast cancer cells, FEBS Lett. (2013), https://doi.org/10.1016/j.febslet.2013.06.039.

[24] I. Charalampopoulos, A. Vicario, I. Pediaditakis, A. Gravanis, A. Simi, C.F. Ibáñez, Genetic dissection of neurotrophin signaling through the p75 neurotrophin receptor, Cell Rep. (2012), https://doi.org/10.1016/j.celrep.2012.11.009.

[25] Y. Hayakawa, K. Sakitani, M. Konishi, S. Asfaha, R. Niikura, H. Tomita, B.W. Renz, Y. Tailor, M. Macchini, M. Middelhoff, Z. Jiang, T. Tanaka, Z.A. Dubeykovskaya, W. Kim, X. Chen, A.M. Urbanska, K. Nagar, C.B. Westphalen, M. Quante, C.S. Lin, M.D. Gershon, A. Hara, C.M. Zhao, D. Chen, D.L. Worthley, K. Koike, T.C. Wang, Nerve growth factor promotes gastric tumorigenesis through aberrant cholinergic signaling, Cancer Cell (2017), https://doi.org/10.1016/j.ccell.2016.11.005.

[26] C. Festuccia, P. Muzi, G.L. Gravina, D. Millimaggi, S. Speca, V. Dolo, E. Ricevuto, C. Vicentini, M. Bologna, Tyrosine kinase inhibitor CEP-701 blocks the NTRK1/NGF receptor and limits the invasive capability of prostate cancer cells in vitro, Int. J. Oncol. 30 (1) (2007 Jan) 193–200.

[27] S. Yust-Katz, D. Liu, Y. Yuan, V. Liu, S. Kang, M. Groves, V. Puduvalli, V. Levin, C. Conrad, H. Colman, S. Hsu, W.K.A. Yung, M.R. Gilbert, Phase 1/1b Study of Lonafarnib and Temozolomide in Patients with Recurrent or Temozolomide Refractory Glioblastoma, Cancer, 2013, https://doi.org/10.1002/cncr.28031.

[28] E. Carra, F. Barbieri, D. Marubbi, A. Pattarozzi, R.E. Favoni, T. Florio, A. Daga, Sorafenib selectively depletes human glioblastoma tumor-initiating cells from primary cultures, Cell Cycle (2013), https://doi.org/10.4161/cc.23372.

[29] T.N. Kreisl, L. Kim, K. Moore, P. Duic, C. Royce, I. Stroud, N. Garren, M. Mackey, J.A. Butman, K. Camphausen, J. Park, P.S. Albert, H.A. Fine, Phase II trial of single-agent bevacizumab followed by bevacizumab plus irinotecan at tumor progression in recurrent glioblastoma, J. Clin. Oncol. (2009), https://doi.org/10.1200/JCO.2008.16.3055.

[30] N. Butowski, S.M. Chang, K.R. Lamborn, M.Y. Polley, R. Pieper, J.F. Costello, S. Vandenberg, R. Parvataneni, A. Nicole, P.K. Sneed, J. Clarke, E. Hsieh, B.M. Costa, R.M. Reis, M. Hristova-Kazmierski, S.J. Nicol, D.E. Thornton, M.D. Prados, Phase II and pharmacogenomics study of enzastaurin plus temozolomide during and following radiation therapy in patients with newly diagnosed glioblastoma multiforme and gliosarcoma, Neuro Oncol. (2011), https://doi.org/10.1093/neuonc/nor130.

[31] D.A. Reardon, B. Neyns, M. Weller, J.C. Tonn, L.B. Nabors, R. Stupp, Cilengitide: an RGD pentapeptide $\alpha v\beta 3$ and $\alpha v\beta 5$ integrin inhibitor in development for glioblastoma and other malignancies, Future Oncol. (2011), https://doi.org/10.2217/fon.11.8.

[32] B. Jutten, L. Dubois, Y. Li, H. Aerts, B.G. Wouters, P. Lambin, J. Theys, G. Lammering, Binding of cetuximab to the EGFRvIII deletion mutant and its biological consequences in malignant glioma cells, Radiother. Oncol. (2009), https://doi.org/10.1016/j.radonc.2009.06.021.

[33] J. Mendelsohn, J. Baselga, Epidermal growth factor receptor targeting in cancer, Semin. Oncol. (2006), https://doi.org/10.1053/j.seminoncol.2006.04.003.

[34] E. Arwert, S. Hingtgen, J.L. Figueiredo, H. Bergquist, U. Mahmood, R. Weissleder, K. Shah, Visualizing the dynamics of EGFR activity and antiglioma therapies in vivo, Cancer Res. (2007), https://doi.org/10.1158/0008-5472.CAN-07-0077.

[35] S.A. Greenall, J.F. Donoghue, M. Van Sinderen, V. Dubljevic, S. Budiman, M. Devlin, I. Street, T.E. Adams, T.G. Johns, EGFRvIII-mediated transactivation of receptor tyrosine kinases in glioma: mechanism and therapeutic implications, Oncogene (2015), https://doi.org/10.1038/onc.2014.448.

[36] E. Ranza, G. Mazzini, A. Facoetti, R. Nano, In-vitro effects of the tyrosine kinase inhibitor imatinib on glioblastoma cell proliferation, J. Neurooncol. (2010), https://doi.org/10.1007/s11060-009-9975-4.

[37] J. Drukala, K. Urbanska, A. Wilk, M. Grabacka, E. Wybieralska, L. Del Valle, Z. Madeja, K. Reiss, ROS accumulation and IGF-IR inhibition contribute to fenofibrate/PPARα -mediated inhibition of Glioma cell motility in vitro, Mol. Canc. (2010), https://doi.org/10.1186/1476-4598-9-159.

[38] E. Carrasco-García, M. Saceda, I. Martínez-Lacaci, Role of receptor tyrosine kinases and their ligands in glioblastoma, Cells (2014), https://doi.org/10.3390/cells3020199.

[39] D.R. Premkumar, E.P. Jane, I.F. Pollack, Co-administration of NVP-AEW541 and dasatinib induces mitochondrial- mediated apoptosis through Bax activation in malignant human glioma cell lines, Int. J. Oncol. (2010), https://doi.org/10.3892/ijo-00000712.

[40] A. Chakravarti, J.S. Loeffler, N.J. Dyson, Insulin-like growth factor receptor I mediates resistance to anti-epidermal growth factor receptor therapy in primary human glioblastoma cells through continued activation of phosphoinositide 3-kinase signaling, Cancer Res. 62 (1) (2002 Jan 1) 200–207.

[41] S.K. Sridhar, S.N. Pandeya, J.P. Stables, A. Ramesh, Anticonvulsant activity of hydrazones, Schiff and Mannich bases of isatin derivatives, Eur. J. Pharm. Sci. 16 (2002) 129–132, https://doi.org/10.1016/S0928-0987(02)00077-5.

[42] R. Sinha, U.V.S. Sara, R.L. Khosa, J. Stables, J. Jain, Nicotinic acid hydrazones: a novel anticonvulsant pharmacophore, Med. Chem. Res. (2011) 1499–1504, https://doi.org/10.1007/s00044-010-9396-0.

[43] S. Rollas, Ş.G. Küçükgüzel, Biological activities of hydrazone derivatives, Molecules 12 (2007) 1910–1939, https://doi.org/10.3390/12081910.

[44] S.N. Pandeya, H. Manjula, P.N. Singh, Antidepressant activity of some phenylaceticacid hydrazones and 2-chlorophenyl semicarbazones [4], Indian J. Physiol. Pharmacol. 44 (2000) 509–510.

[45] S. Neha, R. Ritu, K. Manju, K. Birendra, A review on biological activities of hydrazone derivatives, Int. J. Pharm. Clin. Res. 8 (2016) 162–166.

[46] C.L. S, Analgesic and anti-inflammatory potential of hydrazones, J. Chem. Pharmaceut. Res. 6 (2014) 916–934. http://www.jocpr.com/articles/analgesic-and-antiinflammatory-potential-of-hydrazones.pdf.

[47] N.A. Hamdy, H.A. Abdel-Aziz, G.M. Kamel, I.M.I. Fakhr, Convenient synthesis, anti-inflammatory, analgesic and ulcerogenic activites of some new bis-hydrazones and pyrazole derivatives, Acta Pol. Pharm. - Drug Res. 70 (2013) 469–480.

[48] A. Kajal, S. Bala, N. Sharma, S. Kamboj, V. Saini, Therapeutic potential of hydrazones as anti-inflammatory agents, Int. J. Med. Chem. 2014 (2014) 1–11, https://doi.org/10.1155/2014/761030.

[49] C.M. Moldovan, O. Oniga, A. Pârvu, B. Tiperciuc, P. Verite, A. Pîrnău, O. Crişan, M. Bojiţă, R. Pop, Synthesis and anti-inflammatory evaluation of some new acyl-hydrazones bearing 2-aryl-thiazole, Eur. J. Med. Chem. 46 (2011) 526–534, https://doi.org/10.1016/j.ejmech.2010.11.032.

[50] F.R. Pavan, P.I. d. S. Maia, S.R.A. Leite, V.M. Deflon, A.A. Batista, D.N. Sato, S.G. Franzblau, C.Q.F. Leite, Thiosemicarbazones, semicarbazones, dithiocarbazates and hydrazide/hydrazones: anti - Mycobacterium tuberculosis activity and cytotoxicity, Eur. J. Med. Chem. 45 (2010) 1898–1905, https://doi.org/10.1016/j.ejmech.2010.01.028.

[51] M.T. Cocco, C. Congiu, V. Lilliu, V. Onnis, Synthesis and in vitro antitumoral activity of new hydrazinopyrimidine-5-carbonitrile derivatives, Bioorg. Med. Chem. 14 (2006) 366–372, https://doi.org/10.1016/j.bmc.2005.08.012.

[52] M.S. Alam, D.U. Lee, Synthesis, biological evaluation, drug-likeness, and in silico screening of novel benzylidene-hydrazone analogues as small molecule anticancer agents, Arch. Pharm. Res. 39 (2016) 191–201, https://doi.org/10.1007/s12272-015-0699-z.

[53] R. Nitsch, I. Bechmann, R.A. Deisz, D. Haas, T.N. Lehmann, U. Wendling, F. Zipp, Human brain-cell death induced by tumour-necrosis-factor-related apoptosis-inducing ligand (TRAIL), Lancet (2000), https://doi.org/10.1016/S0140-6736(00)02659-3.

[54] A.P. Demchenko, Beyond annexin V: fluorescence response of cellular membranes to apoptosis, Cytotechnology (2013), https://doi.org/10.1007/s10616-012-9481-y.

[55] G. Zhang, V. Gurtu, S.R. Kain, G. Yan, Early detection of apoptosis using a fluorescent conjugate of annexin V, Biotechniques (1997), https://doi.org/10.2144/97233pf01.

[56] R. Hingorani, J. Deng, J. Elia, C. McIntyre, D. Mittar, Detection of apoptosis using the BD annexin V FITC assay on the BD FACSVerse$^{\text{TM}}$ system, BD Biosci (2011) 1–12.

[57] A.K. Hagan, T. Zuchner, Lanthanide-based time-resolved luminescence immunoassays, Anal. Bioanal. Chem. (2011), https://doi.org/10.1007/s00216-011-5047-7.

[58] S. Palanivel, A. Zhurina, P. Doan, J.G. Chandraseelan, V.K.M. Khandelwal, F.I. Zubkov, K.T. Mahmudov, A.J.L. Pombeiro, O. Yli-Harja, M. Kandhavelu, In vitro characterization of arylhydrazones of active methylene derivatives, Saudi Pharm. J. SPJ Off. Publ. Saudi Pharm. Soc. 26 (2018) 430–436, https://doi.org/10.1016/j.jsps.2017.12.018.

[59] G. Xu, M.C. Abad, P.J. Connolly, M.P. Neeper, G.T. Struble, B.A. Springer, S.L. Emanuel, N. Pandey, R.H. Gruninger, M. Adams, S. Moreno-Mazza, A.R. Fuentes-Pesquera, S.A. Middleton, 4-Amino-6-arylamino-pyrimidine-5-carbaldehyde hydrazones as potent ErbB-2/EGFR dual kinase inhibitors, Bioorg. Med. Chem. Lett (2008), https://doi.org/10.1016/j.bmcl.2008.07.020.

[60] S.M. Abou-Seri, Synthesis and biological evaluation of novel 2,4′-bis substituted diphenylamines as anticancer agents and potential epidermal growth factor receptor tyrosine kinase inhibitors, Eur. J. Med. Chem. (2010), https://doi.org/10.1016/j.ejmech.2010.05.072.

[61] K.T. Mahmudov, M.N. Kopylovich, A. Sabbatini, M.G.B. Drew, L.M.D.R.S. Martins, C. Pettinari, A.J.L. Pombeiro, Cooperative metal-ligand assisted E/Z isomerization and cyano activation at CuIIand CoIIcomplexes of arylhydrazones of active methylene nitriles, Inorg. Chem. (2014), https://doi.org/10.1021/ic501704g.

[62] K.T. Mahmudov, M.F.C.G. Da Silva, M. Sutradhar, M.N. Kopylovich, F.E. Huseynov, N.T. Shamilov, A.A. Voronina, T.M. Buslaeva, A.J.L. Pombeiro, Lanthanide derivatives comprising arylhydrazones of β-diketones: cooperative E/Z isomerization and catalytic activity in nitroaldol reaction, Dalton Trans. (2015), https://doi.org/10.1039/c4dt03788j.

[63] K.T. Mahmudov, A.M. Maharramov, R.A. Aliyeva, I.A. Aliyev, R.K. Askerov, R. Batmaz, M.N. Kopylovich, A.J.L. Pombeiro, 3-(para-Substituted phenylhydrazo)pentane-2,4-diones: physicochemical and solvatochromic properties, J. Photochem. Photobiol. Chem. (2011), https://doi.org/10.1016/j.jphotochem.2011.02.006.

[64] K.T. Mahmudov, A.M. Maharramov, R.A. Aliyeva, I.A. Aliyev, M.N. Kopylovich, A.J.L. Pombeiro, Ion pairs of 5,5-dimethyl-2-(2-hydroxy-3,5-disulfophenylhydrazo)cyclohexane-1,3-dione with cationic surface-active substances as analytical reagent for determination of copper(II), Anal. Lett. (2010), https://doi.org/10.1080/00032711003763665.

[65] M.N. Kopylovich, K.T. Mahmudov, A. Mizar, A.J.L. Pombeiro, Hydrogen bond assisted activation of a dinitrile towards nucleophilic attack, Chem. Commun. (2011), https://doi.org/10.1039/c1cc11696g.

[66] C.A. Montoya, C.F. Gómez, A.B. Paninho, A.V.M. Nunes, K.T. Mahmudov, V. Najdanovic-Visak, L.M.D.R.S. Martins, M.F.C. Guedes Da Silva, A.J.L. Pombeiro, M. Nunes Da Ponte, Cyclic carbonate synthesis from CO2and epoxides using zinc(II) complexes of arylhydrazones of β-diketones, J. Catal. (2016), https://doi.org/10.1016/j.jcat.2015.12.027.

[67] A. Karmakar, A. Paul, K.T. Mahmudov, M.F.C. Guedes Da Silva, A.J.L. Pombeiro, PH dependent synthesis of Zn(ii) and Cd(ii) coordination polymers with dicarboxyl-functionalized arylhydrazone of barbituric acid: photoluminescence properties and catalysts for Knoevenagel condensation, New J. Chem. (2016), https://doi.org/10.1039/c5nj02411k.

[68] M.N. Kopylovich, A.C.C. Nunes, K.T. Mahmudov, M. Haukka, T.C.O. Mac Leod, L.M.D.R.S. Martins, M.L. Kuznetsov, A.J.L. Pombeiro, Complexes of copper(II) with 3-(ortho-substituted phenylhydrazo)pentane-2,4-diones: syntheses, properties and catalytic activity for cyclohexane oxidation, Dalton Trans. (2011), https://doi.org/10.1039/c0dt01527j.

[69] W. Kuznik, M.N. Kopylovich, G.I. Amanullayeva, A.J.L. Pombeiro, A.H. Reshak, K.T. Mahmudov, I.V. Kityk, Role of tautomerism and solvatochromism in UV-VIS spectra of arylhydrazones of β-diketones, J. Mol. Liq. (2012), https://doi.org/10.1016/j.molliq.2012.03.023.

[70] K.T. Mahmudov, M.F.C. Guedes Da Silva, M. Glucini, M. Renzi, K.C.P. Gabriel, M.N. Kopylovich, M. Sutradhar, F. Marchetti, C. Pettinari, S. Zamponi, A.J.L. Pombeiro, Water-soluble heterometallic copper(II)-sodium complex

comprising arylhydrazone of barbituric acid as a ligand, Inorg. Chem. Commun. (2012), https://doi.org/10.1016/j.inoche.2012.06.008.

[71] K.T. Mahmudov, R.A. Rahimov, M.B. Babanly, P.Q. Hasanov, F.G. Pashaev, A.G. Gasanov, M.N. Kopylovich, A.J.L. Pombeiro, Tautomery and acid-base properties of some azoderivatives of benzoylacetone, J. Mol. Liq. (2011), https://doi.org/10.1016/j.molliq.2011.06.005.

[72] K.T. Mahmudov, M.N. Kopylovich, K.V. Luzyanin, A. Mizar, M.F.C. Guedes Da Silva, V. André, A.J.L. Pombeiro, Structural and thermal properties of three cyano-substituted azoderivatives of β-diketones, J. Mol. Struct. (2011), https://doi.org/10.1016/j.molstruc.2011.02.045.

[73] M.N. Kopylovich, K.T. Mahmudov, M.F.C. Guedes Da Silva, L.M.D.R.S. Martins, M.L. Kuznetsov, T.F.S. Silva, J.J.R. Fraústo Da Silva, A.J.L. Pombeiro, Trends in properties of para-substituted 3-(phenylhydrazo)pentane-2,4- diones, J. Phys. Org. Chem. (2011), https://doi.org/10.1002/poc.1824.

[74] K.T. Mahmudov, M.N. Kopylovich, M.F.C. Guedes Da Silva, G.S. Mahmudova, M. Sutradhar, A.J.L. Pombeiro, Copper(II) and cobalt(II,III) complexes of a new carboxylic-functionalized arylhydrazone of 5,5-dimethylcyclohexane-1, 3-dione, Polyhedron (2013), https://doi.org/10.1016/j.poly.2013.05.027.

[75] W.L. Jorgensen, D.S. Maxwell, J. Tirado-Rives, Development and testing of the OPLS all-atom force field on conformational energetics and properties of organic liquids, J. Am. Chem. Soc. (1996), https://doi.org/10.1021/ja9621760.

[76] a G. Robertson, M.J. Banfield, S.J. Allen, J. a Dando, G.G. Mason, S.J. Tyler, G.S. Bennett, S.D. Brain, a R. Clarke, R.L. Naylor, G.K. Wilcock, R.L. Brady, D. Dawbarn, Identification and structure of the nerve growth factor binding site on TrkA, Biochem. Biophys. Res. Commun. (2001), https://doi.org/10.1006/bbrc.2001.4462.

[77] J. Moungjaroen, U. Nimmannit, P.S. Callery, L. Wang, N. Azad, V. Lipipun, P. Chanvorachote, Y. Rojanasakul, Reactive oxygen species mediate caspase activation and apoptosis induced by lipoic acid in human lung epithelial cancer cells through Bcl-2 down-regulation, J. Pharmacol. Exp. Therapeut. 319 (2006) 1062–1069, https://doi.org/10.1124/jpet.106.110965.glutathione.

[78] M. Redza-Dutordoir, D.A. Averill-Bates, Activation of apoptosis signalling pathways by reactive oxygen species, Biochim. Biophys. Acta Mol. Cell Res. (2016), https://doi.org/10.1016/j.bbamcr.2016.09.012.

[79] K. Izeradjene, L. Douglas, D.M. Tillman, A.B. Delaney, J.A. Houghton, Reactive oxygen species regulate caspase activation in tumor necrosis factor-related apoptosis-inducing ligand-resistant human colon carcinoma cell lines, Cancer Res. 65 (2005) 7436–7445, https://doi.org/10.1158/0008-5472.CAN-04-2628.

[80] D.R. Ciocca, S.K. Calderwood, Heat Shock Proteins in Cancer: Diagnostic, Prognostic, Predictive, and Treatment Implications, Cell Stress Chaperones, 2005, https://doi.org/10.1379/CSC-99r.1.

[81] A. Sami, M. Karsy, Targeting the PI3K/AKT/mTOR signaling pathway in glioblastoma: novel therapeutic agents and advances in understanding, Tumor Biol. (2013), https://doi.org/10.1007/s13277-013-0800-5.

[82] Z. Duzgun, Z. Eroglu, C. Biray Avci, Role of mTOR in glioblastoma, Gene (2016), https://doi.org/10.1016/j.gene.2015.08.060.

[83] X. Li, C. Wu, N. Chen, H. Gu, A. Yen, L. Cao, E. Wang, L. Wang, PI3K/Akt/mTOR signaling pathway and targeted therapy for glioblastoma, Oncotarget (2016), https://doi.org/10.18632/oncotarget.7961.

[84] M. Alam, G. Verma, M. Shaquiquzzaman, A. Marella, M. Akhtar, M. Ali, A review exploring biological activities of hydrazones, J. Pharm. BioAllied Sci. 6 (2014) 69, https://doi.org/10.4103/0975-7406.129170.

[85] [a] M. Singh, N. Raghav, Biological activities of hydrazones: a review, Int. J. Pharm. Pharmaceut. Sci. 3 (2011) 26–32, https://doi.org/10.1186/1752-153X-5-2;
[b] S. Rollas, S.G. Kiiciikguzel, Biological activities of hydrazone derivatives, Molecules 12 (2007) 1910–1939;
[c] J. Yadav, S.N. Pandeya, G. Nath, S.P. Singh, Synthesis and antibacterial evaluation of some hydrazones of flavanoid derivatives, J. Chem. Pharmaceut. Res. 2 (4) (2010) 558–563;
[d] S.U. Khan, P. Mullick, S. Pandit, D. Kaushik, Synthesis of hydrazones derivatives of Quinoxaline-prospective antimicrobial and anti-inflammatory agents, Acta Polonica Pharmac 66 (2) (2009 Mar-Apr) 169–172.

[86] M.C. Mandewale, U.C. Patil, S.V. Shedge, U.R. Dappadwad, R.S. Yamgar, A review on quinoline hydrazone derivatives as a new class of potent antitubercular and anticancer agents, Beni-Suef Univ. J. Basic Appl. Sci. (2017), https://doi.org/10.1016/j.bjbas.2017.07.005.

[87] H.S. Naveen Kumar, T. Parumasivam, F. Jumaat, P. Ibrahim, M.Z. Asmawi, A. Sadikun, Synthesis and evaluation of isonicotinoyl hydrazone derivatives as antimycobacterial and anticancer agents, Med. Chem. Res. 23 (2014) 269–279, https://doi.org/10.1007/s00044-013-0632-2.

[88] R.M. Mohareb, D.H. Fleita, O.K. Sakka, Novel synthesis of hydrazide-hydrazone derivatives and their utilization in the synthesis of coumarin, pyridine, thiazole and thiophene derivatives with antitumor activity, Molecules (2011), https://doi.org/10.3390/molecules16010016.

[89] N. Dyson, The regulation of E2F by pRB-family proteins, Genes Dev. (1998), https://doi.org/10.1101/gad.12.15.2245.

[90] D. Avni, H. Yang, F. Martelli, F. Hofmann, W.M. ElShamy, S. Ganesan, R. Scully, D.M. Livingston, Active localization of the retinoblastoma protein in chromatin and its response to S phase DNA damage, Mol. Cell. (2003), https://doi.org/10.1016/S1097-2765(03)00355-1.

PUBLICATION
III

In vitro anti-glioblastoma activity of L-valine derived boroxazolidones

Anisha Viswanathan, Giulia Sebastianelli, Kenna Brown, Janne Raunio, Vili Sipilä, Rafael Candeias Nuno, Olli Yli-Harja, Meenakshisundaram Kandhavelu

European Journal of Pharmacology, Volume 854, 5 July 2019, Pages 194-200
https://doi.org/10.1016/j.ejphar.2019.04.020

Publication reprinted with the permission of the copyright holders.

European Journal of Pharmacology 854 (2019) 194–200

Contents lists available at ScienceDirect

European Journal of Pharmacology

journal homepage: www.elsevier.com/locate/ejphar

Full length article

In vitro anti-glioblastoma activity of L-valine derived boroxazolidones

Anisha Viswanathan[a], Giulia Sebastianelli[a], Kenna Brown[a], Jenna Raunio[b], Vili Sipilä[a], Olli Yli-Harja[c,d], Nuno R. Candeias[b,*], Meenakshisundaram Kandhavelu[a,*]

[a] *Molecular Signaling Lab, Faculty of Medicine and Health Technology, Tampere University and BioMediTech, P.O. Box 553, 33101 Tampere, Finland*
[b] *Faculty of Engineering and Natural Sciences, Tampere University, Korkeakoulunkatu 8, 33101 Tampere, Finland*
[c] *Computational Systems Biology Group, Faculty of Medicine and Health Technology, Tampere University and BioMedi Tech, P.O. Box 553, 33101 Tampere, Finland*
[d] *Institute for Systems Biology, 1441N 34th Street, Seattle, WA 98103-8904, USA*

ARTICLE INFO

Keywords:
Apoptosis
Boroxazolidone
Cell cycle arrest
Cytotoxicity
Glioblastoma

ABSTRACT

In the present study, a series of L-valine derived boroxazolidones, previously synthesized and reported to have residual activity in a human epithelial cell line, have been evaluated *in vitro* for their anti-glioblastoma activity. A boroxazolidone derivative containing 2,4-difluorophenyl moieties (**6**) was found to have higher cytotoxicity than the standard drug, Temozolomide (TMZ). Compound **6** was found to exhibit dose-dependent growth inhibitory effects with an IC_{50} of 49 µM and 53 µM for LN229 and SNB19 cells, respectively. Additionally, **6** was assessed for its role in apoptosis, caspase 3/7 activation and oxidative stress in SNB19 and LN229 cells. SNB19 cells treated with **6** showed 45.3% apoptosis in the population, while TMZ had 24.7%. In LN229 cells, the percentage of apoptotic cells treated with compound **6** and TMZ were the same. Both **6** and TMZ induced apoptosis through the activation of caspase 3/7 in SNB19 and LN229 cells. Interestingly, **6** exhibited a higher effectivity in promoting reactive oxygen species production in LN229, while it was 6-fold less in SNB19. Boroxazolidone-treated GBM cell lines increased reactive oxygen species production, suggesting that such species may be interlinked with the observed programmed cell death. Additionally, the treatment of both GBM cell lines with **6** led to G2/M phase arrest. The magnitude of anti-GBM effect of **6** is significantly higher than the known chemotherapeutic agent TMZ. This work further demonstrates the anticancer properties of L-valine derived boroxazolidones, adding another potential derivative to the collection of promising chemotherapeutic agents for GBM treatment.

1. Introduction

Glioblastoma (GBM) is often treated with the combination of chemotherapy and surgery. However, the application of anticancer drugs for chemotherapy is limited by deleterious side effects, limited activity *in vivo*, and developed drug resistance. Thus, novel, broad-spectrum drugs with less severe side effects are necessary to improve cancer treatment (Doan et al., 2016). Treatment of various cancers has been demonstrated using boron derivatives (Tülüce et al., 2017). The identification of alkyl or aryl boron-containing compounds as serine protease inhibitors (Philipp and Bender, 1971), and the role of this enzymes in cancer progression (Poddar et al., 2017), has triggered several studies on the antitumor properties of boron-containing compounds (Baker et al., 2009). Ultimately, several classes of boron-containing compounds were disclosed to have the ability to reduce tumor cell proliferation and initiate apoptosis (I. Scorei and Popa, 2010). In 2002, boron-containing Bortezomib became the first proteasome inhibitor to be approved by the FDA for multiple myeloma (Paramore and Frantz, 2003). Increased target cell specificity resulting from functionalizing boron with other chemical groups (Żołnierczyk et al., 2016) could decrease the deleterious side effects of anticancer drugs, as they stem from cytotoxic effects towards healthy cells. By reducing chemotherapeutic drug side effects, cancer treatment could be improved (Andrews et al., 1988).

Amino acid-based compounds are stable in a biological environment and catabolically resistant, an advantageous trait for treatment because a high concentration of the compound can be accumulated in target cells. Prodrugs based on amino acid skeletons can be used to increase cellular uptake, while maintaining a consistent intracellular concentration of the anticancer agent, despite efflux caused by various transporters. This strategy has been proven semi-successful with valine prodrug, antitumor SN-38. However, efficacy decreased due to the low stability of the prodrug (Kwak et al., 2012a, 2012b). Boroxazolidones, formed by condensation of a borane with an α-amino acid, have been

---

* Corresponding authors.
E-mail addresses: nuno.rafaelcandeias@tuni.fi (N.R. Candeias), meenakshisundaram.kandhavelu@tuni.fi (M. Kandhavelu).

https://doi.org/10.1016/j.ejphar.2019.04.020
Received 24 January 2019; Received in revised form 5 April 2019; Accepted 8 April 2019
Available online 11 April 2019
0014-2999/ © 2019 Elsevier B.V. All rights reserved.

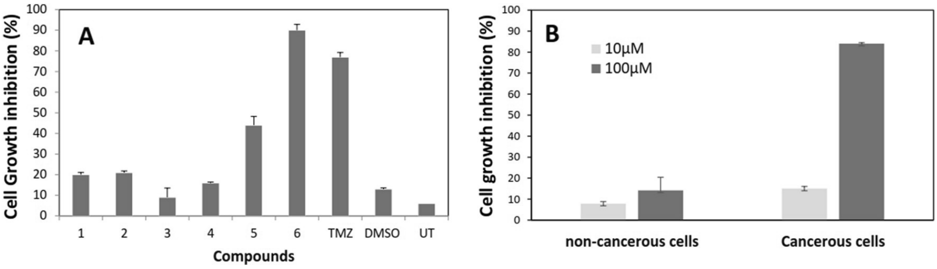

Fig. 1. Synthesis and *in vitro* cytotoxicity assays: A) Testing of boroxazolidones 1–6 against the growth of human glioblastoma LN229 cell line at 100 μM. LN229 cell line was treated with the target compounds for 48 h and cell inhibition was determined with Trypan blue staining. UT - Untreated, DMSO - negative control and TMZ - positive control. B) Percentage of cell growth inhibition versus MEF (non-cancerous cells) and LN229 (glioblastoma cells) (10 μM, non-cancer cells vs cancer cells; $P = 0.0319$ and 100 μM, non-cancer cells vs cancer cells; $P < 0.0001$). Each data point represents mean ± S.E.M of biological and technical replicates.

determined to induce cell death in human epithelial colorectal adenocarcinoma and brain astrocytoma cells (Raunio et al., 2017; Velasco-Bejarano et al., 2007; Velasco et al., 2007) Several methods for the preparation of boroxazolidones have been developed, although most of them rely on reacting an α-amino acid with borane or borinates.

We and others have previously reported modest antitumor properties of boroxazolidones against human epithelial colorectal adenocarcinoma, brain astrocytoma, leukaemia and murine lymphoma cells (Raunio et al., 2017; Velasco-Bejarano et al., 2007; Velasco et al., 2007). However, the antineoplastic effect of boroxazolidones against the growth of various types of GBM is not well understood. Hence, this study aims to investigate the effect of selective compounds against GBM that originates in the parieto-occipital region. The cytotoxic effects of novel derivatives were tested on two GBM cell lines, LN229 and SNB19. Herein we present the results of the *in vitro* cytotoxicity evaluation of L-valine derived boroxazolidones for potential use in GBM treatment. A normal cell (Mouse Embryonic Fibroblast, MEF) line was tested to support that the compound targeted GBM cells. To determine the potential broad-spectrum application of the compound, many *in vitro* studies were performed, including dose-dependent GBM growth inhibition assays. Cell death mechanism was ascertained via apoptosis screening, caspase 3/7, and reactive oxygen species assays, and cell cycle analysis was performed to determine the inhibition of cellular division.

2. Materials and methods

2.1. Chemicals

Dulbecco's Modified Eagle Medium (DMEM) (Sigma-Aldrich, St. Louis, MO), Fetal Bovine Serum (FBS) (Sigma-Aldrich, St. Louis, MO, #F7524), L-glutamine (Sigma-Aldrich, St. Louis, MO #G7513), penicillin and streptomycin (Sigma-Aldrich, St. Louis, MO, P4333), Amphotericin B (Sigma-Aldrich, St. Louis, MO, #A9528), Trypan Blue Solution (Sigma-Aldrich, St. Louis, MO, #T8154), Propidium Iodide (Molecular Probes by Life Technologies, Eugene, OR, #P3566), Trypsin-EDTA solution (Sigma-Aldrich, St. Louis, MO, #59418C), Dead Cell Apoptosis Kit with Annexin V FITC and PI (Thermo Fisher Scientific), Reactive Oxygen Species Detection Reagent (Molecular Probes by Life Technologies, Eugene, OR, #C13293), Caspase-Glo® 3/7 Assay kit (Promega, Madison USA), Dimethyl Sulphoxide (DMSO) Hybri-Max (Sigma-Aldrich, St. Louis, MO, #D2650), Temazolamide (TMZ) (Sigma-Aldrich, USA).

2.2. Chemical preparation

Boroxazolidones **1–6** compounds and TMZ, a chemotherapeutic agent for glioblastoma treatment, were dissolved in DMSO to obtain a final concentration of 100 mM, from which, intermediate dilutions were prepared. For the dose dependent cytotoxicity assay, the final concentrations were prepared in the same culture medium to concentrations of 100 μM, 75 μM, 50 μM, 25 μM, and 10 μM.

2.3. Cell culture

The human glioblastoma cell lines SNB19 and LN229 (ATCC® CRL-2611™/CRL-2611™) and mouse embryonal fibroblast (MEF, normal brain cells) were cultured in DMEM supplemented with 10% FBS, 0.1 mg/ml Streptomycin, 100 U/ml Penicillin, and 0.025 mg/ml Amphotericin B. Cell cultures were incubated at 37 °C supplemented with 5% CO_2 in a humidified incubator. The LN229 cell line was derived from a patient with right frontal parieto-occipital GBM. The line exhibits mutated p53 proteins. SNB19 is a malignant GBM cell line initiated from the surgical resection of a left parietooccipital GBM and also exhibits mutated p53 proteins. The non-cancerous cells, MEFs, have an E10.5 genotype with Vin+/+ (Vinculin) originally obtained from Wolfgang H. Ziegler (Hannover Medical School, Hannover, Germany) (Xu et al., 1998).

2.4. Trypan blue exclusion assay for detecting cells viability

The cytotoxic effects of boron derivatives, reported in Fig. 1, were studied on multiple glioblastoma cell lines, SNB19 and LN229. For this, cells were seeded on 12-well plates with a density of 1×10^5 cell/well. After 48 h, the cells were treated with 100 μM concentration of the compounds of interest. TMZ and DMSO (0.1%) were used, respectively, as a positive control (PC) and negative control. Treated cells were collected after trypsinization, and followed by centrifugation at 153*g* for 10 min. After centrifuging, the cells were resuspended in culture medium, and stained with Trypan blue dye at a ratio of 1:1. To quantify live cell and dead cell populations, a Bürker hemocytometer (Heinz Herenz, Hamburg, Germany) was used. Biological and technical repeats were used to obtain the statistically significant results. The percentage of cell viability inhibition was calculated according to the following equation:

$$Inhibition\ (\%) = \frac{\begin{array}{c}Mean\ No.\ of\ untreated\ cells\ (DMSO\ control)\\ -\ Mean\ No.\ of\ treated\ cells\end{array}}{Mean\ No.\ of\ untreated\ cells\ (DMSO\ control)} x100 \quad (1)$$

2.5. In vitro measurement of dose dependent cytotoxicity

Compound **6** was identified as the most lethal compound from the preliminary cytotoxicity assay, where it exhibited the highest cytotoxicity effect. Dose dependent cytotoxicity was measured after the 24 h exposure to different concentrations **6**; 100, 75, 50, 25, 10 μM concentrations were tested on SNB19 and LN229 cell lines. After treatment, the cells were collected as described in the Trypan blue exclusion assay procedure above. TMZ was used as a positive control. The percentage of mortality was calculated using formula (1). After that, the dose-response curves were plotted using GraphPad software and half-maximal inhibitory concentration (IC_{50}) was calculated from the fitted curves.

2.6. Quantification of apoptosis by annexin V-FITC/PI staining

To quantify apoptosis in the compound **6**-treated cells, the Dead Cell Apoptosis Kit with Annexin V-FITC and PI was used. The procedure for the assay followed the manufacturer's protocol, which is as follows: Glioblastoma cell lines, SNB19 and LN229, were cultured in 6-well-plates with the initial density of 0.3×10^6 cells/well using the complete medium. After 24 h, the complete medium was replaced with serum-free medium and incubated at 37 °C overnight. Post-incubation, the cells were treated with the IC_{50} concentration of the compound of interest, TMZ, and DMSO (0.1%). Treated cultures were incubated for 24 h. Cells were harvested by trypsinization followed by centrifugation at 153*g* for 10 min before being washed in ice-cold PBS. The cell pellets were resuspended in ice-cold 1X annexin-binding buffer. Annexin V-FITC and PI working solutions were added to the cell suspension as suggested by manufacturer protocol. The cells were incubated in dark conditions at room temperature for 15 min prior to fluorescence measurement. An EVOS imaging system (ThermoFisher Scientific) with 20X objective magnification was used to observe apoptotic cells, and images were taken for the quantification of apoptotic and non-apoptotic cell percentages.

2.7. Caspases 3/7 activities assay

Glioblastoma cell lines, SNB19 and LN229, cells were seeded on 96-wellplates with white flat bottoms at an initial density of 1×10^4 cells/well in complete medium. After 24 h, the medium was replaced with 100 µl of serum-free medium and incubated overnight. Post–incubation, the cells were treated with the IC_{50} concentration of **6** and TMZ. Each well had a total volume of 100 µl, and then incubated for 5 h. Glo® 3/7 Assay kit (Promega, Madison USA) was used according to the manufacturer's protocol to determine the caspase activity. A 96-wellplate containing cells was removed from the incubator and allowed to equilibrate to room temperature for 30 min. The 100 µl of Caspase-Glo reagent was added to the treated, untreated, and blank wells. The plate was placed on an agitator for 30 s at 15–25 g. The plate was incubated 1 h in dark conditions. After incubation, the luminescence signal was measured using a plate-reading luminometer (Fluoroskan Ascent FL, Thermo Labsystems). The fold change in caspase 3/7 was calculated using formula (2).

$$Fold\ Change = \frac{F_{test} - F_{blank}}{F_{control} - F_{blank}} \tag{2}$$

Where F_{test} is the luminescence readings from the treated wells, $F_{control}$ is the luminescence readings from the untreated wells, and F_{blank} is the luminescence readings from the unstained wells.

2.8. Detection of intracellular reactive oxygen species

The glioblastoma cell lines, SNB19 and LN229, were grown in 12-well plates with the initial density of 1×10^5 cells/well. After 24 h, the complete medium was replaced with serum-free medium and incubated overnight. Cells were treated with the IC_{50} concentration of **6** and TMZ, then left in a humidified incubator at 37 °C supplied with 5% CO_2 for 5 h. Cells were harvested by centrifugation at 153*g* for 10 min and the cell pellet was suspended in 2 µM 2′,7′-dichlorodihydrofluorescein diacetate (H2DCFDA), and then incubated for 10 min under dark conditions. The cells were centrifuged at 153 g for 10 min, then washed with warm PBS and recovered in warmed complete medium. Cells were incubated at 37 °C for 20 min prior to the fluorescence measurement. Equal volumes of cells in the 96-well plate were used for measuring fluorescence intensity using a plate reader at 485 nm and 538 nm. DMSO was used as a control. The fold change in reactive oxygen species production was calculated from the fluorescence reading using formula (2).

2.9. Analysis of cell cycle arrest

To study the effect of compound **6** on cell cycle arrest in SNB19 and LN229 lines, cells were cultured in 6-well plates with the initial density of 0.3×10^6 cells/well. Cells were incubated overnight at 37 °C with 5% CO_2. After 24 h the complete medium was replaced with serum-free medium. Cultures were incubated overnight before they were treated with the IC_{50} concentration of compound **6** for 48 h. After 48 h from the treatment of the cells, the cells were harvested by trypsinzation. Pellet was resuspended in 1 ml of ice-cold PBS, centrifuged at 153 g for 10 min, and then the cells were resuspended in PBS. 70% ice-cold ethanol was added to the cell suspension and incubated at 4 °C for 15 min. The suspension was centrifuged at 153 g for 10 min and the pellet was washed with ice-cold PBS. 200 µl of PBS containing 20 µg/ml PI, 0.2 mg/ml RNase and 0.1% Triton X-100 was added, and samples were incubated for 15 min at 37 °C. Fluorescent signals of the cells were captured using an EVOS imaging system with 10x objective magnification. The images were analyzed by CellProlifer software to quantify the percentage of cell cycle phases in all treated conditions. The untreated and DMSO controls were used to compare the cell cycle arrest profiles.

2.10. Statistical analysis

Results are expressed as the mean ± standard error of mean (S.E.M) of biological and technical replicates. Statistical significance was evaluated by ANOVA test, when GraphPad Software (GraphPad Software, USA) was used, or by *equal variance t-tests* between samples. Results were considered statistically significant if $p < 0.05$.

3. Results

3.1. Cytotoxicity effect of L-valine-derived boroxazolidones 1-6

First, L-valine derived boroxazolidones **1–6** were prepared as previously described elsewhere (Scheme 1(Kuuloja et al., 2011; Raunio et al., 2017)). Triethylammonium tetra-arylborates were prepared by Grignard reagent addition to $NaBF_4$. This was followed by cation exchange and condensation with L-valine in overnight refluxing toluene, providing pure boroxazolidones after precipitation or recrystallization.

The biological study was performed by determining the cytotoxicity of the compounds against glioblastoma cell line, LN229, using Trypan blue exclusion assay. Compound **6** showed high cytotoxicity at 100 µM concentration, inhibiting more than 90% of cell growth. Compound **5** induced 44% cell death, and boroxazolidones **1–4** displayed less cell growth inhibition. The results indicate that **6** had 13% higher cytotoxicity than the positive control, TMZ. Fig. 1A demonstrates **6** as the top cytotoxic compound compared to the cell death percentage of the negative controls of DMSO and untreated cells. Given the substantial cytotoxic increase of tetrafluorinated derivative **6** when compared with the other boroxazolidones, subsequent analyses on such compound were carried out. Compared to our previous findings, the cytotoxic effect of **6** compound was 40% higher in parieto-occipital GBM. Thus, this result suggest that **6** has selectivity for parieto-occipital GBM cells. Boroxazolidone **6** was further evaluated against the growth of normal brain cells, mouse embryonal fibroblast (MEF). Different concentrations of **6** (10 and 100 µM) were tested on MEF cells followed by a Trypan blue exclusion assay. Fig. 1B shows that at 10 µM and 100 µM treatment

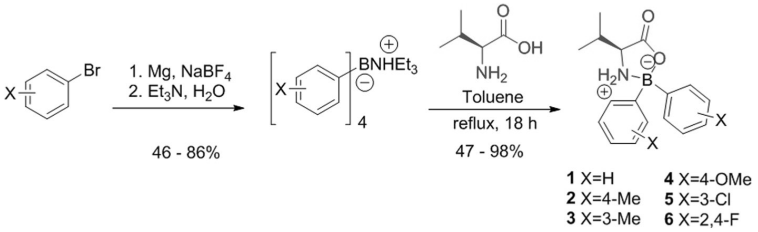

Scheme 1. Synthesis of L-valine derived boroxazolidones.

there was 7.8% and 14% cell death, respectively. The comparative analysis of inhibition percentage between cancer and non-cancerous cells treated with these concentrations suggests that compound **6** has cell line specific activity (10 μM, non-cancer cells vs cancer cells; $P = 0.0319$ and 100 μM, non-cancer cells vs cancer cells; $P < 0.0001$). Overall, the cytotoxicity of the boroxazolidones is dependent on the phenyl rings' substitutions.

3.2. *Dynamics of inhibiting effect*

LN229 and SNB19 cell lines were treated with drug concentrations of 10, 25, 50, 75, and 100 μM to characterize the cellular effects of **6**'s inhibition in glioblastoma. The identified molecule reduced cell proliferation in all cell lines tested (Fig. 2A and B). Phase-contrast microscopy images were investigated to observe whether the compounds under study exert morphological changes through cytotoxicity activity. These computer-assisted morphological observations show that the appearance of the LN229 and SNB19 glioblastoma cells treated with the various concentrations of **6** were markedly different. It is evident that compound **6**-treated cells appeared shrunk in their morphology, while the untreated cells appeared thin and flattened, typical of attached morphology. The observed morphological changes were dose-dependent, which can be seen in Fig. 2A for 10 μM and 100 μM treated conditions. From Fig. 2, it is apparent that compound **6** affected cell growth in a dose dependent manner. The IC_{50} of compound **6** was inferred to be 49 μM and 53 μM, respectively, for LN229 and SNB19**.** The same compound exhibited significant cytotoxic effects in both glioblastoma cells over these concentrations. Effect of TMZ against the growth of Sbn19 and LN229 was also tested and IC^{50} was calculated as 87.7614 ± 6.919 and 84.389 ± 2.599 for LN229 and Snb19, respectively (data not shown). The cytotoxic effect of 6 is significantly higher than TMZ. Hence, compound **6**, which produced inhibitory activity in a dose-dependent manner, was selected for further analysis.

3.3. *Apoptosis mediated cell death induced by compound 6*

To determine the apoptotic effect induced by compound **6**, Annexin V/PI double staining was performed. The percentage of apoptotic cells was calculated based on the results of cellular staining. Apoptotic cells presented with Annexin V-FITC positive/PI negative and both Annexin V-FITC/PI positive. In untreated (Fig. 3A, left panel) and DMSO treated (Fig. 3A, middle panel) samples, the live cells exhibited both as Annexin V/PI negative. Apoptotic cells are cells which possess high levels of Annexin V and low levels of PI expression. From the microscopy images, it is evident that **6** induced cell death by apoptosis when cells expressed as Annexin V/PI positive (Fig. 3A, last panel). Fig. 3B shows the percentage of live and apoptotic cells of LN229 and SNB19 when treated with **6** and TMZ. Generally, apoptosis induction was observed in both cell lines. Results were normalized against an untreated control and compared with a positive control. The percentage of apoptotic SNB19 cells treated with **6** was 45.3% while TMZ treated cells was 24.7% (**6** vs TMZ; $P < 0.0001$). In the case of LN229 cells, the percentage of apoptotic cells was approximately equal in **6** and TMZ treated conditions (**6** vs TMZ; $P < 0.0001$). These results demonstrate that both **6** and TMZ trigger apoptosis mediated cell death in SNB19 and LN229 cells.

3.4. *Caspase 3/7 and reactive oxygen species activation by 6*

Caspase activation is one of the key signalling pathways leading to apoptosis in cancer cells. Caspase 3, 7, 8, and 9 are the different types of caspases associated with apoptotic cell death. However, caspases 3/7 are directly linked to apoptosis through the intrinsic and extrinsic signalling pathway interactions (Walsh et al., 2008). To examine the molecular mechanism underlying apoptosis upon the treatment of boroxazolidone **6**, caspase 3/7 activity was measured. As shown in Fig. 4A, compound **6** induced the activation of caspases 3/7. In general, caspases 3/7 activity increased in **6** and TMZ treated samples in comparison to the untreated ones. A slight increase in caspase activation was observed for **6**-treated LN229 cells, when compared with treatment with TMZ (**6** vs TMZ; $P = 0.1271$). Approximately 1-fold and 1.2-fold increase in caspase 3/7 was found in LN229 cells treated with **6** and TMZ, respectively (Fig. 4A). A different profile was determined for SNB19 cells, where similar increases in caspase 3/7 activity levels were observed regardless of the cytotoxic agent used (6 vs TMZ; $p = 0.4519$). It is notable that the production of reactive oxygen species in ln229 was higher than snb19, which is similar to the trend of caspase 3/7 change. This suggests that there is a possibility of signalling pathway interaction between reactive oxygen species and caspase 3/7. In addition, both snb19 and ln229 cells expressed moderately higher levels of caspase 3/

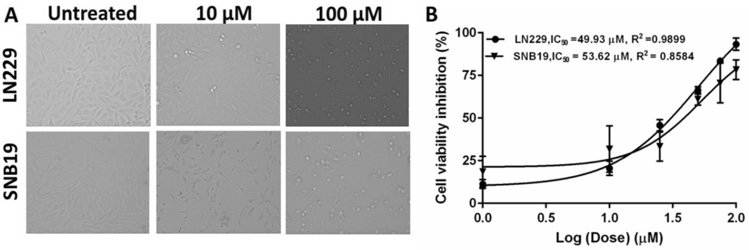

Fig. 2. Compound 6 inhibits glioma cell proliferation. (A) Representative phase-contrast micrographs of glioma cell lines left untreated (control) or treated for 48 h with 10 μM and 100 μM of boroxazolidone 6. (B) Different concentrations including 1, 10, 25, 50, 75 and 100 μM were added in LN229 and SNB19 cells, then incubated for 48 h. Trypan blue staining was used to determine cell viability. The represented data is normalized against vehicle control, DMSO. Each data point represents an average of biological and technical replicates. A R^2 value of about 1 indicates that the regression predictions fits the data.

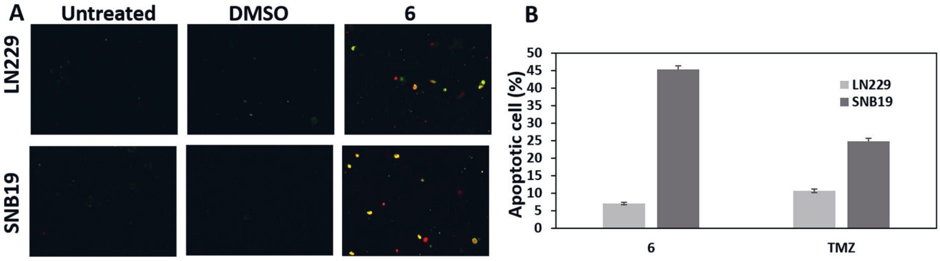

Fig. 3. Apoptosis induction determination using Annexin V and Propidium Iodide. A) Microscopic images of the cells stained with Annexin V-FITC and PI in SNB19 and LN229 cells. Images panels: Untreated, DMSO and 6 treated cells. B) Percentage of apoptosis cells in 6 and TMZ treated conditions (6 vs TMZ; $P < 0.0001$). Each bar represents mean ± S.E.M. Baseline effect due to DMSO has been deducted.

7 compared to the caspase 3/7 level of cells treated with TMZ. Overall, the data suggests that **6** and TMZ induced the intrinsic caspase pathway in snb19 and ln229 cells.

Reactive oxygen species are produced in cancer cells and crucial to several cellular processes, including cell proliferation, metastasis, and angiogenesis. (Clerkin et al., 2008; Giles, 2006; Ushio-Fukai and Nakamura, 2008; Wu and Hua, 2007). Reactive oxygen species induces apoptosis and cell cycle arrest in cancer cells during chemotherapeutic treatment (Circu and Aw, 2010; Toler et al., 2006). in our study, the effects of **6**, H_2O_2 and TMZ on the levels of reactive oxygen species in snb119 and ln229 cells were assessed using reactive oxygen species production assay (Walsh et al., 2008). The increase of reactive oxygen species in ln229 cells treated with **6** was higher than in H_2O_2 and TMZ treated cultures (Fig. 4b). as seen in Fig. 4b, ln229 cells treated with **6** increased their reactive oxygen species production by 5.2-fold and 6.4-fold in comparison with TMZ and H_2O_2 treatment, respectively (**6** vs TMZ; $p < 0.0001$ and **6** vs H_2O_2 $p < 0.0001$). Interestingly, reactive oxygen species production in snb19 cells treated with **6** was lower than in H_2O_2 and TMZ treated samples (**6** vs TMZ; $p < 0.0001$ and **6** vs H_2O_2 $p < 0.0001$). However, compared to the untreated condition, there was a 0.2-fold increase in reactive oxygen species production in snb19. When comparing between ln229 and snb19, **6** had better effectiveness in promoting reactive oxygen species production in ln229, while it was 6-fold less in snb19. Both cell lines produced higher reactive oxygen species levels when compared to the untreated condition, suggesting that it could be interlinked with the observed apoptotic cell death of ln229 and snb19 upon treatment with **6**.

3.5. Cell cycle G2/M phases arrest by boroxazolidone 6

Cellular DNA content analysis following propidium iodide (PI) staining is a well-established method for quantifying the percentage of cells in cell cycle arrest. The deconvolution of the cellular DNA content frequency and histogram analysis allows observation of the fraction of cells in each cycle phase (G0/G1, S and G2/M). It is established that DNA damage can induce cell cycle arrest in cancer cells during chemotherapeutic treatment. In the present study, cell cycle progression was imaged using PI fluorescent staining and microscopy. Different phases of the cell cycle were determined based on the signature fluorescence signals corresponding to each cell cycle phase. In this study, similar trends in cell cycle arrest were observed in both LN229 and SNB19 cell lines after treatment.

In LN229 cells, the control (DMSO treated) conditions resulted in the highest number of cells in the G2/M phases, moderate numbers of cells in the G0/G1 phases, and the least number of cells in the S phase. When treated with compound **6**, the percentage of G2/M phase cells increased, while G0/G1 and S phase cells decreased compared to the control cells, but the overall relationship between the percentages of cells in each phase was similar to the control (Fig. 5A). SNB19 had a similar trend to LN229; however, G0/G1 and G2/M were switched. Where the percentage of G0/G1 phase cells was the highest, followed by G2/M phases, and then the S phase. This may be explained by unequal growth rates in a population of proliferating cells. It is well known than, the LN229 is faster growing than SNB19(Al-Moujahed et al., 2017; Diao et al., 2019; Howard and Pelc, 1986). Therefore, the percentage of SNB19 cells in the G0/G1phases was higher than LN229 cells. Suggesting that many cells were in the resting phase or entering into the G1 phase in LN229 due to fast growth rate. When SNB19 was treated with **6**, the percentage of G2/M phase cells increased by one fold, while the percentage in other phases decreased (Fig. 5B). According to these results, it is concluded that SNB19 and LN229 cells were arrested at G2/M phase when they were treated with **6**.

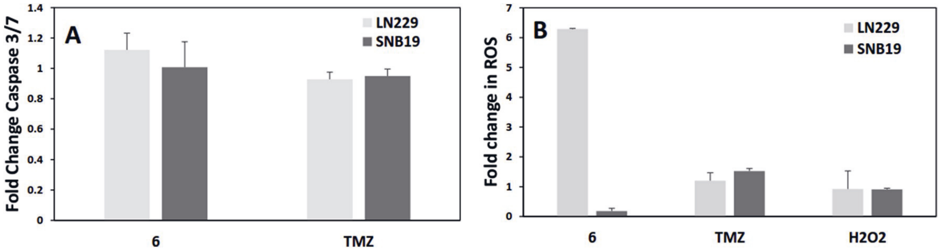

Fig. 4. Effect of compound 6 in caspase 3/7 and intracellular reactive oxygen species: A) Induction of caspase 3/7 in LN229 (6 vs TMZ; $P = 0.1271$) and SNB119 cells (6 vs TMZ; $P = 0.4519$). Cells were treated with IC_{50} concentrations of 6 and TMZ. Activity of caspases 3/7 was measured using luminescence reader. B) Quantification of reactive oxygen species level in LN229 and SNB119 cells treated with 6, H_2O_2 a positive control, and TMZ as a drug control. Biological and technical repeats were used for each condition (6 vs TMZ; $P < 0.0001$ and 6 vs H_2O_2 $P < 0.0001$). Each bar represents a mean ± S.E.M. Each treatment was performed with biological and technical replicates.

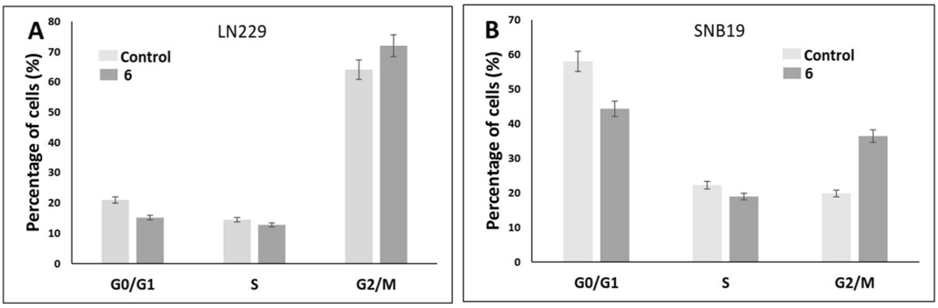

Fig. 5. Cell cycle analysis using PI staining. A. Percentage of total cell in different phases when they were treated with boroxazolidone 6 and DMSO (control) in LN229 and B) SNB119. Each bar represents a mean ± S.E.M. Each treatment was performed with biological and technical replicates.

4. Discussion

Our previous studies have reported the synthesis of several new L-valine derived boroxazolidones and evaluated their anticancer activity against the growth of human brain astrocytoma and colorectal adenocarcinoma cells. As a continuation of previous studies, we presently report the biological activity of L-valine derived boroxazolidones against the growth of human glioblastoma. From a small collection of six compounds, fluorinated derivative **6** demonstrated superior cytotoxic effects against GBM cancer cell lines when compared with the other boroxazolidones tested. In addition, the present study shows that this compound has a higher mortality rate in glioblastoma cells than in colon cancer cells, therefore, suggesting selective inhibition of the brain tumor cells. This boroxazolidone induced cell death via apoptosis and caspase 3/7 activation.

Reactive oxygen species, such as hydrogen peroxide, hydroxyl radicals, and superoxide anions are produced in living cells, and played significant roles in many cellular functions (Pelicano et al., 2004). increased reactive oxygen species production in cancer cells may lead to genetic mutation, genetic instability, and result in cellular damage (Fang et al., 2009; Kovacic and Jacintho, 2001; Pelicano et al., 2004; Shi et al., 2014; Tominaga et al., 2004). Cancer cells usually possess higher level of reactive oxygen species compared to the normal cells, and it was previously reported that boron-containing molecules increased cellular oxidative stress, thus, inducing apoptosis in many cancer cell types. Our current observations are in agreement with such reports as higher levels of reactive oxygen species production were observed in glioblastoma cells, therefore being a plausible cause for apoptotic pathway induction. Given the pronounced six-fold increase in reactive oxygen species production in ln229 cells, it is probable that such species are responsible for the selective cytotoxicity compound **6** exhibits. Drugs targeted towards changing the reactive oxygen species levels are important for anti-GBM drugs, and compound **6** can be considered to be promising in this regard. Although further pharmacological and biolological studies are required to fully disclose the mechanism of action of compound **6**.

Boroxazolidones-related diaryl borinic acids have been widely demonstrated to be strong inhibitors of serine proteases (Steiner et al., 1994), of store-operated calcium entry (Ozaki et al., 2013; Suzuki et al., 2010) and acyl protein thioesterases 1 and 2 (Zimmermann et al., 2013). Moreover, boroxazolidones derived from amino acids other than valine were demonstrated to have an IC_{50} inhibitory activity on store-operated calcium entry (Ozaki et al., 2013) as low as 0.2 μM. As the influence of the substitution pattern of the aromatic rings was not studied previously, this study suggests that, if the antitumor activity of boroxazolidones relies solely on calcium channel inhibition, the use of other amino acids as the synthetic precursor may provide cytotoxic species of higher potency.

Wild-type p53 is documented to suppress cancer formation in normal cells and protects against stress-induced DNA damage by inducing cell cycle arrest, DNA repair, and apoptosis (Van Meir et al., 1994). However, many types of cancer cells, including glioblastoma cells, over express mutant p53 proteins. GBM cells bearing p53 mutations promote chemo-resistant phenotypes, while wild-type p53 does not (Hientz et al., 2017). p53 mutations may cause resistance to DNA-damaging agents and, as a consequence, cause cellular resistance to multiple cytotoxic agents. Many cytotoxic drugs were developed to modulate the p53 singling pathway and, thus, stop the progression of tumor growth (Stegh, 2012). The present study demonstrates that compound **6** potentiates the cytotoxic effect on LN229 and SNB19 cells, both of which exhibit mutated p53 proteins. However, the effect is lower than that of TMZ. The results suggest that compound **6** may induce the cytotoxic effect by affecting the p53 signalling pathway.

5. Conclusion

Overall, this study demonstrated that boroxazolidone **6**, has a strong cytotoxic effect and was found to have the highest cytotoxicity among the library of compounds tested. Further analyses of the mechanism of cell death induction by **6** suggests that cell death occurs through apoptosis and has the potential to activate caspase 3/7 pathways, reactive oxygen species induction, and cell cycle arrest of GBM. The magnitude of anti-GBM effect of **6** is significantly higher than known chemotherapeutic agent TMZ. However, testing effects of **6** in an *in vivo* model, patient derived xenografts, could allow this compound to be used as a potential therapeutic agent for glioma treatment.

Author contributions

JR and NRC synthesized and characterized the compounds, AV and GS executed the experiments and data analysis. VS executed the cell cycle image analysis. KB performed the experiment on the normal brain cell line. MK, OY and NRC conceived and managed all studies. All the authors contributed to writing the manuscript.

Funding sources

MK, AV and OYH acknowledge the Academy of Finland for the project grant support (decision no. 297200) and Tampere University of Technology for Instrumental facility grant support. NRC acknowledges the Academy of Finland (decision no. 287954) for the financial support.

Conflicts of interest statement

All the authors report that they do not have conflicts of interests.

Appendix A. Supplementary data

Supplementary data to this article can be found online at https://doi.org/10.1016/j.ejphar.2019.04.020.

References

Al-Moujahed, A., Brodowska, K., Stryjewski, T.P., Efstathiou, N.E., Vasilikos, I., Cichy, J., Miller, J.W., Gragoudas, E., Vavvas, D.G., 2017. Verteporfin inhibits growth of human glioma in vitro without light activation. Sci. Rep. 7, 7602. https://doi.org/10.1038/s41598-017-07632-8.

Andrews, P.L., Rapeport, W.G., Sanger, G.J., 1988. Neuropharmacology of emesis induced by anti-cancer therapy. Trends Pharmacol. Sci. 9, 334–341. https://doi.org/10.1016/0165-6147(88)90106-X.

Baker, S.J., Ding, C.Z., Akama, T., Zhang, Y.-K., Hernandez, V., Xia, Y., 2009. Therapeutic potential of boron-containing compounds. Future Med. Chem. 1, 1275–1288. https://doi.org/10.4155/fmc.09.71.

Circu, M.L., Aw, T.Y., 2010. Reactive oxygen species, cellular redox systems, and apoptosis. Free Radic. Biol. Med. 48, 749–762. https://doi.org/10.1016/j.freeradbiomed.2009.12.022.

Clerkin, J.S., Naughton, R., Quiney, C., Cotter, T.G., 2008. Mechanisms of ROS modulated cell survival during carcinogenesis. Cancer Lett. 266 (1), 30–36. https://doi.org/10.1016/j.canlet.2008.02.029.

Diao, W., Tong, X., Yang, C., Zhang, F., Bao, C., Chen, H., Liu, L., Li, M., Ye, F., Fan, Q., Wang, J., Ou-Yang, Z.-C., 2019. Behaviors of glioblastoma cells in in vitro microenvironments. Sci. Rep. 9, 85. https://doi.org/10.1038/s41598-018-36347-7.

Doan, P., Karjalainen, A., Chandraseelan, J.G., Sandberg, O., Yli-Harja, O., Rosholm, T., Franzen, R., Candeias, N.R., Kandhavelu, M., 2016. Synthesis and biological screening for cytotoxic activity of N-substituted indolines and morpholines. Eur. J. Med. Chem. 120, 296–303. https://doi.org/10.1016/j.ejmech.2016.05.024.

Fang, J., Seki, T., Maeda, H., 2009. Therapeutic strategies by modulating oxygen stress in cancer and inflammation. Adv. Drug Deliv. Rev. 61, 290–302. https://doi.org/10.1016/j.addr.2009.02.005.

Giles, G.I., 2006. The redox regulation of thiol dependent signaling pathways in cancer. Curr. Pharmaceut. Des. 12, 4427–4443. https://doi.org/10.2174/138161206779010549.

Hientz, K., Mohr, A., Bhakta-Guha, D., Efferth, T., 2017. The role of p53 in cancer drug resistance and targeted chemotherapy. Oncotarget 8, 8921–8946. https://doi.org/10.18632/oncotarget.13475.

Howard, A., Pelc, S.R., 1986. Synthesis of desoxyribonucleic acid in normal and irradiated cells and its relation to chromosome breakage. Int. J. Radiat. Biol. Relat. Stud. Phys. Chem. Med. 49, 207–218. https://doi.org/10.1080/09553008514552501.

Kovacic, P., Jacintho, J.D., 2001. Mechanisms of carcinogenesis: focus on oxidative stress and electron transfer. Curr. Med. Chem. 8, 773–796. https://doi.org/10.2174/0929867013373084.

Kuuloja, N.M., Kylmälä, T.M., Tois, J.E., Sjöholm, R.E., Franzén, R.G., 2011. Preparation of triethylammonium tetra-arylborates (TEATABs): coupling partners for the Suzuki reaction. Synth. Commun. 41, 1052–1063. https://doi.org/10.1080/00397911003718086.

Kwak, E.-Y., Choi, M.-K., Yang, S.-G., Shim, C.-K., Shim, W.-S., 2012a. Investigation into the efficacy of val-SN-38, a valine-ester prodrug of the anti-cancer agent SN-38. Biomol. Ther. 20, 326–331. https://doi.org/10.4062/biomolther.2012.20.3.326.

Kwak, E.-Y., Shim, W.-S., Chang, J.-E., Chong, S., Kim, D.-D., Chung, S.-J., Shim, C.-K., 2012b. Enhanced intracellular accumulation of a non-nucleoside anti-cancer agent via increased uptake of its valine ester prodrug through amino acid transporters. Xenobiotica 42, 603–613. https://doi.org/10.3109/00498254.2011.646339.

Ozaki, S., Suzuki, A.Z., Bauer, P.O., Ebisui, E., Mikoshiba, K., 2013. 2-Aminoethyl diphenylborinate (2-APB) analogues: regulation of Ca2+ signaling. Biochem. Biophys. Res. Commun. 441, 286–290. https://doi.org/10.1016/j.bbrc.2013.08.102.

Paramore, A., Frantz, S., 2003. Bortezomib. Nat. Rev. Drug Discov. 2, 611–612. https://doi.org/10.1038/nrd1159.

Pelicano, H., Carney, D., Huang, P., 2004. ROS stress in cancer cells and therapeutic implications. Drug Res. 7 (2), 97–110. Updat. https://doi.org/10.1016/j.drup.2004.01.004.

Philipp, M., Bender, M.L., 1971. Inhibition of serine proteases by arylboronic acids. Proc. Natl. Acad. Sci. U. S. A 68, 478–480. https://doi.org/10.1073/pnas.68.2.478.

Poddar, N.K., Maurya, S.K., Saxena, V., 2017. Role of serine proteases and inhibitors in cancer. In: Chakraborti, S., Dhalla, N.S. (Eds.), Proteases in Physiology and Pathology. Springer Singapore, Singapore, pp. 257–287. https://doi.org/10.1007/978-981-10-2513-6_12.

Raunio, J., Mannoja, J., Nguyen, T., Ahmad, N., Kemppainen, N.M., Franzén, R.G., Kandhavelu, M., Candeias, N.R., 2017. Base catalysed N-functionalisation of boroxazolidones. RSC Adv. 7, 20620–20627. https://doi.org/10.1039/C7RA03266H.

Scorei, R.I., Popa, R., 2010. Boron-containing compounds as preventive and chemotherapeutic agents for cancer. ACAMC 10, 346–351. https://doi.org/10.2174/187152010791162289.

Shi, J., Zuo, H., Ni, L., Xia, L., Zhao, L., Gong, M., Nie, D., Gong, P., Cui, D., Shi, W., Chen, J., 2014. An IDH1 mutation inhibits growth of glioma cells via GSH depletion and ROS generation. Neurol. Sci. 35, 839–845. https://doi.org/10.1007/s10072-013-1607-2.

Stegh, A.H., 2012. Targeting the p53 signaling pathway in cancer therapy - the promises, challenges and perils. Expert Opin. Ther. Targets 16, 67–83. https://doi.org/10.1517/14728222.2011.643299.

Steiner, S.J., Bien, J.T., Smith, B.D., 1994. Diphenylborinic acid is a strong inhibitor of serine proteases. Bioorg. Med. Chem. Lett 4, 2417–2420. https://doi.org/10.1016/S0960-894X(01)80401-7.

Suzuki, A.Z., Ozaki, S., Goto, J.-I., Mikoshiba, K., 2010. Synthesis of bisboron compounds and their strong inhibitory activity on store-operated calcium entry. Bioorg. Med. Chem. Lett 20, 1395–1398. https://doi.org/10.1016/j.bmcl.2009.12.108.

Toler, S., Noe, D., Sharma, a, 2006. Selective enhancement of cellular oxidative stress by chloroquine: implications for the treatment of glioblastoma multiforme. Neurosurg. Focus 21, E10. https://doi.org/10.3171/foc.2006.21.6.1.

Tominaga, H., Kodama, S., Matsuda, N., Suzuki, K., Watanabe, M., 2004. Involvement of reactive oxygen species (ROS) in the induction of genetic instability by radiation. J. Radiat. Res. 45, 181–188. [pii]. https://doi.org/JST.JSTAGE/jrr/45.181.

Tülüce, Y., Lak, P.T.A., Koyuncu, İ., Kılıç, A., Durgun, M., Özkol, H., 2017. The apoptotic, cytotoxic and genotoxic effect of novel binuclear boron-fluoride complex on endometrial cancer. Biometals 30, 933–944. https://doi.org/10.1007/s10534-017-0060-8.

Ushio-Fukai, M., Nakamura, Y., 2008. Reactive oxygen species and angiogenesis: NADPH oxidase as target for cancer therapy. Cancer Lett. 266 (2), 37–52. https://doi.org/10.1016/j.canlet.2008.02.044.

Van Meir, E.G., Kikuchi, T., Tada, M., Li, H., Diserens, A.C., Wojcik, B.E., Huang, H.J., Friedmann, T., de Tribolet, N., Cavenee, W.K., 1994. Analysis of the p53 gene and its expression in human glioblastoma cells. Cancer Res. 54, 649–652.

Velasco, B., Trujillo-Ferrara, J.G., Castillo, L.H.F., Miranda, R., Sánchez-Torres, L.E., 2007. In vitro apoptotic activity of 2,2-diphenyl-1,3,2-oxazaborolidin-5-ones in L5178Y cells. Life Sci. 80, 1007–1013. https://doi.org/10.1016/j.lfs.2006.11.034.

Velasco-Bejarano, B., Trujillo-Ferrara, J., Miranda, R., 2007. Preparation of apoptotic inducers, 2,2-Diphenyl-1,3,2-oxazaborolidin-5-ones, under alkaline conditions. Synlett 921–924 2007. https://doi.org/10.1055/s-2007-973886.

Walsh, J.G., Cullen, S.P., Sheridan, C., Lüthi, A.U., Gerner, C., Martin, S.J., 2008. Executioner caspase-3 and caspase-7 are functionally distinct proteases. Proc. Natl. Acad. Sci. U. S. A 105, 12815–12819. https://doi.org/10.1073/pnas.0707715105.

Wu, X.J., Hua, X., 2007. Targeting ROS: selective killing of cancer cells by a cruciferous vegetable derived pro-oxidant compound. Cancer Biol. Ther. 6 (5), 646–647. https://doi.org/10.4161/cbt.6.5.4092.

Xu, W., Baribault, H., Adamson, E.D., 1998. Vinculin knockout results in heart and brain defects during embryonic development. Development 125, 327–337.

Zimmermann, T.J., Bürger, M., Tashiro, E., Kondoh, Y., Martinez, N.E., Görmer, K., Rosin-Steiner, S., Shimizu, T., Ozaki, S., Mikoshiba, K., Watanabe, N., Hall, D., Vetter, I.R., Osada, H., Hedberg, C., Waldmann, H., 2013. Boron-based inhibitors of acyl protein thioesterases 1 and 2. Chembiochem 14, 115–122. https://doi.org/10.1002/cbic.201200571.

Żołnierczyk, J.D., Olejniczak, A.B., Mieczkowski, A., Błoński, J.Z., Kiliańska, Z.M., Robak, T., Leśnikowski, Z.J., 2016. In vitro antileukemic activity of novel adenosine derivatives bearing boron cluster modification. Bioorg. Med. Chem. 24, 5076–5087. https://doi.org/10.1016/j.bmc.2016.08.028.

PUBLICATION
IV

Battling Glioblastoma: A Novel Tyrosine Kinase Inhibitor with Multi-dimensional Anti-tumor Effect

Anisha Viswanathan, Aliyu Musa, Akshaya Murugesan, João R. Vale, Saravanan Konda Mani, Carlos A. M. Afonso, Rafael Candeias Nuno, Olli Yli-Harja, Meenakshisundaram Kandhavelu

Cells, 12 Dec 2019, 8(12), 1624
https://doi.org/10.3390/cells8121624

Publication reprinted with the permission of the copyright holders.

cells

Article

Battling Glioblastoma: A Novel Tyrosine Kinase Inhibitor with Multi-Dimensional Anti-Tumor Effect (Running Title: Cancer Cells Death Signalling Activation)

Anisha Viswanathan [1], Aliyu Musa [2], Akshaya Murugesan [1,3], João R. Vale [4,5], Carlos A. M. Afonso [5], Saravanan Konda Mani [6], Olli Yli-Harja [7,8], Nuno R. Candeias [4,*] and Meenakshisundaram Kandhavelu [1,*]

[1] Molecular Signaling Lab, Faculty of Medicine and Health Technology, Tampere University, BioMeditech and Tays Cancer Center, Tampere University Hospital, P.O. Box 553, 33101 Tampere, Finland; anisha.viswanathan@tuni.fi (A.V.); akshaya.murugesan@tuni.fi (A.M.)
[2] Predictive Medicine and Data Analytics Lab, Faculty of Medicine and Health Technology, Tampere University and BioMediTech, P.O. Box 553, 33101 Tampere, Finland; aliyu.musa@tuni.fi
[3] Department of Biotechnology, Lady Doak College, Madurai 625002, India
[4] Faculty of Engineering and Natural Sciences, Tampere University, 33101 Tampere, Finland; rafael.camposdovale@tuni.fi
[5] Instituto de Investigação do Medicamento (iMed.ULisboa), Faculdade de Farmácia, Universidade de Lisboa, Av. Prof. Gama Pinto, 1649-003 Lisboa, Portugal; carlosafonso@ff.ulisboa.pt
[6] Shenzhen Institutes of Advanced Technology, Chinese Academy of Sciences, Shenzhen 518055, China; saravananbioinform@gmail.com
[7] Computational Systems Biology Group, Faculty of Medicine and Health Technology, Tampere University and BioMediTech, P.O. Box 553, 33101 Tampere, Finland; olli.yli-harja@tuni.fi
[8] Institute for Systems Biology, 1441N 34th Street, Seattle, WA 98103-8904, USA
* Correspondence: nuno.rafaelcandeias@tuni.fi (N.R.C.); meenakshisundaram.kandhavelu@tuni.fi (M.K.); Tel.: +358-468857306 (N.R.C.); +358-417488772 (M.K.)

Received: 26 November 2019; Accepted: 9 December 2019; Published: 12 December 2019

Abstract: Glioblastoma (GB), a grade IV glioma, with high heterogeneity and chemoresistance, obligates a multidimensional antagonist to debilitate its competence. Considering the previous reports on thioesters as antitumor compounds, this paper investigates on use of this densely functionalized sulphur rich molecule as a potent anti-GB agent. Bio-evaluation of 12 novel compounds, containing α-thioether ketone and orthothioester functionalities, identified that five analogs exhibited better cytotoxic profile compared to standard drug cisplatin. Detailed toxicity studies of top compound were evaluated in two cell lines, using cell viability test, apoptotic activity, oxidative stress and caspase activation and RNA-sequencing analysis, to obtain a comprehensive molecular profile of drug activity. The most effective molecule presented half maximal inhibitory concentration (IC_{50}) values of 27 μM and 23 μM against U87 and LN229 GB cells, respectively. Same compound effectively weakened various angiogenic pathways, mainly MAPK and JAK-STAT pathways, downregulating VEGF. Transcriptome analysis identified significant promotion of apoptotic genes, and genes involved in cell cycle arrest, with concurrent inhibition of various tyrosine kinase cascades and stress response genes. Docking and immunoblotting studies suggest EGFR as a strong target of the orthothioester identified. Therefore, orthothioesters can potentially serve as a multi-dimensional chemotherapeutic possessing strong cytotoxic, anti-angiogenic and chemo-sensitization activity, challenging glioblastoma pathogenesis.

Keywords: glioblastoma; thioester; anti-angiogenesis; tyrosine kinase inhibitor

1. Introduction

Glioblastoma (GB) is a type of brain tumor with almost 100% recurrence rate and high resistance to current treatment modalities. The high heterogeneity exhibited within GB tumors render it unresponsive to single-target cytotoxic/anti-angiogenic agents and demands a significant clinical need for new multi-dimensional oncogenic inhibitors for GB.

Angiogenesis is a significant feature of GB, attributed to the overexpression of vascular endothelial growth factor (*VEGF*). Few of the most significant proangiogenic regulators that stimulate angiogenesis indirectly by inducing *VEGF* mRNA expression include the growth factors epidermal growth factor (*EGF*), transforming growth factor (*TGF-α* and *TGF-β*), tumor necrosis factor α (*TNF-α*), keratinocyte growth factor, insulin-like growth factor I (*IGF-I*), fibroblast growth factor (*FGF*), platelet-derived growth factor/(*PDGF*), and cytokines (interleukin (*IL*)-*1α* and *IL-6*) and amplifications of *Ras*/*Raf* genes [1]. Multiple strategies have been developed to target VEGF/VEGF receptor (*VEGFR*)–mediated angiogenesis, including VEGF blockade, VEGF Trap, and suppression of VEGFR signaling via receptor tyrosine kinase inhibitors (TKIs) [2–4]. *EGFR* belongs to the *ErbB* family receptors of Class I receptor tyrosine kinases (*RTKs*). Almost 60% of glioblastoma patients have some kind of genomic alteration affecting EGFR pathway [5]. Downstream effects of *EGFR* is mediated through phosphoinositide 3-kinase (*PI3K*), mitogen-activated protein kinase (*MAPK*), signal transducer and activator of transcription 3 (*STAT3*) pathways, and *Src* family kinases [6]. A number of studies have focused on inhibiting both *VEGFR* and *EGFR* so as to improve drug efficiency, including monotherapy with a multi-targeted tyrosine kinase inhibitor (e.g., vandetanib, AEE788, BMS-690514) [7,8]. Other significant pathways regulating tumor angiogenesis directly or indirectly via VEGF includes MAPK pathway [9], JAK-STAT pathway [10,11], and PI3K-AKT [12] pathway. Thus, a multi-targeted chemoagent that can effectively sequester multiple pathways involved in VEGF regulation would be an effective solution to tackle tumor pathogenesis.

Some of us have recently reported the unprecedented autoxidative condensation of 2-aryl-2-lithio-1,3-dithianes (Scheme 1) [13]. The result of such transformation was a small library of highly functionalized molecules containing α-thioether ketones and orthothioesters functionalities, among others. Motivated by the desire to find new agents capable of multi-target inhibition as promising approaches in the development of glioblastoma cancer drugs [14], we have set to assess the antitumor properties of these intricate molecules.

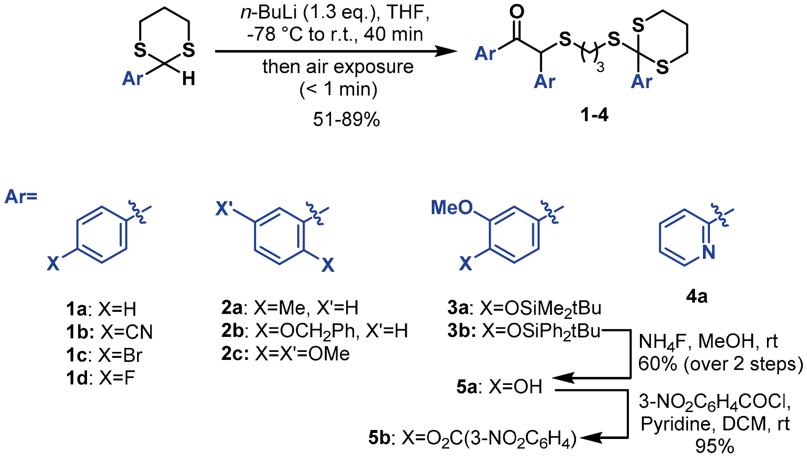

Scheme 1. Synthesis and structures of studied orthothioesters.

2. Materials and Methods

2.1. Synthesis of Orthothioesters

Reactions were monitored through thin-layer chromatography (TLC) with commercial silica gel plates (Merck silica gel, 60 F254). Visualization of the developed plates was performed under UV lights at 254 nm and by staining with cerium ammonium molybdate, 2,4-dinitrophenylhydrazine and vanillin stains. Flash column chromatography was performed on silica gel 60 (40–63 µm) as a stationary phase. NMR spectra were recorded with Varian Mercury 300 MHz or Jeol ECZR 500 instruments using $CDCl_3$ as solvent and calibrated using tetramethylsilane as internal standard. Chemical shifts (δ) are reported in ppm referenced to the $CDCl_3$ residual peak (δ 7.26) or TMS peak (δ 0.00) for ^{1}H-NMR and to $CDCl_3$ (δ 77.16) for ^{13}C-NMR. The following abbreviations were used to describe peak splitting patterns: s = singlet, d = doublet, t = triplet, m = multiplet. Coupling constants, *J*, were reported in Hertz (Hz). High-resolution mass spectra (HR-MS) were recorded on a Waters ESI-TOF MS spectrometer. Tetrahydrofuran (THF) was dried by distillation under argon with sodium metal and benzophenone as indicator. Dichloromethane (DCM) was dried by distillation under argon with calcium hydride. Structural elucidation of all compounds tested in biological assays was performed by ^{1}H and ^{13}C-NMR, and HR-MS. All compounds of interest were isolated by chromatography and their purity (>97%) assessed by NMR.

Compounds **1**–**4** were prepared and characterized as reported elsewhere [13], through autoxidative condensation of 2-aryl-2-lithium-1,3-dithianes, prepared from treatment of 2-aryl-1,3-dithianes with *n*-BuLi followed by air exposure.

5a: (4-(1,3-Dithian-2-yl)-2-methoxyphenoxy)(*tert*-butyl)diphenylsilane (1.09 g, 2.27 mmol) was dissolved in dry THF (10 mL) in an argon purged round-bottom flask. The solution was cooled to −78 °C in an acetone/liquid nitrogen bath. *n*-BuLi (1.3 equivalents) was added dropwise to the reaction mixture at −78 °C. After addition, the solution was left stirring at −78 °C for 20 min, and then left to warm up to room temperature for 40 min. The argon balloon was replaced with an atmospheric air balloon and an additional needle was inserted in the septum as to allow air flow through the surface of the solution. After one minute, the solution was quenched with saturated aqueous NH_4Cl solution (20 mL). Et_2O (20 mL) was added and the layers separated. The organic phase was collected and the aqueous phase was extracted with Et_2O (2 × 20 mL). The organic phases were combined and dried over $MgSO_4$. The solvent was filtered and evaporated to yield crude 3b. The mixture was dissolved in dry methanol (8 mL) in an argon purged round-bottom flask. Then, ammonium fluoride (95 mg, 2.56 mmol, 1.1 equivalents) was added and the solution was stirred overnight at room temperature. The methanol was evaporated and water (10 mL) was added. The aqueous phase was extracted with DCM (3 × 10 mL) and the organic phases were combined and dried over $MgSO_4$. The solvent was evaporated and the product was purified by flash chromatography, eluent hexane: ethyl acetate (1:1), to give product **5a** as an amorphous orange solid (286 mg, 0.45 mmol) in 60% yield. ^{1}H-NMR (500 MHz, $CDCl_3$) δ ppm 7.56–7.49 (m, 3H), 7.44 (dd, *J* = 8.4, 2.1 Hz, 1H), 6.98 (s, 1H), 6.89–6.82 (m, 4H), 6.07 (s, 1H), 5.68 (s, 1H), 5.61 (s, 1H), 5.45 (s, 1H), 3.90 (s, 3H), 3.89 (s, 3H), 3.86 (s, 3H), 3.27 (t, *J* = 12.5 Hz, 2H), 2.74–2.70 (m, 2H), 2.57–2.44 (m, 4H), 2.10–2.05 (m, 1H), 1.92–1.85 (m, 1H), 1.77–1.71 (m, 2H). ^{13}C-NMR (125 MHz, $CDCl_3$) δ ppm 194.0, 150.7, 147.1, 146.8, 146.4, 145.8, 145.6, 133.3, 128.8, 128.5, 124.3, 122.1, 121.3, 114.3, 114.0, 113.9, 111.0, 110.8, 110.6, 64.3, 56.2 (×2), 56.1, 55.2, 32.8, 30.7, 29.4, 28.5, 24.4. HR-MS (ESI) *m*/*z* calculated for $C_{30}H_{34}O_7S_4Na^+$ $[M + Na]^+$ 657.1080, found 657.1068.

5b: Triphenol **5a** (100 mg, 0.158 mmol) was dissolved in dry DCM (3 mL) in an argon purged round-bottom flask. Pyridine (48 µL, 0.591 mmol, 3.75 equivalents) was added to the solution, followed by 3-nitrobenzoyl chloride (91 mg, 0.488 mmol, 3.1 equivalents). The reaction was left stirring at room temperature for 72 h. Water (10 mL) was added to the mixture and the aqueous phase was extracted with DCM (3 × 10 mL). The organic phases were combined and dried over $MgSO_4$. The solvent was evaporated and the product was purified by flash chromatography, eluent hexane: ethyl acetate (3:2), to give the benzoyl derivative **5b** as an amorphous white solid (163 mg, 0.151 mmol) in 95% yield.

^{1}H NMR (500 MHz, CDCl$_3$) δ ppm 9.02 (s, 3H), 8.51–8.48 (m, 6H), 7.76–7.67 (m, 6H), 7.62 (dd, J = 8.4, 2.0 Hz, 1H), 7.25–7.08 (m, 5H), 5.56 (s, 1H), 3.86 (s, 3H), 3.85 (s, 3H), 3.83 (s, 3H), 3.31 (dd, J = 13.3, 11.2 Hz, 2H), 2.79 (dd, J = 14.3, 3.6 Hz, 2H), 2.70–2.58 (m, 4H), 2.14–2.11 (m, 1H), 1.98–1.91 (m, 1H), 1.86–1.81 (m, 2H). ^{13}C-NMR (125 MHz, CDCl$_3$) δ 193.8, 162.6, 162.6, 162.2, 151.7, 151.6, 151.0, 148.5, 148.5, 143.8, 140.9, 139.5, 139.4, 136.1, 136.1, 135.9, 134.9, 131.2, 131.2, 130.8, 130.1, 130.0, 128.3, 128.1, 128.1, 125.5, 125.4, 122.9, 122.4, 122.3, 121.4, 120.6, 112.9, 112.8, 64.1, 56.3, 56.2, 56.2, 55.1, 32.8, 30.9, 29.5, 28.5, 24.3. HR-MS (ESI) m/z calculated for $C_{51}H_{43}N_3O_{16}S_4Na^+$ $[M + Na]^+$ 1104.1418, found 1104.1385.

2.2. Cell Culture

Human GB cell lines, U87 cells were grown in Minimum Essential Medium (MEM, Product# 51416C, Sigma-Aldrich, St. Louis, MO, USA) with 10% Fetal Bovine Serum(FBS) 2 mM sodium pyruvate (Product# S8636, Sigma-Aldrich, St. Louis, MO), 1% Penicillin-Streptomycin and 0.025 mg/mL Amphotericin B. LN229 and non-cancerous cell line, mouse embryonic fibroblast (MEF) cells were cultured in Dulbecco's Modified Eagle Medium—high glucose (DMEM, Catalog# L0102, Biowest, Riverside, CA, USA) containing 5% FBS (Product # F1051, Sigma-Aldrich, St. Louis, MO), 1% Penicillin-Streptomycin (Product # P4333, Sigma-Aldrich, St. Louis, MO) and 0.025 mg/mL Amphotericin B (Sigma-Aldrich, St. Louis, MO). U87 and LN229 are the standard cell lines derived from malignant gliomas used commonly for cytotoxicity study. MEF Cells were maintained at 37 °C in a humidified incubator supplemented with 5% CO_2. Three biological and technical repeats were used for each condition.

2.3. In Vitro Cytotoxicity Assay

Cytotoxicity assay was performed to determine the cell growth inhibitory effect of the compounds following treatment for 48 h on the GB cell lines, U87, LN229. This assay was performed in two stages. At first, a high concentration, 100 µM, of compounds were used as well as for the positive control Cisplatin, CIS (Sigma-Aldrich, USA). Following this, the top compound was selected, and different concentrations (100 µM, 75 µM, 50 µM, 25 µM, and 10 µM) of the compound were tested to determine the IC_{50}. Treated cells were harvested by centrifugation at 1200 rpm for 10 min. Cell viability was determined using trypan blue staining. The number of live and dead cells were counted using a Countess II Automated Cell Counter (Thermo Fisher Scientific, Carlsbad, CA, USA). The proliferation inhibition percentage of each sample was determined using the following formula to determine the dose-response curve. From the dose-response curve, the IC_{50} value of each compound was calculated. The cytotoxicity of the top compound and Cisplatin at a concentration of 10 µM was also evaluated in normal brain cells (MEF). Percentage of inhibition of cell proliferation was calculated using the following formula:

$$\text{Proliferation inhibition } (\%) = \frac{Mean\ No.\ of\ untreated\ cells\ (DMSO\ control) - Mean\ No.\ of\ treated\ cells \times 100}{Mean\ No.\ of\ untreated\ cells\ (DMSO\ control)}$$

2.4. Double Staining Assay

U87 and LN229 cell lines were grown as described previously, followed by cells treatment with IC_{50} concentration of 5a and incubated for 48 h. Untreated (Negative) and Cisplatin (positive) controls were also maintained. Apoptosis/necrosis detection was carried out using Annexin V-FITC and PI (Thermo Fisher Scientific). The apoptosis determination was performed following the standard protocol suggest by the manufacturer. Briefly, the cells were cultured in 6-well plate with an initial cell density of 7×10^5 cells/well. The cells were incubated for 48 h with 5a, positive control and untreated cells conditions and then harvested and washed in cold phosphate buffered saline (PBS). The cell pellets were then resuspended in 1× Annexin-binding buffer provided in the kit. Consequently, 5 µL of FITC conjugated Annexin V and 1 µL of the 100 µg/mL PI working solutions were added to the 100 µL of cell suspension. The cells were incubated in dark for 15 min, at room temperature, after which the stained cells were observed for fluorescence to distinguish apoptotic cells. The image acquisition was done by using an EVOS imaging system (ThermoFisher Scientific) with 20× objective magnification. More than 300 cells were used for each analysis. The percentage of apoptosis was quantified based on the cells stained with Annexin V-FITC positive and PI negative and both Annexin V-FITC and PI positive. The percentage of necrosis was calculated based on the cells with Annexin V-FITC negative and PI positive [15–17]. The fold change in apoptosis was calculated against the untreated cells.

2.5. Caspase Activity Assay

In-vitro caspase-3 and caspase-7 activity was determined using Caspase-Glo® 3/7 Assay Systems (Promega Corporation, Madison, WI, USA). The reagent was prepared as mentioned in the manufacturer protocol. The U87 and LN229 cells were grown overnight in a 96-well plate and were treated with an IC_{50} of 5A. Negative control, positive control and blank (medium+ Dimethyl sulfoxide (DMSO)+ dye) were also maintained. Cells were incubated at 37 °C in a humidified incubator supplemented with 5% CO_2 for 5 h and then equilibrated at room temperature for 30 min. 100 µL of Caspase-Glo 3/7 reagent was added to 100 µL of cells/well and was incubated in a dark-chamber. The luminescence signal was quantified (Chameleon Multi-label Detection Platform) at one hour after treatment. Magnitude of fold change in luminescence between treated and untreated cells were determined using the following formula:

$$Fold\ increase = \frac{F_{test} - F_{blank}}{F_{control} - F_{blank}}$$

2.6. Intracellular Redox Potential Test

To evaluate the redox potential of 5a, a comparative test, using H_2O_2 and standard drug against untreated cells, was performed using H2DCFDA (Catalog no.# D399 Life Technologies, Eugene, OR, USA). The U87 and LN229 cells were grown overnight in a 96-well plate and were treated with an IC_{50} of 5a for 5 h at 37 °C in a humidified incubator supplemented with 5% CO_2. Negative control, positive control and blank were maintained. Baseline effect due to solvent was determined as well. After 5 h of treatment, cells were harvested by centrifugation at 3000 rpm for 10 min and incubated with 200 µL of 2 µM H2DCFDA for 30 min at 37 °C in the CO_2 incubator. Cells were then washed with pre-warmed PBS and resuspended in 200 µL of pre-warmed medium. Next, 100 µL of suspension was transferred to each well, in a 96-well plate and incubated at room temperature for 20 min. Finally, fluorescence signal was measured using Chameleon Multi-label Detection Platform (Excitation 485 nm, Emission 535 nm).

2.7. RNA Isolation and Gene Expression Evaluation

Cell were incubated with IC_{50} of test compound and standard drug Cisplatin for 48 h at 37 °C in a humidified incubator supplemented with 5% $CO_{2.}$ A negative control was maintained as well. All conditions were conducted in triplicated samples for the isolation of RNA. Total RNA of >9.25 ng/µL was isolated using GeneJET RNA purification kit (Catalog no #K0731), according to the manufacturer's instructions. The yield was then measured spectrophotometrically using NanoDrop-1000 (Thermoscientific, Wilmington, NC, USA). After quantification, the cells were considered for quality assessment by TapeStation. The gene expression analysis was performed by using Illumina Next Seq High throughput profiling (Illumina NextSeq 500). The sequencing produced data in bcl format which was converted into FASTQ file format.

2.8. Transcriptome Analysis

Differential expression (DE) and statistical analysis were performed using DESeq2 [18] (release 3.3) in R (version 3.2.4) (https://bioconductor.org/packages/release/bioc/vignettes/DESeq2/inst/doc/DESeq2.html). *p*-values were adjusted for multiple testing using the Benjamini-Hochberg procedure [19]. A false discovery rate adjusted *p*-value (i.e., *q*-value) < 0.05 was set for the selection of DE genes.

2.9. Phosphorylation of MAPKs and Other Serine/Threonine Kinases

The U87 cells were treated with an IC_{50} concentration of **5a** and DMSO, maintained in CO_2 humidified temperature for 48 h. The total protein was extracted using RnD protein extraction kit for the immunoblotting experiment. The phosphorylation of three families of mitogen-activated protein kinases (*MAPKs*), including the extracellular signal-regulated kinases (*ERK1/2*), c-Jun N-terminal kinases (*JNK1-3*), and different p38 isoforms, was analyzed following the manufacturer protocol, RnD Human Phospho-MAPK array kit. In detail, cell lysates are mixed with a cocktail of biotinylated detection antibodies and incubated with Proteome Profiler Human Phospho-MAPK Array. Streptavidin-HRP and chemiluminescent detection reagents are added and the signals that are produced at each spot correspond to the amount of phosphorylated protein bound. The captured and control antibodies have been spotted in duplicate on nitrocellulose membranes. The signals are measured using ChemiPro Luminescence detection system. The relative level of phosphorylation was analysed for 26 *MAPK* proteins as described in the manufacturer's protocol.

2.10. Gene Ontology (GO) and Pathway Analysis

Gene ontology [20] and ClusterProfiler package [21] was used for pathway analyses. We performed with the over-representation test for the GO biological process and KEGG pathways [22]. The package supports the human genome. We used the binomial test and Bonferroni correction for multiple testing and displayed z-scores to indicate whether a potential regulator was activated or inhibited. We used the default settings for statistical analysis in both the KEGG pathways and GO terms. In this analysis, pathways and GO terms only with a p-value < 0.05 were included.

2.11. Evaluation of Structure-Activity Relationship

In order to make a comparative study on the binding of **5a** with different receptors, sequences and structures of six receptors taken from Protein Data Bank (PDB)—Fibroblast Growth Factor receptor (*FGFR*, PDB ID: 2FDB), Epidermal growth Factor Receptor (*EGFR*, PDB ID: 4UIP), Platelet-Derived Growth Factor Receptor (*PDGFR*, PDB ID: 1PDG), *c-MET* Receptor (PDB ID: 3DKC), c-KIT Receptors (PDB ID: 6GQK) and Vascular Endothelial Growth Factor receptors (PDB ID: 3V2A) were obtained from the Protein Data bank. To study the binding efficiency and to identify the important amino acid residues contribute to the binding, Patchdock molecular docking program was used. The default parameters were used for the molecular docking in this study. Patchdock carries out rigid docking, with surface variability implicitly addressed through liberal intermolecular penetration.

2.12. Statistical Analysis

All experiments described in the present study were performed as with three biological and technical repeats. The data were presented as the mean ± standard error of mean. Statistical analyses between two groups were performed by Student's t-test. Differences among multiple groups were tested by one-way analysis of variance following by a Dunnett's multiple comparison test (GraphPad Prism 7.04, San Diego, CA, USA). $p < 0.05$ was considered to indicate a statistically significant difference.

3. Results

3.1. Synthesis of Orthothioesters

The orthothioesters **1-4** were synthesized through autoxidative condensation of 2-aryl-2-lithium-1,3-dithianes, prepared in situ from treatment of 2-aryl-1,3-dithianes with *n*-BuLi followed by air exposure. The presence of bromide when preparing **1c** demanded for replacement of *n*-BuLi by lithium diisopropylamide (LDA) in order to avoid transmetalation. The compounds were obtained in reasonable yields and pure after quenching with NH_4Cl saturated aqueous solution, usual work-up and purification by silica chromatography. The silyl ether group in compound **3b** was cleaved by treatment with 1 equivalent of NH_4F to yield phenol **5a**. Derivatization of **5a** with *m*-nitrobenzoyl chloride delivered carboxylic ester **5b** in excellent yield. Purity evaluation results of the novel compounds are given in the Supplementary file 1.

3.2. *5a Inhibited Proliferation of Glioma Cells*

The cytotoxicity of the orthothioesters **1-5** against the growth of U87 GB cell line was performed with 100 μM concentration of the compounds as described in the method section. Upon evaluation of the 12 compounds depicted in Scheme 1, **5a** was identified to be the most cytotoxic compound inducing 90% cell death and **5b** was the least cytotoxic with 0% cell death. This was a 20-fold higher activity compared to the standard drug cisplatin and 31.8-fold compared to the negative control (Figure 1a) The analysis of cytotoxic data of all compounds tested shows that while the presence of halogens or nitrile in the 4-position of the aromatic rings is detrimental for cytotoxicity (as for compounds **1b**–**d**), having a methoxy group in the 3-position has an opposite effect. Compounds **2c**, **3a** and **5a**, decorated with a 3-methoxy substituent in the aromatic rings, showed cytotoxicity similar to or higher than **1a**. Compounds **3b** and **5b** on the other hand, also decorated with the same 3-methoxy substituent but having bulky substituents in the vicinal 4-position, have residual or absent cytotoxicity. No improvement on cytotoxicity was observed when replacing the aryl groups by heteroaryl such as pyridyl in **4a**. The cytotoxicity on normal brain cells, MEF, was also performed for the top compound **5a** (Figure 1b) and cisplatin at a concentration of 10 μM. The results show that **5a** have 11% of growth inhibition, whereas cisplatin have 48% of inhibition, suggesting that **5a** is more toxic to the cancer cells than the normal cells (Figure 1c).

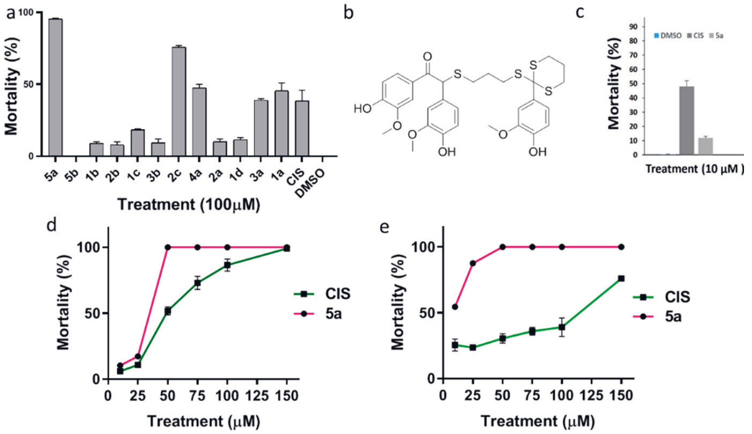

Figure 1. In vitro screening and evaluation of dose response of thioester compounds (**a**). The percentage of mortality rate on treating U87 cells with novel panel of 12 thioester derivatives along with CIS (positive control) 1% DMSO (negative control), at a 100 μM concentration (**b**). Chemical structure of the investigative drug **5a**. (**c**) Cytotoxicity analysis of non-cancerous brain cells, MEF and cisplatin at 10 μM concentration. (**d**) Dose response curve of U87 cells (left) and (**e**) LN229 (right) cells treated with the top compound (**5a**), CIS and 1% DMSO was analyzed to determine IC_{50} value. Treatment was carried out at 48h and cellular viability was measured by Trypan Blue exclusion method. Data points and error bars represent mean ± standard error of the mean (SEM) (n = 6 per group). Significant when $p < 0.05$, one-way ANOVA.

In order to investigate the in vitro anticancer activity of **5a** and to determine its IC_{50} value, we evaluated cytotoxicity against cell lines, U87 and LN229 in the presence of increasing concentrations of this compound for 24 h, ranging from 0 μM–150 μM. The viability of cells was determined according to cell counting based on Trypan Blue assay and the IC_{50} value of **5a** was determined as 27 μM in U87 cells and 23 µM in LN229 cells (Figure 1d,e). The IC_{50} value of cisplatin was identified as 53 µM in U87 cells and 115 µM in LN229.

3.3. *5a Induced Negligible Oxidative Stress and Promoted Caspase Activation*

Reactive oxygen species (ROS) mediated caspase activation of tumor cells during stress and subsequent cell death has been repeatedly reported by various studies [23,24]. In the present study, both intracellular ROS and caspase in U87 cells were quantified to verify oxidative stress and cellular response upon **5a** treatment. After exposure of U87 cells to **5a** at IC_{50} for 5 h, we detected an oxidative increase of 3.3% increase in the **5a** treated cells when compared to untreated cells. The standard drug cisplatin and positive control H_2O_2 on the other hand, marked a 4.2% and 2.2% increase in oxidative response respectively (Figure 2a). Similarly, exposure of LN229 cells to **5a** at IC_{50} for 5 h demonstrated negligible change in the treated cells when compared to untreated cells (Figure 2a). The difference between treated and untreated conditions was confirmed to be statistically insignificant per ANOVA test (*p*-value <0.05), establishing that the **5a** does not increase ROS in the tested GB cells.

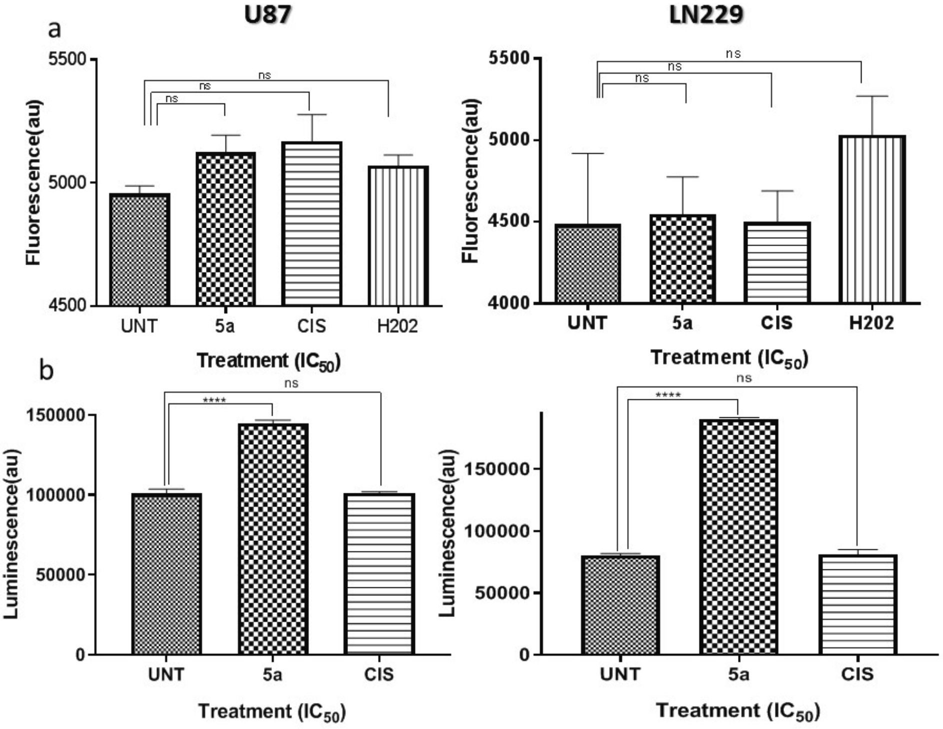

Figure 2. Comparative evaluation of oxidative stress response and caspase activation by the **5a** in two different cell lines (**a**) Effect of **5a** on intracellular reactive oxygen species (ROS) production by GB cells as interpreted by fluorescence level. Evaluation suggested no significant increase in ROS level upon drug treatment ($\alpha = 0.05$). (**b**) Caspase activity displayed by GB cells analyzed using caspase 3/7 luminescence assay. Significant increase in caspase activity of cells was observed after treatment with IC_{50} of **5a** for 5h compared to control. The values are expressed as means ± standard error of the mean (SEM) of triplicate measurements of biological repeats (n = 3). Significance: **** $p < 0.0001$.

Considering the role of Caspase activation, we determined the caspase activity of U87 cells using caspase3/7 assay after a treatment period of 5 h with **5a** at IC_{50}. Interestingly, U87 **5a**-treated cells displayed an increase of caspase 3/7, displaying a 0.43-fold increase in comparison to untreated cancer cells, whereas positive control displayed no significant increase (0.003) in caspase activity (Figure 2b). Similarly, in LN229 cells **5a**-treated cells demonstrated 1.37-fold increase with respect to untreated cells, whereas the standard drug cisplatin exhibited 0.05 fold increase in caspase levels. The difference between treated and untreated conditions was confirmed to be statistically significant per ANOVA test (p-value < 0.05).

*3.4. **5a** Enhanced Apoptosis and Cell Cycle Arrest*

Defective apoptotic machinery enhances tumor pathogenesis by permitting survival of genetically unstable cells leading to treatment resistance. To understand if the decrease in viability was due to apoptosis, we treated U87 cells with IC_{50} of 5a and we determined the apoptosis effect using double staining method.

The results revealed that **5a** was much effective in inducing apoptosis exhibiting a 3.75-fold increase in programmed cell death, whereas the standard drug cisplatin induced a 1.7-fold increase when compared to untreated cells (Figure 3a,b). To explore in detail the effect of 5a transcriptomics, data analysis was carried out, and we identified 1148 differentially expressed genes (DEGs) when **5a** is compared with untreated (negative control) samples (q-value < 0.05). We also compared the **5a** and cisplatin samples as a positive control group, both individually and combined as a single "affected" group. In these comparisons, 3132 DEGs were identified, with the largest number of DEGs identified in comparison with the cisplatin samples. In total, 595 out of 4280 DEGs were common in both comparisons. The complete lists of DEGs from the cell line analysis and all pairs of comparisons are provided in Supplementary file 2. Gene expression analysis indicated that **5a** has a multidimensional impact on various tumorogenic features, especially on tyrosine kinase signaling (Figures 4 and 5a) and was effective in increasing expression of agonists of cell death such as *DKK1*, *ADM*, *HMGA2*, and *CAV1*. In addition, downregulation of chemoprotective factors such as *HMOX1*, *HSPs*, and *CYP1B1* were detected. Adding to its cytotoxic effects, **5a** was also found to suppress mitochondrial membrane stability as evident by dysregulated levels of *HSPA1A* and *BNIP3*.

Gene expression analysis also points out that treatment of U87 cells with **5a** leads to inhibition of G1/S transition leading to cell cycle arrest. Upregulation of cell cycle inhibitory genes involved in G1/S such as *DACT1*, *SUSD2*, and *CTDSP1* signifies the efficiency of the drug as a cell cycle inhibitor (Figure 5c). Additionally, genes favoring G1/S transition such as *PLRG1* and *ADAM17* were effectively downregulated due to **5a** treatment. The cell cycle interruption is further strengthened by suppression of *CCND3* affecting the *CDK4* activity associated with this cyclin, which is necessary for cell cycle progression. Several studies have proposed that agents that interfere with DNA repair can act as a therapeutic strategy targeting double-strand break repair pathways or abrogate cell cycle checkpoints. *HMGA2* gene involved in negative regulation of double-strand break repair via non-homologous end joining was found to be risen upon the treatment with **5a** demonstrating its genotoxicity leading to the apoptotic death of cancer cells. Additionally, notable chemo-sensitizing was visible in treated cells as evident from transcriptome levels of *HSPA1*, *CLU*, and *TXN* (Table 1).

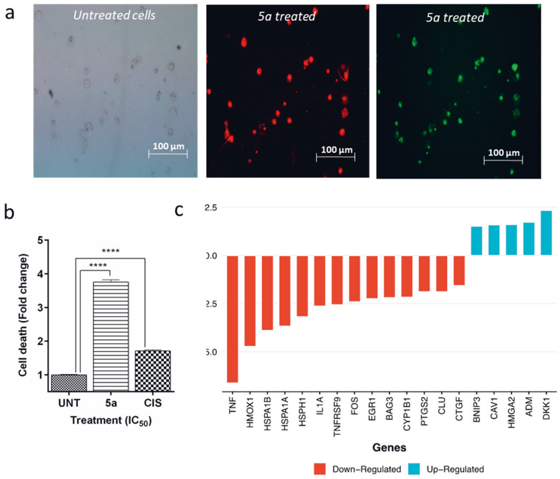

Figure 3. Evaluation of apoptotic activity induced by **5a**. (**a**). Phase contrast image of non-apoptotic cells in untreated condition (left); fluorescence image of U87 cells exhibited upon PI (middle) and Annexin V (right) staining. **5a** was found to effectively induce apoptotic cell death when compared to untreated cells. (**b**) The histogram represents quantification of apoptosis after treating the cell lines with IC_{50} of **5a**, for 48 h, in U87 cell line. Cisplatin was used as a positive control and untreated cells as negative control. The fold change of apoptosis has been calculated against untreated U87 cells. The values are expressed as means ± standard error of the mean (SEM) of triplicate measurements of biological repeats (n = 3). **** $p < 0.0001$ as produced by ANOVA test. (**c**) Key genes involved in Apoptotic process and their log2(fold-change), that are differentially expressed upon R114 treatment, compared to untreated. log 2(fold-change) cutoff = 1.5.

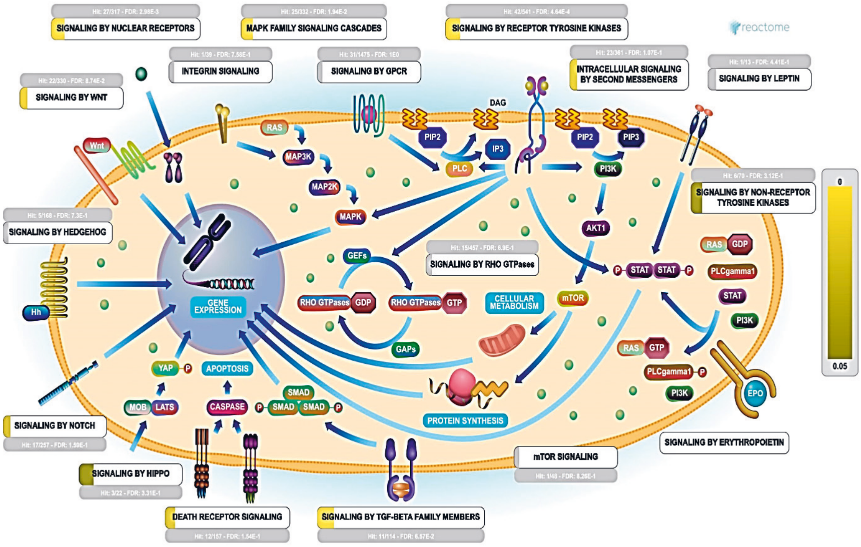
Hit: 27/317 - FDR: 2.98E-3
SIGNALING BY NUCLEAR RECEPTORS
Hit: 25/332 - FDR: 1.94E-2
MAPK FAMILY SIGNALING CASCADES
Hit: 42/541 - FDR: 4.64E-4
SIGNALING BY RECEPTOR TYROSINE KINASES
reactome
Hit: 1/39 - FDR: 7.58E-1
INTEGRIN SIGNALING
Hit: 31/1475 - FDR: 1E0
SIGNALING BY GPCR
Hit: 23/361 - FDR: 1.07E-1
INTRACELLULAR SIGNALING BY SECOND MESSENGERS
Hit: 1/13 - FDR: 4.41E-1
SIGNALING BY LEPTIN
Hit: 22/330 - FDR: 8.74E-2
SIGNALING BY WNT
DAG
RAS
PIP2
IP3
PIP2
PIP3
Wnt
MAP3K
PLC
PI3K
MAP2K
Hit: 6/70 - FDR: 3.12E-1
SIGNALING BY NON-RECEPTOR TYROSINE KINASES
0
MAPK
AKT1
Hit: 5/168 - FDR: 7.3E-1
SIGNALING BY HEDGEHOG
Hit: 15/457 - FDR: 6.9E-1
SIGNALING BY RHO GTPases
RAS
GDP
GEFs
P
STAT
STAT
P
PLCgamma1
STAT
Hh
GENE EXPRESSION
RHO GTPases
GDP
RHO GTPases
GTP
CELLULAR METABOLISM
mTOR
PI3K
GAPs
RAS
GTP
YAP
P
APOPTOSIS
PLCgamma1
P
0.05
SMAD
PI3K
EPO
MOB
LATS
CASPASE
P
SMAD
SMAD
P
PROTEIN SYNTHESIS
SIGNALING BY NOTCH
Hit: 17/257 - FDR: 1.59E-1
SIGNALING BY ERYTHROPOIETIN
mTOR SIGNALING
Hit: 1/48 - FDR: 8.26E-1
SIGNALING BY HIPPO
Hit: 3/22 - FDR: 3.31E-1
DEATH RECEPTOR SIGNALING
Hit: 12/157 - FDR: 1.54E-1
SIGNALING BY TGF-BETA FAMILY MEMBERS
Hit: 11/114 - FDR: 6.57E-2

Figure 4. Representation of DEGs in major signal transduction pathways, in **5a** treated cells. The color code denotes over-representation of that pathway by DEGs. FDR represents the corrected over-representation probability. Color scale denotes the proportion of entities identified among the total entities enriched in a pathway (Image generated via the reactome pathway analysis tool; https://reactome.org/PathwayBrowser/).

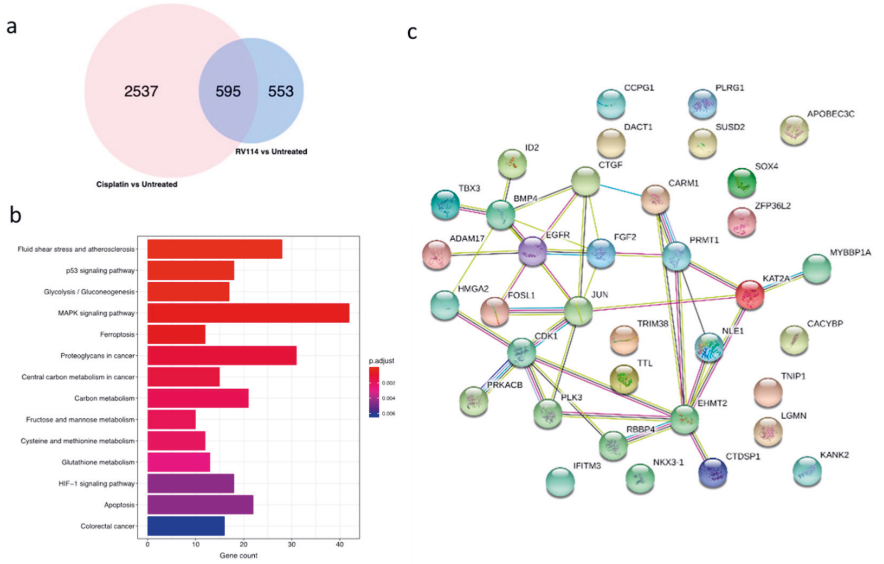

Figure 5. Transcriptional profile of **5a** compared to standard drug (**a**) Venn diagram showing 595 genes commonly differentially expressed in both treatments versus control, as assessed by RNA-seq data analysis of U87 cell line. (**b**) Visual representation of top 14 pathways associated with differentially expressed genes upon **5a** treatment with reference to control. (**c**) Gene interaction network of cell cycle genes affected upon **5a** treatment.

Table 1. Key genes affected by the top drug-like compound.

Key Genes Dysregulated in Major Pathways						
Signalling Pathways	**MAPK**	**TNF**	**PI3K-Akt**	**STAT**	**ErbB**	**NF-kB**
	AREG CASP3 CRK	CASP3 FOS IL15	AREG CCND3 CDKN1A	CCND3 CDKN1A IL15	AREG CDKN1A CRK	BCL10 IL1R1 PTGS2
Downregulated genes	FGF2 FOS	IL18R1 JUN	FGF2 MCL1	MCL1 STAT1	HBEGF JUN	RIPK1 TNF
	IL1A IL1R1 JUN LAMTOR3 PGF TNF	JUNB PTGS2 RIPK1 TNF	PGF SGK1 THBS1			
Upregulated genes	DUSP6 EGFR EPHA2 MET MYC PDGFA PDGFB RPS6KA5 STMN1 TGFA VEGFA BMP4 RASA3	JAG1 LIF RPS6KA5	BCL2L1 EGFR EPHA2 F2R GNG4 IRS1 ITGA6 MET MYC PDGFA PDGFB TGFA VEGFA	BCL2L1 EGFR LIF MYC PDGFA PDGFB PTPN2	EGFR MYC TGFA	BCL2L1

3.5. **5a** *Is an Anti-Angiogenic Agent*

To gain more insight on anti-angiogenic efficacy of **5a**, we analyzed the modulation of genes in U87 glioma cells treated with the investigative drug. **5a** was found to adversely affect the cytokine receptor pathway exerting its effect through interaction of multiple pathways, eventually downregulating *VEGF* expression. *VEGFD* itself exhibited a $\log_2$ (fold change) of −4.5. Other key genes (*TNF*, *HMOX*, *IL1A*, *CYP1B1*, and *PTGS1*) involved in positive regulation of *VEGF* were identified to be downregulated by more than 1.75-fold. Key genes involved in inhibition of angiogenesis, including *NR2F1*, *SEM3A*, *ERRFI1*, *SPRY1*, *ADM*, *NRP1*, etc., were found to be upregulated ($\log_2$ (fold change) > 1.5). Moreover, enhancers of migration and angiogenesis such as *GPNMB*, *PTGS2*, *CD274*, and *ZNF703* were significantly downregulated suggesting suppression of tumor malignancy (Table 1 and Supplementary file 2).

5a advocates inhibition of angiogenesis targeting VEGF pathway, via multiple pro-angiogenic regulators. The mRNA levels of *VEGF* were markedly decreased in the U87 cells treated with the IC_{50} concentrations of **5a**. Moreover, other angiogenic enhancers such as *HMOX1*, *IL1A*, *CYP1B1* *PGF*, and *FGF* were effectively suppressed by **5a**. Additionally, such a molecule potentially weakened angiogenesis by affecting pathways involved in the crosstalk by interrupting key regulators involved. The phosphorylation of multiple kinase proteins involved in the VEGF signaling pathway were quantified using immunoblotting. The upregulation of *CREB*, *GSK-3α/β*, *GSK-3β*, *MSK2*, *p38α*, *p38γ*, and *p53* and down regulation of *JNK1* validates that the VEGF pathway might be targeted by **5a** (Figure 6a–c).

3.6. **5a** *Restricts MAPK Signaling Cascade and Downregulates TNF Expression*

Activation of the MAPK pathway leads to the transcription of genes that encode proteins involved in the regulation of essential cellular functions, such as cell growth, cell proliferation, and cell differentiation [25]. U87 glioma cells treated with IC_{50} concentrations of **5a** exhibited downregulation of positive regulators of MAPK pathway such as *GADDs*, *RIPK*, *CTNNB1* and *PSAP*, whereas, it enhanced the expression of inhibitors of MAPK signaling such as *MYC*, *SPRY1*, *EZR*, *RASA3* and *CAV1*. Additionally, **5a** reduced the expression of activators of ERK cascade (*TNF*, *CTGF*, *FGF*, *JUN*) and enhanced its negative modulators such as *C1QL4* and *TNIP1* (Figure 5b, Table 1 and Supplementary file 2). *TNF* exerts its biological functions by activating distinct signaling pathways such as nuclear factor κB (*NF-κB*) and c-Jun N-terminal kinase (*JNK*). We observed a significant reduction of TNF levels in 5a treated cells compared to untreated cells. Inhibitors of TNF production like *ERRIF1*, *RARA*, *VSIR* and *AXL* were found to be overexpressed explaining the reduction in TNF level. Additionally, immunoblotting revealed the phosphorylation of *CREB*, *p38*, *JNK* proteins involved in MAPK/TNF signaling pathway. The relative higher-level expression of *CREB*, *p38* and reduced expression of *JNK* protein, also validates the inhibition of MAPK signaling cascade by **5a** in U87 cells (Figure 6a–c).

3.7. **5a** *Negatively Affects JAK-STAT Pathway*

The direct and mediated mechanisms of JAK-STAT signaling in tumor cell survival, proliferation, and invasion have made the JAK-STAT pathway a feasible target for drug development and cancer therapy. Interactions of JAK/STAT pathway with the RTK/Ras/MAPK pathway, TGF- β signaling pathway and PI3K pathway amplifies the effect mediated through the regulation of JAK-STAT signaling [26]. The current study revealed that **5a** is a strong suppressor of JAK-STAT pathway causing notable downregulation of major and downstream genes such as *STAT1*, *MCL1*, *CCND3*, *CDKN1A*, and *IL15* (Table 1 and Supplementary file 2). Upregulation of *PTPN2*, an inhibitor of *JAK* expression was observed, which is also a contributor of endoplasmic reticulum stress-induced intrinsic apoptotic signaling pathway. Additionally, upregulation of *CAV1* and *HMGA* was identified explaining the downregulation of JAK-STAT pathway. Phosphorylation analysis of multiple kinases shows the upregulation of *CREB* and *p38* proteins, suggesting a role of **5a** in inhibiting JAK-STAT signaling pathway (Figure 6a–c).

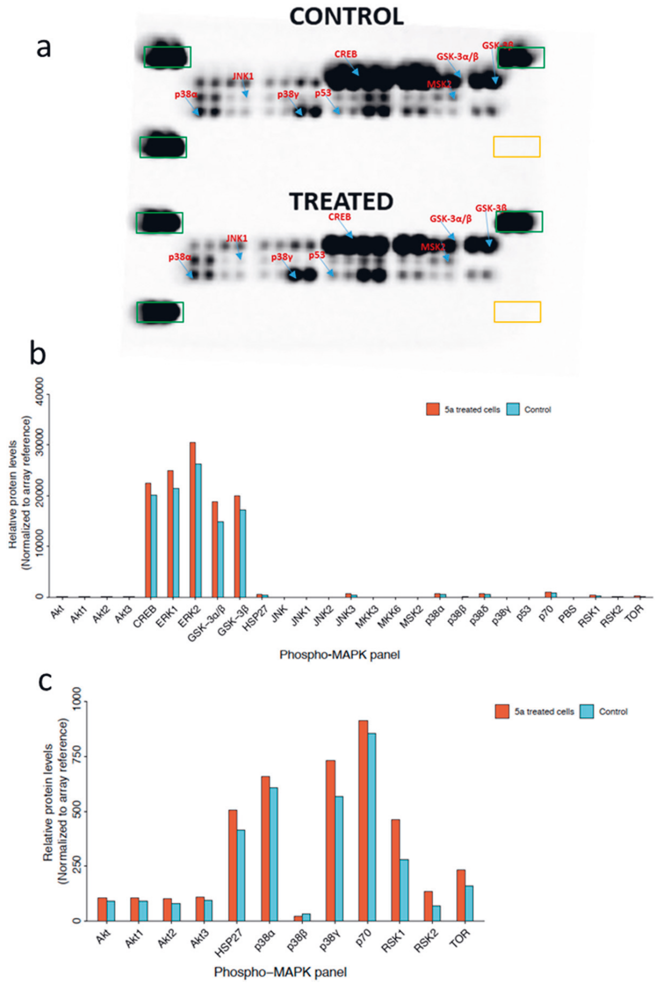

Figure 6. Analysis of phosphor–MAPK array. (**a**) The array images are shown for both DMSO control and **5a** treated cells and the eight phosphorylated proteins are marked in blue arrow. Positive reference spots are represented in green box and the negative reference spot (PBS) is represented in yellow box. (**b**) The complete set of *MAPKs* was presented according to the relative level of intensity of phosphorylation. (**c**) Absolute values of integrated pixel intensity of a few kinases are displayed for better resolution.

Several cross-family interactions among tyrosine kinases may significantly alter angiogenic signaling, leading to anti-angiogenic drug resistance. Reports say *FGF*-driven angiogenesis is blocked by *VEGF* inhibition, which suggests that *FGF* controls angiogenesis upstream of *VEGF* by modulating *VEGF* function [27]. Additionally, in the case of glioma tumorigenesis, *PDGF*- expression is assumed to contribute to the expansion of an established tumor as well as the regulation of the angiogenic switch for initial tumor development [28]. Studies also testify that there are cross family interactions between *VEGF* and *PDGFR* [29]. In addition, *cKIT* and *MET* are another two important *RTKs* to be explored as angiogenic drivers [30]. c-KIT signaling promotes cell proliferation and survival, exerting its effect through Ras-Erk pathway as well as JAK/STAT pathway [31]. Chen et al. asserted that intracrine *VEGF* function can be regulated by MET signaling and plays a significant role in controlling *VEGFR2* [32].

In this context, we sought to explore interactions between promising orthothioester 5a and six different tyrosine kinase receptors-*FGFR*, *EGFR*, *PDGFR*, *c-MET*, *cKIT*, and *VEGFR-2*, by in silico docking study. The results show that the Epidermal growth Factor Receptor shows good binding efficiency with thioester with high docking score (7256) (Figure 7a). The two-dimensional ligand interaction diagram of thioester with *EGFR* is shown in Figure 7b. Conclusively, our study evidences a multidimensional anti-tumor effect of the novel thioester drug **5a**.

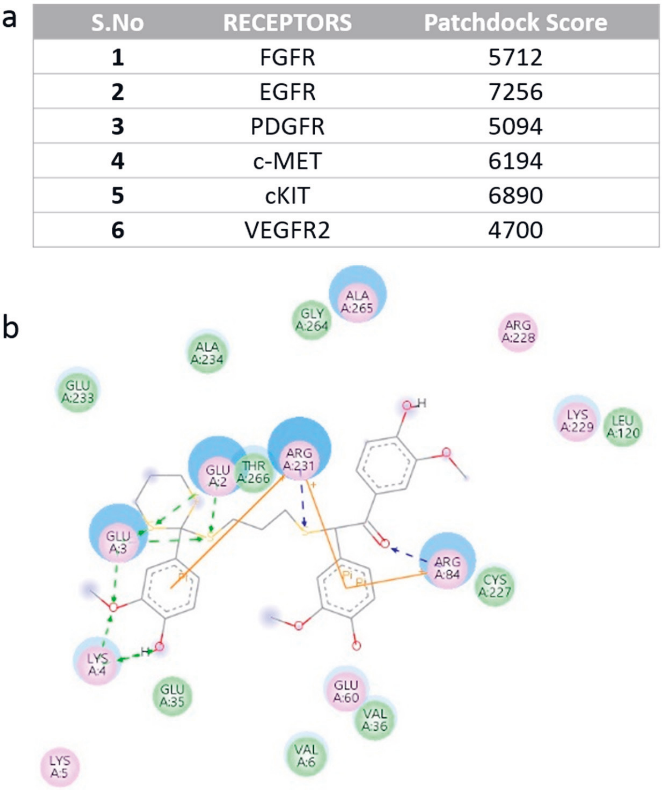

a

S.No	RECEPTORS	Patchdock Score
1	FGFR	5712
2	EGFR	7256
3	PDGFR	5094
4	c-MET	6194
5	cKIT	6890
6	VEGFR2	4700

Figure 7. Docking score of **5a** with various kinase receptors (**a**) Docking analysis of various cytokine receptors (Fibroblast Growth Factor receptor—*FGFR*, PDB ID: 2FDB, Epidermal growth Factor Receptor—*EGFR*, PDB ID: 4UIP, Platelet-Derived Growth Factor Receptor—*PDGFR*, PDB ID: 1PDG, c-MET Receptor, PDB ID: 3DKC, *c-KIT* Receptor- PDB ID: 6GQK, and Vascular Endothelial Growth Factor receptors PDB ID: 3V2A) with **5a**. Docking study was carried out using the Patchdock program. (**b**) 2-dimensional interaction diagram of EGFR with ligand.

*3.8. **5a** Induced Phosphorylation of MAPKs and Other Serine/Threonine Kinases*

The effect of **5a** on the phosphorylation levels of three families of *MAPKs*, such as *ERK1/2*, *JNK1–3* and different p38 isoforms, was analyzed. The arrays used in the experiments are based on the analysis of kinase specific antibodies which are spotted in duplicates along with three reference spots and PBS as negative spots. The mixture of biotinylated anti-phospho-kinase antibodies and streptavidin-HRP conjugate differentiates the phosphorylated and non-phosphorylated protein between the control and **5a** treated cells. The luminescence induced by the addition of chemiluminescence reagent was captured using the ChemiPro detection system (Figure 6a). In detail, the relative levels of phosphorylation of 26 kinases such as *Akt1*, *Akt2*, *Akt3*, *Akt*, *CREB*, *ERK1*, *ERK2*, *GSK-3α/β*, *GSK-3β*, *HSP27*, *JNK1*, *JNK2*, *JNK3*, *JNK*, *MKK3*, *MKK6*, *MSK2*, *p38α*, *p38β*, *p38δ*, *p38γ*, *p53*, *p70*, *RSK1*, *RSK2*, and *TOR* (Figure 7b) were analyzed. The phosphorylation level of *CREB* (Ser^{133}), *GSK-3α/β* (Ser^{21}/Ser^{9}), *GSK-3β* (Ser^{9}), *MSK2* (Ser^{360}), *p38α* (Thr^{180}/Tyr^{182}), *p38γ* (Thr^{183}/Tyr^{185}) and *p53* (Ser^{46}) were significantly increased in 5a treated U87 cells, whereas the phosphorylation level for *JNK1* (Thr^{183}/Tyr^{185}) was found to be reduced relative to the control (Figure 6c). The results suggest that the EGFR signaling pathway was suppressed by **5a**, which is confirmed by the phosphorylation of not only the *MAPKs* and other serine threonine kinases. Thus, the **5a** suppression of *EGFR* further substantiates that 5a as TK inhibitor.

4. Discussion

In order to challenge tumor recurrence and resistance of GB, agents that can synergistically confront multiple oncogenic pathways are gaining great importance in GB drug discovery. In a pursuit to identify a multi-targeted chemo-agent against glioblastoma, we assessed bioactivity of a panel of new orthothioester derivatives as anti-GB agents in vitro.

Cytotoxicity evaluation identified an orthothioester **5a**, which has inhibited tumor cell growth in a dose-dependent manner in GB cell lines. In addition, it displayed a more effective anti-tumor activity than current standard drug cisplatin in both GB cell lines U87 and LN229. Gene expression profiling revealed that this effect is due to the suppression of multiple kinase signaling pathways regulating *VEGF* levels in GB cells suggesting the possible anti-angiogenic effect. Additionally, inhibition of *HMOX1* abrogates VEGF-induced endothelial activation and subsequent angiogenesis [33]. A robust silencing of *HMOX1* observed in our study convinces curbing of VEGF-induced pathogenic angiogenesis.

Virtual binding studies using bioinformatics tools suggests *EGFR* as a key target of **5a**, exerting its effect through multiple pathways leading to the inhibition of angiogenesis, cell cycle arrest, and apoptosis. Considering previous reports that *EGFR* can activate β-catenin via receptor tyrosine kinase-PI3K/Akt pathway [34], inhibitory ligand binding on *EGFR* is expected to diminish WNT signaling. Our observation of weakened expression of *CTNNB1* and other positive regulators of WNT pathway (*DAB2*, *GSKIP*) corresponds to this notion.

The candidate drug **5a** seems to be an attractive anti-angiogenic agent acting beyond VEGF/VEGFR pathway. Notable downregulation of growth factors (*VEGFD*, *FGF2*, *PGF*, *TNF-α*) and *cytokine IL-1A* was observed in tumor cells upon treatment with 5a. FGF can act synergistically with *VEGF* to amplify tumor angiogenesis and are implicated in the emerging phenomenon of resistance to VEGF inhibition. FGFs have been reported to have potent proangiogenic effects through the stimulation and release of other proangiogenic factors [35]. **5a** was found to effectively reduce *FGF* levels, causing a synergistic anti-angiogenic effect as well as increased sensitization to *VEGF* suppression. Additionally, potent inhibition of *TNF-α* by **5a** may also contribute to its anti-angiogenic impact. Though *TNF* is widely promoted as a antineoplastic agent, its dual role as a angiogenesis promoter and inhibitor has been discussed in multiple reports [36–38]. A study by Giraudo et al. discussed the *VEGF* mediated role of *TNF-α* in the initiation and maintenance of angiogenesis and increased vascular permeability [39]. Furthermore, the investigative drug also effectively induced chemo-sensitization by suppressing stress proteins such as *HSPs, CLU, SNAI1, PTGS2,* and *MCL1.* Taken together, we postulate **5a** as a multi-targeted agent against GB signaling pathway and highlighting its significance as anti-tumor agent. Additionally, **5a** exerts its cytostatic effect via key genes involved in regulation of cell cycle pathways as observed in our experimental results. The present research thus suggests **5a** as a candidate GB chemotherapeutic with multiple anti-cancer properties.

5. Conclusions

Drugs that can act as multi-targeted agents can enhance efficacy and confront chemoresistance exhibited by GB cells. Thioesters has been investigated as an antitumor agent in multiple studies [40,41]. The present study validates potential of a novel orthothioester **5a**, as an excellent pharmacological scaffold possessing strong cytotoxic, anti-angiogenic, and chemo-sensitization activity. The compound **5a** exerted extensive killing effects on two different glioma cell lines by effectively weakening resistance pathways and enhancing apoptotic machinery. Additionally, **5a** is a strong cytostatic agent acting on key genes involved in regulation of cell cycle pathways. In particular, the capability of **5a** to impede various pathogenic signaling cascades leading to GB pathogenesis, by acting on multiple tyrosine kinase pathways, makes it an appealing anti-GB agent. Taken together, our report provides new insights on how underexplored thioester derivatives can act as a potent pharmacological scaffold against glioblastoma.

Supplementary Materials: The following are available online at http://www.mdpi.com/2073-4409/8/12/1624/s1: NMR spectroscopy results of previously unreported compounds are attached as Supplementary file 1. List of differentially expressed genes and pathway analysis are attached as Supplementary file 2.

Author Contributions: J.R.V., C.A.M.A., and N.R.C. synthesized and characterized the compounds and A.V. executed the experiments and data analysis. S.K.M. executed docking studies. A.M (Akshaya Murugesan) executed protein studies. A.M. (Aliyu Musa) analyzed RNA-seq data. O.Y.-H. and M.K. conceived and managed all studies. All the authors contributed to writing the manuscript.

Funding: M.K., A.V., and O.Y.H. acknowledge the Academy of Finland for the project grant support (decision no. 297200) and Tampere University of Technology for Instrumental facility grant support. N.R.C. acknowledges the Academy of Finland (decision no. 287954) for the financial support. FCT is acknowledged for financial support to J.R.V., (SFRH/BD/120119/2016)

Acknowledgments: We thank Rahul Mangayil and Ville Santala for providing the access to Fluorescence Plate reader instrumental facility at Tampere University.

Conflicts of Interest: The authors declare that they have no conflicting interests.

Abbreviations

GB	Glioblastoma
TKI	Tyrosine Kinase Inhibitor
RTK	Receptor Tyrosine Kinases
ROS	Reactive Oxygen Species
GO	Gene Ontology
TLC	Thin-Layer Chromatography
DCM	Dichloromethane
TCF	Tetrahydrofuran
DE	Differential expression
DEG	Differentially expressed gene

References

1. Ferrara, N.; Gerber, H.P.; LeCouter, J. The biology of VEGF and its receptors. *Nat. Med.* **2003**, *9*, 669. [CrossRef]
2. Fuchs, C.S.; Tomasek, J.; Yong, C.J.; Dumitru, F.; Passalacqua, R.; Goswami, C.; Safran, H.; Dos Santos, L.V.; Aprile, G.; Ferry, D.R.; et al. Ramucirumab monotherapy for previously treated advanced gastric or gastro-oesophageal junction adenocarcinoma (REGARD): An international, randomised, multicentre, placebo-controlled, phase 3 trial. *Lancet* **2014**, *383*, 31–39. [CrossRef]
3. Ferrara, N.; Hillan, K.J.; Gerber, H.P.; Novotny, W. Discovery and development of bevacizumab, an anti-VEGF antibody for treating cancer. *Nat. Rev. Drug Discov.* **2004**, *3*, 391. [CrossRef] [PubMed]
4. Holash, J.; Davis, S.; Papadopoulos, N.; Croll, S.D.; Ho, L.; Russell, M.; Boland, P.; Leidich, R.; Hylton, D.; Burova, E.; et al. VEGF-Trap: A VEGF blocker with potent antitumor effects. *Proc. Natl. Acad. Sci. USA* **2002**, *99*, 11393–11398. [CrossRef] [PubMed]
5. Maire, C.L.; Ligon, K.L. Molecular pathologic diagnosis of epidermal growth factor receptor. *Neuro. Oncol.* **2014**, *16*, viii1–viii6. [CrossRef] [PubMed]
6. Mizoguchi, M.; Betensky, R.A.; Batchelor, T.T.; Bernay, D.C.; Louis, D.N.; Nutt, C.L. Activation of STAT3, MAPK, and AKT in malignant astrocytic gliomas: Correlation with EGFR status, tumor grade, and survival. *J. Neuropathol. Exp. Neurol.* **2006**, *556*, 1181–1188. [CrossRef] [PubMed]
7. Tabernero, J. The Role of VEGF and EGFR Inhibition: Implications for Combining Anti-VEGF and Anti-EGFR Agents. *Mol. Cancer Res.* **2007**, *5*, 203–220. [CrossRef]

8. Pennell, N.A.; Lynch, T.J. Combined Inhibition of the VEGFR and EGFR Signaling Pathways in the Treatment of NSCLC. *Oncologist* **2009**, *14*, 399–411. [CrossRef]
9. Mori, K.; Tani, M.; Kamata, K.; Kawamura, H.; Urata, Y.; Goto, S.; Kuwano, M.; Shibata, S.; Kondo, T. Mitogen-activated protein kinase, ERK1/2, is essential for the induction of vascular endothelial growth factor by ionizing radiation mediated by activator protein-1 in human glioblastoma cells. *Free Radic. Res.* **2000**, *33*, 157–166. [CrossRef]
10. Xie, T.; Wei, D.; Liu, M.; Gao, A.C.; Ali-Osman, F.; Sawaya, R.; Huang, S. Stat3 activation regulates the expression of matrix metalloproteinase-2 and tumor invasion and metastasis. *Oncogene* **2004**, *23*, 3550. [CrossRef]
11. Chen, Z.; Zhong, C.H. STAT3: A critical transcription activator in angiogenesis. *Med. Res. Rev.* **2008**, *28*, 185–200. [CrossRef] [PubMed]
12. Jiang, B.H.; Liu, L.Z. PI3K/PTEN signaling in tumorigenesis and angiogenesis. *Biochim. Biophys. Acta Proteins Proteomics* **2008**, *1784*, 150–158. [CrossRef] [PubMed]
13. Vale, J.R.; Rimpiläinen, T.; Sievänen, E.; Rissanen, K.; Afonso, C.A.M.; Candeias, N.R. Pot-economy autooxidative condensation of 2-Aryl-2-lithio-1,3-dithianes. *J. Org. Chem.* **2018**, *83*, 1948–1958. [CrossRef] [PubMed]
14. Sestito, S.; Runfola, M.; Tonelli, M.; Chiellini, G.; Rapposelli, S. New multitarget approaches in the war against glioblastoma: A mini-perspective. *Front. Pharmacol.* **2018**, *9*, 874. [CrossRef]
15. Doan, P.; Musa, A.; Candeias, N.R.; Emmert-Streib, F.; Yli-Harja, O.; Kandhavelu, M. Alkylaminophenol induces G1/S phase cell cycle arrest in glioblastoma cells through p53 and cyclin-dependent kinase signaling pathway. *Front. Pharmacol.* **2019**, *10*, 330. [CrossRef]
16. Chowdhury, S.; Kandhavelu, M.; Yli-Harja, O.; Ribeiro, A.S. An interacting multiple model filter-based autofocus strategy for confocal time-lapse microscopy. *J. Microsc.* **2012**, *245*, 265–275. [CrossRef]
17. Vaiyapuri, P.S.; Ali, A.A.; Mohammad, A.A.; Kandhavelu, J.; Kandhavelu, M. Time lapse microscopy observation of cellular structural changes and image analysis of drug treated cancer cells to characterize the cellular heterogeneity. *Environ. Toxicol.* **2015**, *30*, 724–734. [CrossRef]
18. Love, M.I.; Huber, W.; Anders, S. Moderated estimation of fold change and dispersion for RNA-seq data with DESeq2. *Genome Biol.* **2014**, *15*, 550. [CrossRef]
19. Benjamini, Y.; Hochberg, Y. Controlling the false discovery rate: A practical and powerful approach to multiple testing. *J. R. Stat. Soc. Ser. B* **1995**, *57*, 289–300. [CrossRef]
20. Ashburner, M.; Ball, C.A.; Blake, J.A.; Botstein, D.; Butler, H.; Cherry, J.M.; Davis, A.P.; Dolinski, K.; Dwight, S.S.; Eppig, J.T.; et al. Gene ontology: Tool for the unification of biology. *Nat. Genet.* **2000**, *25*, 25. [CrossRef]
21. Yu, G.; Wang, L.-G.; Han, Y.; He, Q.-Y. clusterProfiler: An R Package for Comparing Biological Themes Among Gene Clusters. *Omi. A J. Integr. Biol.* **2012**, *16*, 284–287. [CrossRef] [PubMed]
22. Ogata, H.; Goto, S.; Sato, K.; Fujibuchi, W.; Bono, H.; Kanehisa, M. KEGG: Kyoto encyclopedia of genes and genomes. *Nucleic Acids Res.* **1999**, *28*, 27–30. [CrossRef] [PubMed]
23. Izeradjene, K.; Douglas, L.; Tillman, D.M.; Delaney, A.B.; Houghton, J.A. Reactive oxygen species regulate caspase activation in tumor necrosis factor-related apoptosis-inducing ligand-resistant human colon carcinoma cell lines. *Cancer Res.* **2005**, *65*, 7436–7445. [CrossRef] [PubMed]
24. Chanvorachote, P.; Nimmannit, U.; Azad, N.; Wang, L.; Moungjaroen, J.; Lipipun, V.; Rojanasakul, Y.; Callery, P.S. Reactive Oxygen Species Mediate Caspase Activation and Apoptosis Induced by Lipoic Acid in Human Lung Epithelial Cancer Cells through Bcl-2 Down-Regulation. *J. Pharmacol. Exp. Ther.* **2006**, *319*, 1062–1069.
25. Kim, E.K.; Choi, E.J. Pathological roles of MAPK signaling pathways in human diseases. *Biochim. Biophys. Acta Mol. Basis Dis.* **2010**, *1802*, 396–405. [CrossRef]
26. Moustakas, A.; Ardley, H.C. Smad signalling network. *J. Cell Sci.* **2002**, *115*, 3355–3356.
27. Murakami, M.; Simons, M. Fibroblast growth factor regulation of neovascularization. *Curr. Opin. Hematol.* **2008**, *15*, 215. [CrossRef]
28. Plate, K.H.; Breier, G.; Farrell, C.L.; Risau, W. Platelet-derived growth factor receptor-beta is induced during tumor development and upregulated during tumor progression in endothelial cells in human gliomas. *Lab. Investig.* **1992**, *67*, 529–534.

29. Mamer, S.B.; Chen, S.; Weddell, J.C.; Palasz, A.; Wittenkeller, A.; Kumar, M.; Imoukhuede, P.I. Discovery of High-Affinity PDGF-VEGFR Interactions: Redefining RTK Dynamics. *Sci. Rep.* **2017**, *7*, 16439. [CrossRef]
30. Stankov, K.; Popovic, S.; Mikov, M. C-KIT signaling in cancer treatment. *Curr. Pharm. Des.* **2014**, *20*, 2849–2880. [CrossRef]
31. Abbaspour Babaei, M.; Kamalidehghan, B.; Saleem, M.; Huri, H.Z.; Ahmadipour, F. Receptor tyrosine kinase (c-Kit) inhibitors: A potential therapeutic target in cancer cells. *Drug Des. Devel. Ther.* **2016**, *10*, 2443–2459. [CrossRef] [PubMed]
32. Chen, T.T.; Filvaroff, E.; Peng, J.; Marsters, S.; Jubb, A.; Koeppen, H.; Merchant, M.; Ashkenazi, A. MET Suppresses Epithelial VEGFR2 via Intracrine VEGF-induced Endoplasmic Reticulum-associated Degradation. *EBioMedicine* **2015**, *2*, 406–420. [CrossRef] [PubMed]
33. Bussolati, B.; Mason, J.C. Dual role of VEGF-induced heme-oxygenase-1 in angiogenesis. *Antioxid. Redox Signal.* **2006**, *8*, 1153–1163. [CrossRef] [PubMed]
34. Hu, T.; Li, C. Convergence between Wnt-β-catenin and EGFR signaling in cancer. *Mol. Cancer* **2010**, *9*, 236. [CrossRef] [PubMed]
35. Giavazzi, R.; Sennino, B.; Coltrini, D.; Garofalo, A.; Dossi, R.; Ronca, R.; Tosatti, M.P.M.; Presta, M. Distinct role of fibroblast growth factor-2 and vascular endothelial growth factor on tumor growth and angiogenesis. *Am. J. Pathol.* **2003**, *162*, 1913–1926. [CrossRef]
36. Madhusudan, S.; Foster, M.; Mathuramalingam, S.R.; Braybrooke, J.P.; Wilner, S.; Kaur, K.; Han, C.; Hoare, S.; Balkwill, F.; Talbot, D.C.; et al. A phase II study of etanercept (Enbrel), a tumor necrosis factor α inhibitor in patients with metastatic breast cancer. *Clin. Cancer Res.* **2004**, *10*, 6528–6534. [CrossRef]
37. Cordero, J.B.; Macagno, J.P.; Stefanatos, R.K.; Strathdee, K.E.; Cagan, R.L.; Vidal, M. Oncogenic ras diverts a host TNF tumor suppressor activity into tumor promoter. *Dev. Cell* **2010**, *18*, 999–1011. [CrossRef]
38. Nabors, L.B.; Suswam, E.; Huang, Y.; Yang, X.; Johnson, M.J.; King, P.H. Tumor necrosis factor α induces angiogenic factor up-regulation in malignant glioma cells: A role for RNA stabilization and HuR. *Cancer Res.* **2003**, *63*, 4181–4187.
39. Giraudo, E.; Primo, L.; Audero, E.; Gerber, H.P.; Koolwijk, P.; Soker, S.; Klagsbrun, M.; Ferrara, N.; Bussolino, F. Tumor necrosis factor-alpha regulates expression of vascular endothelial growth factor receptor-2 and of its co-receptor neuropilin-1 in human vascular endothelial cells. *J. Biol. Chem.* **1998**, *273*, 22128–22135. [CrossRef]
40. El-Azab, A.S.; Abdel-Aziz, A.A.M.; Abou-Zeid, L.A.; El-Husseiny, W.M.; ElMorsy, A.M.; El-Gendy, M.A.; El-Sayed, M.A.A. Synthesis, antitumour activities and molecular docking of thiocarboxylic acid ester-based NSAID scaffolds: COX-2 inhibition and mechanistic studies. *J. Enzyme Inhib. Med. Chem.* **2018**, *33*, 989–998. [CrossRef]
41. Ashizawa, T.; Kawashima, K.; Kanda, Y.; Goml, K.; Okabe, M.; Ueda, K.; Tamaoki, T. Antitumor activity of KF22678, a novel thioester derivative of leinamycin. *Anticancer. Drugs* **1999**, *10*, 829–836. [CrossRef] [PubMed]

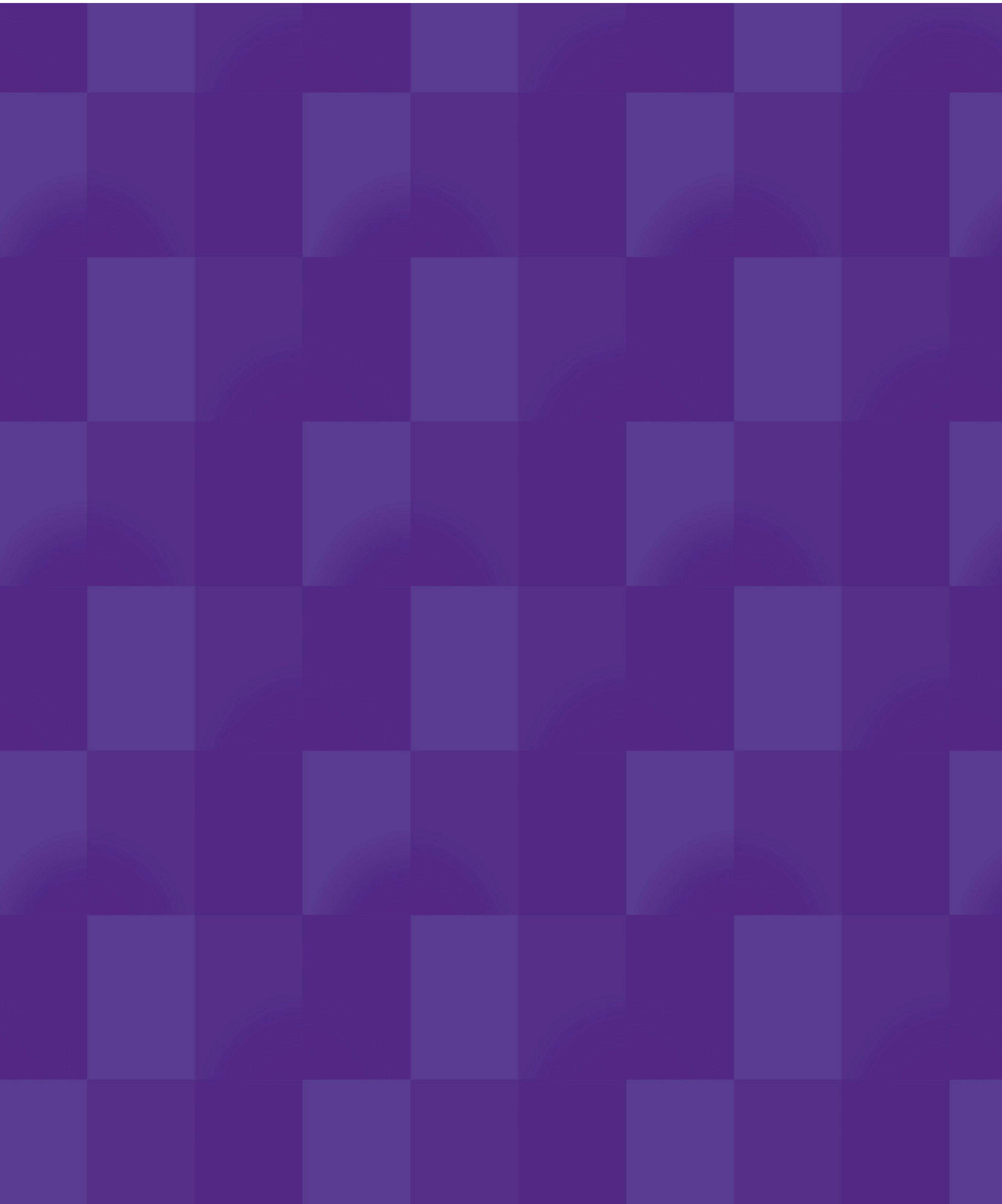© 2019 by the authors. Licensee MDPI, Basel, Switzerland. This article is an open access article distributed under the terms and conditions of the Creative Commons Attribution (CC BY) license (http://creativecommons.org/licenses/by/4.0/).